Geotechnical Engineering

Environmental Engineering

Hydrogeology

Geological Engineering

Materials Testing

Building Science

Noise and Vibration Studies

Paterson Group Inc.
Consulting Engineers
154 Colonnade Road South
Ottawa (Nepean), Ontario
Canada K2E 7S8

Tel: (613) 226-7381
Fax: (613) 226-6344
www.patersongroup.ca

patersongroup

Geotechnical Investigation

Proposed Residential Building
1185 Beaverwood Road
Ottawa, Ontario

Prepared For

ARK Construction Ltd.

December 16, 2022

Report: PG6160-1
Revision 2

Table of Contents

Appendices

1.0 Introduction

Paterson Group (Paterson) was commissioned by ARK Construction Ltd. to conduct a geotechnical investigation for the proposed residential building to be located at 1185 Beaverwood Road in the City of Ottawa (refer to Figure 1 - Key Plan in Appendix 2 of this report).

The objectives of the geotechnical investigation were to:

- Determine the subsoil and groundwater conditions at this site by means of test holes.
- Provide geotechnical recommendations pertaining to design of the proposed development including construction considerations which may affect the design.

The following report has been prepared specifically and solely for the aforementioned project which is described herein. It contains our findings and includes geotechnical recommendations pertaining to the design and construction of the subject development as they are understood at the time of writing this report.

Investigating for the presence or potential presence of contamination on the subject property was not part of the scope of work of the present investigation. Therefore, the present report does not address environmental issues.

2.0 Proposed Development

Based on the available drawings, it is understood that the proposed development will consist of a multi-storey residential building with a partial below-grade level which will daylight to the east. At finished grades, the proposed building will be surrounded by landscaped areas and asphalt-paved access lanes and parking areas. It is also understood that the proposed building will be municipally serviced.

3.0 Method of Investigation

3.1 Field Investigation

Field Program

The field program for the geotechnical investigation was carried out on March 1, 2022 and consisted of advancing a total of 4 boreholes to a maximum depth of 4.5 m below existing ground surface. The test hole locations were distributed in a manner to provide general coverage of the subject site and taking into consideration underground utilities and site features. The borehole locations are shown on Drawing PG6160-1 - Test Hole Location Plan included in Appendix 2.

The boreholes were completed using a low clearance drill rig operated by a two-person crew. All fieldwork was conducted under the full-time supervision of Paterson personnel under the direction of a senior engineer. The testing procedure consisted of augering and excavating to the required depth at the selected location and sampling the overburden.

Sampling and In Situ Testing

Soil samples were recovered using a 50 mm diameter split-spoon sampler or from the auger flights. The split-spoon and auger samples were classified on site and placed in sealed plastic bags. All samples were transported to our laboratory. The depths at which the split-spoon and auger samples were recovered from the boreholes are shown as SS and AU, respectively, on the Soil Profile and Test Data sheets in Appendix 1.

The Standard Penetration Test (SPT) was conducted in conjunction with the recovery of the split-spoon samples. The SPT results are recorded as “N” values on the Soil Profile and Test Data sheets. The “N” value is the number of blows required to drive the split-spoon sampler 300 mm into the soil after a 150 mm initial penetration using a 63.5 kg hammer falling from a height of 760 mm.

The subsurface conditions observed in the boreholes were recorded in detail in the field. The soil profiles are logged on the Soil Profile and Test Data sheets in Appendix 1 of this report.

Groundwater

Borehole BH 4-22 was fitted with a 51 mm diameter PVC groundwater monitoring well. The other boreholes were fitted with flexible piezometers to allow for groundwater level monitoring. The groundwater observations are discussed in Section 4.3 and are presented on the Soil Profile and Test Data sheets in Appendix 1.

Sample Storage

All samples will be stored in the laboratory for a period of one (1) month after issuance of this report. They will then be discarded unless we are otherwise directed.

3.2 Field Survey

The test hole locations and ground surface elevation at each test hole location were surveyed by Paterson using a handheld GPS and referenced to a geodetic datum. The locations of the boreholes, and the ground surface elevation at each borehole location, are presented on Drawing PG6160 - 1 - Test Hole Location Plan in Appendix 2.

3.3 Laboratory Testing

Soil samples were recovered from the subject site and visually examined in our laboratory to review the results of the field logging. A total of 2 grain size distribution analyses and 1 Atterberg limit test were completed on selected soil samples. The results of the testing are presented in Section 4.2 and on the Grain Size Distribution and Hydrometer Testing Results, and Atterberg Limits Testing Results sheets presented in Appendix 1.

3.4 Analytical Testing

One (1) soil sample was submitted for analytical testing to assess the corrosion potential for exposed ferrous metals and the potential of sulphate attacks against subsurface concrete structures. The samples were submitted to determine the concentration of sulphate and chloride, the resistivity, and the pH of the samples. The results are presented in Appendix 1 and are discussed further in Section 6.7.

4.0 Observations

4.1 Surface Conditions

The subject site is currently occupied by a residential dwelling and detached shed, which are located on the western portion of the site. The remainder of the site generally consists of landscaped areas. The site is bordered by Beaverwood Road to the south, Scharfield Road to the east, and residential properties to the north and west. The existing ground surface across the site slopes downward moderately from west to east, from approximate geodetic elevation 94 m at the west property line, down to approximate geodetic elevation 90 m at the east property line.

4.2 Subsurface Profile

Generally, the subsurface profile at the test hole locations consists of a thin layer of topsoil or asphalt overlying a layer of fill extending to depths ranging from 0.2 to 1.2 m below the existing ground surface. The fill was generally observed to consist of a silty sand to silty clay with trace gravel.

With the exception of borehole BH 2-22, a hard to stiff silty clay was encountered underlying the fill, extending to approximate depths of 1.5 to 3.4 m below the existing ground surface. Based on an Atterberg Limits test at borehole BH 4-22 from approximate depths of 2.2 to 2.9 m, the in-situ moisture content of the clay (45.2%) at this location and depth exceeds the liquid limit of 40%. The results of the Atterberg Limits test is provided in Table 1 on the next page.

A glacial till deposit was generally encountered underlying the silty clay, consisting of a compact, brown silty sand to sandy silt with gravel, cobbles, and boulders.

Practical refusal to augering was encountered at approximate depths ranging from 0.2 m at the west end of the site, to 4.5 m at the east end of the site. Where auger refusal was encountered at depths of less than 2.5 m, a second borehole was drilled (BH 1A-22, BH 2A-22 and BH 3A-22) in the vicinity of the initial borehole, in order to confirm the refusal depth.

The shallow refusals (less than 2.5 m depth) are considered to be indicative of boulders in the glacial till deposit. The deeper refusal at borehole BH 4-22 at a depth of 4.5 m approximately coincides with the bedrock depths of 5 to 10 m in the available geological mapping, and is considered to be indicative of the bedrock surface.

Reference should be made to the Soil Profile and Test Data sheets in Appendix 1 for the details of the soil profile encountered at each test hole location.

Bedrock

Based on available geological mapping, the bedrock in the subject area consists of Paleozoic Dolomite of the Oxford formation, with an overburden drift thickness of 5 to 10 m depth.

Atterberg Limits Testing

Atterberg limits testing was completed on a recovered silty clay sample from borehole BH 4-22. The result of the Atterberg limits test is presented in Table 1 and on the Atterberg Limits Testing Results sheet in Appendix 1.

Table 1 - Atterberg Limits Results

Sample	Depth (m)	LL (%)	PL (%)	PI (%)	w (%)	Classification
BH 4-22 SS4	2.2-2.9	40	23	17	45.2	CL

Notes: LL: Liquid Limit; PL: Plastic Limit; PI: Plasticity Index; w: water content;
CL: Inorganic Clays of Low Plasticity

Grain Size Distribution and Hydrometer Testing

Grain size distribution (sieve and hydrometer analysis) was also completed on 2 selected soil samples. The results of the grain size analysis are summarized in Table 2 and are presented on the Grain-Size Distribution and Hydrometer Testing Results sheet in Appendix 1.

Table 2 - Summary of Grain Size Distribution Analysis

Test Hole	Sample	Gravel (%)	Sand (%)	Silt (%)	Clay (%)
BH 3-22	SS3	0.4	17.1	82.5	
BH 4-22	SS3	0.0	12.8	87.2	

4.3 Groundwater

Groundwater levels were measured in the monitoring wells and piezometers installed at the borehole locations on March 9 and November 25, 2022. The measured groundwater levels noted at that time are presented in Table 3 on the next page.

Additional groundwater level readings will be obtained once per season through spring 2023.

Table 3 – Summary of Groundwater Levels

Test Hole Number	Ground Surface Elevation (m)	March 9, 2022		November 25, 2022	
		Depth (m)	Elevation (m)	Depth (m)	Elevation (m)
BH 1-22	94.24	1.23	93.01	1.54	92.70
BH 3-22	91.65	Dry	-	Not Found	-
BH 4-22	90.67	3.14	87.53	3.95	86.72

Note: The ground surface elevation at each borehole location was surveyed using a handheld GPS and are referenced to a geodetic datum.

It should be noted that surface water can become trapped within a backfilled borehole that can lead to higher than typical groundwater level observations. Based on the site observations, the long-term groundwater table can be expected at approximate geodetic elevation 87 to 92 m.

The recorded groundwater levels are noted on the applicable Soil Profile and Test Data sheet presented in Appendix 1.

It should be noted that groundwater levels are subject to seasonal fluctuations. Therefore, the groundwater levels could vary at the time of construction.

5.0 Discussion

5.1 Geotechnical Assessment

From a geotechnical perspective, the subject site is considered suitable for the proposed residential building. It is recommended that the proposed building be supported on conventional spread footings bearing on the undisturbed silty clay, glacial till, or clean surface sounded bedrock.

Based on the results of the geotechnical investigation, boulder removal is anticipated to be required to complete the basement levels and/or site servicing works. All contractors should be prepared for oversized boulder removal.

Due to the presence of the silty clay layer, the subject site will have a permissible grade raise restriction where the silty clay was observed. The permissible grade raise recommendations are discussed in Section 5.3.

The above and other considerations are discussed in the following sections.

5.2 Site Grading and Preparation

Stripping Depth

Topsoil and deleterious fill, such as those containing organic materials, should be stripped from under any buildings, paved areas, pipe bedding and other settlement sensitive structures. Care should be taken not to disturb adequate bearing soils below the founding level during site preparation activities. Disturbance of the subgrade may result in having to sub-excavate the disturbed material and the placement of additional suitable fill material.

Existing foundation walls and other construction debris should be entirely removed from within the building perimeter. Under paved areas, existing construction remnants, such as foundation walls, should be excavated to a minimum of 1 m below final grade.

Boulder Removal

Boulder removal may be required at the subject site and can be accomplished by hoe ramming the boulders into smaller fragments, which then can be excavated and handled the same as other soils.

Vibration Considerations

Construction operations are also the cause of vibrations, and possibly, sources of nuisance to the community. Therefore, means to reduce the vibration levels should be incorporated in the construction operations to maintain, as much as possible, a cooperative environment with the residents.

The following construction equipment could be a source of vibrations: piling rig, hoe ram, compactor, dozer, crane, truck traffic, etc. Vibrations, whether caused by blasting operations or by others construction operations, could be the source of detrimental vibrations on the nearby buildings and structures. Therefore, it is recommended that all vibrations be limited.

Two parameters are used to determine the permissible vibrations, namely, the maximum peak particle velocity and the frequency. For low frequency vibrations, the maximum allowable peak particle velocity is less than that for high frequency vibrations. As a guideline, the peak particle velocity should be less than 15 mm/s between frequencies of 4 to 12 Hz, and 50 mm/s above a frequency of 40 Hz (interpolate between 12 and 40 Hz).

It should be noted that these guidelines are for today's construction standards. Considering that these guidelines are above perceptible human level and, in some cases, could be very disturbing to some people, it is recommended that a pre-construction survey be completed to minimize the risks of claims during or following the construction of the proposed buildings.

Fill Placement

Fill placed for grading beneath the building areas should consist, unless otherwise specified, of clean imported granular fill, such as Ontario Provincial Standard Specifications (OPSS) Granular A or Granular B Type II. The imported fill material should be tested and approved prior to delivery. The fill, where required, should be placed in maximum 300 mm thick loose lifts and compacted by suitable compaction equipment. Fill placed beneath the buildings should be compacted to a minimum of 98% of the standard Proctor maximum dry density (SPMDD).

Non-specified existing fill along with site-excavated soil could be placed as general landscaping fill where settlement of the ground surface is of minor concern. These materials should be spread in lifts with a maximum thickness of 300 mm and compacted by the tracks of the spreading equipment to minimize voids.

Non-specified existing fill and site-excavated soils are not suitable for placement as backfill against foundation walls, unless used in conjunction with a geocomposite drainage membrane, such as Miradrain G100N or Delta Drain 6000.

5.3 Foundation Design

Conventional spread footings, placed on an undisturbed, stiff silty clay, compact glacial till, or clean surface sounded bedrock subgrade can be designed using a bearing resistance value at serviceability limit states (SLS) of **170 kPa** and a factored bearing resistance value at ultimate limit states (ULS) of **255 kPa**. A geotechnical resistance factor of 0.5 was applied to the above noted bearing resistance value at ULS.

The bearing resistance value at SLS will be subjected to potential post-construction total and differential settlements of 25 and 20 mm, respectively.

An undisturbed soil bearing surface consists of a surface from which all topsoil and deleterious materials, such as loose, frozen, or disturbed soil, whether in situ or not, have been removed, in the dry, prior to the placement of concrete for footings.

Lateral Support

The bearing medium under footing-supported structures is required to be provided with adequate lateral support with respect to excavations and different foundation levels.

Adequate lateral support is provided to the in-situ bearing medium soils above the groundwater table when a plane extending down and out from the bottom edges of the footing, at a minimum of 1.5H:1V, passes only through in situ soil or engineered fill of the same or higher capacity as that of the bearing medium.

Permissible Grade Raise Recommendations

Due to the presence of a silty clay deposit at the subject site, permissible grade raise restriction of **2.5 m** is recommended for development.

If higher than permissible grade raises are required, preloading with or without a surcharge, lightweight fill, and/or other measures should be investigated to reduce the risks of unacceptable long-term post construction total and differential settlements.

5.4 Design for Earthquakes

The site class for seismic site response can be taken as **Class D**. If a higher seismic site class is required (Class C), a site specific shear wave velocity test may be completed to accurately determine the applicable seismic site classification for foundation design of the proposed building, as presented in Table 4.1.8.4.A of the Ontario Building Code 2012.

Reference should be made to the latest revision of the Ontario Building Code 2012 for a full discussion of the earthquake design requirements.

Soils underlying the subject site are not susceptible to liquefaction. The coarse-grained soils at the subject site have been evaluated for liquefaction potential in accordance with the "Liquefaction Resistance of Soils" document prepared by Youd et al. (2001), and were determined to have suitable factors of safety greater than 1.1 against liquefaction potential.

The fine-grained soils at the subject site have been evaluated for cyclic failure potential in accordance with the "Evaluating The Potential For Liquefaction or Cyclic Failure of Silts and Clays" document prepared by Boulanger & Idriss (2004), and were determined to have suitable factors of safety greater than 1.1 against cyclic failure.

The studies referenced above are provided in Appendix 3.

5.5 Basement Slab / Slab-on-Grade Construction

With the removal of all topsoil and deleterious fill within the footprints of the proposed buildings, the native soil subgrade will be considered an acceptable subgrade upon which to commence backfilling for floor slab construction.

As the proposed below-grade level will mostly consist of vehicle parking, the recommended pavement structure noted in Table 5 in Section 5.7 below will be applicable for the parking level of the proposed building.

However, when storage or other uses of the lower level will involve the construction of a concrete floor slab, it is recommended that the upper 200 mm of subfloor fill consists of 19 mm clear crushed stone. It is also recommended to install an underslab drainage system, consisting of lines of perforated drainage pipe subdrains connected to a positive outlet, below lowest level floor. This is discussed further in Section 6.1.

5.6 Pavement Design

For design purposes, it is recommended that the rigid pavement structure for the underground parking level should consist of Category C2, 32 MPa concrete at 28 days with air entrainment of 5 to 8%. The recommended rigid pavement structure is further presented in Table 4 below.

Table 4 - Recommended Rigid Pavement Structure – Underground Parking Areas	
Thickness (mm)	**Material Description**
150	**Exposure Class C2 – 32 MPa Concrete** (5 to 8 % Air Entrainment)
300	**BASE** - OPSS Granular A Crushed Stone
SUBGRADE Top of Raft Foundation	

To control cracking due to shrinking of the concrete floor slab, it is recommended that strategically located saw cuts be used to create control joints within the concrete floor slab of the underground parking level. The control joints are generally recommended to be located at the center of the column lines and spaced at approximately 24 to 36 times the slab thickness (for example, a 0.15 m thick slab should have control joints spaced between 3.6 and 5.4 m). The joints should be cut between 25 and 30% of the thickness of the concrete floor slab and completed as early as 4 hours after the concrete has been poured during warm temperatures and up to 12 hours during cooler temperatures.

The following flexible pavement structures presented in Tables 5 and 6 should be used for exterior, at-grade parking areas and access lanes, respectively.

Table 5 – Recommended Pavement Structure – Driveways and at-grade car parking areas	
Thickness (mm)	**Material Description**
50	**Wear Course –** HL-3 or Superpave 12.5 Asphaltic Concrete
150	**BASE –** OPSS Granular A Crushed Stone
300	**SUBBASE –** OPSS Granular B Type II
Subgrade – Either fill, in-situ soil, or OPSS Granular B Type I or II material placed over in-situ soil or fill.	

Table 6 – Recommended Pavement Structure – Local Residential Roadways and Access Lanes	
Thickness (mm)	**Material Description**
40	**Wear Course –** HL-3 or Superpave 12.5 Asphaltic Concrete
50	**Binder Course –** HL-8 or Superpave 19.0 Asphaltic Concrete
150	**BASE –** OPSS Granular A Crushed Stone
450	**SUBBASE –** OPSS Granular B Type II
Subgrade – Either fill, in-situ soil, or OPSS Granular B Type I or II material placed over in-situ soil or fill.	

If soft spots develop in the subgrade during compaction or due to construction traffic, the affected areas should be excavated and replaced with OPSS Granular B Type II material. Weak subgrade conditions may be experienced over service trench fill materials. This may require the use of geotextile, thicker subbase or other measures that can be recommended at the time of construction as part of the field observation program.

Minimum Performance Graded (PG) 58-34 asphalt cement should be used for this project. For residential driveways and car only parking areas, an Ontario Traffic Category A will be used. For local roadways, an Ontario traffic Category B should be used for design purposes. The pavement granular base and subbase should be placed in maximum 300 mm thick lifts and compacted to a minimum of 99% of the material's SPMDD using suitable compaction equipment.

6.0 Design and Construction Precautions

6.1 Foundation Drainage and Backfill

Foundation Drainage

A perimeter foundation drainage system is recommended for the proposed structure. The system should consist of a 100 to 150 mm diameter, geotextile-wrapped, perforated and corrugated plastic pipe which is surrounded by 150 mm of 19 mm clear crushed stone and placed at the footing level around the exterior perimeter of the structure. The perimeter drainage pipe should have a positive outlet, such as gravity connection to the storm sewer.

Underslab Drainage

Underslab drainage will be required to control water infiltration below the lowest level floor slab. For preliminary design purposes, we recommend that 150 or 100 mm diameter perforated pipes be placed at approximate 6 m centres. The spacing of the underslab drainage system should be confirmed at the time of completing the excavation when water infiltration can be better assessed.

Foundation Backfill

Backfill against the exterior sides of the foundation walls should consist of free draining, non-frost susceptible granular materials. The site excavated materials will be frost susceptible and, as such, are not recommended for re-use as backfill unless a composite drainage system (such as system Miradrain G100N or Delta Drain 6000) connected to a drainage system is provided. Imported granular materials, such as clean sand or OPSS Granular B Type I granular material should otherwise be used for this purpose.

6.2 Protection of Footings Against Frost Action

Perimeter footings of heated structures are required to be insulated against the deleterious effects of frost action. A minimum 1.5 m thick soil cover, or an equivalent combination of soil cover and foundation insulation, should be provided in this regard.

Exterior unheated footings, such as for isolated piers, are more prone to deleterious movement associated with frost action. These should be provided with a minimum 2.1 m thick soil cover, or an equivalent combination of soil cover and foundation insulation.

6.3 Excavation Side Slopes

The side slopes of shallow excavations anticipated at this site should either be cut back at acceptable slopes or retained by shoring systems from the start of the excavation until the structure is backfilled.

Due to the proposed depth of excavation below existing site grades and the proximity to the property line, a temporary shoring system is anticipated to be required along the western boundary of the site, and the western portion of the northern boundary of the site. For the remainder of the site, due to the proposed depth of excavation below the existing site grades and the setback from the property lines, it is anticipated that the excavation can be sloped as per the recommendations below.

Unsupported Excavations

The excavation side slopes above the groundwater level extending to a maximum depth of approximately 3 m should be stable cut back at 1H:1V. Flatter slopes could be required for deeper excavations or for excavations below the groundwater level. Where such side slopes are not permissible or practical, temporary shoring systems should be used.

The subsoil at this site is considered to be mainly a Type 2 or 3 soil according to the Occupational Health and Safety Act and Regulations for Construction Projects.

Excavated soil should not be stockpiled directly at the top of excavations and heavy equipment should be kept away from the excavation sides.

Slopes in excess of 3 m in height should be periodically inspected by the geotechnical consultant in order to detect if the slopes are exhibiting signs of distress.

Excavation side slopes around the building excavation should be protected from erosion by surface water and rainfall events by the use of secured tarpaulins spanning the length of the side slopes, or other means of erosion protection along their footprint. Efforts should also be made to maintain dry surfaces at the bottom of the excavation footprints and along the bottom of side slopes. Additional measures may be recommended at the time of construction by the geotechnical consultant.

It is recommended that a trench box be used at all times to protect personnel working in trenches with steep or vertical sides. It is expected that services will be installed by “cut and cover” methods and excavations will not be left open for extended periods of time.

Temporary Shoring

Temporary shoring may be required for the overburden soil to complete the required excavations at the western boundary of the site, and the western portion of the northern boundary of the site. The shoring requirements will depend on the depth of the excavation and the proximity of the adjacent structures.

If a temporary shoring system is considered, the design and approval of the shoring system will be the responsibility of the shoring contractor and the shoring designer who is a licensed professional engineer and is hired by the shoring contractor. It is the responsibility of the shoring contractor to ensure that the temporary shoring is in compliance with safety requirements, designed to avoid any damage to adjacent structures, and include dewatering control measures.

Geotechnical information provided below is to assist the designer in completing a suitable and safe shoring system. In the event that subsurface conditions differ from the approved design during the actual installation, it is the responsibility of the shoring contractor to commission the required experts to re-assess the design and implement the required changes.

The designer should also take into account the impact of a significant precipitation event and designate design measures to ensure that a precipitation will not negatively impact the shoring system or soils supported by the system. Any changes to the approved shoring design system should be reported immediately to the owner's representative prior to implementation.

The temporary shoring system, where required, may generally consist of a soldier pile and lagging system which could be cantilevered, anchored or braced.

The shoring system is recommended to be adequately supported to resist toe failure. Any additional loading due to street traffic, construction equipment, adjacent structures and facilities, etc., should be added to the earth pressures described below. The earth pressures acting on the temporary shoring system may be calculated using the following parameters.

Table 7 – Soil Parameters for Shoring System Design

Parameters	Values
Active Earth Pressure Coefficient (K_a)	0.33
Passive Earth Pressure Coefficient (K_p)	3
At-rest Earth Pressure Coefficient (K_o)	0.5
Total Unit Weight (γ), kN/m^3	20
Submerged Unit Weight (γ'), kN/m^3	13

The active earth pressure should be calculated where wall movements are permissible while the at-rest pressure should be calculated if no movement is permissible.

The dry unit weight should be used above the groundwater level while the effective unit weight should be used below the groundwater level.

The hydrostatic groundwater pressure should be added to the earth pressure distribution wherever the effective unit weights are used for earth pressure calculations. If the groundwater level is lowered, the dry unit weight for the soil should be used full weight, with no hydrostatic groundwater pressure component. For design purposes, the minimum factor of safety of 1.5 should be calculated.

Based on the subsurface soil conditions observed, the groundwater conditions, and the proposed depth of excavation for the proposed residential building, basal heaving is not considered an issue at the subject site.

6.4 Pipe Bedding and Backfill

Bedding and backfill materials should be in accordance with the most recent Material Specifications and Standard Detail Drawings from the Department of Public Works and Services, Infrastructure Services Branch of the City of Ottawa.

The pipe bedding for sewer and water pipes placed on a relatively dry, undisturbed subgrade surface should consist of at least 150 mm of OPSS Granular A material. Where the bedding is located within the silty clay, the thickness of the bedding material should be increased to a minimum of 300 mm. The bedding should extend to the spring line of the pipe. Cover material, from the spring line to at least 300 mm above the obvert of the pipe, should consist of OPSS Granular A or Granular B Type II with a maximum size of 25 mm. The bedding and cover materials should be placed in maximum 225 mm thick lifts compacted to 99% of the material's standard Proctor maximum dry density.

It should generally be possible to re-use the upper portion of the dry to moist (not wet) silty clay above the cover material if the excavation and filling operations are carried out in dry weather conditions. Any stones greater than 200 mm in their longest dimension should be removed from these materials prior to placement.

Where hard surface areas are considered above the trench backfill, the trench backfill material within the frost zone (about 1.8 m below finished grade) should match the soils exposed at the trench walls to reduce potential differential frost heaving. The backfill should be placed in maximum 225 mm thick loose lifts and compacted to a minimum of 95% of the material's SPMDD.

6.5 Groundwater Control

Groundwater Control for Building Construction

Based on our observations, it is anticipated that groundwater infiltration into the excavations should be low to moderate and controllable using open sumps. The contractor should be prepared to direct water away from all bearing surfaces and subgrades, regardless of the source, to prevent disturbance to the founding medium.

Permit to Take Water

A temporary Ministry of the Environment, Conservation and Parks (MECP) permit to take water (PTTW) may be required for this project if more than 400,000 L/day of ground and/or surface water is to be pumped during the construction phase. A minimum 4 to 5 months should be allowed for completion of the PTTW application package and issuance of the permit by the MECP.

For typical ground or surface water volumes being pumped during the construction phase, typically between 50,000 to 400,000 L/day, it is required to register on the Environmental Activity and Sector Registry (EASR). A minimum of two to four weeks should be allotted for completion of the EASR registration and the Water Taking and Discharge Plan to be prepared by a Qualified Person as stipulated under O.Reg. 63/16. If a project qualifies for a PTTW based upon anticipated conditions, an EASR will not be allowed as a temporary dewatering measure while awaiting the MECP review of the PTTW application.

6.6 Winter Construction

Precautions must be taken if winter construction is considered for this project.

The subsoil conditions at this site consist of frost susceptible materials. In the presence of water and freezing conditions, ice could form within the soil mass. Heaving and settlement upon thawing could occur.

In the event of construction during below zero temperatures, the founding stratum should be protected from freezing temperatures using straw, propane heaters and tarpaulins or other suitable means. In this regard, the base of the excavations should be insulated from sub-zero temperatures immediately upon exposure and until such time as heat is adequately supplied to the building and the footings are protected with sufficient soil cover to prevent freezing at founding level.

Trench excavations and pavement construction are also difficult activities to complete during freezing conditions without introducing frost in the subgrade or in the excavation walls and bottoms. Precautions should be taken if such activities

are to be carried out during freezing conditions. Additional information could be provided, if required.

Impacts on Neighbouring Structures

The proposed structure is not anticipated to extend significantly below the groundwater level. Therefore, no adverse effects from short term and/or long term dewatering are expected for the surrounding structures.

6.7 Corrosion Potential and Sulphate

The results of analytical testing show that the sulphate content is less than 0.1%. This result is indicative that Type 10 Portland cement (normal cement) would be appropriate for this site.

The chloride content and the pH of the sample indicate that they are not significant factors in creating a corrosive environment for exposed ferrous metals at this site, whereas the resistivity is indicative of a low to slightly aggressive corrosive environment.

6.8 Landscaping Considerations

Tree Planting Restrictions

Paterson completed a soils review of the site to determine the applicable tree planting setbacks, in accordance with the City of Ottawa Tree Planting in Sensitive Marine Clay Soils (2017 Guidelines). Atterberg limits testing was completed for a recovered silty clay sample. Sieve analysis testing was also completed on a selected soil sample. The above-noted testing was completed on a sample taken at a depth between the anticipated underside of footing elevation and a 3 m depth below finished grade. The results of the testing are presented in Tables 1 and 2 in Section 4.2 and in Appendix 1.

Based on the results of our review, the plasticity index was found to be less than 40%. Therefore, the following tree planting setbacks are recommended for the silty clay deposit. Large trees (mature height over 14 m) can be planted within the silty clay areas provided a tree to foundation setback equal to the full mature height of the tree can be provided (e.g., in a park or other green space). Tree planting setback limits may be reduced to **4.5 m** for small (mature height up to 7.5 m) and medium size trees (mature tree height 7.5 to 14 m), provided that the conditions noted below are met.

- ❒ The underside of footing (USF) is 2.1 m or greater below the lowest finished grade must be satisfied for footings within 10 m from the tree, as measured from the centre of the tree trunk and verified by means of the Grading Plan as indicated procedural changes below.

- ❒ A small tree must be provided with a minimum 25 m^3 of available soil volume while a medium tree must be provided with a minimum of 30 m^3 of available soil volume, as determined by the Landscape Architect. The developer is to ensure that the soil is generally un-compacted when backfilling in street tree planting locations.

- ❒ The tree species must be small (mature tree height up to 7.5 m) to medium size (mature tree height 7.5 m to 14 m) as confirmed by the Landscape Architect.

- ❒ The foundation walls are to be reinforced at least nominally (minimum of two upper and two lower 15M bars in the foundation wall).

- ❒ Grading surrounding the tree must promote drainage to the tree root zone (in such a manner as not to be detrimental to the tree).

It is well documented in the literature, and is our experience, that fast-growing trees located near buildings founded on cohesive soils that shrink on drying can result in long-term differential settlements of the structures. Tree varieties that have the most pronounced effect on foundations are seen to consist of poplars, willows, and some maples (i.e., Manitoba Maples) and, as such, they should not be considered in the landscaping design.

6.9 Slope Stability Assessment

Due to the slope across the site, it is understood that a slope stability assessment is required in accordance with the City of Ottawa guidelines. Accordingly, a slope stability assessment of the proposed site conditions was conducted using SLIDE, a computer program which permits a two-dimensional stability analysis using several methods including the Bishop's method, which is a widely used and accepted analysis method. A horizontal acceleration of 0.16 g (50% of PGA = 0.32g) was utilized for the seismic analysis.

The program calculates a factor of safety, which represents the ratio of the forces resisting failure to those favouring failure. Theoretically, a factor of safety (F.o.S.) of 1.0 represents a condition where the slope is stable. However, due to intrinsic limitations of the calculation methods and the variability of the subsoil and groundwater conditions, a F.o.S. greater than one is usually required to ascertain that the risks of failure are acceptable. A minimum F.o.S. of 1.5 is generally recommended for static analysis conditions and a mimimum F.o.S. of 1.1 is

generally recommended for seismic analysis conditions, where the failure of the slope would endanger permanent structures.

The cross-section A-A (location indicated on Drawing PG6160-1 in Appendix 2) was analyzed based on the proposed site conditions and a review of the available topographic mapping.

The effective strength soil parameters used for static analysis were chosen based on the subsoil information recovered during the geotechnical investigation and in general accordance with the typical ranges of values provided in the City of Ottawa's "Slope Stability Guidelines for Development Applications". The effective strength soil parameters used for static analysis are presented in Table 8 below.

Table 8 - Effective Strength Soil and Material Parameters (Static Analysis)

Soil Layer	Unit Weight (kN/m^3)	Friction Angle (degrees)	Cohesion (kPa)
Fill	18	33	0
Brown Silty Clay	17	33	7
Glacial Till	20	36	0

The total strength soil parameters used for seismic analysis were also chosen based on the subsoil information recovered during the geotechnical investigation and in general accordance with the typical ranges of values provided in the City of Ottawa's "Slope Stability Guidelines for Development Applications".

The strength parameters used for seismic analysis at the slope cross-sections are presented in Table 9 below:

Table 9 - Total Strength Soil and Material Parameters (Seismic Analysis)

Soil Layer	Unit Weight (kN/m^3)	Friction Angle (degrees)	Cohesion (kPa)
Fill	18	33	0
Brown Silty Clay	17	0	100
Glacial Till	20	36	0

The results for the slope stability analyses under static and seismic conditions at cross-section A-A are shown on Figures 2 and 3, which are provided in Appendix 2. The results of the slope stability analyses indicate that the factor of safety exceeds 1.5 and 1.1 under static and seismic analysis conditions, respectively.

Therefore, the slope stability for the proposed site conditions is considered acceptable, from a geotechnical perspective.

Global Stability Analysis

Retaining walls with heights greater than 1 m were noted on the available grading plan at the northwest corner of the site (cross-section B-B), along the north side of the parking lot (cross-section C-C), and on the south side of the building (cross-section D-D). In accordance with City of Ottawa guidelines, global stability analyses are required for all retaining walls greater than 1 m in height.

The global stability analyses of the retaining walls were conducted using SLIDE. A horizontal acceleration of 0.16 g (50% of PGA = 0.32g) was utilized for the seismic analysis.

The results for the global stability analyses under static conditions for cross-sections B-B, C-C, and D-D are shown in Figures 4, 6 and 8, which are attached in Appendix 2. The results of the global stability analyses indicate that the factor of safety exceeds 1.5 under static conditions.

The results for the global stability analyses under seismic conditions at cross-sections B-B, C-C, and D-D are shown on Figure 5, 7 and 9, which are also attached in Appendix 2. The results of this analyses indicate that the factor of safety exceeds 1.1 under seismic conditions.

Therefore, the proposed retaining walls at the subject site are considered stable, from a global stability perspective.

In accordance with the “Slope Stability Guidelines for Development Applications in the City of Ottawa”, retaining wall failure modes such as toppling, forward sliding, structural failure, and bearing capacity are to be addressed at the detailed design stage of the project.

7.0 Recommendations

It is a requirement for the foundation design data provided herein to be applicable that the following material testing and observation program be performed by the geotechnical consultant.

- Review detailed grading plan(s) from a geotechnical perspective.
- Observation of all bearing surfaces prior to the placement of concrete.
- Periodic observation of the condition of unsupported excavation side slopes in excess of 3 m in height, if applicable.
- Observation of all subgrades prior to placing backfilling material.
- Sampling and testing of the concrete and fill materials.
- Observation of clay seal placement at specified locations.
- Field density tests to determine the level of compaction achieved.
- Sampling and testing of the bituminous concrete including mix design reviews.

All excess soils must be handled as per *Ontario Regulation 406/19: On-Site and Excess Soil Management*.

A report confirming that these works have been conducted in general accordance with our recommendations could be issued upon the completion of a satisfactory inspection program by the geotechnical consultant.

8.0 Statement of Limitations

The recommendations provided are in accordance with the present understanding of the project. Paterson requests permission to review the recommendations when the drawings and specifications are completed.

A soils investigation is a limited sampling of a site. Should any conditions at the site be encountered which differ from those at the test locations, Paterson requests immediate notification to permit reassessment of our recommendations.

The recommendations provided herein should only be used by the design professionals associated with this project. They are not intended for contractors bidding on or undertaking the work. The latter should evaluate the factual information provided in this report and determine the suitability and completeness for their intended construction schedule and methods. Additional testing may be required for their purposes.

The present report applies only to the project described in this document. Use of this report for purposes other than those described herein or by person(s) other than ARK Construction Ltd. or their agents is not authorized without review by Paterson for the applicability of our recommendations to the alternative use of the report.

Paterson Group Inc.

Otillia McLaughlin B.Eng.

Scott S. Dennis, P.Eng.

Report Distribution:

- ❑ ARK Construction Ltd. (e-mail copy)
- ❑ Paterson Group (1 copy)

APPENDIX 1

SOIL PROFILE AND TEST DATA SHEETS

SYMBOLS AND TERMS

GRAIN SIZE DISTRIBUTION AND HYDROMETER TESTING RESULTS

ATTERBERG LIMIT TESTING RESULTS

ANALYTICAL TESTING RESULTS

patersongroup Consulting Engineers

9 Auriga Drive, Ottawa, Ontario K2E 7T9

SOIL PROFILE AND TEST DATA

Geotechnical Investigation
Proposed Development - 1185 Beaverwood Road
Ottawa, Ontario

DATUM Geodetic

REMARKS

BORINGS BY CME-55 Low Clearance Drill **DATE** March 1, 2022

FILE NO. PG6160

HOLE NO. BH 1-22

SOIL DESCRIPTION	STRATA PLOT	SAMPLE TYPE	SAMPLE NUMBER	SAMPLE % RECOVERY	SAMPLE N VALUE or RQD	DEPTH (m)	ELEV. (m)
GROUND SURFACE						0	94.24
Asphaltic concrete 0.05							
FILL: Brown silty sand trace gravel and topsoil 0.69		AU	1				
Very stiff, brown **SILTY CLAY,** trace sand and gravel		SS	2	50	6	1	93.24
1.52							
GLACIAL TILL: Compact, brown silty sand to sandy silt with gravel, cobbles, trace clay and boulders 1.98		SS	3	56	50		
End of Borehole							
Practical refusal to augering at 1.98m depth.							
(GWL @ 1.34m - March 9, 2022)							
(GWL at 1.54m - Nov. 25, 2022)							

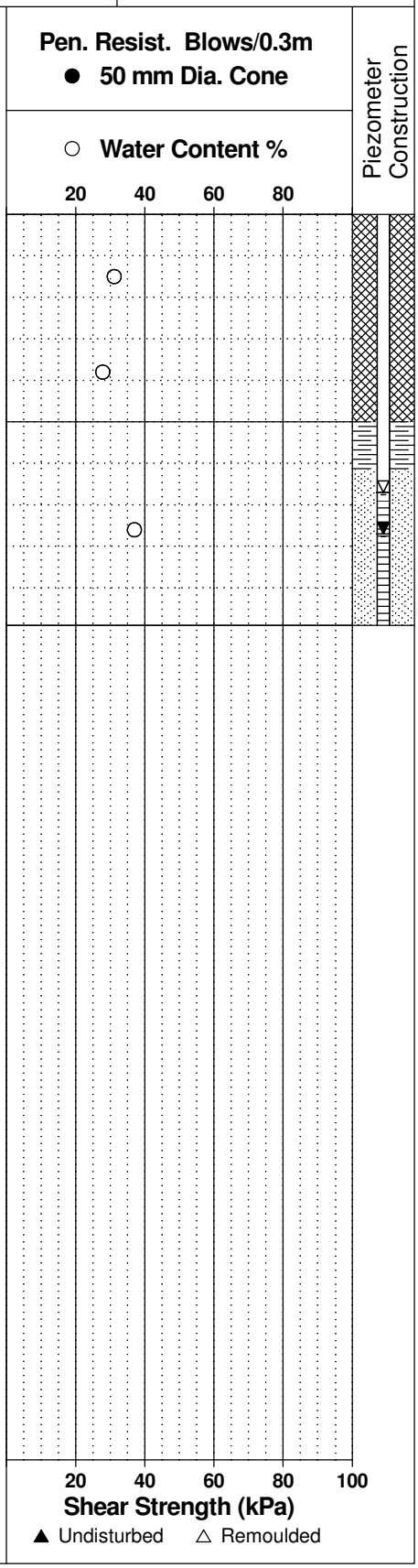

patersongroup Consulting Engineers

9 Auriga Drive, Ottawa, Ontario K2E 7T9

SOIL PROFILE AND TEST DATA

Geotechnical Investigation
Proposed Development - 1185 Beaverwood Road
Ottawa, Ontario

DATUM Geodetic

REMARKS Moved east approx 1 m from BH 1-22 location

BORINGS BY CME-55 Low Clearance Drill **DATE** March 1, 2022

FILE NO. PG6160

HOLE NO. BH 1A-22

SOIL DESCRIPTION	STRATA PLOT	SAMPLE TYPE	SAMPLE NUMBER	SAMPLE % RECOVERY	SAMPLE N VALUE or RQD	DEPTH (m)	ELEV. (m)	Pen. Resist. Blows/0.3m ● 50 mm Dia. Cone ○ Water Content %	Piezometer Construction
GROUND SURFACE									
Asphaltic concrete 0.05						0	94.24		
OVERBURDEN						1	93.24		
2.13						2	92.24		
End of Borehole Practical refusal to augering at 2.13m depth									

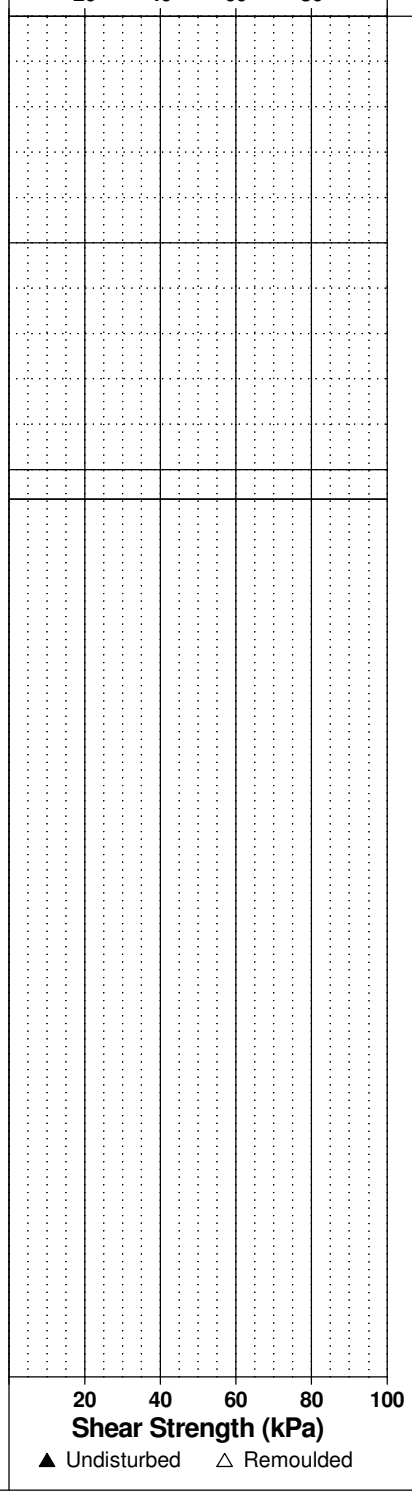

patersongroup Consulting Engineers

9 Auriga Drive, Ottawa, Ontario K2E 7T9

SOIL PROFILE AND TEST DATA

Geotechnical Investigation
Proposed Development - 1185 Beaverwood Road
Ottawa, Ontario

DATUM Geodetic

REMARKS

BORINGS BY CME-55 Low Clearance Drill **DATE** March 1, 2022

FILE NO. PG6160

HOLE NO. BH 2-22

SOIL DESCRIPTION	STRATA PLOT	SAMPLE TYPE	SAMPLE NUMBER	SAMPLE % RECOVERY	SAMPLE N VALUE or RQD	DEPTH (m)	ELEV. (m)	Pen. Resist. Blows/0.3m ● 50 mm Dia. Cone ○ Water Content %	Piezometer Construction
GROUND SURFACE									
Asphaltic concrete 0.05						0	94.46		
FILL: Brown silty sand with gravel and crushed stone 0.23		AU	1						
End of Borehole									
Practical refusal to augering at 0.23m depth									

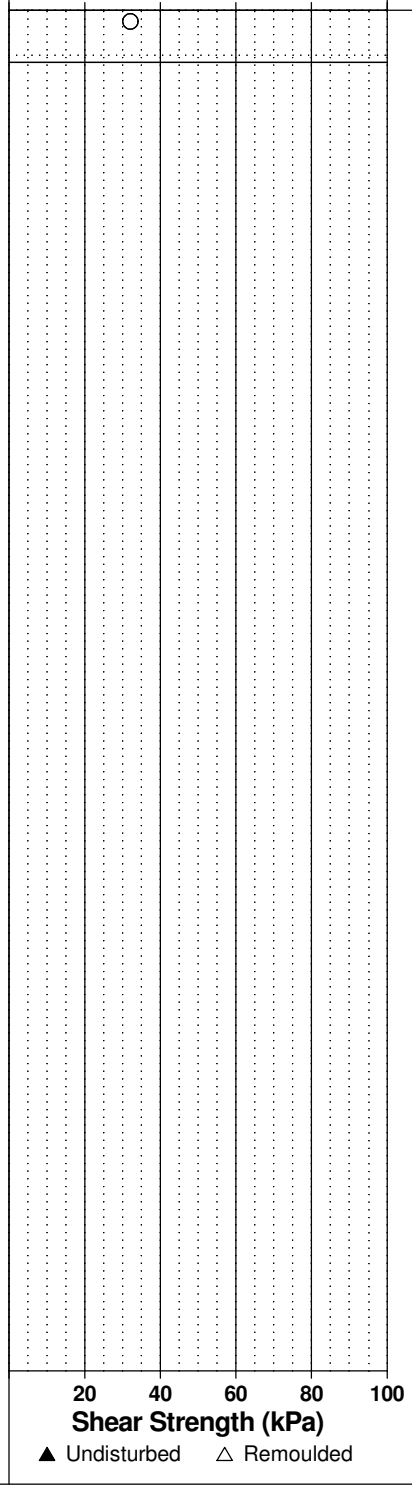

patersongroup Consulting Engineers

9 Auriga Drive, Ottawa, Ontario K2E 7T9

SOIL PROFILE AND TEST DATA

Geotechnical Investigation
Proposed Development - 1185 Beaverwood Road
Ottawa, Ontario

DATUM Geodetic

REMARKS Moved north approx 1 m from BH 2-22 location

BORINGS BY CME-55 Low Clearance Drill **DATE** March 1, 2022

FILE NO. PG6160

HOLE NO. BH 2A-22

SOIL DESCRIPTION	STRATA PLOT	SAMPLE TYPE	SAMPLE NUMBER	SAMPLE % RECOVERY	SAMPLE N VALUE or RQD	DEPTH (m)	ELEV. (m)	Pen. Resist. Blows/0.3m ● 50 mm Dia. Cone ○ Water Content %	Piezometer Construction
GROUND SURFACE						0	94.46		
Asphaltic concrete 0.05									
OVERBURDEN 0.23									
End of Borehole									
Practical refusal to augering at 0.23m depth									

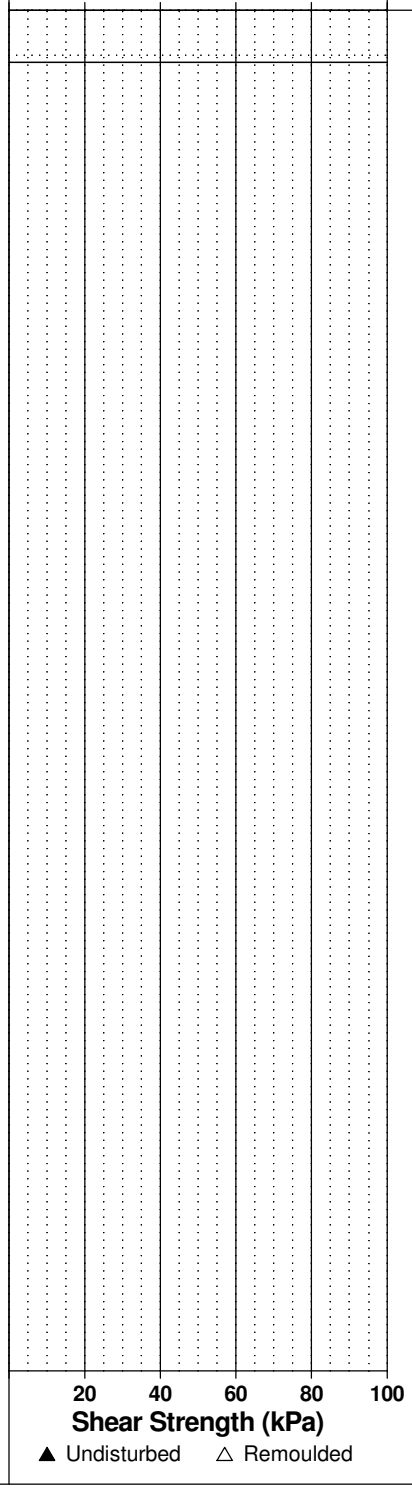

patersongroup Consulting Engineers

9 Auriga Drive, Ottawa, Ontario K2E 7T9

SOIL PROFILE AND TEST DATA

Geotechnical Investigation
Proposed Development - 1185 Beaverwood Road
Ottawa, Ontario

DATUM Geodetic

REMARKS

BORINGS BY CME-55 Low Clearance Drill **DATE** March 1, 2022

FILE NO. PG6160

HOLE NO. BH 3-22

SOIL DESCRIPTION	STRATA PLOT	SAMPLE TYPE	SAMPLE NUMBER	SAMPLE % RECOVERY	SAMPLE N VALUE or RQD	DEPTH (m)	ELEV. (m)
GROUND SURFACE						0	91.65
TOPSOIL 0.10							
FILL: Brown silty clay trace sand and gravel		AU	1				
		SS	2	33	11	1	90.65
1.22							
Very stiff, brown **SILTY CLAY**							
1.68							
GLACIAL TILL: Compact, brown silty sand to sandy silt with gravel, trace clay, cobbles and boulders		SS	3	90	12	2	89.65
2.18							
End of Borehole							
Practical refusal to augering at 2.18m depth							
(BH dry - March 9, 2022)							

Pen. Resist. Blows/0.3m
● **50 mm Dia. Cone**
○ **Water Content %**

20 40 60 80

Piezometer Construction

20 40 60 80 100

Shear Strength (kPa)

▲ Undisturbed △ Remoulded

patersongroup Consulting Engineers

9 Auriga Drive, Ottawa, Ontario K2E 7T9

SOIL PROFILE AND TEST DATA

Geotechnical Investigation
Proposed Development - 1185 Beaverwood Road
Ottawa, Ontario

DATUM Geodetic

REMARKS Moved north approx 1 m from BH 3-22 location

BORINGS BY CME-55 Low Clearance Drill **DATE** March 1, 2022

FILE NO. PG6160

HOLE NO. BH 3A-22

SOIL DESCRIPTION	STRATA PLOT	SAMPLE TYPE	SAMPLE NUMBER	SAMPLE % RECOVERY	SAMPLE N VALUE or RQD	DEPTH (m)	ELEV. (m)	Pen. Resist. Blows/0.3m ● 50 mm Dia. Cone ○ Water Content %	Piezometer Construction
GROUND SURFACE									
TOPSOIL 0.10						0	91.65		
OVERBURDEN						1	90.65		
2.18						2	89.65		
End of Borehole Practical refusal to augering at 2.18m depth									

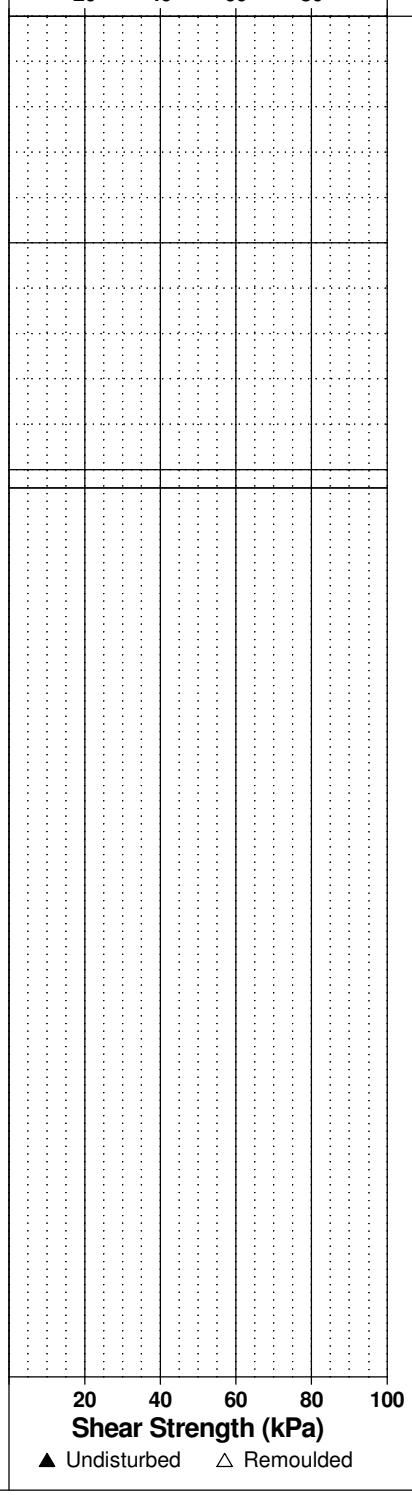

patersongroup Consulting Engineers

9 Auriga Drive, Ottawa, Ontario K2E 7T9

SOIL PROFILE AND TEST DATA

Geotechnical Investigation
Proposed Development - 1185 Beaverwood Road
Ottawa, Ontario

DATUM Geodetic

REMARKS

BORINGS BY CME-55 Low Clearance Drill **DATE** March 1, 2022

FILE NO. PG6160

HOLE NO. BH 4-22

SOIL DESCRIPTION	STRATA PLOT	SAMPLE TYPE	SAMPLE NUMBER	SAMPLE % RECOVERY	SAMPLE N VALUE or RQD	DEPTH (m)	ELEV. (m)
GROUND SURFACE						0	90.67
TOPSOIL 0.10							
FILL: Brown silty clay trace sand		AU	1				
0.69		SS	2	75	10	1	89.67
Brown **SILTY CLAY**		SS	3	42	7	2	88.67
		SS	4	42	4	3	87.67
3.35		SS	5	50	2		
GLACIAL TILL: Compact, brown silty sand to sandy silt with gravel, trace clay, cobbles and boulders		SS	6	50	30	4	86.67
4.52							
End of Borehole							
Practical refusal to augering at 4.52m depth							
(GWL @ 3.14m - March 9, 2022)							
(GWL at 3.95m - Nov. 25, 2022)							

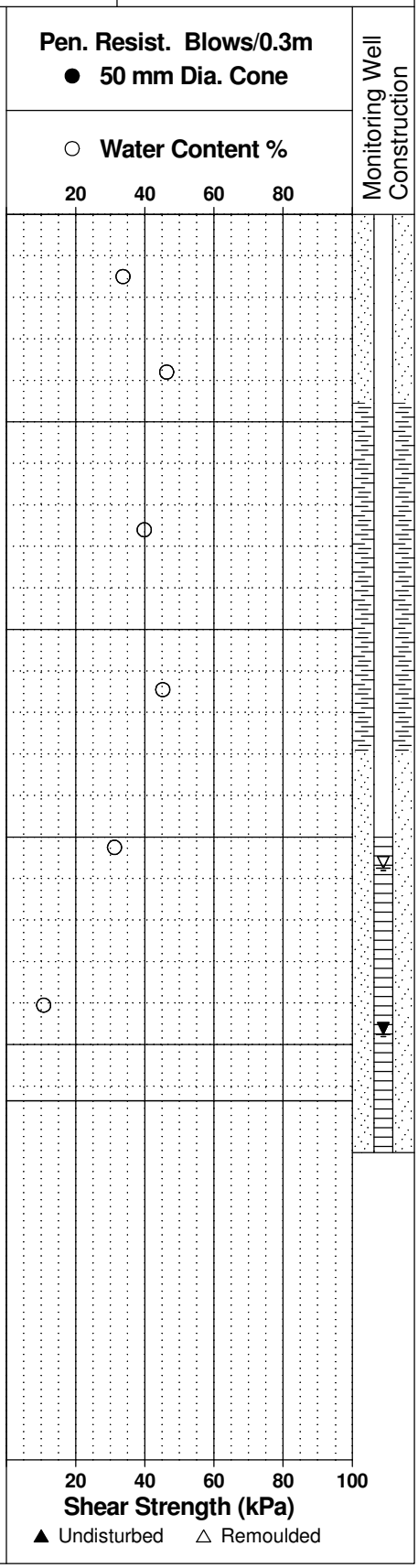

SYMBOLS AND TERMS (continued)

SOIL DESCRIPTION (continued)

Cohesive soils can also be classified according to their “sensitivity”. The sensitivity is the ratio between the undisturbed undrained shear strength and the remoulded undrained shear strength of the soil.

Terminology used for describing soil strata based upon texture, or the proportion of individual particle sizes present is provided on the Textural Soil Classification Chart at the end of this information package.

ROCK DESCRIPTION

The structural description of the bedrock mass is based on the Rock Quality Designation (RQD).

The RQD classification is based on a modified core recovery percentage in which all pieces of sound core over 100 mm long are counted as recovery. The smaller pieces are considered to be a result of closely-spaced discontinuities (resulting from shearing, jointing, faulting, or weathering) in the rock mass and are not counted. RQD is ideally determined from NXL size core. However, it can be used on smaller core sizes, such as BX, if the bulk of the fractures caused by drilling stresses (called “mechanical breaks”) are easily distinguishable from the normal in situ fractures.

RQD %	ROCK QUALITY
90-100	Excellent, intact, very sound
75-90	Good, massive, moderately jointed or sound
50-75	Fair, blocky and seamy, fractured
25-50	Poor, shattered and very seamy or blocky, severely fractured
0-25	Very poor, crushed, very severely fractured

SAMPLE TYPES

SS	-	Split spoon sample (obtained in conjunction with the performing of the Standard Penetration Test (SPT))
TW	-	Thin wall tube or Shelby tube
PS	-	Piston sample
AU	-	Auger sample or bulk sample
WS	-	Wash sample
RC	-	Rock core sample (Core bit size AXT, BXL, etc.). Rock core samples are obtained with the use of standard diamond drilling bits.

SYMBOLS AND TERMS (continued)

GRAIN SIZE DISTRIBUTION

MC%	-	Natural moisture content or water content of sample, %
LL	-	Liquid Limit, % (water content above which soil behaves as a liquid)
PL	-	Plastic limit, % (water content above which soil behaves plastically)
PI	-	Plasticity index, % (difference between LL and PL)
Dxx	-	Grain size which xx% of the soil, by weight, is of finer grain sizes These grain size descriptions are not used below 0.075 mm grain size
D10	-	Grain size at which 10% of the soil is finer (effective grain size)
D60	-	Grain size at which 60% of the soil is finer
Cc	-	Concavity coefficient = $(D30)^2$ / (D10 x D60)
Cu	-	Uniformity coefficient = D60 / D10

Cc and Cu are used to assess the grading of sands and gravels:
Well-graded gravels have: $1 < Cc < 3$ and $Cu > 4$
Well-graded sands have: $1 < Cc < 3$ and $Cu > 6$
Sands and gravels not meeting the above requirements are poorly-graded or uniformly-graded.
Cc and Cu are not applicable for the description of soils with more than 10% silt and clay
(more than 10% finer than 0.075 mm or the #200 sieve)

CONSOLIDATION TEST

p'_o	-	Present effective overburden pressure at sample depth
p'_c	-	Preconsolidation pressure of (maximum past pressure on) sample
Ccr	-	Recompression index (in effect at pressures below p'_c)
Cc	-	Compression index (in effect at pressures above p'_c)
OC Ratio		Overconsolidaton ratio = p'_c / p'_o
Void Ratio		Initial sample void ratio = volume of voids / volume of solids
Wo	-	Initial water content (at start of consolidation test)

PERMEABILITY TEST

k	-	Coefficient of permeability or hydraulic conductivity is a measure of the ability of water to flow through the sample. The value of k is measured at a specified unit weight for (remoulded) cohesionless soil samples, because its value will vary with the unit weight or density of the sample during the test.

SYMBOLS AND TERMS (continued)

STRATA PLOT

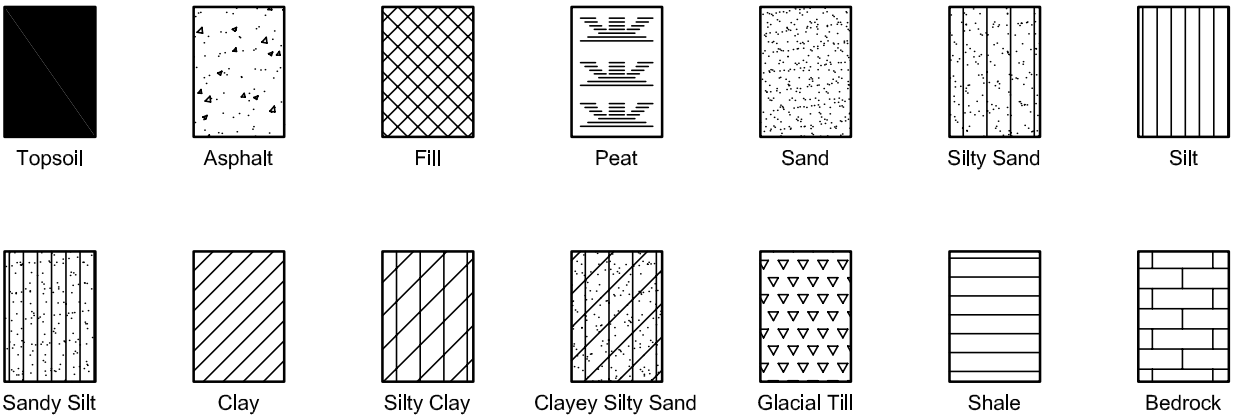

MONITORING WELL AND PIEZOMETER CONSTRUCTION

MONITORING WELL CONSTRUCTION

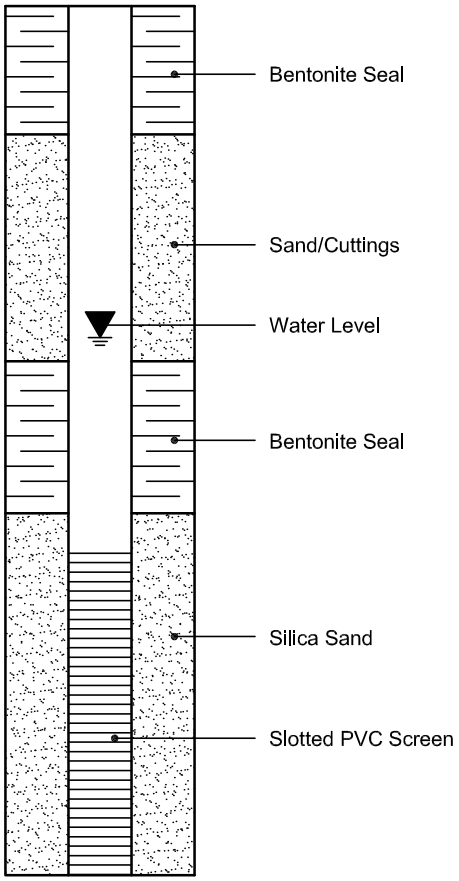

PIEZOMETER CONSTRUCTION

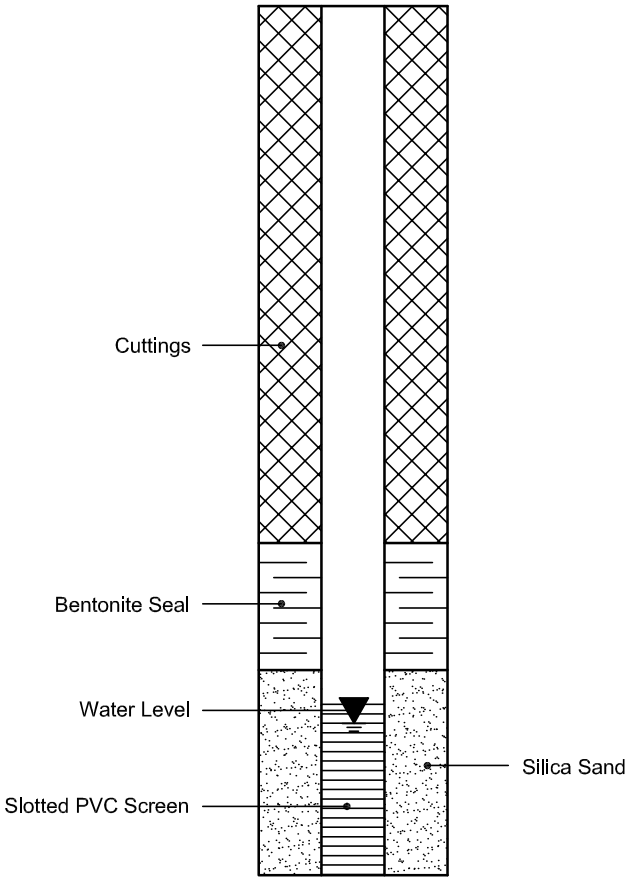

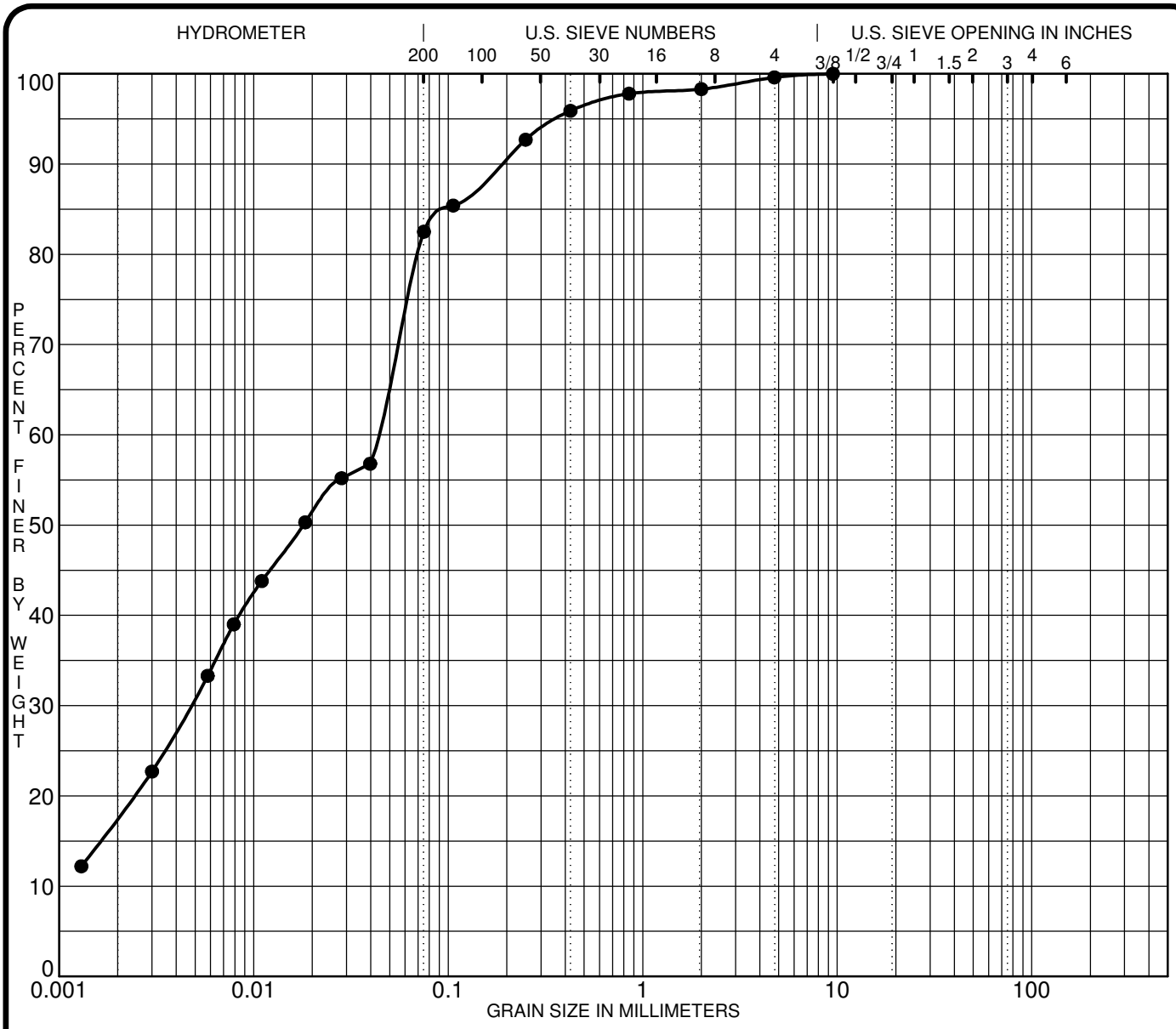

CLAY	SILT	SAND			GRAVEL		COBBLES
		fine	medium	coarse	fine	coarse	

Specimen Identification	Classification	MC%	LL	PL	PI	Cc	Cu
● **BH 3-22 SS3**		**30.1**					
⊠							
▲							
★							

Specimen Identification	D100	D60	D30	D10	%Gravel	%Sand	%Silt	%Clay
● **BH 3-22 SS3**	**9.50**	**0.04**	**0.005**		**0.4**	**17.1**	**64.0**	**18.5**
⊠								
▲								
★								

CLIENT **Ark Construction** FILE NO. **PG6160**

PROJECT **Geotechnical Investigation - Proposed Development** DATE **1 Mar 22**

patersongroup Consulting Engineers
154 Colonnade Road South, Ottawa, Ontario K2E 7J5

GRAIN SIZE DISTRIBUTION

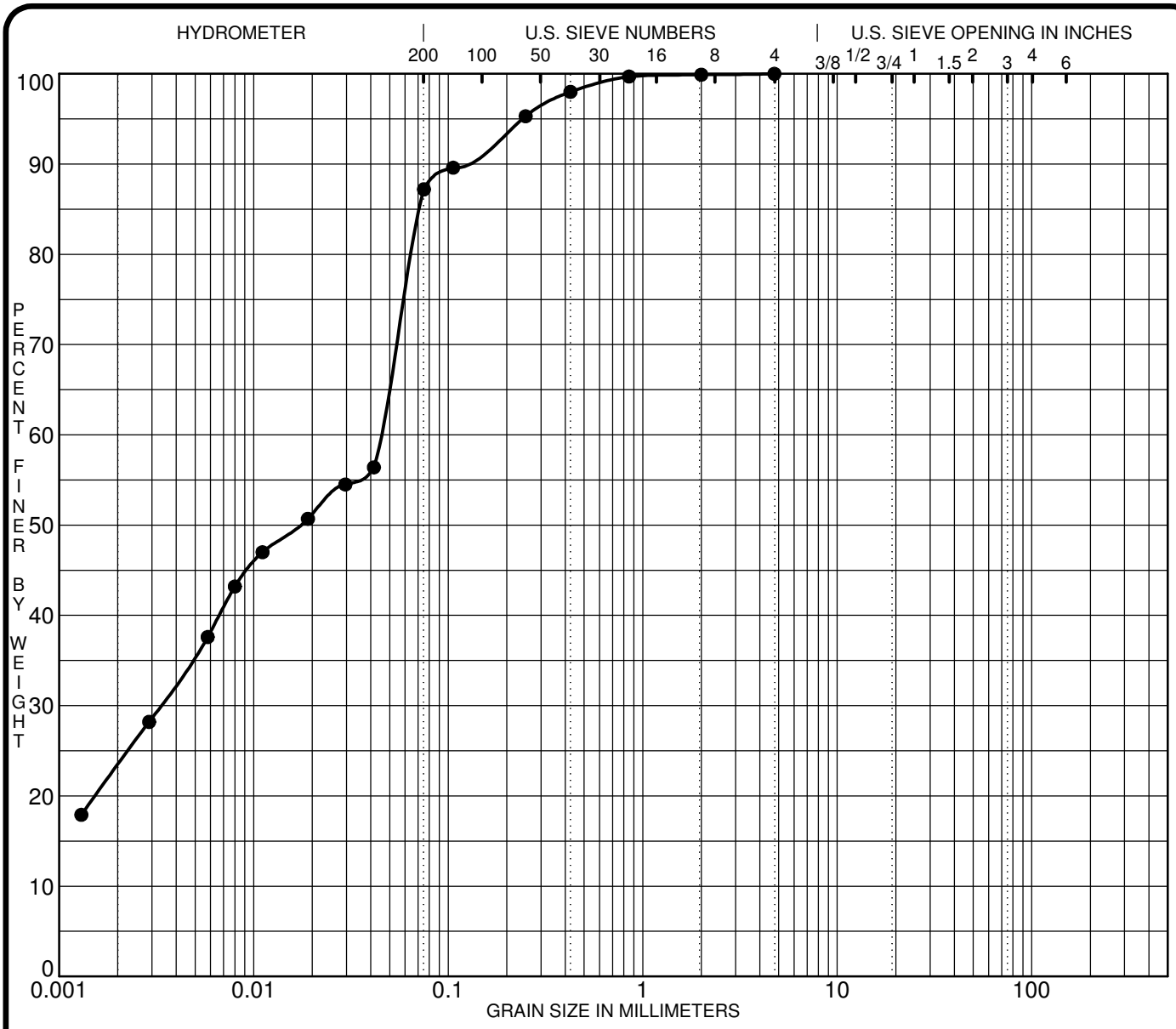

CLAY	SILT	SAND			GRAVEL		COBBLES
		fine	medium	coarse	fine	coarse	

	Specimen Identification	Classification	MC%	LL	PL	PI	Cc	Cu
●	**BH 4-22 SS3**		**33.6**					
⊠								
▲								
★								

	Specimen Identification	D100	D60	D30	D10	%Gravel	%Sand	%Silt	%Clay
●	**BH 4-22 SS3**	**4.75**	**0.04**	**0.003**		**0.0**	**12.8**	**64.2**	**23.0**
⊠									
▲									
★									

CLIENT **Ark Construction** FILE NO. **PG6160**

PROJECT **Geotechnical Investigation - Proposed Development** DATE **1 Mar 22**

patersongroup Consulting Engineers
154 Colonnade Road South, Ottawa, Ontario K2E 7J5

GRAIN SIZE DISTRIBUTION

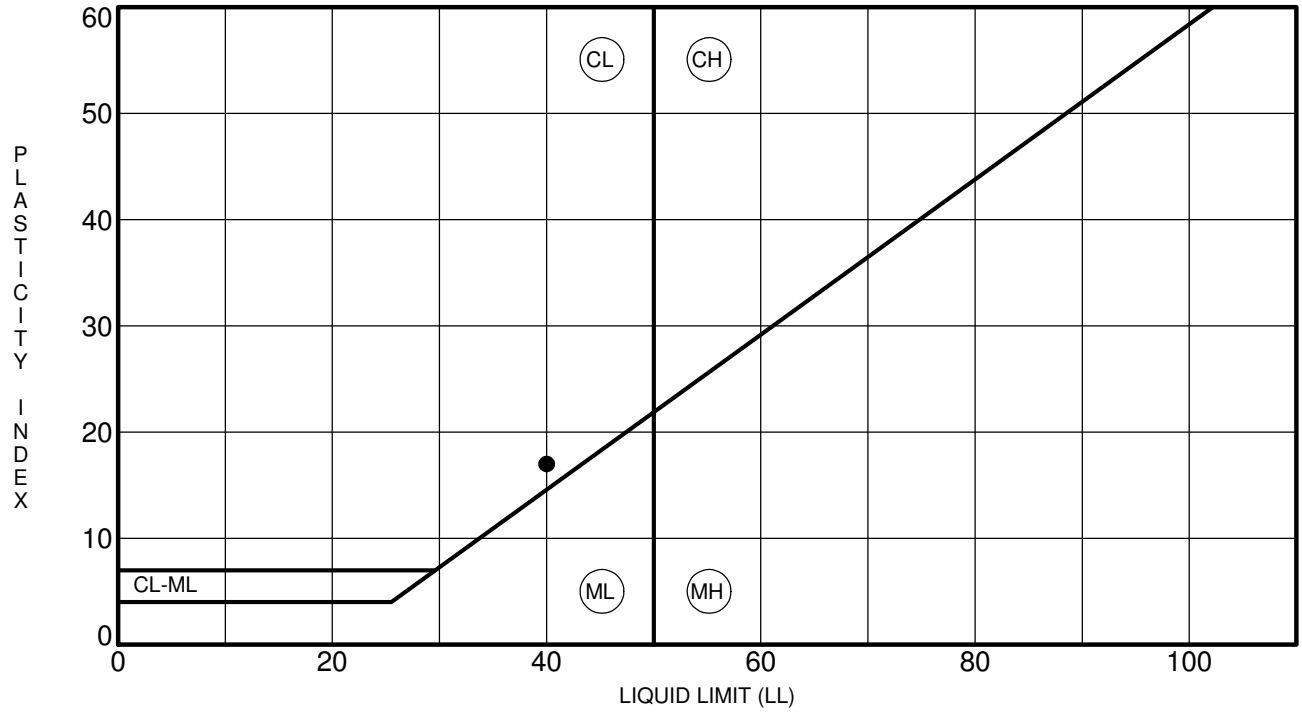

	Specimen Identification	LL	PL	PI	Fines	Classification
●	**BH 4-22 SS4**	**40**	**23**	**17**		**CL = Inorganic Clays of Low Plasticity**

CLIENT	**Ark Construction**	FILE NO.	**PG6160**
PROJECT	**Geotechnical Investigation - Proposed Development**	DATE	**1 Mar 22**

patersongroup Consulting Engineers
154 Colonnade Road South, Ottawa, Ontario K2E 7J5

ATTERBERG LIMITS' RESULTS

Certificate of Analysis

Report Date: 04-Mar-2022

Client: Paterson Group Consulting Engineers

Order Date: 2-Mar-2022

Client PO: 33999

Project Description: PG6160

	Client ID:	BH4-22 (SS2)	-	-	-
	Sample Date:	01-Mar-22 09:00	-	-	-
	Sample ID:	2210363-01	-	-	-
	MDL/Units	Soil	-	-	-
Physical Characteristics					
% Solids	0.1 % by Wt.	69.7	-	-	-
General Inorganics					
pH	0.05 pH Units	7.43	-	-	-
Resistivity	0.10 Ohm.m	83.4	-	-	-
Anions					
Chloride	5 ug/g dry	11	-	-	-
Sulphate	5 ug/g dry	<5	-	-	-

APPENDIX 2

FIGURE 1 – KEY PLAN

FIGURES 2 & 3 – SLOPE STABILITY ANALYSIS CROSS-SECTIONS

FIGURES 4 TO 9 – GLOBAL STABILITY ANALYSIS CROSS-SECTIONS

DRAWING PG6160-1 – TEST HOLE LOCATION PLAN

FIGURE 1

KEY PLAN

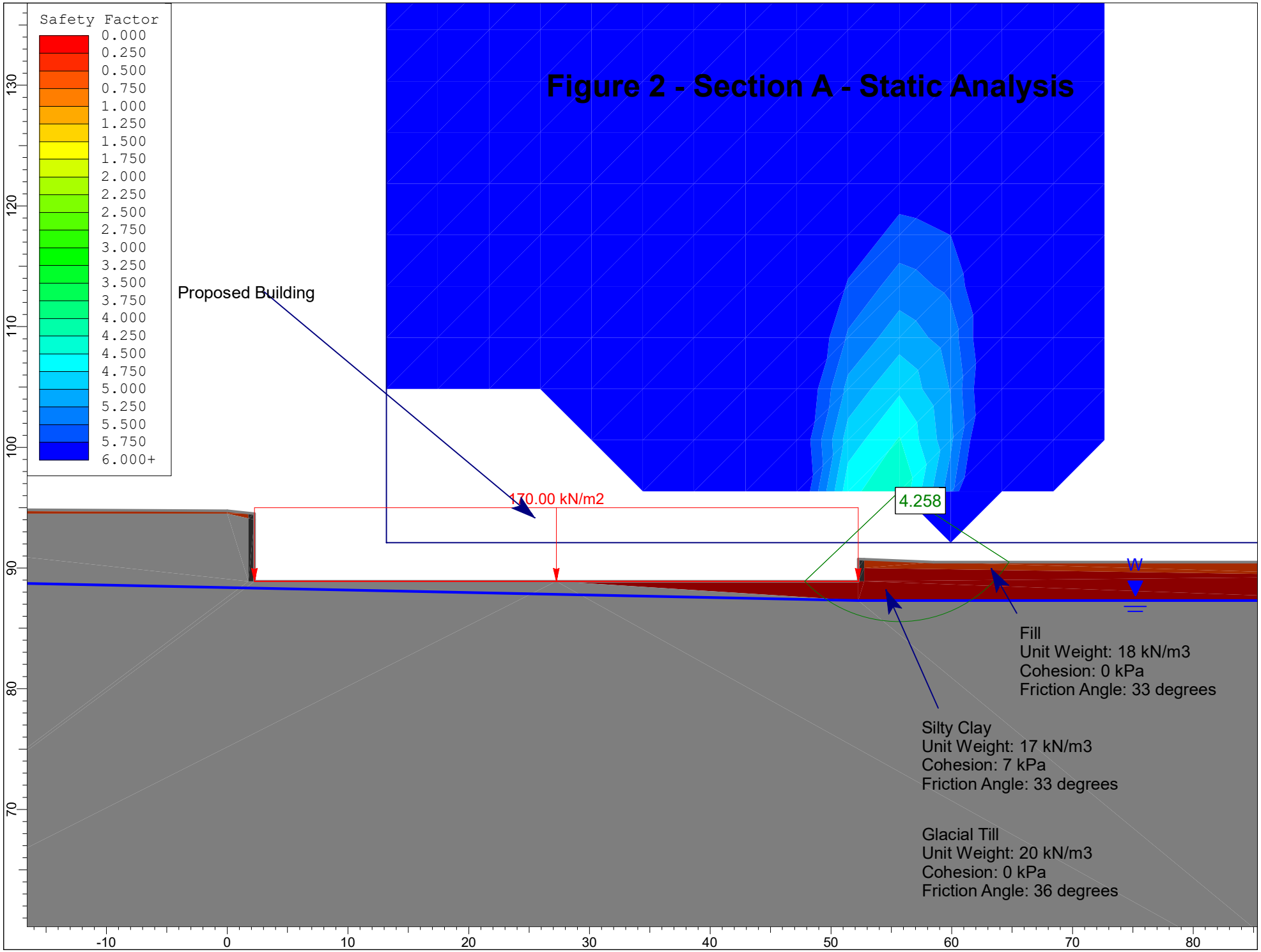
Figure 2 - Section A - Static Analysis
Safety Factor
0.000
0.250
0.500
0.750
1.000
1.250
1.500
1.750
2.000
2.250
2.500
2.750
3.000
3.250
3.500
3.750
4.000
4.250
4.500
4.750
5.000
5.250
5.500
5.750
6.000+
Proposed Building
170.00 kN/m2
4.258
W
Fill
Unit Weight: 18 kN/m3
Cohesion: 0 kPa
Friction Angle: 33 degrees
Silty Clay
Unit Weight: 17 kN/m3
Cohesion: 7 kPa
Friction Angle: 33 degrees
Glacial Till
Unit Weight: 20 kN/m3
Cohesion: 0 kPa
Friction Angle: 36 degrees
130
120
110
100
90
80
70
-10
0
10
20
30
40
50
60
70
80

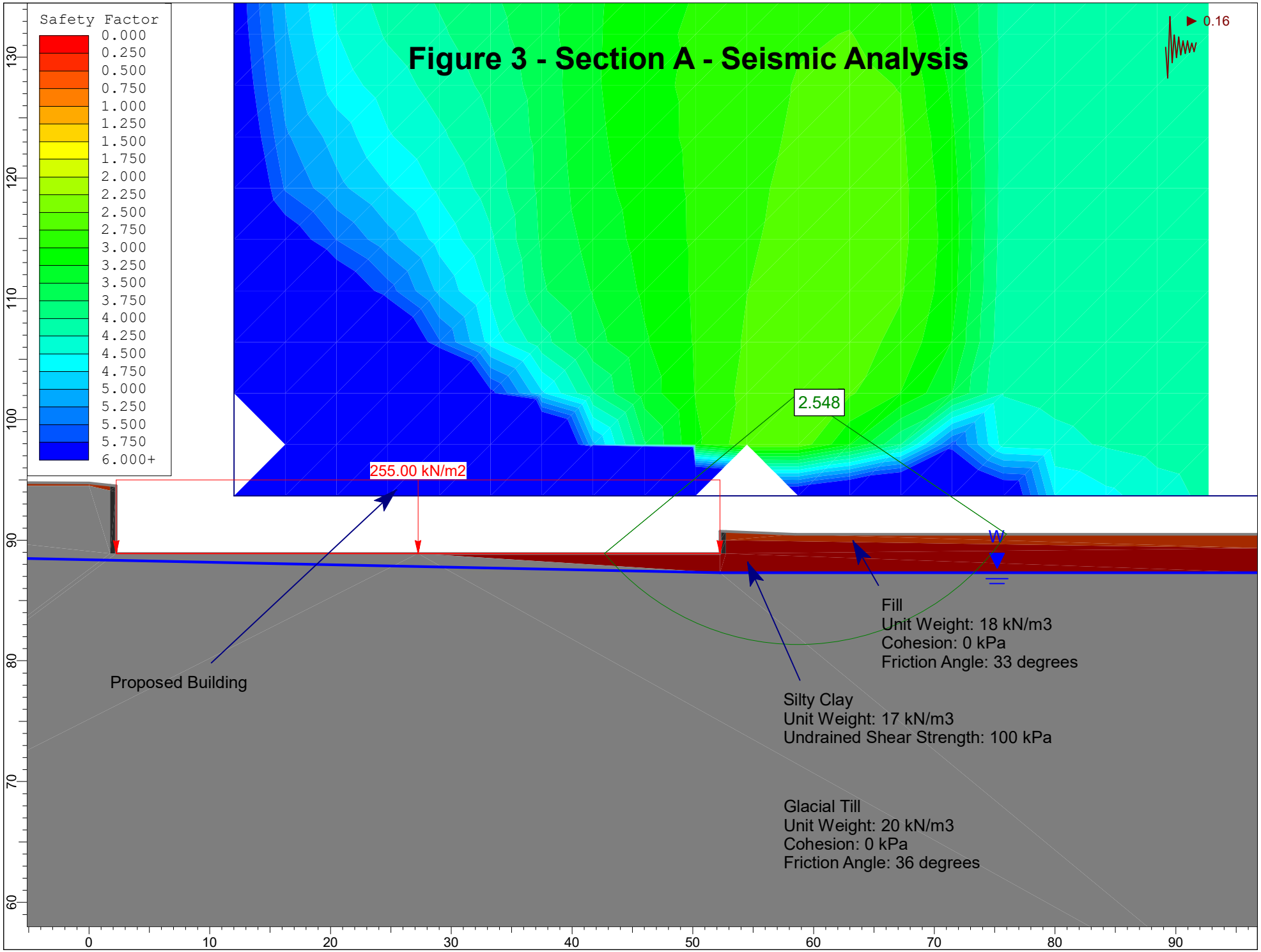
Figure 3 - Section A - Seismic Analysis
Safety Factor
0.000
0.250
0.500
0.750
1.000
1.250
1.500
1.750
2.000
2.250
2.500
2.750
3.000
3.250
3.500
3.750
4.000
4.250
4.500
4.750
5.000
5.250
5.500
5.750
6.000+
0.16
2.548
255.00 kN/m2
W
Fill
Unit Weight: 18 kN/m3
Cohesion: 0 kPa
Friction Angle: 33 degrees
Proposed Building
Silty Clay
Unit Weight: 17 kN/m3
Undrained Shear Strength: 100 kPa
Glacial Till
Unit Weight: 20 kN/m3
Cohesion: 0 kPa
Friction Angle: 36 degrees
130
120
110
100
90
80
70
60
0
10
20
30
40
50
60
70
80
90

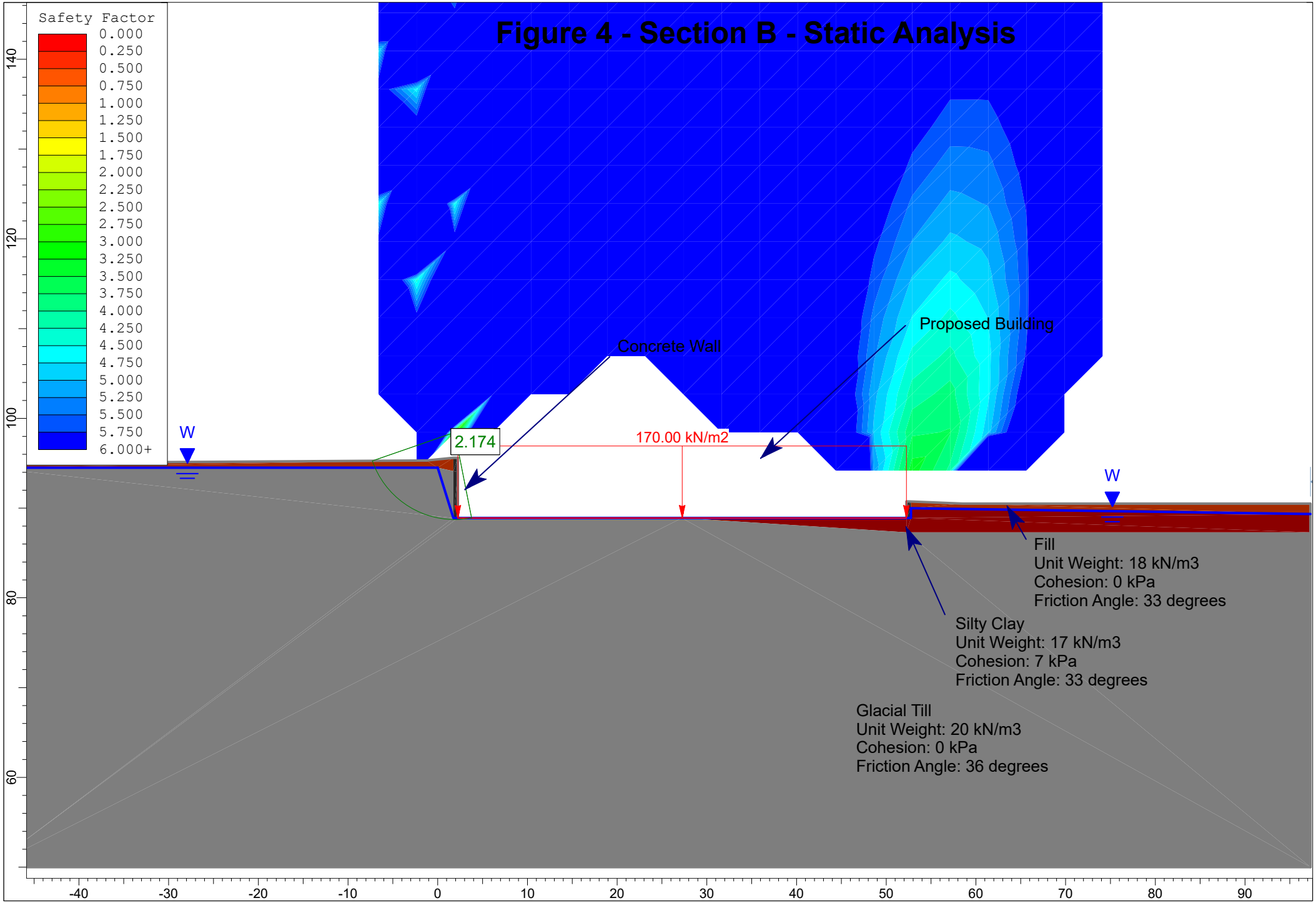
Figure 4 - Section B - Static Analysis
Safety Factor
0.000
0.250
0.500
0.750
1.000
1.250
1.500
1.750
2.000
2.250
2.500
2.750
3.000
3.250
3.500
3.750
4.000
4.250
4.500
4.750
5.000
5.250
5.500
5.750
6.000+
Concrete Wall
Proposed Building
W
2.174
170.00 kN/m2
W
Fill
Unit Weight: 18 kN/m3
Cohesion: 0 kPa
Friction Angle: 33 degrees
Silty Clay
Unit Weight: 17 kN/m3
Cohesion: 7 kPa
Friction Angle: 33 degrees
Glacial Till
Unit Weight: 20 kN/m3
Cohesion: 0 kPa
Friction Angle: 36 degrees
140
120
100
80
60
-40
-30
-20
-10
0
10
20
30
40
50
60
70
80
90

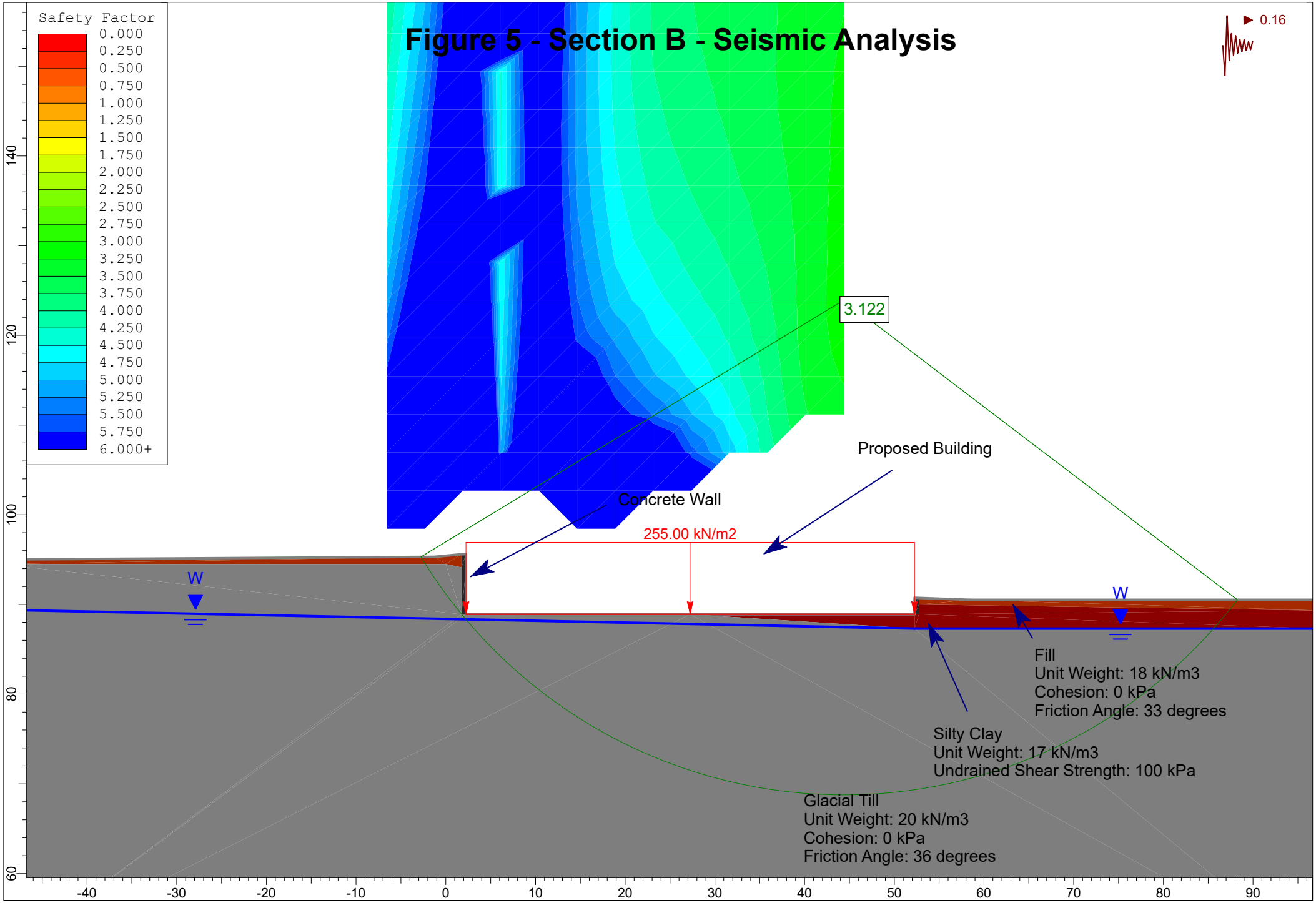
Figure 5 - Section B - Seismic Analysis
Safety Factor
0.000
0.250
0.500
0.750
1.000
1.250
1.500
1.750
2.000
2.250
2.500
2.750
3.000
3.250
3.500
3.750
4.000
4.250
4.500
4.750
5.000
5.250
5.500
5.750
6.000+
0.16
3.122
Proposed Building
Concrete Wall
255.00 kN/m2
W
W
Fill
Unit Weight: 18 kN/m3
Cohesion: 0 kPa
Friction Angle: 33 degrees
Silty Clay
Unit Weight: 17 kN/m3
Undrained Shear Strength: 100 kPa
Glacial Till
Unit Weight: 20 kN/m3
Cohesion: 0 kPa
Friction Angle: 36 degrees
140
120
100
80
60
-40
-30
-20
-10
0
10
20
30
40
50
60
70
80
90

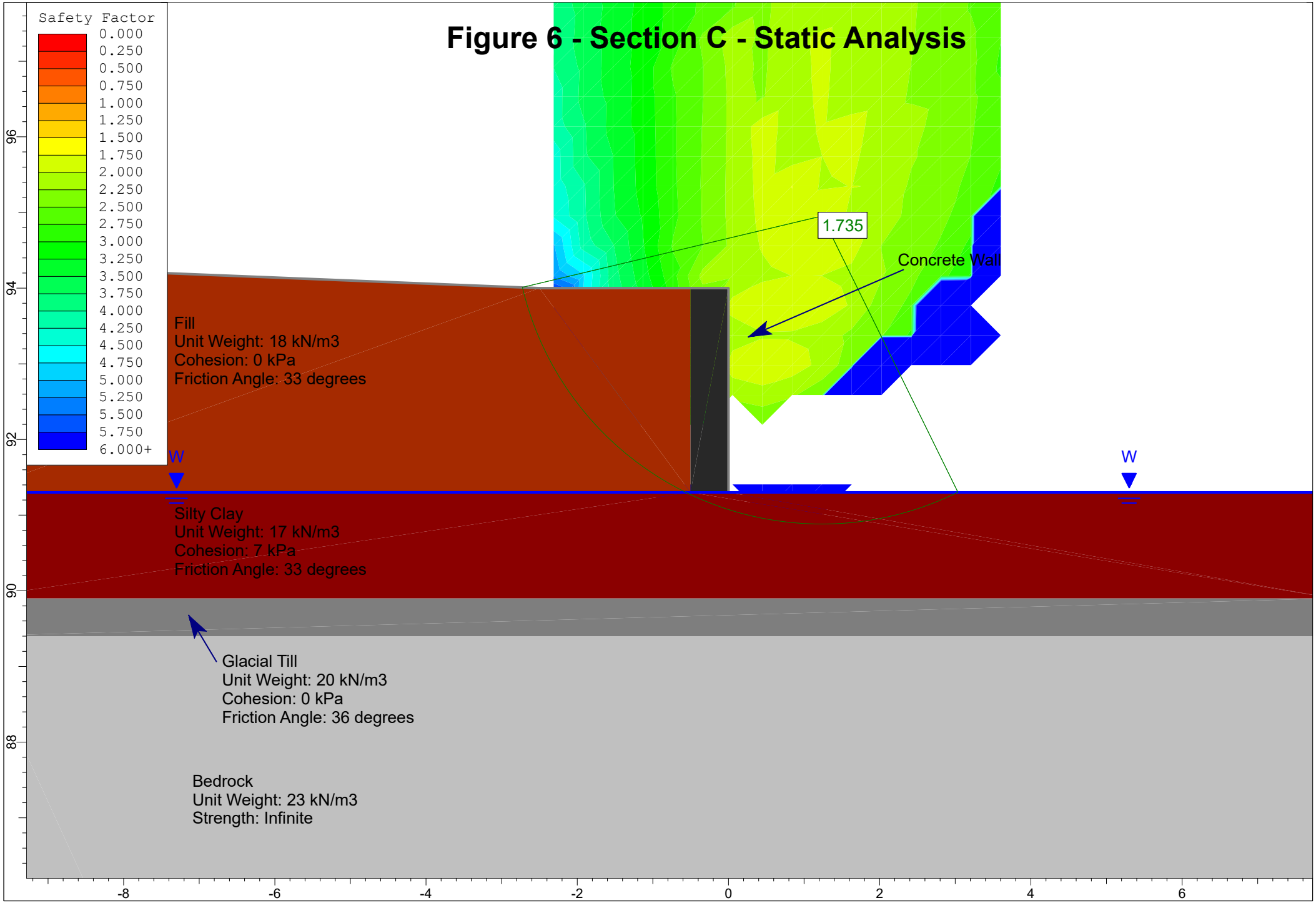
Figure 6 - Section C - Static Analysis
Safety Factor
0.000
0.250
0.500
0.750
1.000
1.250
1.500
1.750
2.000
2.250
2.500
2.750
3.000
3.250
3.500
3.750
4.000
4.250
4.500
4.750
5.000
5.250
5.500
5.750
6.000+
1.735
Concrete Wall
Fill
Unit Weight: 18 kN/m3
Cohesion: 0 kPa
Friction Angle: 33 degrees
W
W
Silty Clay
Unit Weight: 17 kN/m3
Cohesion: 7 kPa
Friction Angle: 33 degrees
Glacial Till
Unit Weight: 20 kN/m3
Cohesion: 0 kPa
Friction Angle: 36 degrees
Bedrock
Unit Weight: 23 kN/m3
Strength: Infinite
96
94
92
90
88
-8
-6
-4
-2
0
2
4
6

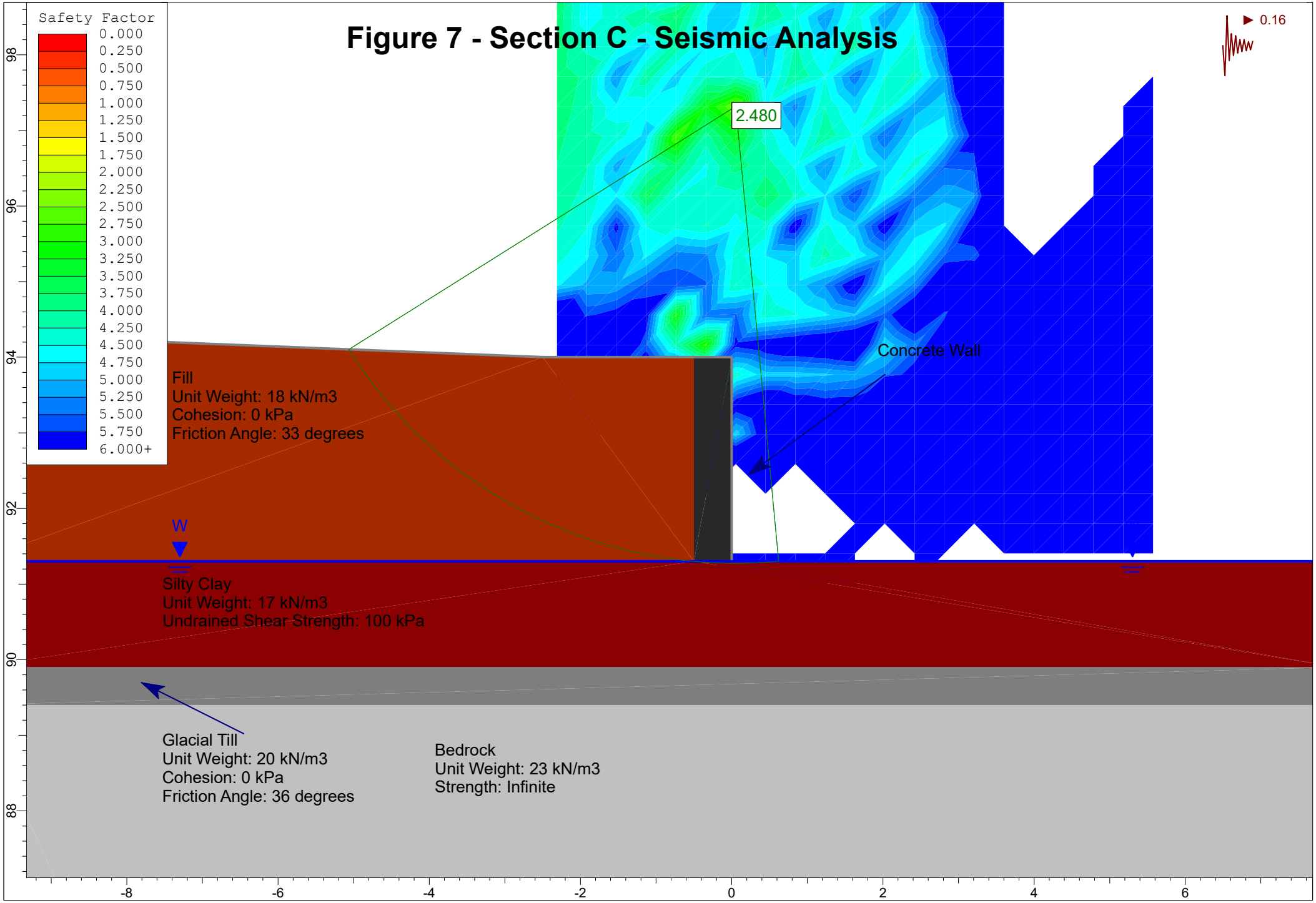
Figure 7 - Section C - Seismic Analysis
Safety Factor
0.000
0.250
0.500
0.750
1.000
1.250
1.500
1.750
2.000
2.250
2.500
2.750
3.000
3.250
3.500
3.750
4.000
4.250
4.500
4.750
5.000
5.250
5.500
5.750
6.000+
0.16
2.480
Concrete Wall
Fill
Unit Weight: 18 kN/m3
Cohesion: 0 kPa
Friction Angle: 33 degrees
W
Silty Clay
Unit Weight: 17 kN/m3
Undrained Shear Strength: 100 kPa
Glacial Till
Unit Weight: 20 kN/m3
Cohesion: 0 kPa
Friction Angle: 36 degrees
Bedrock
Unit Weight: 23 kN/m3
Strength: Infinite
98
96
94
92
90
88
-8
-6
-4
-2
0
2
4
6

Figure 8 - Section D - Static Analysis

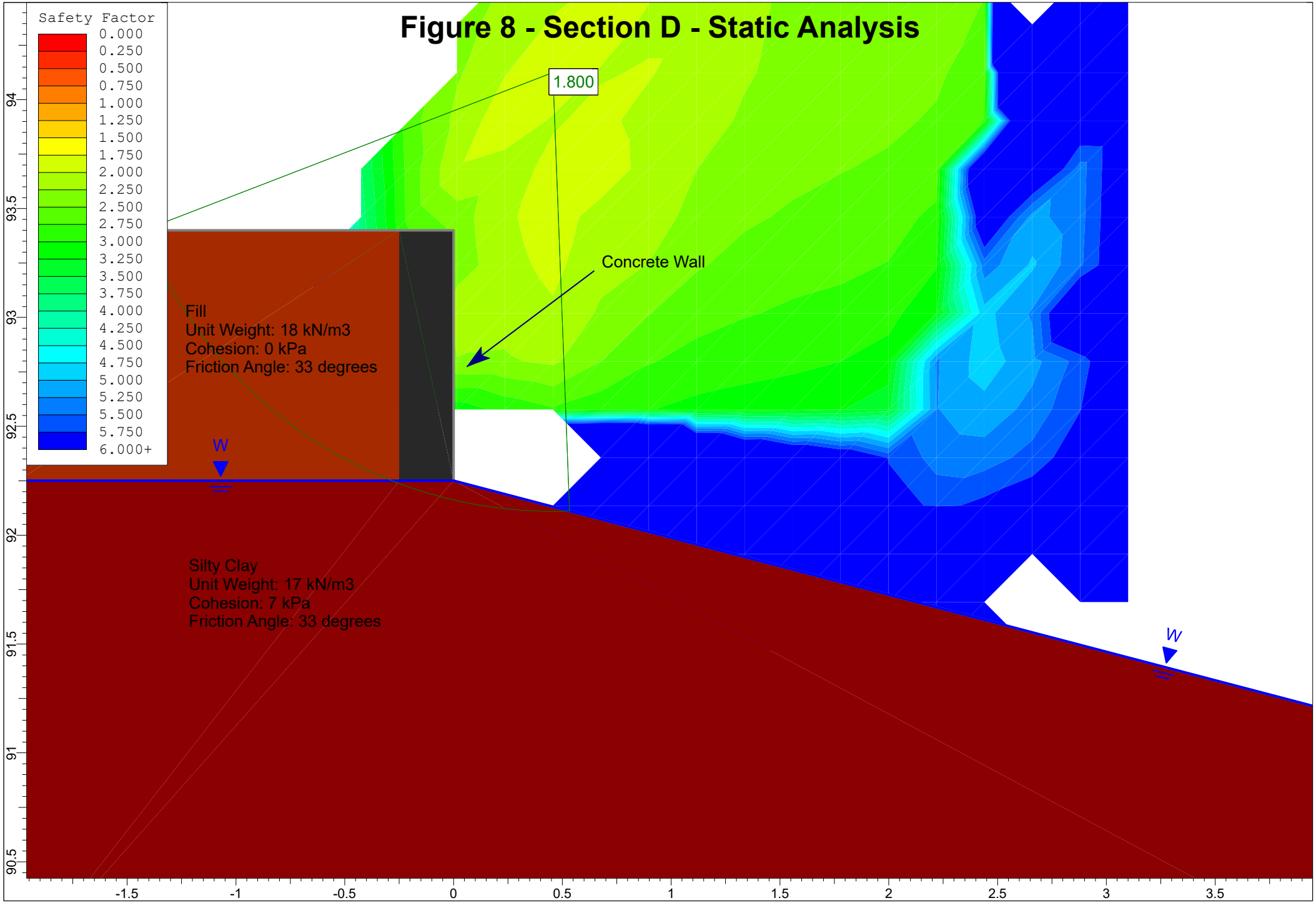

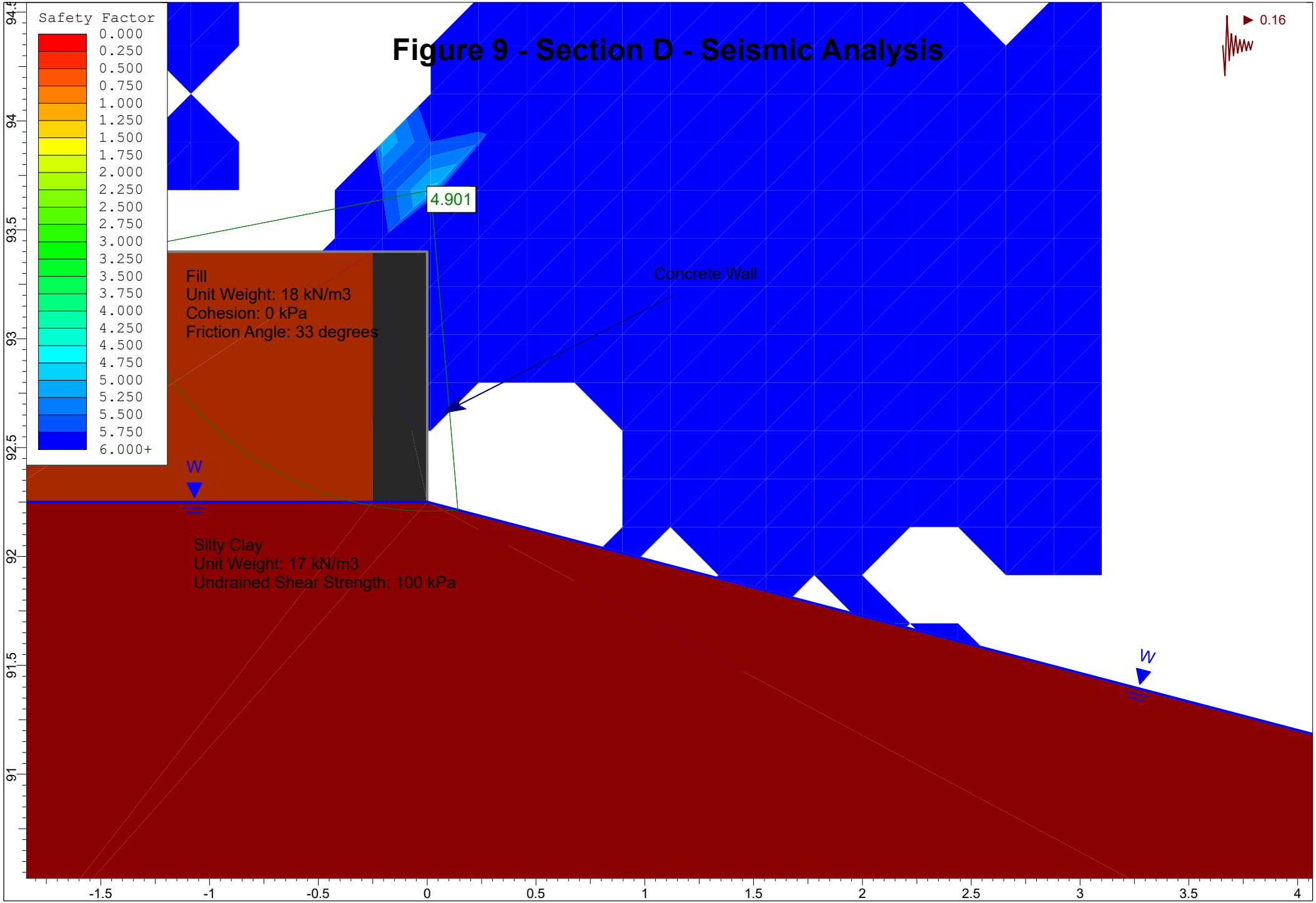
Figure 9 - Section D - Seismic Analysis
Safety Factor
0.000
0.250
0.500
0.750
1.000
1.250
1.500
1.750
2.000
2.250
2.500
2.750
3.000
3.250
3.500
3.750
4.000
4.250
4.500
4.750
5.000
5.250
5.500
5.750
6.000+
0.16
4.901
Concrete Wall
Fill
Unit Weight: 18 kN/m3
Cohesion: 0 kPa
Friction Angle: 33 degrees
W
Silty Clay
Unit Weight: 17 kN/m3
Undrained Shear Strength: 100 kPa
W
94.5
94
93.5
93
92.5
92
91.5
91
-1.5
-1
-0.5
0
0.5
1
1.5
2
2.5
3
3.5
4

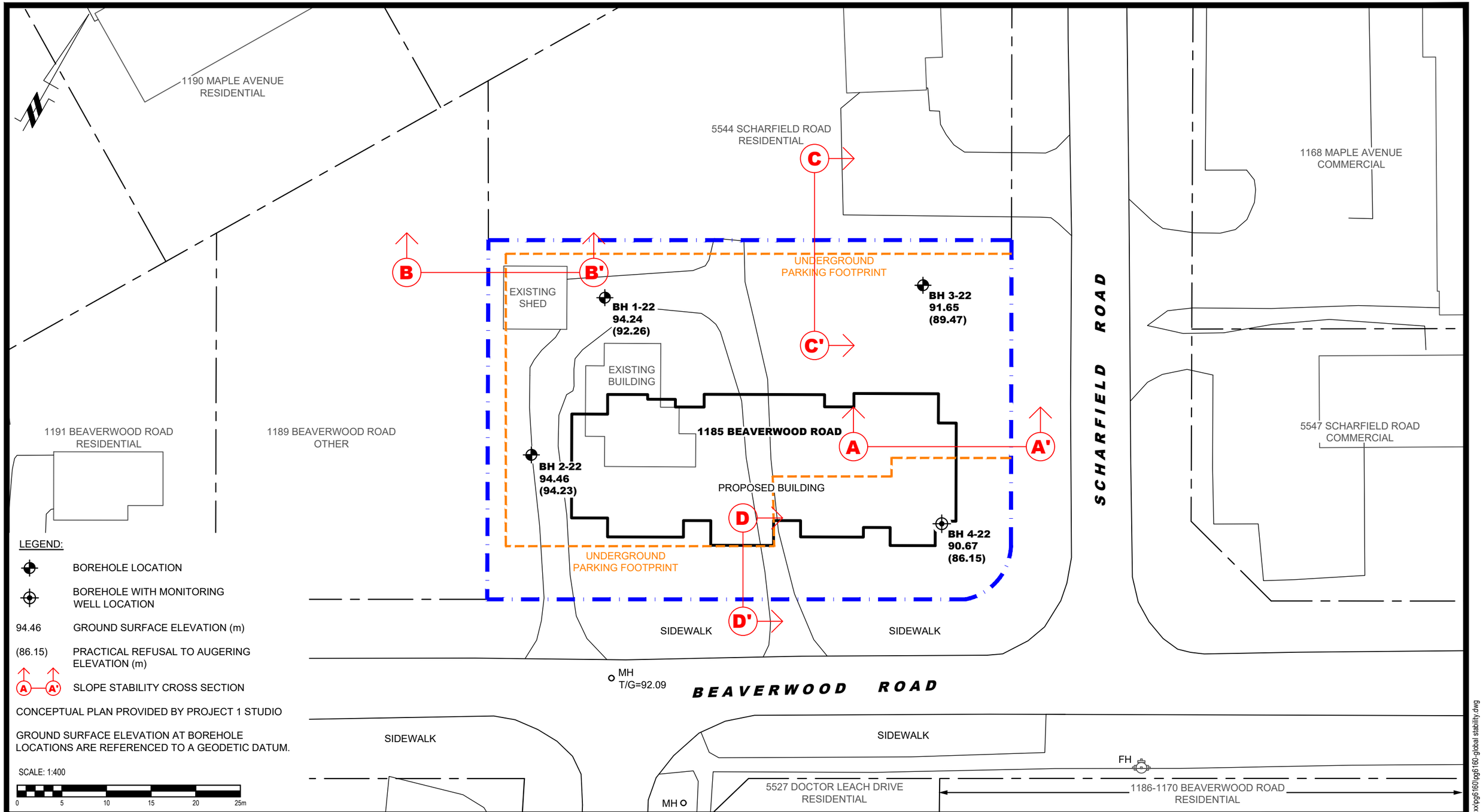

LEGEND:

- BOREHOLE LOCATION
- BOREHOLE WITH MONITORING WELL LOCATION
- 94.46 GROUND SURFACE ELEVATION (m)
- (86.15) PRACTICAL REFUSAL TO AUGERING ELEVATION (m)
- A A' SLOPE STABILITY CROSS SECTION

CONCEPTUAL PLAN PROVIDED BY PROJECT 1 STUDIO

GROUND SURFACE ELEVATION AT BOREHOLE LOCATIONS ARE REFERENCED TO A GEODETIC DATUM.

SCALE: 1:400

0 5 10 15 20 25m

patersongroup
consulting engineers

154 Colonnade Road South
Ottawa, Ontario K2E 7J5
Tel: (613) 226-7381 Fax: (613) 226-6344

NO.	REVISIONS	DATE	INITIAL

ARK CONSTRUCTION

GEOTECHNICAL INVESTIGATION
PROPOSED DEVELOPMENT
1185 BEAVERWOOD ROAD

OTTAWA, ONTARIO

Title:

TEST HOLE LOCATION PLAN

Scale: 1:400	Date: 09/2022
Drawn by: NFRV	Report No.: PG6160-1
Checked by: OM	Dwg. No.: PG6160-1
Approved by: SD	Revision No.:

p:\autocad drawings\geotechnical\pg61xx\pg6160\pg6160-global stability.dwg

APPENDIX 3

LIQUEFACTION RESISTANCE OF SOILS
BY YOUD ET AL. (2001)

EVALUATING THE POTENTIAL FOR LIQUEFACTION OR CYCLIC FAILURE
OF SILTS AND CLAYS
BY BOULANGER & IDRISS (2004)

Preface

Evaluation of soil liquefaction resistance is an important aspect of geotechnical engineering practice. To update and enhance criteria that are routinely applied in practice, workshops were convened in 1996 and 1998 to gain consensus from 20 experts on updates and augmentations that should be made to standard procedures that have evolved over the past 30 years. At the outset, the goal was to develop this state-of-the-art summary of consensus recommendations. A commitment was also made to those who participated in the workshops that all would be listed as co-authors. Unfortunately, the previous publication of this summary paper (April 2001) listed only the co-chairs of the workshop, Profs. Youd and Idriss, as authors; the remaining workshop participants were acknowledged in a footnote. In order to correct this error and to fully acknowledge and credit those who significantly contributed to the work, this paper is being republished in its entirety, at the request of the journal's editors, with all the participants named as co-authors. All further reference to this paper should be to this republication. The previous publication should no longer be cited. Also, several minor errors are corrected in this republication.

Liquefaction Resistance of Soils: Summary Report from the 1996 NCEER and 1998 NCEER/NSF Workshops on Evaluation of Liquefaction Resistance of Soils[a]

By T. L. Youd,[1] Chair, Member, ASCE, I. M. Idriss,[2] Co-Chair, Fellow, ASCE, Ronald D. Andrus,[3] Ignacio Arango,[4] Gonzalo Castro,[5] John T. Christian,[6] Richardo Dobry,[7] W. D. Liam Finn,[8] Leslie F. Harder Jr.,[9] Mary Ellen Hynes,[10] Kenji Ishihara,[11] Joseph P. Koester,[12] Sam S. C. Liao,[13] William F. Marcuson III,[14] Geoffrey R. Martin,[15] James K. Mitchell,[16] Yoshiharu Moriwaki,[17] Maurice S. Power,[18] Peter K. Robertson,[19] Raymond B. Seed,[20] and Kenneth H. Stokoe II[21]

Abstract: Following disastrous earthquakes in Alaska and in Niigata, Japan in 1964, Professors H. B. Seed and I. M. Idriss developed and published a methodology termed the "simplified procedure" for evaluating liquefaction resistance of soils. This procedure has become a standard of practice throughout North America and much of the world. The methodology which is largely empirical, has evolved over years, primarily through summary papers by H. B. Seed and his colleagues. No general review or update of the procedure has occurred, however, since 1985, the time of the last major paper by Professor Seed and a report from a National Research Council workshop on liquefaction of soils. In 1996 a workshop sponsored by the National Center for Earthquake Engineering Research (NCEER) was convened by Professors T. L. Youd and I. M. Idriss with 20 experts to review developments over the previous 10 years. The purpose was to gain consensus on updates and augmentations to the simplified procedure. The following topics were reviewed and recommendations developed: (1) criteria based on standard penetration tests; (2) criteria based on cone penetration tests; (3) criteria based on shear-wave velocity measurements; (4) use of the Becker penetration test for gravelly soil; (4) magnitude scaling factors; (5) correction factors for overburden pressures and sloping ground; and (6) input values for earthquake magnitude and peak acceleration. Probabilistic and seismic energy analyses were reviewed but no recommendations were formulated.

[a]This Summary Report, originally published in April 2001, is being republished so that the contribution of all workshop participants as authors can be officially recognized. The original version listed only two authors, plus a list of 19 workshop participants. This was incorrect; all 21 individuals should have been identified as authors. ASCE deeply regrets the error.

[1]Prof., Brigham Young Univ., Provo, UT 84602.
[2]Prof., Univ. of California at Davis, Davis, CA 95616.
[3]Prof., Clemson Univ., Clemson, SC 29634-0911; formerly, Nat. Inst. of Standards and Technol., Gaithersburg, MD.
[4]Bechtel Corp., San Francisco, CA 94119-3965.
[5]PhD, GEI Consultants, Inc., Winchester, MA 01890.
[6]PhD, Engrg. Consultant, Waban, MA 02468-1103.
[7]Prof., Rensselaer Polytechnic Inst., Troy, NY 12180.
[8]Prof., Univ. of British Columbia, Vancouver, BC, Canada.
[9]California Dept. of Water Resour., Sacramento, CA 94236-0001.
[10]U.S. Army Engr. Wtrwy. Experiment Station, Vicksburg, MS 39180.
[11]Prof., Sci. Univ. of Tokyo, Tokyo, Japan.
[12]U.S. Army Engr. Wtrwy. Experiment Station, Vicksburg, MS 39180.
[13]Parsons Brinckerhoff, Boston, MA 02116.
[14]PhD, U.S. Army Engr. Wtrwy. Experiment Station, Vicksburg, MS 39180.
[15]Prof., Univ. of Southern California, Los Angeles, CA 90089-2531.
[16]Prof., Virginia Polytechnic Inst., Blacksburg, VA 24061.
[17]PhD, Prin., Geomatrix Consultants, Santa Ana, CA 94612.
[18]Geomatrix Consultants, Oakland, CA 94612.
[19]Prof., Univ. of Alberta, Edmonton, Alberta, Canada.
[20]Prof., Univ. of California, Berkeley, CA 94720.
[21]Prof., Univ. of Texas at Austin, Austin, TX 78712.

Note. Discussion open until March 1, 2002. To extend the closing date one month, a written request must be filed with the ASCE Manager of Journals. The manuscript for this paper was submitted for review and possible publication on January 18, 2000; revised November 14, 2000. This paper is part of the *Journal of Geotechnical and Geoenvironmental Engineering*, Vol. 127, No. 10, October, 2001. ©ASCE, ISSN 1090-0241/01/0010-0817–0833/$8.00 + $.50 per page. Paper No. 22223.

INTRODUCTION

Over the past 25 years a methodology termed the "simplified procedure" has evolved as a standard of practice for evaluating the liquefaction resistance of soils. Following disastrous earthquakes in Alaska and in Niigata, Japan in 1964, Seed and Idriss (1971) developed and published the basic "simplified procedure." That procedure has been modified and improved periodically since that time, primarily through landmark papers by Seed (1979), Seed and Idriss (1982), and Seed et al. (1985). In 1985, Professor Robert V. Whitman convened a workshop on behalf of the National Research Council (NRC) in which 36 experts and observers thoroughly reviewed the state-of-knowledge and the state-of-the-art for assessing liquefaction hazard. That workshop produced a report (NRC 1985) that has become a widely used standard and reference for liquefaction hazard assessment. In January 1996, T. L. Youd and I. M. Idriss convened a workshop of 20 experts to update the simplified procedure and incorporate research findings from the previous decade. This paper summarizes recommendations from that workshop (Youd and Idriss 1997).

To keep the workshop focused, the scope of the workshop was limited to procedures for evaluating liquefaction resistance of soils under level to gently sloping ground. In this context, liquefaction refers to the phenomena of seismic generation of large pore-water pressures and consequent softening of granular soils. Important postliquefaction phenomena, such as residual shear strength, soil deformation, and ground failure, were beyond the scope of the workshop.

The simplified procedure was developed from empirical evaluations of field observations and field and laboratory test data. Field evidence of liquefaction generally consisted of surficial observations of sand boils, ground fissures, or lateral spreads. Data were collected mostly from sites on level to gently sloping terrain, underlain by Holocene alluvial or fluvial sediment at shallow depths (<15 m). The original procedure was verified for, and is applicable only to, these site conditions. Similar restrictions apply to the implementation of the updated procedures recommended in this report.

Liquefaction is defined as the transformation of a granular material from a solid to a liquefied state as a consequence of increased pore-water pressure and reduced effective stress (Marcuson 1978). Increased pore-water pressure is induced by the tendency of granular materials to compact when subjected to cyclic shear deformations. The change of state occurs most readily in loose to moderately dense granular soils with poor drainage, such as silty sands or sands and gravels capped by or containing seams of impermeable sediment. As liquefaction occurs, the soil stratum softens, allowing large cyclic deformations to occur. In loose materials, the softening is also accompanied by a loss of shear strength that may lead to large shear deformations or even flow failure under moderate to high shear stresses, such as beneath a foundation or sloping ground. In moderately dense to dense materials, liquefaction leads to transient softening and increased cyclic shear strains, but a tendency to dilate during shear inhibits major strength loss and large ground deformations. A condition of cyclic mobility or cyclic liquefaction may develop following liquefaction of moderately dense granular materials. Beneath gently sloping to flat ground, liquefaction may lead to ground oscillation or lateral spread as a consequence of either flow deformation or cyclic mobility. Loose soils also compact during liquefaction and reconsolidation, leading to ground settlement. Sand boils may also erupt as excess pore water pressures dissipate.

CYCLIC STRESS RATIO (CSR) AND CYCLIC RESISTANCE RATIO (CRR)

Calculation, or estimation, of two variables is required for evaluation of liquefaction resistance of soils: (1) the seismic demand on a soil layer, expressed in terms of CSR; and (2) the capacity of the soil to resist liquefaction, expressed in terms of CRR. The latter variable has been termed the cyclic stress ratio or the cyclic stress ratio required to generate liquefaction, and has been given different symbols by different writers. For example, Seed and Harder (1990) used the symbol CSRℓ, Youd (1993) used the symbol CSRL, and Kramer (1996) used the symbol CSR_L to denote this ratio. To reduce confusion and to better distinguish induced cyclic shear stresses from mobilized liquefaction resistance, the capacity of a soil to resist liquefaction is termed the CRR in this report. This term is recommended for engineering practice.

EVALUATION OF CSR

Seed and Idriss (1971) formulated the following equation for calculation of the cyclic stress ratio:

$$CSR = (\tau_{av}/\sigma'_{vo}) = 0.65(a_{max}/g)(\sigma_{vo}/\sigma'_{vo})r_d \quad (1)$$

where a_{max} = peak horizontal acceleration at the ground surface generated by the earthquake (discussed later); g = acceleration of gravity; σ_{vo} and σ'_{vo} are total and effective vertical overburden stresses, respectively; and r_d = stress reduction coefficient. The latter coefficient accounts for flexibility of the soil profile. The workshop participants recommend the following minor modification to the procedure for calculation of CSR.

For routine practice and noncritical projects, the following equations may be used to estimate average values of r_d (Liao and Whitman 1986b):

$$r_d = 1.0 - 0.00765z \quad \text{for } z \le 9.15 \text{ m} \quad (2a)$$

$$r_d = 1.174 - 0.0267z \quad \text{for } 9.15 \text{ m} < z \le 23 \text{ m} \quad (2b)$$

where z = depth below ground surface in meters. Some investigators have suggested additional equations for estimating r_d at greater depths (Robertson and Wride 1998), but evaluation of liquefaction at these greater depths is beyond the depths where the simplified procedure is verified and where routine applications should be applied. Mean values of r_d calculated from (2) are plotted in Fig. 1, along with the mean and range of values proposed by Seed and Idriss (1971). The workshop participants agreed that for convenience in programming spreadsheets and other electronic aids, and to be consistent with past practice, r_d values determined from (2) are suitable for use in routine engineering practice. The user should understand, however, that there is considerable variability in the

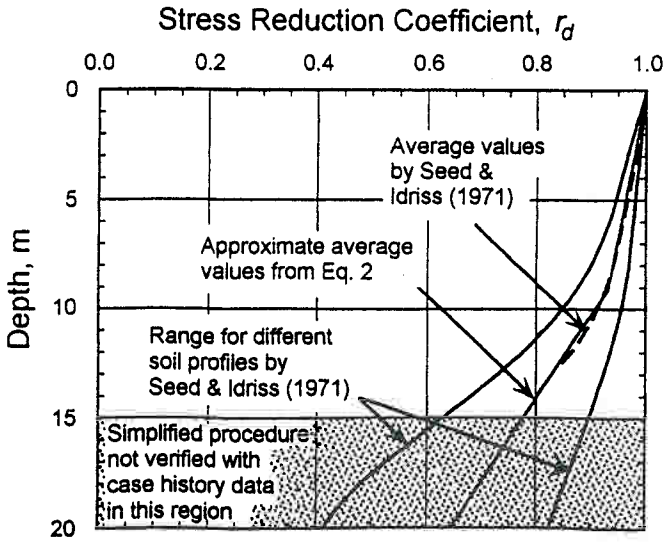

FIG. 1. r_d versus Depth Curves Developed by Seed and Idriss (1971) with Added Mean-Value Lines Plotted from Eq. (2)

flexibility and thus r_d at field sites, that r_d calculated from (2) are the mean of a wide range of possible r_d, and that the range of r_d increases with depth (Golesorkhi 1989).

For ease of computation, T. F. Blake (personal communication, 1996) approximated the mean curve plotted in Fig. 1 by the following equation:

$$r_d = \frac{(1.000 - 0.4113z^{0.5} + 0.04052z + 0.001753z^{1.5})}{(1.000 - 0.4177z^{0.5} + 0.05729z - 0.006205z^{1.5} + 0.001210z^2)} \quad (3)$$

where z = depth beneath ground surface in meters. Eq. (3) yields essentially the same values for r_d as (2), but is easier to program and may be used in routine engineering practice.

I. M. Idriss [Transportation Research Board (TRB) (1999)] suggested a new procedure for determining magnitude-dependent values of r_d. Application of these r_d require use of a corresponding set of magnitude scaling factors that are compatible with the new r_d. Because these r_d were developed after the workshop and have not been independently evaluated by other experts, the workshop participants chose not to recommend the new factors at this time.

EVALUATION OF LIQUEFACTION RESISTANCE (CRR)

A major focus of the workshop was on procedures for evaluating liquefaction resistance. A plausible method for evaluating CRR is to retrieve and test undisturbed soil specimens in the laboratory. Unfortunately, in situ stress states generally cannot be reestablished in the laboratory, and specimens of granular soils retrieved with typical drilling and sampling techniques are too disturbed to yield meaningful results. Only through specialized sampling techniques, such as ground freezing, can sufficiently undisturbed specimens be obtained. The cost of such procedures is generally prohibitive for all but the most critical projects. To avoid the difficulties associated with sampling and laboratory testing, field tests have become the state-of-practice for routine liquefaction investigations.

Several field tests have gained common usage for evaluation of liquefaction resistance, including the standard penetration test (SPT), the cone penetration test (CPT), shear-wave velocity measurements (V_s), and the Becker penetration test (BPT). These tests were discussed at the workshop, along with associated criteria for evaluating liquefaction resistance. The participants made a conscientious attempt to correlate liquefaction resistance criteria from each of the various field tests to provide generally consistent results, no matter which test is applied. SPTs and CPTs are generally preferred because of the more extensive databases and past experience, but the other tests may be applied at sites underlain by gravelly sediment or where access by large equipment is limited. Primary advantages and disadvantages of each test are listed in Table 1.

SPT

Criteria for evaluation of liquefaction resistance based on the SPT have been rather robust over the years. Those criteria are largely embodied in the CSR versus $(N_1)_{60}$ plot reproduced in Fig. 2. $(N_1)_{60}$ is the SPT blow count normalized to an overburden pressure of approximately 100 kPa (1 ton/sq ft) and a hammer energy ratio or hammer efficiency of 60%. The normalization factors for these corrections are discussed in the section entitled Other Corrections. Fig. 2 is a graph of calculated CSR and corresponding $(N_1)_{60}$ data from sites where liquefaction effects were or were not observed following past earthquakes with magnitudes of approximately 7.5. CRR curves on this graph were conservatively positioned to separate regions with data indicative of liquefaction from regions with data indicative of nonliquefaction. Curves were developed for granular soils with the fines contents of 5% or less, 15%, and 35% as shown on the plot. The CRR curve for fines contents <5% is the basic penetration criterion for the simplified procedure and is referred to hereafter as the "SPT clean-sand base curve." The CRR curves in Fig. 2 are valid only for magnitude 7.5 earthquakes. Scaling factors to adjust CRR curves to other magnitudes are addressed in a later section of this report.

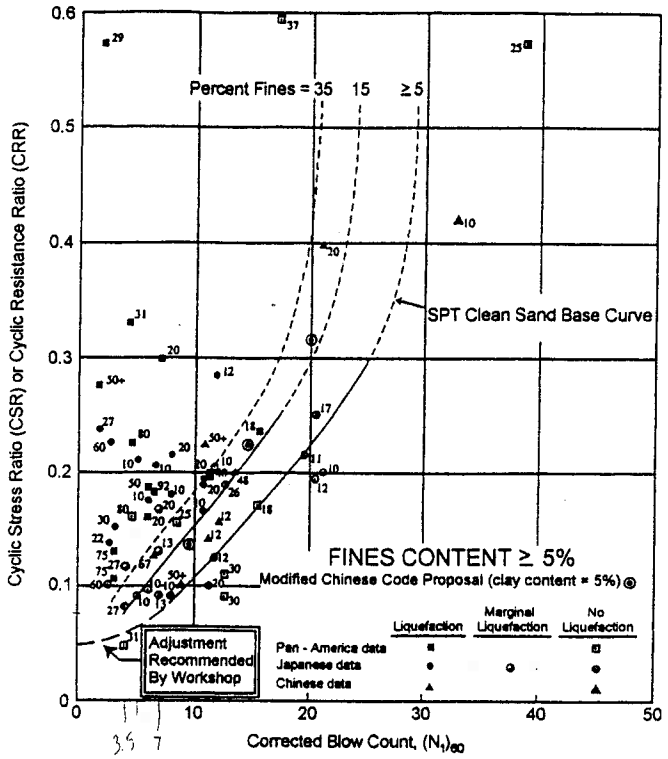

FIG. 2. SPT Clean-Sand Base Curve for Magnitude 7.5 Earthquakes with Data from Liquefaction Case Histories (Modified from Seed et al. 1985)

SPT Clean-Sand Base Curve

Several changes to the SPT criteria are recommended by the workshop participants. The first change is to curve the trajec-

TABLE 1. Comparison of Advantages and Disadvantages of Various Field Tests for Assessment of Liquefaction Resistance

Feature	Test Type			
	SPT	CPT	V_s	BPT
Past measurements at liquefaction sites	Abundant	Abundant	Limited	Sparse
Type of stress-strain behavior influencing test	Partially drained, large strain	Drained, large strain	Small strain	Partially drained, large strain
Quality control and repeatability	Poor to good	Very good	Good	Poor
Detection of variability of soil deposits	Good for closely spaced tests	Very good	Fair	Fair
Soil types in which test is recommended	Nongravel	Nongravel	All	Primarily gravel
Soil sample retrieved	Yes	No	No	No
Test measures index or engineering property	Index	Index	Engineering	Index

tory of the clean-sand base curve at low $(N_1)_{60}$ to a projected intercept of about 0.05 (Fig. 2). This adjustment reshapes the clean-sand base curve to achieve greater consistency with CRR curves developed for the CPT and shear-wave velocity procedures. Seed and Idriss (1982) projected the original curve through the origin, but there were few data to constrain the curve in the lower part of the plot. A better fit to the present empirical data is to bow the lower end of the base curve as indicated in Fig. 2.

At the University of Texas, A. F. Rauch (personal communication, 1998), approximated the clean-sand base curve plotted in Fig. 2 by the following equation:

$$CRR_{7.5} = \frac{1}{34 - (N_1)_{60}} + \frac{(N_1)_{60}}{135} + \frac{50}{[10 \cdot (N_1)_{60} + 45]^2} - \frac{1}{200} \quad (4)$$

This equation is valid for $(N_1)_{60} < 30$. For $(N_1)_{60} \geq 30$, clean granular soils are too dense to liquefy and are classed as nonliquefiable. This equation may be used in spreadsheets and other analytical techniques to approximate the clean-sand base curve for routine engineering calculations.

Influence of Fines Content

In the original development, Seed et al. (1985) noted an apparent increase of CRR with increased fines content. Whether this increase is caused by an increase of liquefaction resistance or a decrease of penetration resistance is not clear. Based on the empirical data available, Seed et al. developed CRR curves for various fines contents reproduced in Fig. 2. A revised correction for fines content was developed by workshop attendees to better fit the empirical database and to better support computations with spreadsheets and other electronic computational aids.

The workshop participants recommend (5) and (6) as approximate corrections for the influence of fines content (FC) on CRR. Other grain characteristics, such as soil plasticity, may affect liquefaction resistance as well as fines content, but widely accepted corrections for these factors have not been developed. Hence corrections based solely on fines content should be used with engineering judgment and caution. The following equations were developed by I. M. Idriss with the assistance of R. B. Seed for correction of $(N_1)_{60}$ to an equivalent clean sand value, $(N_1)_{60cs}$:

$$(N_1)_{60cs} = \alpha + \beta(N_1)_{60} \quad (5)$$

where α and β = coefficients determined from the following relationships:

$$\alpha = 0 \quad \text{for FC} \leq 5\% \quad (6a)$$

$$\alpha = \exp[1.76 - (190/FC^2)] \quad \text{for } 5\% < FC < 35\% \quad (6b)$$

$$\alpha = 5.0 \quad \text{for FC} \geq 35\% \quad (6c)$$

$$\beta = 1.0 \quad \text{for FC} \leq 5\% \quad (7a)$$

$$\beta = [0.99 + (FC^{1.5}/1{,}000)] \quad \text{for } 5\% < FC < 35\% \quad (7b)$$

$$\beta = 1.2 \quad \text{for FC} \geq 35\% \quad (7c)$$

These equations may be used for routine liquefaction resistance calculations. A back-calculated curve for a fines content of 35% is essentially congruent with the 35% curve plotted in Fig. 2. The back-calculated curve for a fines contents of 15% plots to the right of the original 15% curve.

Other Corrections

Several factors in addition to fines content and grain characteristics influence SPT results, as noted in Table 2. Eq. (8) incorporates these corrections

TABLE 2. Corrections to SPT (Modified from Skempton 1986) as Listed by Robertson and Wride (1998)

Factor	Equipment variable	Term	Correction
Overburden pressure	—	C_N	$(P_a/\sigma'_{vo})^{0.5}$
Overburden pressure	—	C_N	$C_N \leq 1.7$
Energy ratio	Donut hammer	C_E	0.5–1.0
Energy ratio	Safety hammer	C_E	0.7–1.2
Energy ratio	Automatic-trip Donut-type hammer	C_E	0.8–1.3
Borehole diameter	65–115 mm	C_B	1.0
Borehole diameter	150 mm	C_B	1.05
Borehole diameter	200 mm	C_B	1.15
Rod length	<3 m	C_R	0.75
Rod length	3–4 m	C_R	0.8
Rod length	4–6 m	C_R	0.85
Rod length	6–10 m	C_R	0.95
Rod length	10–30 m	C_R	1.0
Sampling method	Standard sampler	C_S	1.0
Sampling method	Sampler without liners	C_S	1.1–1.3

$$(N_1)_{60} = N_m C_N C_E C_B C_R C_S \quad (8)$$

where N_m = measured standard penetration resistance; C_N = factor to normalize N_m to a common reference effective overburden stress; C_E = correction for hammer energy ratio (ER); C_B = correction factor for borehole diameter; C_R = correction factor for rod length; and C_S = correction for samplers with or without liners.

Because SPT N-values increase with increasing effective overburden stress, an overburden stress correction factor is applied (Seed and Idriss 1982). This factor is commonly calculated from the following equation (Liao and Whitman 1986a):

$$C_N = (P_a/\sigma'_{vo})^{0.5} \quad (9)$$

where C_N normalizes N_m to an effective overburden pressure σ'_{vo} of approximately 100 kPa (1 atm) P_a. C_N should not exceed a value of 1.7 [A maximum value of 2.0 was published in the National Center for Earthquake Engineering Research (NCEER) workshop proceedings (Youd and Idriss 1997), but later was reduced to 1.7 by consensus of the workshop participants] Kayen et al. (1992) suggested the following equation, which limits the maximum C_N value to 1.7, and in these writers' opinion, provides a better fit to the original curve specified by Seed and Idriss (1982):

$$C_N = 2.2/(1.2 + \sigma'_{vo}/P_a) \quad (10)$$

Either equation may be used for routine engineering applications.

The effective overburden pressure σ'_{vo} applied in (9) and (10) should be the overburden pressure at the time of drilling and testing. Although a higher ground-water level might be used for conservatism in the liquefaction resistance calculations, the C_N factor must be based on the stresses present at the time of the testing.

The C_N correction factor was derived from SPT performed in test bins with large sand specimens subjected to various confining pressures (Gibbs and Holtz 1957; Marcuson and Bieganousky 1997a,b). The results of several of these tests are reproduced in Fig. 3 in the form of C_N curves versus effective overburden stress (Castro 1995). These curves indicate considerable scatter of results with no apparent correlation of C_N with soil type or gradation. The curves from looser sands, however, lie in the lower part of the C_N range and are reasonably approximated by (9) and (10) for low effective overburden pressures [200 kPa (<2 tsf)]. The workshop participants endorsed the use of (9) for calculation of C_N, but acknowledged that for overburden pressures >200 kPa (2 tsf) the results are uncertain. Eq. (10) provides a better fit for overburden

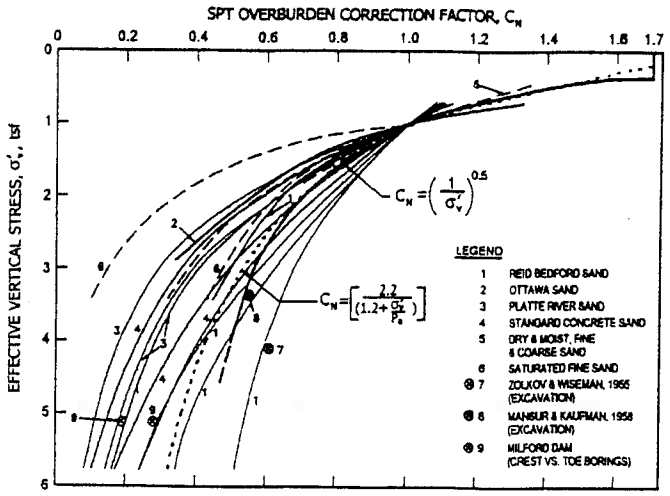

FIG. 3. C_N Curves for Various Sands Based on Field and Laboratory Test Data along with Suggested C_N Curve Determined from Eqs. (9) and (10) (Modified from Castro 1995)

pressures up to 300 kPa (3 tsf). For pressures >300 kPa (3 tsf), the uncertainty is so great that (9) should not be applied. At these high pressures, which are generally below the depth for which the simplified procedure has been verified, C_N should be estimated by other means.

Another important factor is the energy transferred from the falling hammer to the SPT sampler. An ER of 60% is generally accepted as the approximate average for U.S. testing practice and as a reference value for energy corrections. The ER delivered to the sampler depends on the type of hammer, anvil, lifting mechanism, and the method of hammer release. Approximate correction factors (C_E = ER/60) to modify the SPT results to a 60% energy ratio for various types of hammers and anvils are listed in Table 2. Because of variations in drilling and testing equipment and differences in testing procedures, a rather wide range in the energy correction factor C_E has been observed as noted in the table. Even when procedures are carefully monitored to conform to established standards, such as ASTM D 1586-99, some variation in C_E may occur because of minor variations in testing procedures. Measured energies at a single site indicate that variations in energy ratio between blows or between tests in a single borehole typically vary by as much as 10%. The workshop participants recommend measurement of the hammer energy frequently at each site where the SPT is used. Where measurements cannot be made, careful observation and notation of the equipment and procedures are required to estimate a C_E value for use in liquefaction resistance calculations. Use of good-quality testing equipment and carefully controlled testing procedures conforming to ASTM D 1586-99 will generally yield more consistent energy ratios and C_E with values from the upper parts of the ranges listed in Table 2.

Skempton (1986) suggested and Robertson and Wride (1998) updated correction factors for rod lengths <10 m, borehole diameters outside the recommended interval (65–125 mm), and sampling tubes without liners. Range for these correction factors are listed in Table 2. For liquefaction resistance calculations and rod lengths <3 m, a C_R of 0.75 should be applied as was done by Seed et al. (1985) in formulating the simplified procedure. Although application of rod-length correction factors listed in Table 2 will give more precise $(N_1)_{60}$ values, these corrections may be neglected for liquefaction resistance calculations for rod lengths between 3 and 10 m because rod-length corrections were not applied to SPT test data from these depths in compiling the original liquefaction case history databases. Thus rod-length corrections are implicitly incorporated into the empirical SPT procedure.

A final change recommended by workshop participants is the use of revised magnitude scaling factors rather than the original Seed and Idriss (1982) factors to adjust CRR for earthquake magnitudes other than 7.5. Magnitude scaling factors are addressed later in this report.

CPT

A primary advantage of the CPT is that a nearly continuous profile of penetration resistance is developed for stratigraphic interpretation. The CPT results are generally more consistent and repeatable than results from other penetration tests listed in Table 1. The continuous profile also allows a more detailed definition of soil layers than the other tools listed in the table. This stratigraphic capability makes the CPT particularly advantageous for developing liquefaction-resistance profiles. Interpretations based on the CPT, however, must be verified with a few well-placed boreholes preferably with standard penetration tests, to confirm soil types and further verify liquefaction-resistance interpretations.

Fig. 4 provides curves prepared by Robertson and Wride (1998) for direct determination of CRR for clean sands (FC ≤ 5%) from CPT data. This figure was developed from CPT case history data compiled from several investigations, including those by Stark and Olson (1995) and Suzuki et al. (1995). The chart, valid for magnitude 7.5 earthquakes only, shows calculated cyclic resistance ratio plotted as a function of dimensionless, corrected, and normalized CPT resistance q_{c1N} from sites where surface effects of liquefaction were or were not observed following past earthquakes. The CRR curve conservatively separates regions of the plot with data indicative of liquefaction from regions indicative of nonliquefaction.

Based on a few misclassified case histories from the 1989 Loma Prieta earthquake, I. M. Idriss suggested that the clean sand curve in Fig. 4 should be shifted to the right by 10–15%. However, a majority of workshop participants supported a curve in its present position, for three reasons. First, a purpose of the workshop was to recommend criteria that yield roughly equivalent CRR for the field tests listed in Table 1. Shifting the base curve to the right makes the CPT criteria generally more conservative. For example, for $(N_1)_{60} > 5$, q_{c1N}:$(N_1)_{60}$ ra-

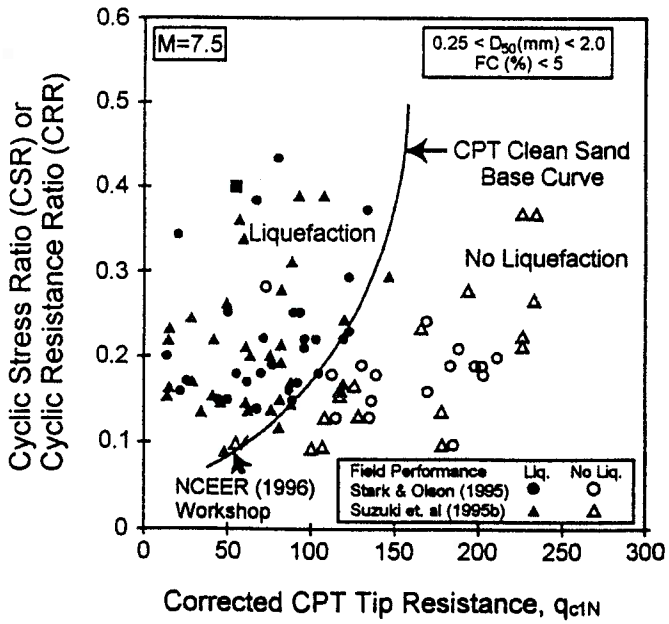

FIG. 4. Curve Recommended for Calculation of CRR from CPT Data along with Empirical Liquefaction Data from Compiled Case Histories (Reproduced from Robertson and Wride 1998)

tios between the two clean-sand base curves, plotted in Figs. 4 and 2, respectively, range from 5 to 8—values that are slightly higher than those expected for clean sands. Shifting the CPT base curve to the right by 10 to 15% would increase those ratios to unusually high values ranging from 6 to 9. Second, base curves, such as those plotted in Figs. 2 and 4, were intended to be conservative, but not necessarily to encompass every data point on the plot. Thus the presence of a few points beyond the base curve should be allowable. Finally, several studies have confirmed that the CPT criteria in Fig. 4 are generally conservative. Robertson and Wride (1998) verified these criteria against SPT and other data from sites they investigated. Gilstrap and Youd (1998) compared calculated liquefaction resistances against field performance at 19 sites and concluded that the CPT criteria correctly predicted the occurrence or nonoccurrence of liquefaction with >85% reliability.

The clean-sand base curve in Fig. 4 may be approximated by the following equation (Robertson and Wride 1998):

$$\text{If } (q_{c1N})_{cs} < 50 \quad \text{CRR}_{7.5} = 0.833[(q_{c1N})_{cs}/1{,}000] + 0.05 \tag{11a}$$

$$\text{If } 50 \leq (q_{c1N})_{cs} < 160 \quad \text{CRR}_{7.5} = 93[(q_{c1N})_{cs}/1{,}000]^3 + 0.08 \tag{11b}$$

where $(q_{c1N})_{cs}$ = clean-sand cone penetration resistance normalized to approximately 100 kPa (1 atm).

Normalization of Cone Penetration Resistance

The CPT procedure requires normalization of tip resistance using (12) and (13). This transformation yields normalized, dimensionless cone pentration resistance q_{c1N}

$$q_{c1N} = C_Q(q_c/P_a) \tag{12}$$

where

$$C_Q = (P_a/\sigma'_{vo})^n \tag{13}$$

and where C_Q = normalizing factor for cone penetration resistance; P_a = 1 atm of pressure in the same units used for σ'_{vo}; n = exponent that varies with soil type; and q_c = field cone penetration resistance measured at the tip. At shallow depths C_Q becomes large because of low overburden pressure; however, values >1.7 should not be applied. As noted in the following paragraphs, the value of the exponent n varies from 0.5 to 1.0, depending on the grain characteristics of the soil (Olsen 1997).

The CPT friction ratio (sleeve resistance f_s divided by cone tip resistance q_c) generally increases with increasing fines content and soil plasticity, allowing rough estimates of soil type and fines content to be determined from CPT data. Robertson and Wride (1998) constructed the chart reproduced in Fig. 5 for estimation of soil type. The boundaries between soil types 2–7 can be approximated by concentric circles and can be used to account for effects of soil characteristics on q_{c1N} and CRR. The radius of these circles, termed the soil behavior type index I_c is calculated from the following equation:

$$I_c = [(3.47 - \log Q)^2 + (1.22 + \log F)^2]^{0.5} \tag{14}$$

where

$$Q = [(q_c - \sigma_{vo})/P_a][(P_a/\sigma'_{vo})^n] \tag{15}$$

and

$$F = [f_s/(q_c - \sigma_{vo})] \times 100\% \tag{16}$$

The soil behavior chart in Fig. 5 was developed using an exponent n of 1.0, which is the appropriate value for clayey soil types. For clean sands, however, an exponent value of 0.5 is more appropriate, and a value intermediate between 0.5 and

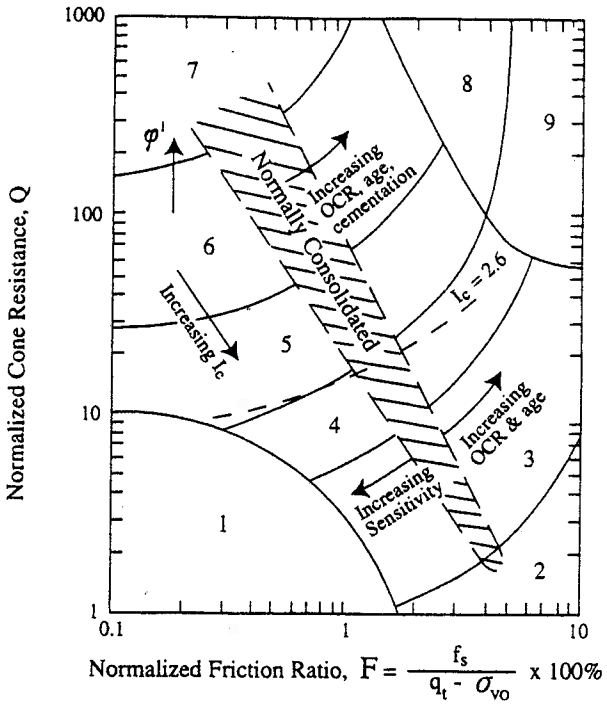

1. Sensitive, fine grained
2. Organic soils - peats
3. Clays - silty clay to clay
4. Silt mixtures - clayey silt to silty clay
5. Sand mixtures - silty sand to sandy silt
6. Sands - clean sand to silty sand
7. Gravelly sand to dense sand
8. Very stiff sand to clayey sand*
9. Very stiff, fine grained*

**Heavily overconsolidated or cemented*

FIG. 5. CPT-Based Soil Behavior-Type Chart Proposed by Robertson (1990)

1.0 would be appropriate for silts and sandy silts. Robertson and Wride recommended the following procedure for calculating the soil behavior type index I_c. The first step is to differentiate soil types characterized as clays from soil types characterized as sands and silts. This differentiation is performed by assuming an exponent n of 1.0 (characteristic of clays) and calculating the dimensionless CPT tip resistance Q from the following equation:

$$Q = [(q_c - \sigma_{vo})/P_a][P_a/\sigma'_{vo}]^{1.0} = [(q_c - \sigma_{vo})/\sigma'_{vo}] \tag{17}$$

If the I_c calculated with an exponent of 1.0 is >2.6, the soil is classified as clayey and is considered too clay-rich to liquefy, and the analysis is complete. However, soil samples should be retrieved and tested to confirm the soil type and liquefaction resistance. Criteria such as the Chinese criteria might be applied to confirm that the soil is nonliquefiable. The so-called Chinese criteria, as defined by Seed and Idriss (1982), specify that liquefaction can only occur if all three of the following conditions are met:

1. The clay content (particles smaller than 5 μ) is <15% by weight.
2. The liquid limit is <35%.
3. The natural moisture content is >0.9 times the liquid limit.

If the calculated I_c is <2.6, the soil is most likely granular in nature, and therefore C_q and Q should be recalculated using an exponent n of 0.5. I_c should then be recalculated using (14). If the recalculated I_c is <2.6, the soil is classed as nonplastic and granular. This I_c is used to estimate liquefaction resistance, as noted in the next section. However, if the recalculated I_c is

>2.6, the soil is likely to be very silty and possibly plastic. In this instance, q_{c1N} should be recalculated from (12) using an intermediate exponent n of 0.7 in (13). I_c is then recalculated from (14) using the recalculated value for q_{c1N}. This intermediate I_c is then used to calculate liquefaction resistance. In this instance, a soil sample should be retrieved and tested to verify the soil type and whether the soil is liquefiable by other criteria, such as the Chinese criteria.

Because the relationship between I_c and soil type is approximate, the consensus of the workshop participants is that all soils with an I_c of 2.4 or greater should be sampled and tested to confirm the soil type and to test the liquefiability with other criteria. Also, soil layers characterized by an $I_c > 2.6$, but with a normalized friction ratio $F < 1.0\%$ (region 1 of Fig. 5) may be very sensitive and should be sampled and tested. Although not technically liquefiable according to the Chinese criteria, such sensitive soils may suffer softening and strength loss during earthquake shaking.

Calculation of Clean-Sand Equivalent Normalized Cone Penetration Resistance ($q_{c1N})_{cs}$

The normalized penetration resistance (q_{c1N}) for silty sands is corrected to an equivalent clean sand value ($q_{c1N})_{cs}$, by the following relationship:

$$(q_{c1N})_{cs} = K_c q_{c1N} \tag{18}$$

where K_c, the correction factor for grain characteristics, is defined by the following equation (Robertson and Wride 1998):

$$\text{for } I_c \leq 1.64 \quad K_c = 1.0 \tag{19a}$$

$$\text{for } I_c > 1.64 \quad K_c = -0.403I_c^4 + 5.581I_c^3 - 21.63I_c^2 + 33.75I_c - 17.88 \tag{19b}$$

The K_c curve defined by (19) is plotted in Fig. 6. For $I_c > 2.6$, the curve is shown as a dashed line, indicating that soils in this range of I_c are most likely too clay-rich or plastic to liquefy.

With an appropriate I_c and K_c, (11) and (19) can be used to calculate $CRR_{7.5}$. To adjust CRR to magnitudes other than 7.5, the calculated $CRR_{7.5}$ is multiplied by an appropriate magnitude scaling factor. The same magnitude scaling factors are used with CPT data as with SPT data. Magnitude scaling factors are discussed in a later section of this report.

Olsen (1997) and Suzuki et al. (1995) Procedures

Olsen (1997), who pioneered many of the techniques for assessing liquefaction resistance from CPT soundings, suggested a somewhat different procedure for calculating CRR from CPT data. Reasons for recommending the Robertson and Wride (1998) procedure over that of Olsen are the ease of application and the ease with which relationships can be quantified for computer-aided calculations. Results from Olsen's procedure, however, are consistent with results from the procedure proposed here for shallow (<15 m deep) sediment beneath level to gently sloping terrain. Olsen (1997) noted that almost any CPT normalization technique will give results consistent with his normalization procedure for soil layers in the 3–15 m depth range. For deeper layers, significant differences may develop between the two procedures. Those depths are also beyond the depth for which the simplified procedure has been verified. Hence any procedure based on the simplified procedure yields rather uncertain results at depths >15 m.

Suzuki et al. (1995) also developed criteria for evaluating CRR from CPT data. Those criteria are slightly more conservative than those of Robertson and Wride (1998) and were considered by the latter investigators in developing the criteria recommended herein.

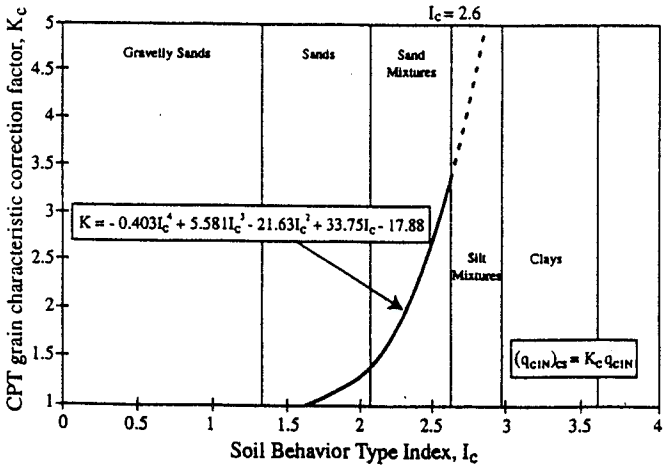

FIG. 6. Grain-Characteristic Correction Factor K_c for Determination of Clean-Sand Equivalent CPT Resistance (Reproduced from Robertson and Wride 1998)

Correction of Cone Penetration Resistance for Thin Soil Layers

Theoretical as well as laboratory studies indicate that CPT tip resistance is influenced by softer soil layers above or below the cone tip. As a result, measured CPT tip resistance is smaller in thin layers of granular soils sandwiched between softer layers than in thicker layers of the same granular soil. The amount of the reduction of penetration resistance in soft layers is a function of the thickness of the softer layer and the stiffness of the stiffer layers.

Using a simplified elastic solution, Vreugdenhil et al. (1994) developed a procedure for estimating the thick-layer equivalent cone penetration resistance of thin stiff layers lying within softer strata. The correction applies only to thin stiff layers embedded within thick soft layers. Because the corrections have a reasonable trend, but appear rather large, Robertson and Fear (1995) recommended conservative corrections from the $q_{cA}/q_{cB} = 2$ curve sketched in Fig. 7.

Further analysis of field data by Gonzalo Castro and Peter Robertson for the NCEER workshop indicates that corrections based on the $q_{cA}/q_{cB} = 2$ curve may still be too large and not adequately conservative. They suggested, and the workshop participants agreed, that the lower bound of the range of field data plotted by G. Castro in Fig. 7 provides more conservative K_H values that should be used until further field studies and analyses indicate that higher values are viable. The equation for the lower bound of the field curve is

$$K_H = 0.25[((H/d_c)/17) - 1.77]^2 + 1.0 \tag{20}$$

where H = thickness of the interbedded layer in mm; q_{cA} and q_{cB} = cone resistances of the stiff and soft layers, respectively; and d_c = diameter of the cone in mm (Fig. 7).

V_s

Andrus and Stokoe (1997, 2000) developed liquefaction resistance criteria from field measurements of shear wave velocity V_s. The use of V_s as a field index of liquefaction resistance is soundly based because both V_s and CRR are similarly, but not proportionally, influenced by void ratio, effective confining stresses, stress history, and geologic age. The advantages of using V_s include the following: (1) V_s measurements are possible in soils that are difficult to penetrate with CPT and SPT or to extract undisturbed samples, such as gravelly soils, and at sites where borings or soundings may not be permitted; (2) V_s is a basic mechanical property of soil materials, directly related to small-strain shear modulus; and (3) the

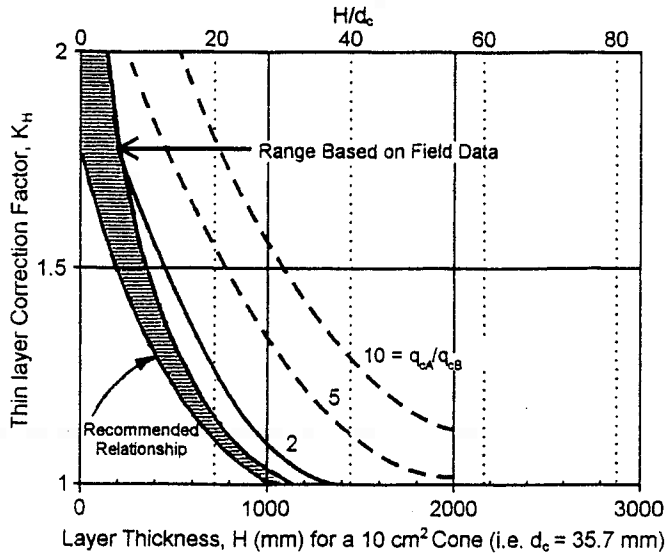

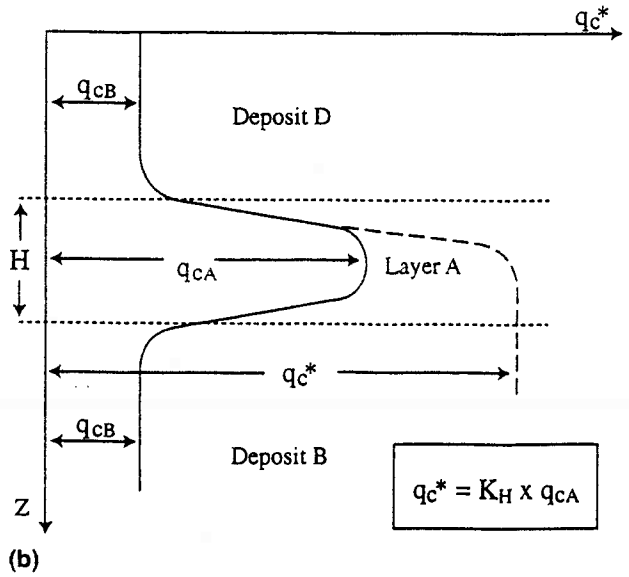

FIG. 7. Thin-Layer Correction Factor K_H for Determination of Equivalent Thick-Layer CPT Resistance (Modified from Robertson and Fear 1995)

small-strain shear modulus is a parameter required in analytical procedures for estimating dynamic soil response and soil-structure interaction analyses.

Three concerns arise when using V_s for liquefaction-resistance evaluations: (1) seismic wave velocity measurements are made at small strains, whereas pore-water pressure buildup and the onset of liquefaction are medium- to high-strain phenomena; (2) seismic testing does not provide samples for classification of soils and identification of nonliquefiable soft clay-rich soils; and (3) thin, low V_s strata may not be detected if the measurement interval is too large. Therefore the preferred practice is to drill sufficient boreholes and conduct in situ tests to detect and delineate thin liquefiable strata, nonliquefiable clay-rich soils, and silty soils above the ground-water table that might become liquefiable should the water table rise. Other tests, such as the SPT or CPT, are needed to detect liquefiable weakly cemented soils that may have high V_s values.

V_s Criteria for Evaluating Liquefaction Resistance

Following the traditional procedures for correcting penetration resistance to account for overburden stress, V_s is also corrected to a reference overburden stress using the following equation (Sykora 1987; Kayen et al. 1992; Robertson et al. 1992):

$$V_{s1} = V_s \left(\frac{P_a}{\sigma'_{vo}}\right)^{0.25} \tag{21}$$

where V_{s1} = overburden-stress corrected shear wave velocity; P_a = atmospheric pressure approximated by 100 kPa (1 TSF); and σ'_{vo} = initial effective vertical stress in the same units as P_a. Eq. (21) implicitly assumes a constant coefficient of earth pressure K'_o which is approximately 0.5 for sites susceptible to liquefaction. Application of (21) also implicitly assumes that V_s is measured with both the directions of particle motion and wave propagation polarized along principal stress directions and that one of those directions is vertical (Stokoe et al. 1985).

Fig. 8 compares seven CRR-V_{s1} curves. The "best fit" curve by Tokimatsu and Uchida (1990) was determined from laboratory cyclic triaxial test results for various sands with <10% fines and 15 cycles of loading. The more conservative "lower bound" curve for Tokimatsu and Uchida's laboratory test results is also shown as a lower bound for liquefaction occurrences. The bounding curve by Robertson et al. (1992) was developed using field performance data from sites in Imperial Valley, Calif., along with data from four other sites. The curves by Kayen et al. (1992) and Lodge (1994) are from sites that did and did not liquefy during the 1989 Loma Prieta earthquake. Andrus and Stokoe's (1997) curve was developed for uncemented, Holocene-age soils with 5% or less fines using field performance data from 20 earthquakes and over 50 measurement sites. Andrus and Stokoe (2000) revised this curve based on new information and an expanded database that includes 26 earthquakes and more than 70 measurement sites.

Andrus and Stokoe (1997) proposed the following relationship between CRR and V_{s1}:

$$\text{CRR} = a\left(\frac{V_{s1}}{100}\right)^2 + b\left(\frac{1}{V^*_{s1} - V_{s1}} - \frac{1}{V^*_{s1}}\right) \tag{22}$$

where V^*_{s1} = limiting upper value of V_{s1} for liquefaction occurrence; and a and b are curve fitting parameters. The first parenthetical term of (22) is based on a modified relationship

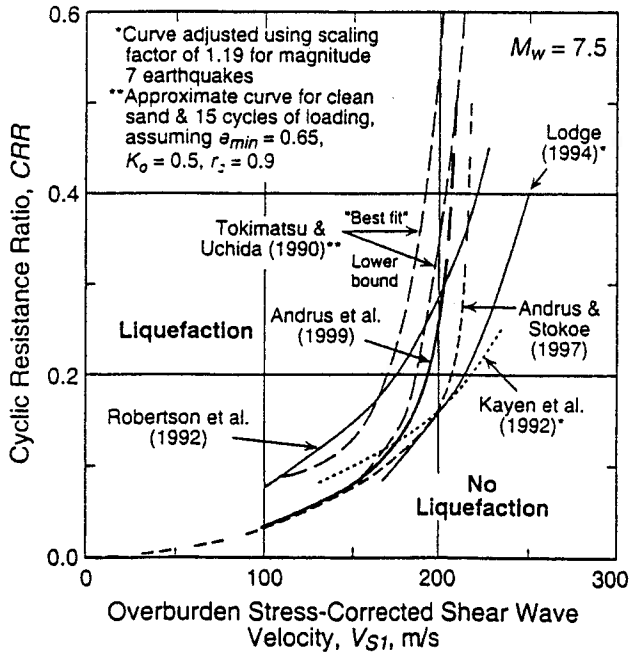

FIG. 8. Comparison of Seven Relationships between Liquefaction Resistance and Overburden Stress-Corrected Shear Wave Velocity for Granular Soils

between V_{s1} and CSR for constant average cyclic shear strain suggested by R. Dobry (personal communication to R. D. Andrus, 1996). The second parenthetical term is a hyperbola with a small value at low V_{s1}, and a very large value as V_{s1} approaches V_{s1}^*, a constant limiting velocity for liquefaction of soils.

CRR versus V_{s1} curves recommended for engineering practice by Andrus and Stokoe (2000) for magnitude 7.5 earthquakes and uncemented Holocene-age soils with various fines contents are reproduced in Fig. 9. Also plotted and presented in Fig. 9 are points calculated from liquefaction case history information for magnitude 5.9–8.3 earthquakes. The three curves shown were determined through an iterative process of varying the values of a and b until nearly all the points indicative of liquefaction were bounded by the curves with the least number of nonliquefaction points plotted in the liquefaction region. The final values of a and b used to draw the curves were 0.022 and 2.8, respectively. Values of V_{s1}^* were assumed to vary linearly from 200 m/s for soils with fines content of 35% to 215 m/s for soils with fines content of 5% or less.

The recommended curves shown in Fig. 9 are dashed above CRR of 0.35 to indicate that field-performance data are limited in that range. Also, they do not extend much below 100 m/s, because there are no field data to support extending them to the origin. The calculated CRR is 0.033 for a V_{s1} of 100 m/s. This minimal CRR value is generally consistent with intercept CRR values assumed for the CPT and SPT procedures. Eq. (22) can be scaled to other magnitude values through use of magnitude scaling factors. These factors are discussed in a later section of this paper.

BPT

Liquefaction resistance of nongravelly soils has been evaluated primarily through CPT and SPT, with occasional V_s measurements. CPT and SPT measurements, however, are not generally reliable in gravelly soils. Large gravel particles may interfere with the normal deformation of soil materials around the penetrometer and misleadingly increase penetration resistance. Several investigators have employed large-diameter penetrometers to surmount these difficulties; the Becker penetration test (BPT) in particular has become one of the more effectively and widely used larger tools. The BPT was developed in Canada in the late 1950s and consists of a 168-mm diameter, 3-m-long double-walled casing driven into the ground with a double-acting diesel-driven pile hammer. The hammer impacts are applied at the top of the casing and peneration is continuous. The Becker penetration resistance is defined as the number of blows required to drive the casing through an increment of 300 mm.

The BPT has not been standardized, and several different types of equipment and procedures have been used. There are currently very few liquefaction sites from which BPT data have been obtained. Thus the BPT cannot be directly correlated with field behavior, but rather through estimating equivalent SPT N-values from BPT data and then applying evaluation procedures based on the SPT. This indirect method introduces substantial additional uncertainty into the calculated CRR.

To provide uniformity, Harder and Seed (1986) recommended newer AP-1000 drill rigs equipped with supercharged diesel hammers, 168-mm outside diameter casing, and a plugged bit. From several sites where both BPT and SPT tests were conducted in parallel soundings, Harder and Seed (1986) developed a preliminary correlation between Becker and standard penetration resistance [Fig. 10(a)]. Additional comparative data compiled since 1986 are plotted in Fig. 10(b). The original Harder and Seed correlation curve (solid line) is drawn in Fig. 10(b) along with dashed curves representing 20% over- and underpredictions of SPT blow counts. These plots indicate that SPT blow counts can be roughly estimated

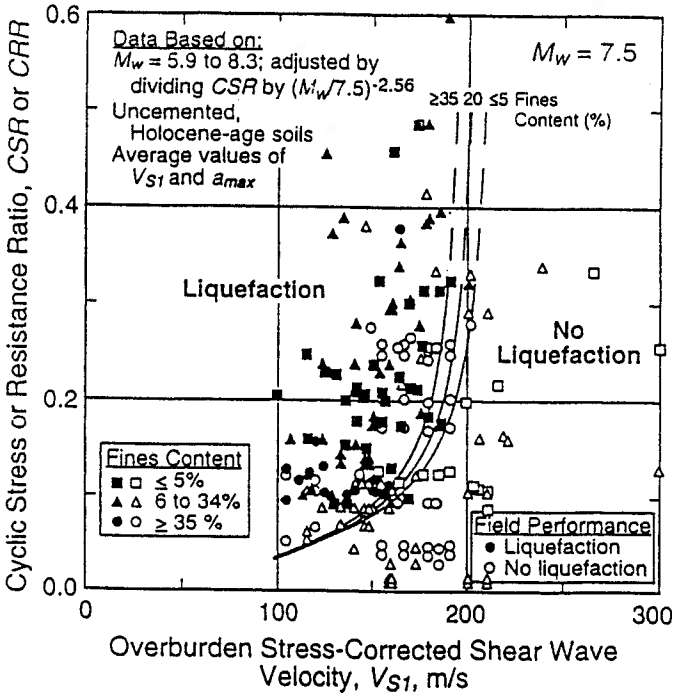

FIG. 9. Liquefaction Relationship Recommended for Clean, Uncemented Soils with Liquefaction Data from Compiled Case Histories (Reproduced from Andrus and Stokoe 2000)

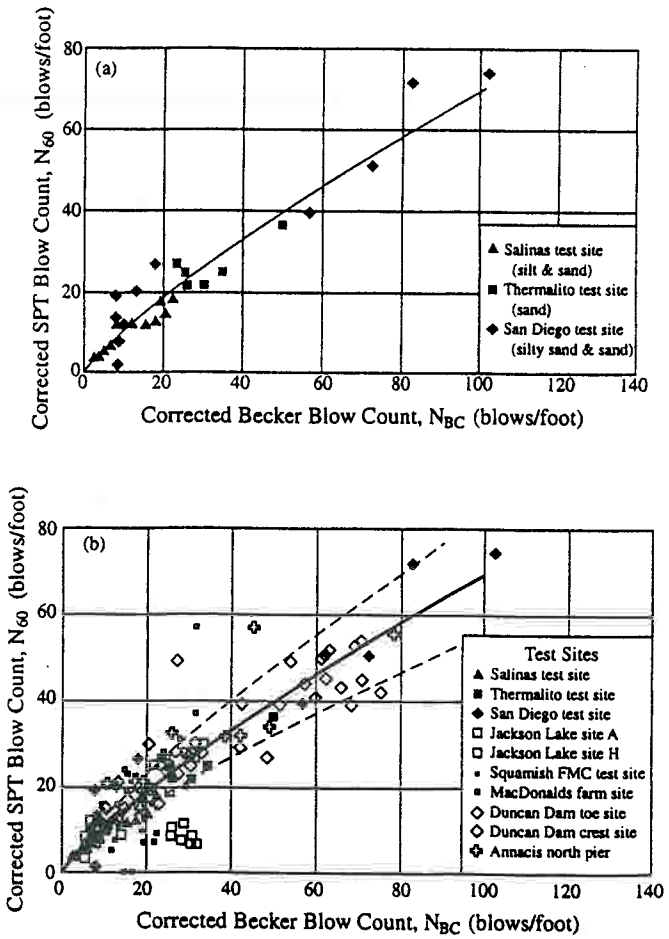

FIG. 10. Correlation between Corrected Becker Penetration Resistance N_{BC} and Corrected SPT Resistance N_{60}: (a) Harder and Seed (1986); (b) Data from Additional Sites (Reproduced from Harder 1997)

from BPT measurements. These plots indicate that although SPT blow counts can be roughly estimated from BPT measurements, there can be considerable uncertainty for calculating liquefaction resistance because the data scatter is greatest in the range of greatest importance [N-values of 0–30 blows/300 mm (ft)].

A major source of variation in BPT blow counts is deviations in hammer energy. Rather than measuring hammer energy directly, Harder and Seed (1986) monitored bounce-chamber pressures and found that uniform combustion conditions (e.g., full throttle with a supercharger) correlated rather well with variations in Becker blow count. From this information, Harder and Seed developed an energy correction procedure based on measured bounce-chamber pressure.

Direct measurement of transmitted hammer energy could provide a more theoretically rigorous correction for Becker hammer efficiency. Sy and Campanella (1994) and Sy et al. (1995) instrumented a small length of Becker casing with strain gauges and accelerometers to measure transferred energy. They analyzed the recorded data with a pile-driving analyzer to determine strain, force, acceleration, and velocity. The transferred energy was determined by time integration of force times velocity. They were able to verify many of the variations in hammer energy previously identified by Harder and Seed (1986), including effects of variable throttle settings and energy transmission efficiencies of various drill rigs. However, they were unable to reduce the amount of scatter and uncertainty in converting BPT blow counts to SPT blow counts. Because the Sy and Campanella procedure requires considerably more effort than monitoring of bounce-chamber pressure without producing greatly improved results, the workshop participants agreed that the bounce-chamber technique is adequate for routine practice.

Friction along the driven casing also influences penetration resistance. Harder and Seed (1986) did not directly evaluate the effect of casing friction; hence, the correlation in Fig. 10(b) intrinsically incorporates an unknown amount of casing friction. However, casing friction remains a concern for depths >30 m and for measurement of penetration resistance in soft soils underlying thick deposits of dense soil. Either of these circumstances could lead to greater casing friction than is intrinsically incorporated in the Harder and Seed correlation.

The following procedures are recommended for routine practice: (1) the BPT should be conducted with newer AP-1000 drill rigs equipped with supercharged diesel hammers to drive plugged 168-mm outside diameter casing; (2) bounce-chamber pressures should be monitored and adjustments made to measured BPT blow counts to account for variations in diesel hammer combustion efficiency—for most routine applications, correlations developed by Harder and Seed (1986) may be used for these adjustments; and (3) the influence of some casing friction is indirectly accounted for in the Harder and Seed BPT-SPT correlation. This correlation, however, has not been verified and should not be used for depths >30 m or for sites with thick dense deposits overlying loose sands or gravels. For these conditions, mudded boreholes may be needed to reduce casing friction, or specially developed local correlations or sophisticated wave-equation analyses may be applied to quantify frictional effects.

MAGNITUDE SCALING FACTORS (MSFs)

The clean-sand base or CRR curves in Figs. 2 (SPT), 4 (CPT), and 10 (V_{s1}) apply only to magnitude 7.5 earthquakes. To adjust the clean-sand curves to magnitudes smaller or larger than 7.5, Seed and Idriss (1982) introduced correction factors termed "magnitude scaling factors (MSFs)." These factors are used to scale the CRR base curves upward or downward on CRR versus $(N_1)_{60}$, q_{c1N}, or V_{s1} plots. Conversely, magnitude weighting factors, which are the inverse of magnitude scaling factors, may be applied to correct CSR for magnitude. Either correcting CRR via magnitude scaling factors, or correcting CSR via magnitude weighting factors, leads to the same final result. Because the original papers by Seed and Idriss were written in terms of magnitude scaling factors, the use of magnitude scaling factors is continued in this report.

To illustrate the influence of magnitude scaling factors on calculated hazard, the equation for factor of safety (FS) against liquefaction is written in terms of CRR, CSR, and MSF as follows:

$$FS = (CRR_{7.5}/CSR)MSF \tag{23}$$

where CSR = calculated cyclic stress ratio generated by the earthquake shaking; and $CRR_{7.5}$ = cyclic resistance ratio for magnitude 7.5 earthquakes. $CRR_{7.5}$ is determined from Fig. 2 or (4) for SPT data, Fig. 4 or (11) for CPT data, or Fig. 9 or (22) for V_{s1} data.

Seed and Idriss (1982) Scaling Factors

Because of the limited amount of field liquefaction data available in the 1970s, Seed and Idriss (1982) were unable to adequately constrain bounds between liquefaction and non-liquefaction regions on CRR plots for magnitudes other than 7.5. Consequently, they developed a set of MSF from average numbers of loading cycles for various earthquake magnitudes and laboratory test results. A representative curve developed by these investigators, showing the number of loading cycles required to generate liquefaction for a given CSR, is reproduced in Fig. 11. The average number of loading cycles for various magnitudes of earthquakes are also noted on the plot. The initial set of magnitude scaling factors was derived by dividing CSR values on the representative curve for the number of loading cycles corresponding to a given earthquake magnitude by the CSR for 15 loading cycles (equivalent to a magnitude 7.5 earthquake). These scaling factors are listed in column 2 of Table 3 and are plotted in Fig. 12. These MSFs have been routinely applied in engineering practice since their introduction in 1982.

Revised Idriss Scaling Factors

In preparing his H. B. Seed Memorial Lecture, I. M. Idriss reevaluated the data that he and the late Professor Seed used to calculate the original (1982) magnitude scaling factors. In so doing, Idriss replotted the data on a log-log plot and suggested that the data should plot as a straight line. He noted, however, that one outlying point had strongly influenced the original analysis, causing the original plot to be nonlinear and characterized by unduly low MSF values for magnitudes <7.5. Based on this reevaluation, Idriss defined a revised set of magnitude scaling factors listed in column 3 of Table 3 and plotted

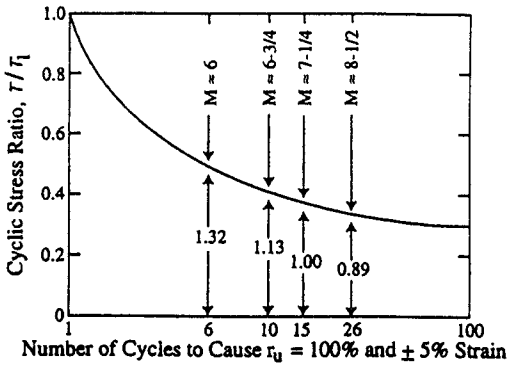

FIG. 11. Representative Relationship between CSR and Number of Cycles to Cause Liquefaction (Reproduced from Seed and Idriss 1982)

TABLE 3. Magnitude Scaling Factor Values Defined by Various Investigators (Youd and Noble 1997a)

Magnitude, M	Seed and Idriss (1982)	Idriss[a]	Ambraseys (1988)	Arango (1996) Distance based	Arango (1996) Energy based	Andrus and Stokoe (1997)	Youd and Noble (1997b) $P_L < 20\%$	Youd and Noble (1997b) $P_L < 32\%$	Youd and Noble (1997b) $P_L < 50\%$
5.5	1.43	2.20	2.86	3.00	2.20	2.8	2.86	3.42	4.44
6.0	1.32	1.76	2.20	2.00	1.65	2.1	1.93	2.35	2.92
6.5	1.19	1.44	1.69	1.60	1.40	1.6	1.34	1.66	1.99
7.0	1.08	1.19	1.30	1.25	1.10	1.25	1.00	1.20	1.39
7.5	1.00	1.00	1.00	1.00	1.00	1.00	—	—	1.00
8.0	0.94	0.84	0.67	0.75	0.85	0.8?	—	—	0.73?
8.5	0.89	0.72	0.44	—	—	0.65?	—	—	0.56?

Note: ? = Very uncertain values.
[a]1995 Seed Memorial Lecture, University of California at Berkeley (I. M. Idriss, personal communication to T. L. Youd, 1997).

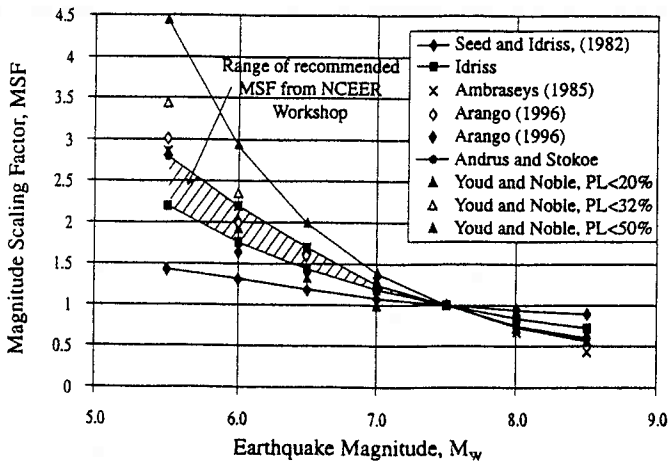

FIG. 12. Magnitude Scaling Factors Derived by Various Investigators (Reproduced from Youd and Noble 1997a)

in Fig. 12. The revised MSFs are defined by the following equation:

$$\text{MSF} = 10^{2.24}/M_w^{2.56} \tag{24}$$

The workshop participants recommend these revised scaling factors as a lower bound for MSF values.

The revised scaling factors are significantly higher than the original scaling factors for magnitudes <7.5 and somewhat lower than the original factors for magnitudes >7.5. Relative to the original scaling factors, the revised factors lead to a reduced calculated liquefaction hazard for magnitudes <7.5, but increase calculated hazard for magnitudes >7.5.

Ambraseys (1988) Scaling Factors

Field performance data collected since the 1970s for magnitudes <7.5 indicate that the original Seed and Idriss (1982) scaling factors are overly conservative. For example, Ambraseys (1988) analyzed liquefaction data compiled through the mid-1980s and plotted calculated cyclic stress ratios for sites that did or did not liquefy versus $(N_1)_{60}$. From these plots, Ambraseys developed empirical exponential equations that define CRR as a function of $(N_1)_{60}$ and moment magnitude M_w. By holding the value of $(N_1)_{60}$ constant in the equations and taking the ratio of CRR determined for various magnitudes of earthquakes to the CRR for magnitude 7.5 earthquakes, Ambraseys derived the magnitude scaling factors listed in column 4 of Table 3 and plotted in Fig. 12. For magnitudes <7.5, the MSFs suggested by Ambraseys are significantly larger than both the original factors developed by Seed and Idriss (column 2, Table 3) and the revised factors suggested by Idriss (column 3). Because they are based on observational data, these factors have validity for estimating liquefaction hazard; however, they have not been widely used in engineering practice.

For magnitudes >7.5, Ambraseys factors are significantly lower and much more conservative than the original (Seed and Idriss 1982) and Idriss's revised scaling factors. Because there are few data to constrain Ambraseys' scaling factors for magnitudes >7.5, they are not recommended for hazard evaluation for large earthquakes.

Arango (1996) Scaling Factors

Arango (1996) developed two sets of magnitude scaling factors. The first set (column 5, Table 3) is based on furthest observed liquefaction effects from the seismic energy source, the estimated average peak accelerations at those distant sites, and the seismic energy required to cause liquefaction. The second set (column 6, Table 3) was developed from energy concepts and the relationship derived by Seed and Idriss (1982) between numbers of significant stress cycles and earthquake magnitude. The MSFs listed in column 5 are similar in value (within about 10%) to the MSFs of Ambraseys (column 4), and the MSFs listed in column 6 are similar in value (within about 10%) to the revised MSFs proposed by Idriss (column 3).

Andrus and Stokoe (1997) Scaling Factors

From their studies of liquefaction resistance as a function of shear wave velocity V_s Andrus and Stokoe (1997) drew bounding curves and developed (22) for calculating CRR from V_s for magnitude 7.5 earthquakes. These investigators drew similar bounding curves for sites where surface effects of liquefaction were or were not observed for earthquakes with magnitudes of 6, 6.5, and 7. The positions of the CRR curves were visually adjusted on each graph until a best-fit bound was obtained. Magnitude scaling factors were then estimated by taking the ratio of CRR for a given magnitude to the CRR for magnitude 7.5 earthquakes. These MSFs are quantified by the following equation:

$$\text{MSF} = (M_w/7.5)^{-2.56} \tag{25}$$

MSFs for magnitudes <6 and >7.5 were extrapolated from this equation. The derived MSFs are listed in column 7 of Table 3, and plotted in Fig. 12. For magnitudes <7.5, the MSFs proposed by Andrus and Stokoe are rather close in value (within about 5%) to the MSFs proposed by Ambraseys. For magnitudes >7.5, the Andrus and Stokoe MSFs are slightly smaller than the revised MSFs proposed by Idriss.

Youd and Noble (1997a) Scaling Factors

Youd and Noble (1997a) used a probabilistic or logistic analysis to analyze case history data from sites where effects of liquefaction were or were not reported following past earthquakes. This analysis yielded the following equation, which

was updated after publication of the NCEER proceedings (Youd and Idriss 1997):

$$\text{Logit}(P_L) = \ln(P_L/(1 - P_L)) = -7.0351 + 2.1738M_w - 0.2678(N_1)_{60cs} + 3.0265 \ln \text{CRR} \quad (26)$$

where P_L = probability that liquefaction occurred; $1 - P_L$ = probability that liquefaction did not occur; and $(N_1)_{60cs}$ = corrected equivalent clean-sand blow count. For magnitudes <7.5, Youd and Noble recommended direct application of this equation to calculate the CRR for a given probability of liquefaction. In lieu of direct application, Youd and Noble defined three sets of MSFs for use with the simplified procedure. These MSFs are for probabilities of liquefaction occurrence <20, 32, and 50%, respectively, and are defined by the following equations:

$$\text{Probability } P_L < 20\% \quad \text{MSF} = 10^{3.81}/M^{4.53} \text{ for } M_w < 7 \quad (27)$$

$$\text{Probability } P_L < 32\% \quad \text{MSF} = 10^{3.74}/M^{4.33} \text{ for } M_w < 7 \quad (28)$$

$$\text{Probability } P_L < 50\% \quad \text{MSF} = 10^{4.21}/M^{4.81} \text{ for } M_w < 7.75 \quad (29)$$

New Recommendation by Idriss

I. M. Idriss (TRB 1999) proposed a new set of MSFs that are compatible with, and are only to be used with, the magnitude-dependent r_d that he also proposed. These new MSFs have lower values than the revised MSFs listed in Table 3, but slightly higher values than the original Seed and Idriss (1982) MSFs. Because the proposed r_d and associated MSFs have not been published and the factors have not been independently verified, the workshop participants chose not to recommend the new r_d or MSFs at this time.

Recommendations for Engineering Practice

The workshop participants reviewed the MSFs listed in Table 3, and all but one (S. S. C. Liao) agree that the original factors were too conservative and that increased MSFs are warranted for engineering practice for magnitudes <7.5. Rather than recommending a single set of factors, the workshop participants suggest a range of MSFs from which the engineer is allowed to choose factors that are requisite with the acceptable risk for any given application. For magnitudes <7.5, the lower bound for the recommended range is the new MSF proposed by Idriss [column 3 in Table 3, or (23)]. The suggested upper bound is the MSF proposed by Andrus and Stokoe [column 7 in Table 3, or (26)]. The upper-bound values are consistent with MSFs suggested by Ambraseys (1988), Arango (1996), and Youd and Noble (1997a) for $P_L < 20\%$.

For magnitudes >7.5, the new factors recommended by Idriss [column 3 in Table 3; (25)] should be used for engineering practice. These new factors are smaller than the original Seed and Idriss (1982) factors, hence their application leads to increased calculated liquefaction hazard compared to the original factors. Because there are only a few well-documented liquefaction case histories for earthquakes with magnitudes >8, MSFs in that range are poorly constrained by field data. Thus the workshop participants agreed that the greater conservatism embodied in the revised MSF by Idriss (column 3, Table 3) should be recommended for engineering practice.

CORRECTIONS FOR HIGH OVERBURDEN STRESSES, STATIC SHEAR STRESSES, AND AGE OF DEPOSIT

Correction factors K_σ and K_α were developed by Seed (1983) to extrapolate the simplified procedure to larger overburden pressure and static shear stress conditions than those embodied in the case history data set from which the simplified procedure was derived. As noted previously, the simplified procedure was developed and validated only for level to gently sloping sites (low static shear stress) and depths less than about 15 m (low overburden pressures). Thus applications using K_σ and K_α are beyond routine practice and require specialized expertise. Because these factors were discussed at the workshop and some new information was developed, recommendations from those discussions are included here. These recommendations, however, apply mostly to liquefaction hazard analyses of embankment dams and other large structures. These factors are applied by extending (23) to include K_σ and K_α as follows:

$$\text{FS} = (\text{CRR}_{7.5}/\text{CSR}) \cdot \text{MSF} \cdot K_\sigma \cdot K_\alpha \quad (30)$$

K_σ Correction Factor

Cyclically loaded laboratory test data indicate that liquefaction resistance increases with increasing confining stress. The rate of increase, however, is nonlinear. To account for the nonlinearity between CRR and effective overburden pressure, Seed (1983) introduced the correction factor K_σ to extrapolate the simplified procedure to soil layers with overburden pressures >100 kPa. Cyclically loaded, isotropically consolidated triaxial compression tests on sand specimens were used to measure CRR for high-stress conditions and develop K_σ values. By taking the ratio of CRR for various confining pressures to the CRR determined for approximately 100 kPa (1 atm) Seed (1983) developed the original K_σ correction curve. Other investigators have added data and suggested modifications to better define K_σ for engineering practice. For example, Seed and Harder (1990) developed the clean-sand curve reproduced in Fig. 13. Hynes and Olsen (1999) compiled and analyzed an enlarged data set to provide guidance and formulate equations for selecting K_σ values (Fig. 14). The equation they derived for calculating K_σ is

$$K_\sigma = (\sigma'_{vo}/P_a)^{(f-1)} \quad (31)$$

where σ'_{vo}, effective overburden pressure; and P_a, atmospheric pressure, are measured in the same units; and f is an exponent that is a function of site conditions, including relative density, stress history, aging, and overconsolidation ratio. The workshop participants considered the work of previous investigators and recommend the following values for f (Fig. 15). For relative densities between 40 and 60%, $f = 0.7-0.8$; for relative densities between 60 and 80%, $f = 0.6-0.7$. Hynes and Olsen recommended these values as minimal or conservative esti-

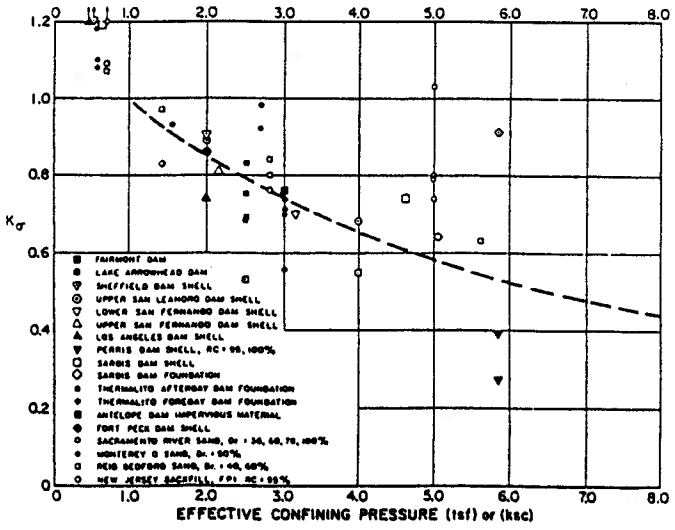

FIG. 13. K_σ-Values Determined by Various Investigators (Reproduced from Seed and Harder 1990)

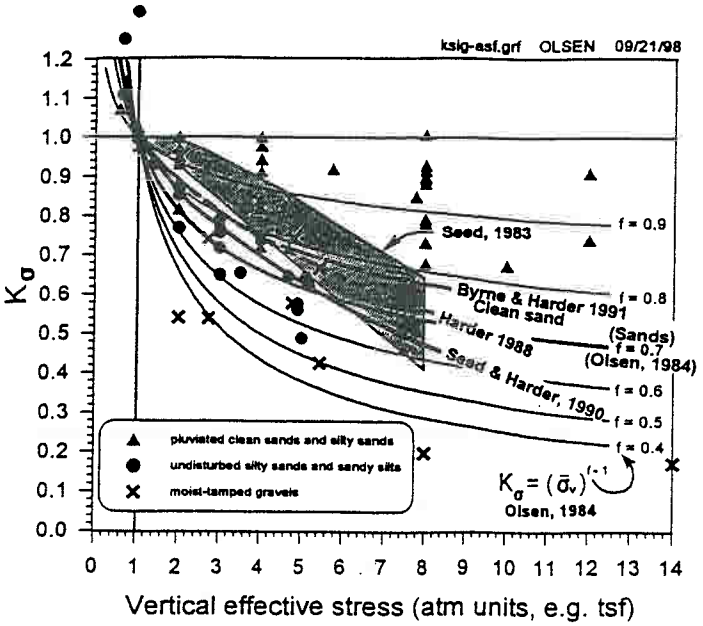

FIG. 14. Laboratory Data and Compiled K_σ Curves (Reproduced from Hynes and Olsen 1999)

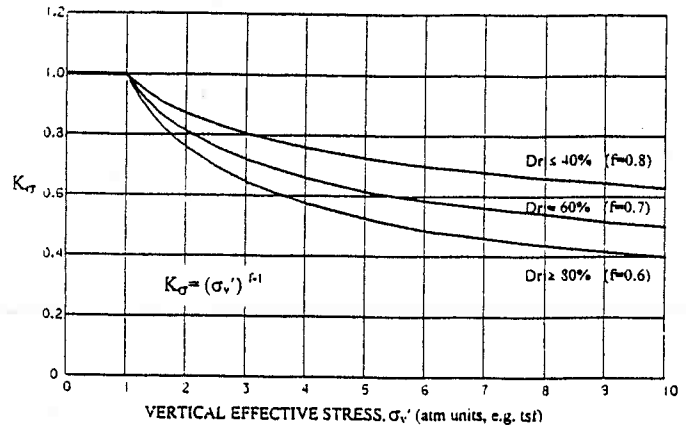

FIG. 15. Recommended Curves for Estimating K_σ for Engineering Practice

mates of K_σ for use in engineering practice for both clean and silty sands, and for gravels. The workshop participants concurred with this recommendation.

K_α Correction Factor for Sloping Ground

The liquefaction resistance of dilative soils (moderately dense to dense granular materials under low confining stress) increases with increased static shear stress. Conversely, the liquefaction resistance of contractive soils (loose soils and moderately dense soils under high confining stress) decreases with increased static shear stresses. To incorporate the effect of static shear stresses on liquefaction resistance, Seed (1983) introduced a correction factor K_α. To generate values for this factor, Seed normalized the static shear stress τ_{zx} acting on a plane with respect to the effective vertical stress σ'_{vo} yielding a parameter α, where

$$\alpha = \tau_{zx}/\sigma'_{vo} \tag{32}$$

Cyclically loaded triaxial compression tests were then used to empirically determine values of the correction factor K_α as a function of α.

For the NCEER workshop, Harder and Boulanger (1997) reviewed past publications, test results, and analyses of K_α. They noted that a wide range of K_α values have been proposed, indicating a lack of convergence and a need for continued research. The workshop participants agreed with this assessment. Although curves relating K_α to α have been published (Harder and Boulanger 1997), these curves should not be used by nonspecialists in geotechnical earthquake engineering or in routine engineering practice.

Influence of Age of Deposit

Several investigators have noted that liquefaction resistance of soils increases with age. For example, Seed (1979) observed significant increases in liquefaction resistance with aging of reconstituted sand specimens tested in the laboratory. Increases of as much as 25% in cyclic resistance ratio were noted between freshly constituted and 100-day-old specimens. Youd and Hoose (1977) and Youd and Perkins (1978) noted that liquefaction resistance increases markedly with geologic age. Sediments deposited within the past few thousand years are generally much more susceptible to liquefaction than older Holocene sediments; Pleistocene sediments are even more resistant; and pre-Pleistocene sediments are generally immune to liquefaction. Although qualitative time-dependent increases have been documented as noted above, few quantitative data have been collected. In addition, the factors causing increased liquefaction resistance with age are poorly understood. Consequently, verified correction factors for age have not been developed.

In the absence of quantitative correction factors, engineering judgment is required to estimate the liquefaction resistance of sediments more than a few thousand years old. For deeply buried sediments dated as more than a few thousand years old, some knowledgeable engineers have omitted application of the K_σ factor as partial compensation for the unquantified, but substantial increase of liquefaction resistance with age. For man-made structures, such as thick fills and embankment dams, aging effects are minimal, and corrections for age should not be applied in calculating liquefaction resistance.

SEISMIC FACTORS

Application of the simplified procedure for evaluating liquefaction resistance requires estimates of two ground motion parameters—earthquake magnitude and peak horizontal ground acceleration. These factors characterize duration and intensity of ground shaking, respectively. The workshop addressed the following questions with respect to selection of magnitude and peak acceleration values for liquefaction resistance analyses.

Earthquake Magnitude

Records from recent earthquakes, such as 1979 Imperial Valley, 1988 Armenia, 1989 Loma Prieta, 1994 Northridge, and 1995 Kobe, indicate that the relationship between duration and magnitude is rather uncertain and that factors other than magnitude also influence duration. For example, unilateral faulting, in which rupture begins at one end of the fault and propagates to the other, usually produces longer shaking duration for a given magnitude than bilateral faulting, in which slip begins near the midpoint on the fault and propagates in both directions simultaneously. Duration also generally increases with distance from the seismic energy source and may vary with tectonic province, site conditions, and bedrock topography (basin effects).

Question: Should correction factors be developed to adjust duration of shaking to account for the influence of earthquake source mechanism, fault rupture mode, distance from the energy source, basin effects, etc.?

Answer: Faulting characteristics and variations in shaking duration are difficult to predict in advance of an earthquake

event. The influence of distance generally is of secondary importance within the range of distances to which damaging liquefaction effects commonly develop. Basin effects are not yet sufficiently predictable to be adequately accounted for in engineering practice. Thus the workshop participants recommend continued use of the generally conservative relationship between magnitude and duration that is embodied in the simplified procedure.

Question: An important difference between eastern U.S. earthquakes and western U.S. earthquakes is that eastern ground motions are generally richer in high-frequency energy and thus could generate more significant stress cycles and equivalently longer durations than western earthquakes of the same magnitude. Is a correction needed to account for higher frequencies of motions generated by eastern U.S. earthquakes?

Answer: The high-frequency motions of eastern earthquakes are generally limited to near-field rock sites. High-frequency motions attenuate or are damped out rather quickly as they propagate through soil layers. This filtering action reduces the high-frequency energy at soil sites and thus reduces differences in numbers of significant loading cycles. Because liquefaction occurs only within soil strata, duration differences on soil sites between eastern and western earthquakes are not likely to be great. Without more instrumentally recorded data from which differences in ground motion characteristics can be quantified, there is little basis for the development of additional correction factors for eastern localities.

Another difference between eastern and western U.S. earthquakes is that strong ground motions generally propagate to greater distances in the east than in the west. By applying present state-of-the-art procedures for estimating peak ground acceleration at eastern sites, differences in amplitudes of ground motions between western and eastern earthquakes are properly taken into account.

Question: Which magnitude scale should be used for selection of earthquake magnitudes for liquefaction resistance analyses?

Answer: Seismologists commonly calculate earthquake magnitudes using five different scales: (1) local or Richter magnitude M_L; (2) surface-wave magnitude M_s; (3) short-period body-wave magnitude m_b; (4) long-period body-wave magnitude m_B; and (5) moment magnitude M_w. Moment magnitude, the scale most commonly used for engineering applications, is the scale preferred for calculation of liquefaction resistance. As Fig. 16 shows, magnitudes from other scales may be substituted directly for M_w within the following limitations—$M_L < 6$, $m_B < 7.5$, and $6 < M_s < 8$—m_b, a scale commonly used for eastern U.S. earthquakes, may be used for magnitudes between 5 and 6, provided m_b values are corrected to equivalent M_w values. The curves plotted in Fig. 16 may be used for this adjustment (Idriss 1985).

Peak Acceleration

In the simplified procedure, peak horizontal acceleration a_{max} is used to characterize the intensity of ground shaking. To provide guidance for estimation of a_{max}, the workshop addressed the following questions.

Question: What procedures are preferred for estimating a_{max} at potentially liquefiable sites?

Answer: The following methods, in order of preference, may be used for estimating a_{max}:

1) The preferred method for estimating a_{max} is through empirical correlations of a_{max} with earthquake magnitude, distance from the seismic energy source, and local site conditions. Several correlations have been published for estimating a_{max} for sites on bedrock or stiff to moderately stiff soils. Preliminary attenuation relationships have also been developed for a limited range of soft soil sites (Idriss 1991). Selection of an attenuation relationship should be based on such factors as region of the country, type of faulting, and site condition.

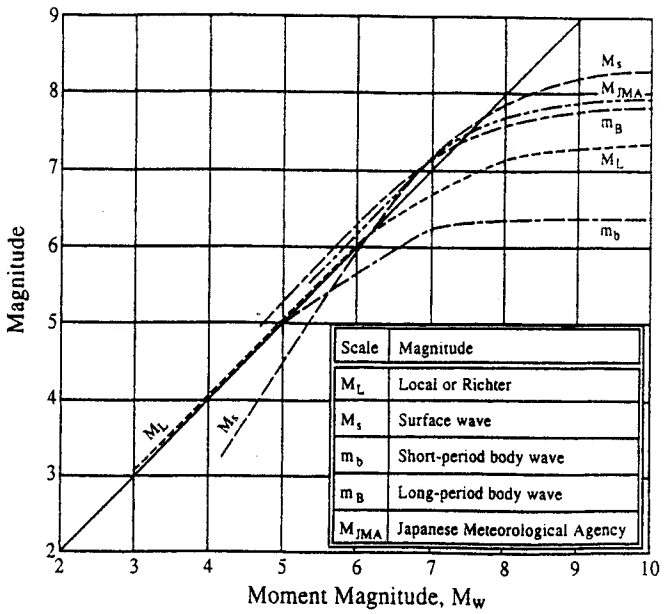

FIG. 16. Relationship between Moment M_w and Other Magnitude Scales (Reproduced from Heaton et al., Unpublished Report, 1982)

2) For soft sites and other soil profiles that are not compatible with available attenuation relationships, a_{max} may be estimated from local site response analyses. Computer programs such as SHAKE and DESRA may be used for these calculations (Schnabel et al. 1972; Finn et al. 1977). Input ground motions in the form of recorded accelerograms are preferable to synthetic records. Accelerograms derived from white noise should be avoided. A suite of plausible earthquake records should be used in the analysis, including as many as feasible from earthquakes with similar magnitudes, source distances, etc.

3) The third and least desirable method for estimating peak ground acceleration is through amplification ratios, such as those developed by Idriss (1990, 1991) and Seed et al. (1994). These factors use a multiplier or ratio by which bedrock outcrop motions are amplified to estimate surface motions at soil sites. Because amplification ratios are influenced by strain level, earthquake magnitude, and frequency content, caution and considerable engineering judgment are required in the application of these relationships.

Question: Which peak acceleration should be used: (1) the largest horizontal acceleration recorded on a three-component accelerogram; (2) the geometric mean (square root of the product) of the two maximum horizontal components; or (3) a vectorial combination of horizontal accelerations?

Answer: According to I. M. Idriss (oral discussion at NCEER workshop, 1996), where recorded motions were available, the larger of the two horizontal peak components of acceleration was used in the compilation of data used to derive the original simplified procedure. Where recorded values were not available, which was the circumstance for most sites, peak acceleration values were estimated from attenuation relationships based on the geometric mean of the two orthogonal peak horizontal accelerations. In nearly all instances where recorded motions were used, the peaks from the two horizontal records were approximately equal. Thus where a single peak was used, the peak and the geometric mean of the two peaks were about the same value. Based on this information, the workshop participants concurred that use of the geometric mean is consistent with the development of the procedure and is preferred for use in engineering practice. However, use of the larger of

the two orthogonal peak accelerations yields a larger estimate of a_{max}, is conservative, and is allowable. Vectorial accelerations are seldom calculated and should not be used. Peak vertical accelerations are generally much smaller than peak horizontal accelerations and are ignored for calculation of liquefaction resistance.

Question: Liquefaction usually develops at soil sites where ground motion amplification may occur and where sediment may soften, reducing motions as excess pore pressure develop. How should investigators account for these factors in estimating peak acceleration?

Answer: The recommended procedure is to calculate or estimate the a_{max} that would occur at the site in the absence of increased pore pressure or the onset of liquefaction. That peak acceleration incorporates the influence of site amplification, but neglects the influence of excess pore-water pressure.

Question: Should high-frequency spikes (periods <0.1 s) in acceleration records be considered or ignored?

Answer: In general, short-duration, high-frequency acceleration spikes are too short in duration to generate significant instability or deformation of granular structures, and should be ignored. By using attenuation relationships for estimation of peak acceleration, as noted above, high-frequency spikes are essentially ignored because few high-frequency peaks are incorporated in databases from which attenuation the relationships were derived. Similarly, ground response analyses programs such as SHAKE and DESRA generally attenuate or filter out high-frequency spikes, reducing their influence. Where amplification ratios are used, engineering judgment should be used to determine which bedrock acceleration is to be amplified.

ENERGY-BASED CRITERIA AND PROBABILISTIC ANALYSES

The workshop considered two additional topics: (1) liquefaction resistance criteria based on seismic energy passing through a liquefiable layer (Kayen and Mitchell 1997; Youd et al. 1997), and probabilistic analyses of case history data (Liao et al. 1988; Youd and Noble 1997b). Although probabilistic or risk analyses have been made for some localities and critical facilities, the workshop participants concluded that probabilistic procedures are still under development and not sufficiently formulated for routine engineering practice. Similarly, new energy-based criteria need to be independently tested before recommendations can be made for general practice. The workshop participants recommend that research and development continue on both of these relatively new and potentially useful procedures.

CONCLUSIONS

The participants in the NCEER workshop reviewed the state-of-the-art for evaluating liquefaction resistance and recommend several augmentations to that procedure. Specific recommendations, including procedures and equations, are listed in each section of this summary paper. Consensus conclusions from the workshop are:

1. Four field tests are recommended for routine evaluation of liquefaction resistance—the cone penetration test (CPT), the standard penetration test (SPT), shear-wave velocity (V_s) measurements, and for gravelly sites the Becker penetration test (BPT). Criteria for each test were reviewed and revised to incorporate recent developments and to achieve consistency between resistances calculated from the various tests. Each test has its advantages and limitations (Table 1). the CPT provides the most detailed soil stratigraphy and robust field-data based liquefaction resistance curves now available. CPT testing should always be accompanied by soil sampling for validation of soil type identification. The SPT has a longer record of application and provides disturbed soil samples from which fines content and other grain characteristics can be determined. Measured shear-wave velocities provide fundamental information on small-strain soil behavior that is useful beyond analyses of liquefaction resistance. V_s is also applicable at sites, such as landfills and gravelly sediments, where CPT and SPT soundings may not be possible or reliable. The BPT test is recommended only for gravelly sites and requires use of rough correlations between BPT and SPT, making the results less certain than other tests. Where possible, two or more test procedures should be applied to assure adequate definition of soil stratigraphy and a consistent evaluation of liquefaction resistance.
2. The magnitude scaling factors originally derived by Seed and Idriss (1982) are overly conservative for earthquakes with magnitudes <7.5. A range of scaling factors is recommended for engineering practice, the lower end of the range being the new MSF recommended by Idriss (column 3, Table 3), and the upper end of the range being the MSF suggested by Andrus and Stokoe (column 7, Table 3). These MSFs are defined by (25) and (26), respectively. For magnitudes >7.5, the new factors by Idriss (column 3, Table 3) should be used. These factors, which are more conservative than the original Seed and Idriss (1982) factors, should be applied.
3. The K_σ factors suggested by Seed and Harder (1990) appear to be overly conservative for some soils and field conditions. The workshop participants recommend K_σ values defined by the curves in Fig. 14 or (31). Because K_σ values are usually applied to depths greater than those verified for the simplified procedure, special expertise is generally required for their application.
4. Procedures for evaluation of liquefaction resistance beneath sloping ground or embankments (slopes greater than about 6%) have not been developed to a level allowable for routine use. Special expertise is required for evaluation of liquefaction resistance beneath sloping ground.
5. Moment magnitude M_w should be used for liquefaction resistance calculations. Magnitude, as used in the simplified procedure, is a measure of the duration of strong ground shaking. The present magnitude criteria are conservative and should not be corrected for source mechanism, style of faulting, distance from the energy source, subsurface bedrock topography (basin effect), or tectonic region (eastern versus western U.S. earthquakes).
6. The peak acceleration a_{max} applied in the procedure is the peak horizontal acceleration that would occur at ground surface in the absence of pore pressure increases or liquefaction. Attenuation relationships compatible with soil conditions at a site should be applied in estimating a_{max}. Relationships based on the geometric mean of the peak horizontal accelerations are preferred, but use of relationships based on peak horizontal acceleration is allowable and conservative. Where site conditions are incompatible with existing attenuation relationships, site-specific response calculations, using programs such as SHAKE or DESRA, should be used. The least preferable technique is application of amplification factors.

ACKNOWLEDGMENTS

Financial support for the January 1996 workshop was provided by the NCEER. Support for a second workshop in August 1998 was provided by both NCEER and the National Science Foundation. Brigham Young

University graduate students Steven Noble, Samuel Gilstrap, and Curt Peterson, assisted in organizing and conducting the workshops.

REFERENCES

Ambraseys, N. N. (1988). "Engineering seismology." *Earthquake Engrg. and Struct. Dynamics*, 17, 1–105.

Andrus, R. D., and Stokoe, K. H., II (1997). "Liquefaction resistance based on shear wave velocity." *Proc., NCEER Workshop on Evaluation of Liquefaction Resistance of Soils*, Nat. Ctr. for Earthquake Engrg. Res., State Univ. of New York at Buffalo, 89–128.

Andrus, R. D., and Stokoe, K. H., II (2000). "Liquefaction resistance of soils from shear-wave velocity." *J. Geotech. and Geoenvir. Engrg.*, ASCE, 126(11), 1015–1025.

Arango, I. (1996). "Magnitude scaling factors for soil liquefaction evaluations." *J. Geotech. Engrg.*, ASCE, 122(11), 929–936.

ASTM. (2000). "Annual book of ASTM standards." *04.08, D 1586-99*, West Conshohocken, Pa.

Castro, G. (1995). "Empirical methods in liquefaction evaluation." Primer Ciclo d Conferencias Internationales, Leonardo Zeevaert, Universidad Nacional Autonoma de Mexico, Mexico City.

Finn, W. D. L., Martin, G. R., and Lee, K. W. (1977). "An effective stress model for liquefaction." *J. Geotech. Engrg Div.*, ASCE, 103(6), 517—533.

Gibbs, H. J., and Holtz, W. G. (1957). "Research on determining the density of sand by spoon penetration testing." *Proc., 4th Int. Conf. on Soil Mech. and Found. Engrg.*, Vol. I, 35–39.

Gilstrap, S. D., and Youd, T. L. (1998). "CPT based liquefaction resistance analyses using case histories." *Tech. Rep. CEG-90-01*, Dept. of Civ. and Envir. Engrg., Brigham Young University, Provo, Utah.

Golesorkhi, R. (1989). "Factors influencing the computational determination of earthquake-induced shear stresses in sandy soils." PhD dissertation, University of California at Berkeley.

Harder, L. F., Jr. (1988). "Use of penetration tests to determine the cyclic loading resistance of gravelly soils during earthquake shaking." PhD dissertation, University of California at Berkeley.

Harder, L. F., Jr. (1997). "Application of the Becker Penetration test for evaluating the liquefaction potential of gravelly soils." *Proc., NCEER Workshop on Evaluation of Liquefaction Resistance of Soils*, National Center for Engineering Research, Buffalo, 129–148.

Harder, L. F., Jr., and Boulanger, R. W. (1997). "Application of K_σ and K_α correction factors." *Proc., NCEER Workshop on Evaluation of Liquefaction Resistance of Soils*, Nat. Ctr. for Earthquake Engrg. Res., State Univ. of New York at Buffalo, 167–190.

Harder, L. F., Jr., and Seed, H. B. (1986). "Determination of penetration resistance for coarse-grained soils using the Becker hammer drill." *Rep. UCB/EERC-86/06*, Earthquake Engrg. Res. Ctr., University of California at Berkeley.

Hynes, M. E., and Olsen, R. S. (1999). "Influence of confining stress on liquefaction resistance." *Proc., Int. Workshop on Phys. and Mech. of Soil Liquefaction*, Balkema, Rotterdam, The Netherlands, 145–152.

Idriss, I. M. (1985). "Evaluating seismic risk in engineering practice." *Proc., 11th Int. Conf. on Soil Mech. and Found. Engrg.*, Vol. 1, 255–320.

Idriss, I. M. (1990). "Response of soft soil sites during earthquakes." *Proc., H. Bolton Seed Memorial Symp.*, Vol. 2, BiTech Publishers, Ltd., Vancouver, 273–290.

Idriss, I. M. (1991). "Earthquake ground motions at soft soil sites." *Proc., 2nd Int. Conf. on Recent Adv. in Geotech. Earthquake Engrg. and Soil Dyn.*, Vol. 3, 2265–2271.

Kayen, R. E., and Mitchell, J. K. (1997). "Assessment of liquefaction potential during earthquakes by Arias intensity." *J. Geotech and Geoenvir. Engrg.*, ASCE, 123(12), 1162–1174.

Kayen, R. E., Mitchell, J. K., Seed, R. B., Lodge, A., Nishio, S., and Coutinho, R. (1992). "Evaluation of SPT-, CPT-, and shear wave-based methods for liquefaction potential assessment using Loma Prieta data." *Proc., 4th Japan-U.S. Workshop on Earthquake-Resistant Des. of Lifeline Fac. and Countermeasures for Soil Liquefaction*, Vol. 1, 177–204.

Kramer S. L. (1996). *Geotechnical earthquake engineering*, Prentice-Hall, Englewood Cliffs, N.J., 653.

Liao, S., and Whitman, R. V. (1986a). "Overburden correction factors for SPT in sand." *J. Geotech. Engrg.*, ASCE, 112(3), 373–377.

Liao, S. S. C., Veneziano, D., and Whitman, R. V. (1988). "Regression models for evaluating liquefaction probability." *J. Geotech. Engrg.*, ASCE, 114(4), 389–411.

Liao, S. S. C., and Whitman, R. V. (1986b). "Catalogue of liquefaction and non-liquefaction occurrences during earthquakes." *Res. Rep.*, Dept. of Civ. Engrg., Massachusetts Institute of Technology, Cambridge, Mass.

Lodge, A. L. (1994). "Shear wave velocity measurements for subsurface characterization." PhD dissertation, University of California at Berkeley.

Marcuson, W. F., III (1978). "Definition of terms related to liquefaction." *J. Geotech. Engrg. Div.*, ASCE, 104(9), 1197–1200.

Marcuson, W. F., III, and Bieganousky, W. A. (1977a). "Laboratory standard penetration tests on fine sands." *J. Geotech. Engrg. Div.*, ASCE, 103(6), 565–588.

Marcuson, W. F., III, and Bieganousky, W. A. (1977b). "SPT and relative density in coarse sands." *J. Geotech. Engrg. Div.*, ASCE, 103(11), 1295–1309.

National Research Council (NRC). (1985). *Liquefaction of soils during earthquakes*, National Academy Press, Washington, D.C.

Olsen, R. S. (1984). "Liquefaction analysis using the cone penetrometer test (CPT)." *Proc., 8th World Conf. on Earthquake Engrg.*, Vol. 3, 247–254.

Olsen, R. S. (1997). "Cyclic liquefaction based on the cone penetration test." *Proc., NCEER Workshop on Evaluation of Liquefaction Resistance of Soils*, Nat. Ctr. for Earthquake Engrg. Res., State Univ. of New York at Buffalo, 225–276.

Robertson, P. K. (1990). "Soil classification using CPT." *Can. Geotech. J.*, Ottawa, 27(1), 151–158.

Robertson, P. K., and Fear, C. E. (1995). "Liquefaction of sands and its evaluation." *Proc., 1st Int. Conf. on Earthquake Geotech. Engrg.*

Robertson, P. K., Woeller, D. J., and Finn, W. D. (1992). "Seismic cone penetration test for evaluating liquefaction potential under cyclic loading." *Can. Geotech. J.*, Ottawa, 29, 686–695.

Robertson, P. K., and Wride, C. E. (1998). "Evaluating cyclic liquefaction potential using the cone penetration test." *Can. Geotech. J.*, Ottawa, 35(3), 442–459.

Schnabel, P. B., Lysmer, J., and Seed, H. B. (1972). "A computer program for earthquake response analysis of horizontally layered sites." *Rep. No. EERC 72-12*, University of California at Berkeley.

Seed, H. B. (1979). "Soil liquefaction and cyclic mobility evaluation for level ground during earthquakes." *J. Geotech. Engrg. Div.*, ASCE, 105(2), 201–255.

Seed, H. B. (1983). "Earthquake-resistant design of earth dams." *Proc., Symp. Seismic Des. of Earth Dams and Caverns*, ASCE, New York, 41–64.

Seed, H. B., and Idriss, I. M. (1971). "Simplified procedure for evaluating soil liquefaction potential." *J. Geotech. Engrg. Div.*, ASCE, 97(9), 1249–1273.

Seed, R. B., Dickenson, S. E., Rau, G. A., White, R. K., and Mok, C. M. (1994). "Site effects on strong shaking and seismic risk: Recent developments and their impact on seismic design codes and practice." *Proc., Struct. Congr. II*, Vol. 1, ASCE, New York, 573–578.

Seed, R. B., and Harder, L. F., Jr. (1990). "SPT-based analysis of cyclic pore pressure generation and undrained residual strength." *Proc., H. Bolton Seed Memorial Symp.*, BiTech Publishers Ltd., Vancouver, 351–376.

Seed, H. B., and Idriss, I. M. (1982). "Ground motions and soil liquefaction during earthquakes." Earthquake Engineering Research Institute Monograph, Oakland, Calif.

Seed, H. B., Tokimatsu, K., Harder, L. F., and Chung, R. M. (1985). "The influence of SPT procedures in soil liquefaction resistance evaluations." *J. Geotech. Engrg.*, ASCE, 111(12), 1425–1445.

Skempton, A. K. (1986). "Standard penetration test procedures and the effects in sands of overburden pressure, relative density, particle size, aging, and overconsolidation." *Géotechnique*, London, 36(3), 425–447.

Stark, T. D., and Olson, S. M. (1995). "Liquefaction resistance using CPT and field case histories." *J. Geotech. Engrg.*, ASCE, 121(12), 856–869.

Stokoe, K. H., II, Lee, S. H. H., and Knox, D. P. (1985). "Shear moduli measurements under true triaxial stresses." *Advances in the art of testing under cyclic conditions*, ASCE, New York, 166–185.

Suzuki, Y., Tokimatsu, K., Koyamada, K., Taya, Y., and Kubota, Y. (1995). "Field correlation of soil liquefaction based on CPT data." *Proc., Int. Symp. on Cone Penetration Testing*, Vol. 2, 583–588.

Sy, A., and Campanella, R. G. (1994). "Becker and standard penetration tests (BPT-SPT) correlations with consideration of casing friction." *Can. Geotech. J.*, Ottawa, 31, 343–356.

Sy, A., Campanella, R. G., and Stewart, R. A. (1995). "BPT-SPT correlations for evaluation of liquefaction resistance in gravelly soils." *Proc., Spec. Session on Dyn. Properties of Gravelly Soil*, ASCE, New York.

Sykora, D. W. (1987). "Creation of a data base of seismic shear wave velocities for correlation analysis." *Geotech. Lab. Misc. Paper GL-87-26*, U.S. Army Engr. Waterways Experiment Station, Vicksburg, Miss.

Transportation Research Board (TRB). (1999). "TRB workshop on new approaches to liquefaction analysis." *Publ. No. FHWA-RD-99-165*, Federal Highway Administration, Washington, D.C. (on CD-ROM).

Tokimatsu, K., and Uchida, A. (1990). "Correlation between liquefaction resistance and shear wave velocity." *Soils and Found.*, Tokyo, 30(2), 33–42.
Vreugdenhil, R., Davis, R., and Berrill, J. (1994). "Interpretation of cone penetration results in multilayered soils." *Int. J. Numer. and Analytical Methods in Geomech.*, 18, 585–599.
Youd, T. L. (1993). "Liquefaction-induced lateral spread displacement." *NCEL Tech. Note N-1862*, U.S. Navy, Port Hueneme, Calif., 44.
Youd, T. L., and Hoose, S. N. (1977). "Liquefaction susceptibility and geologic setting." *Proc., 6th World Conf. on Earthquake Engrg.*, Vol. 3, Prentice-Hall, Englewood Cliffs, N.J., 2189–2194.
Youd, T. L., and Idriss, I. M., eds. (1997). *Proc., NCEER Workshop on Evaluation of Liquefaction Resistance of Soils*, Nat. Ctr. for Earthquake Engrg. Res., State Univ. of New York at Buffalo.
Youd, T. L., Kayen, R. E., and Mitchell, J. K. (1997). "Liquefaction criteria based on energy content of seismograms." *Proc., NCEER Workshop on Evaluation of Liquefaction Resistance of Soils*, Nat. Ctr. for Earthquake Engrg. Res., State Univ. of New York at Buffalo, 217–224.
Youd, T. L., and Noble, S. K. (1997a). "Magnitude scaling factors." *Proc., NCEER Workshop on Evaluation of Liquefaction Resistance of Soils*, Nat. Ctr. for Earthquake Engrg. Res., State Univ. of New York at Buffalo, 149–165.
Youd, T. L., and Noble, S. K. (1997b). "Liquefaction criteria based on statistical and probabilistic analyses." *Proc., NCEER Workshop on Evaluation of Liquefaction Resistance of Soils*, Nat. Ctr. for Earthquake Engrg. Res., State Univ. of New York at Buffalo, 201–215.
Youd, T. L., and Perkins, D. M. (1978). "Mapping of liquefaction-induced ground failure potential." *J. Geotech. Engrg. Div.*, ASCE, 104(4), 433–446.

NOTATION

The following symbols are used in this paper:

a, b = curve fitting parameters for use with V_s criteria for evaluating liquefaction resistance;
a_{max} = peak horizontal acceleration at ground surface;
C_B = correction factor for borehole diameter;
C_E = correction factor for hammer energy;
C_N = correction factor for overburden pressure applied to SPT;
C_Q = correction factor for overburden pressure applied to CPT;
C_R = correction factor for drilling rod length;
C_S = correction factor for split spoon sampler without liners;
$CRR_{7.5}$ = cyclic resistance ratio for $M_w = 7.5$ earthquakes;
d_c = diameter of CPT tip;
F = normalized friction ratio;
f = exponent estimated from site conditions used in calculation of K_σ;
f_s = sleeve friction measured with CPT;
g = acceleration of gravity;
H = thickness of thin granular layer between softer sediment layers;
I_c = soil behavior type index for use with CPT liquefaction criteria;
K_c = correction factor for grain characteristics applied to CPT;
K_H = thin-layer correction factor for use with CPT;
K_α = correction factor for soil layers subjected to large static shear stresses;
K_σ = correction factor for soil layers subjected to large static normal stresses;
M_L = local or Richter magnitude of earthquake;
M_s = surface-wave magnitude of earthquake;
M_w = moment magnitude of earthquake;
m_B = long period body-wave magnitude of earthquake;
m_b = short period body-wave magnitude of earthquake;
N_m = measured standard penetration resistance;
$(N_1)_{60}$ = corrected standard penetration resistance;
$(N_1)_{60cs}$ = $(N_1)_{60}$ adjusted to equivalent clean-sand value;
n = exponent used in normalizing CPT resistance for overburden stress;
P_a = atmospheric pressure, approximately 100 kPa;
P_L = probability of liquefaction;
Q = normalized and dimensionless cone penetration resistance;
q_{c1N} = normalized cone penetration resistance;
$(q_{c1N})_{cs}$ = normalized cone penetration resistance adjusted to equivalent clean-sand value;
r_d = stress reduction coefficient to account for flexibility in soil profile;
V_s = measured shear-wave velocity;
V_{s1} = overburden-stress corrected shear-wave velocity;
V_{s1}^* = limiting upper value of V_{s1} for liquefaction occurrences;
z = depth below ground surface (m);
α, β = coefficients, that are functions of fines content, used to correct $(N_1)_{60}$ to $(N_1)_{60cs}$;
σ'_{vo} = effective overburden pressure;
τ_{av} = average horizontal shear stress acting on soil layer during shaking generated by given earthquake; and
τ_{st} = static shear stress acting on soil element due to gravitational forces.

REPORT NO.
UCD/CGM-04/01

CENTER FOR GEOTECHNICAL MODELING

EVALUATING THE POTENTIAL FOR LIQUEFACTION OR CYCLIC FAILURE OF SILTS AND CLAYS

BY

R. W. BOULANGER
I. M. IDRISS

DEPARTMENT OF CIVIL & ENVIRONMENTAL ENGINEERING
COLLEGE OF ENGINEERING
UNIVERSITY OF CALIFORNIA AT DAVIS

DECEMBER 2004

EVALUATING THE POTENTIAL FOR LIQUEFACTION OR CYCLIC FAILURE OF SILTS AND CLAYS

by

Ross W. Boulanger
I. M. Idriss

Report No. UCD/CGM-04/01

Center for Geotechnical Modeling
Department of Civil & Environmental Engineering
University of California
Davis, California

2004

TABLE OF CONTENTS

1. INTRODUCTION

Evaluating the seismic behavior of a saturated soil, from sand to clay, requires addressing the potential for significant strains or strength loss that can contribute to ground deformations or instability during or following the occurrence of an earthquake. The procedures that are best used to estimate potential strains and strength loss during earthquake loading are different for sand from those for clay, in the same way that the procedures for estimating their static shear strength and stiffness properties are different. The situation is, however, more complicated for low-plasticity silts and clays that are near the transition between "sand-like" and "clay-like" behavior. Recent experiences with ground failure in low-plasticity silts and clays during strong earthquakes have highlighted the need for an improved fundamental understanding of their seismic behavior and for related guidance on the engineering procedures that are most appropriate for evaluating their seismic behavior.

The term "liquefaction" has taken on different meanings in the literature, and it is therefore important to start by defining it and other key terms used in this report. The terms "sand-like" and "clay-like" are used in this report to describe fine-grained soils whose stress-strain behavior during monotonic and cyclic undrained shear loading is fundamentally similar to that of sands and clays, respectively. The term "liquefaction" is used to describe the onset of high excess pore water pressures and large shear strains during undrained cyclic loading of sand-like soils, while the term "cyclic failure" is used to describe the corresponding behavior of clay-like soils. The stress-strain behavior of a sand specimen that develops liquefaction can look quite similar, in some cases, to that of a soft clay specimen that develops cyclic failure. Consequently, the terms liquefaction and cyclic failure do not necessarily imply strong differences in the observed stress-strain response during undrained cyclic shear loading, but rather will be used in reference to soils whose fundamental soil mechanics behaviors are different and whose seismic behaviors are best evaluated using different engineering procedures. The basis for these distinctions is described in more detail in Section 2 of this report.

The purpose of the study described herein was to develop rational guidelines and analytical procedures for evaluating the potential for liquefaction or cyclic failure of low-plasticity silts and clays during earthquake loading. The scope of work involved: (1) developing revised liquefaction susceptibility criteria for fine-grained soils, (2) developing analytical procedures for evaluating the cyclic failure potential of clay-like fine-grained soils, and (3) demonstrating these new criteria and procedures through application to case histories. These tasks are described in more detail at the end of this section, after a brief overview of current liquefaction susceptibility guidelines in engineering practice.

Current guidelines in engineering practice

For the past two decades, the Chinese Criteria have been widely used as a means for evaluating the liquefaction susceptibility of silts and clays. The basis for these criteria came from observations of "liquefaction" in fine-grained soils at various sites in China during strong earthquakes, as reported by Wang (1979). For example, Fig. 1-1 shows Wang's plot identifying those CL, CL-ML, and ML soils that were reported to have liquefied. Wang's paper provided no details regarding how the field data were collected or interpreted, and thus it is not possible to

ascertain whether the true soil behavior would be best described as liquefaction (i.e., sand-like soil behavior) or cyclic failure (i.e., clay-like soil behavior). Nonetheless, there were few data to rely on in 1982, and so Seed and Idriss (1982) incorporated Wang's findings in their monograph, wherein they wrote:

> "Both laboratory tests and field performance data have shown that the great majority of clayey soils will not liquefy during earthquakes. However, recent studies in China (Wang 1979) have shown that certain types of clayey materials may be vulnerable to severe strength loss as a result of earthquake shaking. These soils appear to have the following characteristics (*combined*):
>
> | | |
> |---|---|
> | Percent finer than 0.005 mm | < 15% |
> | Liquid Limit (LL) | < 35 |
> | Water Content | > 0.9 x Liquid Limit |
>
> If soils with these characteristics plot above the A-line on the Plasticity chart, the best means of determining their cyclic loading characteristics is by test. Otherwise, clayey soils may be considered non-vulnerable to liquefaction."

Koester (1992) later showed that LL values determined using the Casagrande cup (US practice) gave LL values that were about 4 percentage points greater than LL values determined using the fall cone device (Chinese practice), and subsequently suggested appropriate changes to these criteria for use in the US.

More recently, Andrews and Martin (2000) reviewed empirical observations from a few case histories, discussed the relevance of various indices, and recommended the following matrix for evaluating liquefaction susceptibility of these soils based on LL and minus 2μm fraction.

Liquefaction susceptibility criteria by Andrews and Martin (2000)

	LL < 32	LL ≥ 32
Minus 2 μm fraction < 10%	Susceptible to liquefaction	Further studies required *[Consider plastic nonclay sized grains]*
Minus 2 μm fraction ≥ 10%	Further studies required [Consider nonplastic clay sized grains]	Not susceptible to liquefaction

LL determined by Casagrande-type percussion apparatus.

Another recent guideline was provided by Seed et al. (2003), who were influenced by observations of ground failure in fine-grained soils in the 1999 Kocaeli and Chi-Chi earthquakes (e.g., Stewart et al. 2003, Bray et al. 2004a,b). The guidelines proposed by Seed et al are graphically shown in Fig. 1-2, wherein the "liquefiability of soils with significant fines content" is described by three zones on the Atterberg Limits Chart; Zone A soils are considered potentially susceptible to "classic cyclically induced liquefaction" if the water content is greater than 80% of the LL; Zone B soils are considered potentially liquefiable with detailed laboratory testing recommended if the water content is greater than 85% of the LL; and Zone C soils (outside Zones A and B) are considered generally not susceptible to classic cyclic liquefaction, although they should be checked for potential sensitivity. These criteria are similar to those

reported by Bray et al. (2004a) based on the results of cyclic triaxial tests on field samples taken from areas of ground failures during the 1999 Kocaeli earthquake. Bray et al. (2004a) concluded that soils with PI≤12 and water contents greater than 85% of the LL were susceptible to liquefaction (note that PI=12 is the upper boundary on Seed et al's Zone A in Fig. 1-2), while soils with 12<PI<20 and water contents greater than 80% of the LL were "systematically more resistant to liquefaction but still susceptible to cyclic mobility" (note that PI=20 is the upper boundary on Seed et al.'s Zone B in Fig. 1-2).

The nature of empirical field data is also well illustrated by the recent results obtained in Adapazari, Turkey by Bray et al. (2004b). They plotted the characteristics of fine-grained soils that were identified as having "liquefied" at 12 building sites during the 1999 Kocaeli earthquake, as shown in Fig. 1-3. The four parts of this figure show gradational characteristics and Atterberg Limits, along with comparisons to the original Chinese Criteria and the criteria by Andrews and Martin (2000). Recognizing that every bullet in these plots is considered a soil that "liquefied," Bray et al concluded that gradational characteristics are not a reliable indicator of liquefaction susceptibility. The guidelines proposed by Seed et al. (2003) and the Atterberg Limits data from Adapazari are compared in Fig. 1-4, showing that Seed et al.'s Zone A provides a close envelope of the data compiled by Bray et al. (2004b). In reviewing these and other field data, the challenge is determining whether a fine-grained soil that appears to have "liquefied" based on damage observations at the ground surface would, in fact, be best described as having fundamentally sand-like rather than clay-like soil mechanics characteristics.

Empirical data and guidelines, like those described above, are best viewed as envelopes of the fine-grained soil types that have been observed to experience significant strains or strength loss during earthquakes. As shown in Figs. 1-1 to 1-4, the field observations have included nonplastic silts (which behave like sands) and soft clays. It would be incorrect, however, to subsequently conclude that the potential for significant strains or strength loss in soil types that fall within these envelopes can be evaluated or predicted using the same set of engineering procedures. In fact, the original statements by Seed and Idriss (1982) recommended cyclic laboratory testing for CL and CL-ML soils (i.e., plotting above the A-line) as opposed to the SPT and CPT procedures that they presented for sands and silty sands. Perlea (2000) presented a recent review of the cyclic loading behavior of "cohesive" soils and similarly concluded that the best way to evaluate their cyclic loading behavior was to perform laboratory testing of field samples. Nonetheless, it has often been assumed that soils classified as "liquefiable" by these various criteria can all be analyzed using the SPT- and CPT-based liquefaction correlations that were derived primarily from case histories involving sands, silty sands, and sandy silts.

It follows that a potential source of confusion in the derivation and use of empirical "liquefaction susceptibility" guidelines for fine-grained soils stems from two related issues: (1) the expectation that the term "liquefaction" should correspond to a single underlying soil mechanics behavior, and (2) the difficulty in accurately inferring fundamental soil mechanics behaviors based on observations of damage at the ground surface. The implicit presumption has commonly been that field observations (e.g., settlements, foundation failures, ground cracking, soil ejecta) can be reliably used to infer the nature of the underlying soil behavior (e.g., sand-like versus clay-like behavior), which is a tenuous situation in many cases. The fact is that the empirical observations, on their own, provide only limited insight into the underlying mechanics

of the soil behavior or the appropriate means to predict that behavior. Without a better basis in soil mechanics, it is impossible to properly judge the applicability of the resulting empirical guidelines to other site and soil conditions. This potential source of confusion can be partly alleviated by maintaining different terms to describe the onset of significant strains in sand-like versus clay-like fine-grained soils, and this is why it is recommended herein that the term "liquefaction" be reserved for describing sand-like soil behavior and the term "cyclic failure" be reserved for describing clay-like soil behavior.

Lastly, a common misuse of empirical liquefaction susceptibility guidelines for fine-grained soils has been the presumption that a classification as "nonliquefiable" means that a soil is not susceptible to strength loss or cyclic failure during an earthquake. This presumption is incorrect as demonstrated by several important case histories, including three that are described in Section 4 of this report.

Purpose and scope of this study

The purpose of this study was to develop rational analytical procedures and guidelines for evaluating the potential for liquefaction or cyclic failure of low-plasticity silts and clays during earthquake loading. The scope consisted of the three main tasks summarized below.

- Establish a soil mechanics framework upon which the undrained cyclic loading behavior of silts and clays with varying levels of plasticity can be grouped and characterized. This task involved a detailed review of experimental test results for fine-grained soils, and included the development of soil-mechanics-based criteria for distinguishing between soils that are susceptible to liquefaction (sand-like behavior) versus cyclic failure (clay-like behavior).
- Develop analysis procedures for evaluating the cyclic failure potential of clay-like soils. The framework for this cyclic failure procedure was kept as similar as possible to the framework that has been used to develop most semi-empirical liquefaction procedures. The resulting procedure offers the ability to directly compare the expected cyclic behavior of saturated sand and clay strata in the same soil profile, and to address the issues of triggering and consequences within the same context for either soil type. Other advantages and insights offered by having a common analysis framework for evaluating both liquefaction and cyclic failure potential are illustrated later in this report.
- Apply the new criteria and procedures to case histories that involved a range of earthquake-induced ground deformations, from acceptable movements to instability, at sites underlain by silt and clay strata. The recommended liquefaction susceptibility criteria and the cyclic failure procedure will be shown to reasonably distinguish between the conditions that did and did not lead to ground deformations at these sites. In addition, these case histories illustrate the limitations inherent in some of the current engineering guidelines and the difficulties with interpreting the underlying soil mechanics behavior of saturated fine-grained soils based solely on the observed ground surface deformation patterns.

The above three tasks are covered in Sections 2, 3, and 4 of this report, respectively, while the major findings and recommendations are summarized in Section 5.

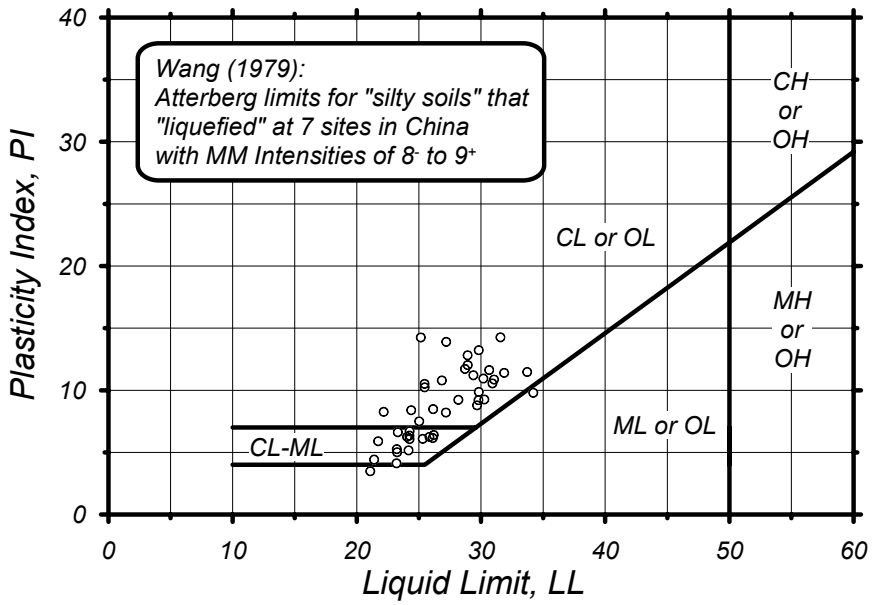

FIG. 1-1: Plasticity chart showing ML-CL and CL soils that were reported to have "liquefied" in China during strong earthquakes (source Wang 1979)

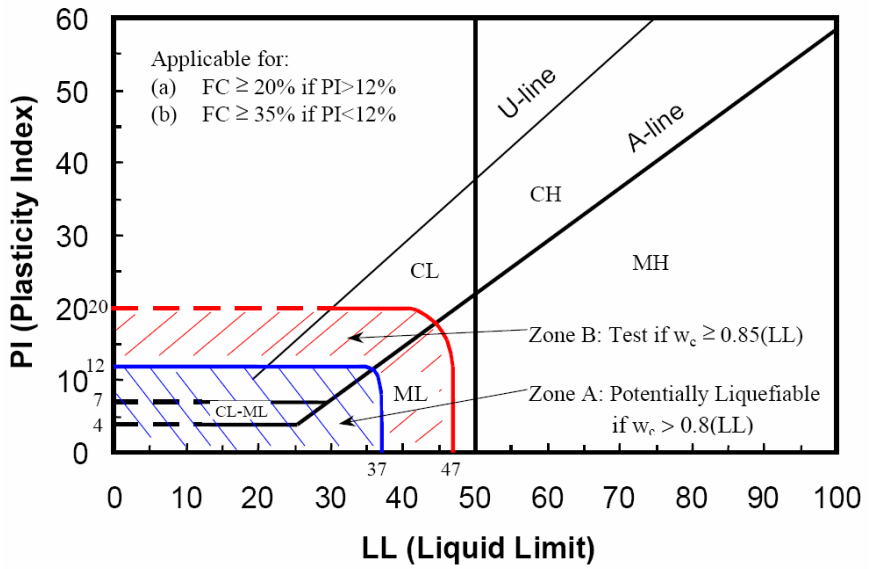

FIG. 1-2: Recommendations by Seed et al. regarding the assessment of "liquefiable" soil types (Seed et al. 2003).

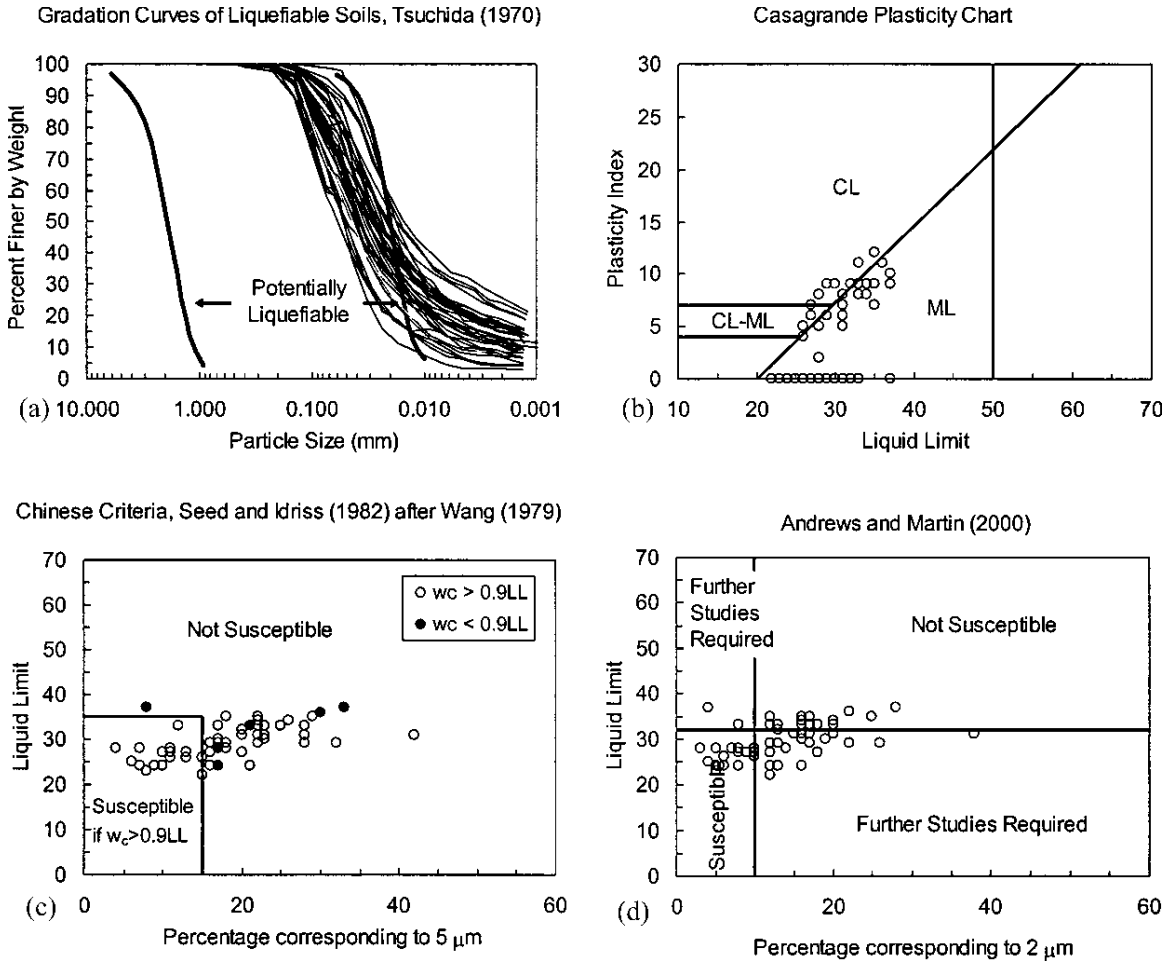

FIG. 1-3: Characteristics of fine-grained soils that were reported by Bray et al. to have "liquefied" at 12 building sites in Adapazari, Turkey during the 1999 Kocaeli earthquake (Bray et al. 2004b): (a) comparison of grain size distributions to the criteria by Tsuchida (1970), (b) Atterberg Limits, (c) LL and percentage finer than 5 μm versus the original Chinese Criteria, and (d) LL and percentage finer than 5 μm versus the criteria by Andrews and Martin (2000).

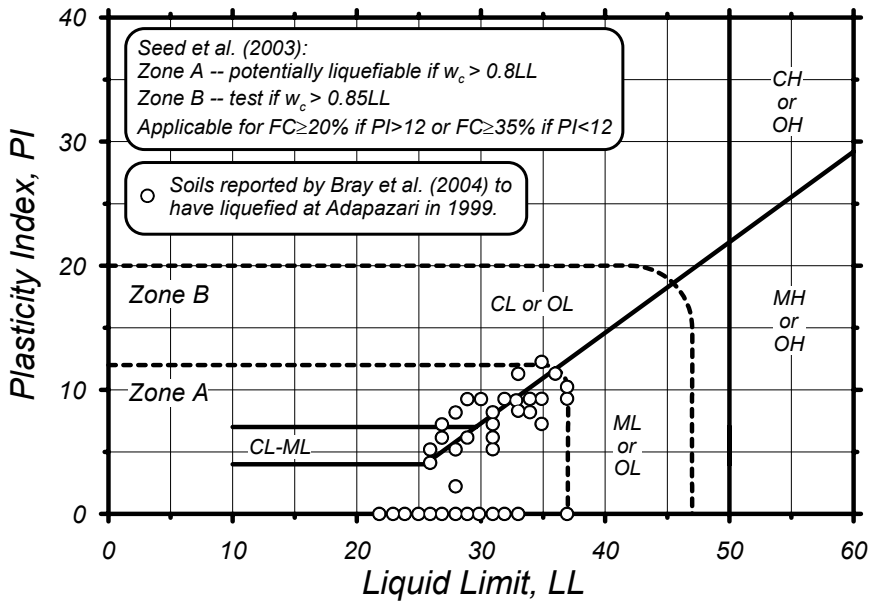

FIG. 1-4: Plasticity chart showing the recommendations by Seed et al. (2003) regarding the assessment of "liquefiable" soil types and the Atterberg Limits of fine-grained soils reported by Bray et al. (2004) to have liquefied in Adapazari during the 1999 Kocaeli earthquake

2. CYCLIC LOADING BEHAVIOR OF FINE-GRAINED SOILS

2.1 Characteristics of sand-like and clay-like soil behavior

Sands and clays have some basic differences in behavior that lead to the use of different engineering procedures for assessing their strength and compressibility characteristics. Classification systems, such as the Unified Soil Classification System (USCS), recognize these differences by emphasizing the importance of particle size and size distribution for coarse-grained soils and the importance of plasticity for fine-grained soils. A review of the basic behavioral differences and corresponding differences in engineering analysis procedures for sands and clays is helpful before addressing the issue of soils with intermediate characteristics.

For sands, some key features of both their behavior and the common engineering procedures used to characterize them are as follows.

- The stress-strain behavior of sand is strongly dependent on its relative density (D_R) and confining stress.
- Sands generally have a small enough compressibility that their D_R does not change significantly as the effective consolidation stress is increased.
- Sands have no unique relation between D_R (or void ratio, e) and confining stress history. Rather, the D_R of sand is more closely determined by the depositional environment and other factors (e.g., seismic loading history).
- The slope of the critical state line in void ratio (e) versus logarithm of mean effective stress (p') space is different from the slope of any virgin consolidation line.
- Sands are highly susceptible to disturbance using conventional tube sampling methods. One contributing factor is that sand can drain during conventional tube sampling, losing most of its effective stress, and therefore becoming easily disturbed by the vibrations and strains imposed during the various steps involved in getting the sample from the bottom of a borehole to the inside of a laboratory device.
- The cyclic loading behavior of sand cannot be reliably determined using laboratory testing of samples obtained using conventional sampling methods because the effects of sampling disturbance are too significant. Recourse to frozen sampling techniques is possible, but the expense makes this a seldom used option.
- SPT and CPT penetration resistances are reasonably sensitive to variations in a sand's D_R and other characteristics, such that these penetration tests can be correlated to various sand behaviors (e.g., from drained effective friction angles to undrained cyclic resistance ratios).
- For the above reasons, it has become common practice to characterize sand deposits using in situ penetration tests and semi-empirical correlations as opposed to laboratory testing of field samples.

For clays, some key features of their behavior and the common engineering procedures used to characterize them are as follows.

- Clays generally have a large enough compressibility that their void ratio or density is highly dependent upon the effective consolidation stress and consolidation stress history.

- Clays can exhibit a relatively unique relation between void ratio and confining stress history.
- The critical state line and virgin consolation lines for many non-cemented clay soils are approximately parallel, which means that the undrained shear strength can be expressed as a relatively unique function of the effective consolidation stress and overconsolidation stress ratio.
- Clays are less susceptible to disturbance from thin-tube sampling techniques, provided sampling is done properly. One contributing factor is that clays are sufficiently impermeable that they remain undrained during sampling, and therefore retain some fraction of their in situ effective confining stress during the sampling process (via negative pore water pressures).
- Monotonic and cyclic undrained strengths of clays can be evaluated using laboratory testing of samples obtained using high-quality sampling techniques. Disturbance effects can be minimized by reconsolidating samples in the laboratory using either the "recompression" or "SHANSEP" techniques, with the choice depending on the characteristics of the particular soil being evaluated (Ladd 1991).
- Determining the preconsolidation stress profile for a clay deposit, whether by consolidation testing or knowledge of the geologic or historical loadings, is usually the single most important step in characterizing a deposit's strength and compressibility characteristics. Subsequently, empirical relations between s_u, σ_{vc}', and OCR for clay can be sufficiently accurate for many engineering applications.
- CPT penetration resistances are directly related to the undrained shear strength of clay and provide a valuable means of assessing the spatial variability of clay deposits. General correlations between undrained shear strength and CPT penetration resistance have significant uncertainty, and thus it is generally advisable to develop site-specific correlations (i.e., laboratory tests or in situ vane shear tests for more accurate point-specific estimates of undrained shear strength that can be used to calibrate the CPT correlation).
- SPT penetration resistances provide only a coarse correlation to the undrained shear strength of clay.
- For the above reasons, it is widely accepted in practice that the most reliable characterization of a clay deposit includes laboratory testing of high quality field samples in combination with a program of in situ testing (e.g., CPT soundings and vane shear testing) and knowledge of the geologic history of the site.

For the broader category of fine-grained soil, the issues are complicated by the transition in engineering behavior that occurs between nonplastic silt (which behaves like sand in many respects) and more plastic clay. The remainder of this section addresses these issues through the following steps:

- The undrained monotonic and cyclic loading behavior of sand is reviewed.
- The undrained monotonic and cyclic loading behavior of clay is reviewed.
- The transition between clay-like and sand-like behavior for fine-grained soils is evaluated and discussed based on experimental observations.
- Index tests for distinguishing between clay-like and sand-like soils are discussed and guidelines for making these distinctions are developed.

- The effects of static shear stresses on the cyclic loading resistances of sand-like and clay-like soils are reviewed, followed by the derivation of simple relations for describing the effects of static shear stresses on the cyclic loading resistances of clay-like soils.

Recall that the terms "sand-like" and "clay-like" were adopted in this study for describing fine-grained soils that exhibit monotonic and cyclic stress-strain behaviors that are fundamentally similar to those of "sands" and "clays," respectively.

2.2 Undrained monotonic and cyclic loading behavior of sand

The behavior of saturated clean sand under undrained monotonic and cyclic loading has been studied extensively, with the resulting behaviors well described in the literature. The purpose of this section is not to provide a complete review of behavior, but rather to draw out some key features that will subsequently provide a useful reference for distinguishing the differences in behavior between sand-like and clay-like fine-grained soils.

The undrained response of saturated sand to monotonic shear loading is illustrated by the triaxial compression test results in Fig. 2-1 for Toyoura sand with D_R of 16, 38, and 64% under consolidation stresses ranging from 10 to 3000 kPa (Ishihara 1993). For any given D_R, the shape of the stress-strain curves and the stress-paths are affected by the consolidation stress (σ_{3c}'), but the undrained shear resistance at large strains is relatively independent of σ_{3c}'. The undrained shear resistance at large strains is, however, very sensitive to D_R, as illustrated by the order of magnitude differences in the scales used to present the results for each value of D_R. The results of these tests are consistent with critical state concepts, in that the undrained critical state strength is strongly dependent on void ratio (or D_R) and essentially independent of initial consolidation stress.

The stress paths for sand in undrained monotonic shearing often show an initially contractive response (positive pore pressure increments since volume change is zero) followed by a transition to an incrementally dilative response (negative pore pressure increments), as illustrated by the data for Toyoura sand in Fig. 2-2. The transition from incrementally contractive to incrementally dilative response during undrained shear is termed phase transformation (Ishihara et al 1975), and it corresponds to a local minimum in the mean effective stress and often a local minimum in the shear resistance (i.e., points P and Q in Fig. 2-2). This local minimum in shear resistance is referred to as a quasi-steady state (QSS) condition (Ishihara 1993), and the line connecting these points on an e-log(p') plot is called the quasi-steady state line (QSSL).

The undrained cyclic loading behavior of saturated sand is illustrated by the results of a stress-controlled cyclic triaxial test on saturated Sacramento River sand shown in Fig. 2-3. As cyclic loading progressed, there was a progressive increase in excess pore water pressure (Δu) and corresponding reduction in mean effective stress (p', expressed as a ratio of the mean consolidation stress $p_c' = (\sigma_{1c}'+\sigma_{2c}'+\sigma_{3c}')/3$). The excess pore pressure ratio ($r_u=\Delta u/\sigma_{3c}'$ for triaxial tests and $r_u=\Delta u/\sigma_{vc}'$ for field conditions) increases to a maximum value of 100%, which corresponds to the sample temporarily having zero effective stress (i.e., p'=0 and q=0). This state of r_u=100% has historically been referred to as "initial liquefaction", although the term

"liquefaction" is also used as a more general term as discussed later. With each cycle of applied shear load (q), the sample alternates between being incrementally dilative (p' increasing) and incrementally contractive (p' decreasing) in its response, with the transition from incrementally contractive to incrementally dilative response being phase transformation. The axial strains remain relatively small until r_u nears 100%, after which the strains grow rapidly with each additional cycle of loading. Note that the triggering of r_u=100% typically corresponds to shear strains of about 2 to 3% (or about 1.4 to 2% axial strain in a triaxial test). The sample strain hardens at the end of each load cycle and develops enough shear strength to resist the peak applied shear load (i.e., it does not develop "flow deformation"). The resulting inverted s-shaped stress-strain loops shown in Fig. 2-3 are an example of what is termed "cyclic mobility," wherein the temporary occurrence of r_u=100% (or initial liquefaction) is accompanied by the development of limited strains.

The undrained cyclic resistance of sand against the triggering of r_u=100% or a specified level of shear strain (e.g., 3%) in some number of equivalent uniform loading cycles is described by a cyclic resistance ratio (CRR), which is the ratio of cyclic stress (τ_{cyc}) to consolidation stress (σ_{vc}'). The in situ CRR of sand is evaluated in practice using semi-empirical correlations such as those shown in Figs. 2-4 and 2-5 for SPT and CPT tests, respectively. These semi-empirical correlations are based on case histories where the occurrence or non-occurrence of liquefaction is judged primarily on the basis of observations of sand boils and ground deformations, such that the actual development of r_u=100% is an inferred condition.

These correlations are developed to be applicable to a σ_{vc}' of about one atmosphere ($P_a \approx 100$ kPa $\approx$ 1 tsf). The increase in CRR with increasing penetration resistance is, in large part, due to the effect of D_R on both CRR and penetration resistance. The extension of these correlations to other σ_{vc}' is accomplished through an overburden stress correction factor, K_σ, as:

$$CRR_{(\sigma'_{vc}/P_a)\neq 1} = K_\sigma CRR_{(\sigma'_{vc}/P_a)=1} \quad (2\text{-}1)$$

The K_σ factor depends on both D_R and σ_{vc}' because of the fact that the relative state of sand depends on both of these parameters. This effect was demonstrated by Boulanger (2003a), after first introducing the relative state parameter index that describes the state of sand relative to an empirical critical state line in e-*log*p' space, as shown in Fig. 2-6. The CRR of sand was then shown to correlate to this relative state parameter index, such that the experimentally observed effects of D_R and σ_{vc}' on CRR could be modeled. The resulting relations were used to derive the K_σ curves shown in Fig. 2-7 (from Boulanger and Idriss 2004).

2.3 Undrained monotonic and cyclic loading behavior of clay

The undrained monotonic and cyclic loading behavior of saturated clay has also been extensively studied and well described in the literature. Similar to the previous section, this section draws out some key features of behavior that are important to subsequent discussions.

First, a key feature of clay stress-strain behavior is that the monotonic undrained shear strength can be closely expressed as a function of consolidation stress history, as illustrated by

the experimental results shown in Figs. 2-8 to 2-10 and discussed in detail by Ladd (1991). The results in Fig. 2-8 illustrate that normalizing shear stresses by the effective vertical consolidation stress can result in relatively unique normalized stress-strain behavior for normally consolidated Maine organic clay in undrained direct simple shear tests. The results in Fig. 2.9 further illustrate that the same stress normalization (i.e., τ/σ_{vc}') produces a normalized stress-strain response that is independent of consolidation stress for Boston Blue clay samples at the same overconsolidation ratio (OCR), based on undrained direct simple shear tests on samples with preconsolidation stresses ranging from 400 to 800 kPa and with OCR of 1 to 8. The lower plot in Fig. 2-9 illustrates how the normalized shear strength can be expressed as a function of OCR. Comparing the stress-strain curves for these clays to those for clean sand in Fig. 2-1, it is clear that the clays show a very plastic stress-strain response (nearly constant shear stress after yield) for OCR of 1 to 8 while the sands showed a range of strain softening to strain hardening behavior that depended on the sand's relative density and confining stress. Note, however, that ACU triaxial compression tests on high-quality intact natural clay samples have shown a larger range of stress-strain behaviors than shown in Fig. 2-9, including significant strain-softening at low OCR and strain-hardening at high OCR.

The test results in Fig. 2-10(a) are for mechanically overconsolidated AGS clay tested according to the SHANSEP (Stress History and Normalized Soil Engineering Properties) technique, whereas the results in Fig. 2-10(b) are for highly sensitive, cemented James Bay clay (i.e., highly structured clay) tested according to the Recompression technique. Recall that the Recompression technique (e.g., Bjerrum 1973) involves re-consolidating samples in the laboratory to the same effective stresses that the sample had been carrying in situ, while the SHANSEP technique (Ladd and Foott 1974) involves re-consolidating samples to effective stresses exceeding the sample's preconsolidation stress, followed by unloading to various levels of overconsolidation ratio. The solid symbols on the James Bay clay plot are for samples consolidated to 1.3 to 3 times the in situ preconsolidation stress (σ_{vp}'), such as would be done for SHANSEP testing. This resulted in a lower undrained strength ratio compared to the recompression results for James Bay clay, illustrating how the SHANSEP technique can be conservative when applied to highly structured clays (Ladd 1991). Both sets of test data illustrate the typical differences in strengths obtained by triaxial compression, direct simple shear, and triaxial extension testing. Most importantly, both sets of data illustrate how the undrained strength of clay can be expressed in the form:

$$\frac{s_u}{\sigma'_{vc}} = S \cdot OCR^m \qquad (2\text{-}2)$$

where S is the value of s_u/σ_{vc}' when the OCR=1 and m is the slope of s_u/σ_{vc}' versus OCR relation on a log-log plot.

Ladd (1991) provided the following recommendations regarding average undrained shear strengths to be used in analyses of staged embankment construction, based on a review of experimental data and field experiences.

- Sensitive marine clays (PI<30%, Liquidity index >1)

  m = 1

  S = 0.20 with nominal standard deviation of 0.015

- Homogenous CL and CH sedimentary clays of low to moderate sensitivity (PI = 20-80%)
  $m = 0.88(1-C_r/C_c)$ or simply $m = 0.8$
  $S = 0.20 + 0.05PI$, or simply $S=0.22$
  [Note that PI is a fraction in the above expression.]
- Northeastern U.S. varved clays
  $m = 0.75$
  $S = 0.16$ (assuming DSS failure mode predominates)
- Sedimentary deposits of silts and organic soils that plot below the A-line on the Atterberg Limits chart (excluding peats) and clays with shells
  $m = 0.88(1-C_r/C_c)$ or simply $m = 0.8$
  $S = 0.25$ with nominal standard deviation of 0.05

Ladd (1991) further noted that a careful assessment of a clay deposit's stress history is required for staged construction analyses at any level of sophistication, and that "this fact, plus the observation that $s_u(ave)/\sigma_{vc}'$ versus OCR for most soils (except varved clays) falls within a fairly narrow range, means that consolidation testing usually represents the single most important experimental component for the design of staged construction projects."

The cyclic stress-strain and stress-path responses of saturated clays are illustrated by the "slow" cyclic triaxial test results for normally consolidated Cloverdale clay in Fig. 2-11 (Zergoun and Vaid 1994). The term "slow" means that the tests were performed sufficiently slow to ensure reliable measurements of pore water pressure, as opposed to the more common seismic loading rates of 1 Hz at which pore pressure measurements are unreliable for clay samples. Similar to the results shown previously for clean sand, the undrained cyclic loading of this clay sample results in a progressive increase in excess pore water pressure (decreasing effective stress) to some limiting level, at which time the sample develops rapidly increasing strains with each subsequent loading cycle. For this clay, the excess pore pressure ratio reaches a limiting value of about r_u=80%, such that the sample never has less than about 20% of its initial effective stress. The stress-strain loops after this limiting r_u has been reached, dissipate considerably more energy than observed for clean sand (i.e., the hysteresis loops are broader). Furthermore, the stress-strain loops for clay do not develop the very flat middle portions (where the shear stiffness is essentially zero) that are observed for sands after they temporarily develop r_u=100%.

The cyclic strength of saturated clays can be expressed as a relatively unique function of the clay's undrained monotonic shear strength, as illustrated by the experimental results summarized in Fig. 2-12 for different natural clays with OCR's of 1 to 4. These results show the cyclic stress ratios required to generate shear strains of 3% during uniform cyclic loading in both triaxial and direct simple shear devices. The cyclic stress ratios, expressed as the ratio τ_{cyc}/s_u, have all been adjusted to an equivalent uniform cyclic loading frequency of 1 Hz based on the observation that cyclic strengths increase about 9% per log cycle of loading rate (e.g., Lefebvre and LeBouef 1987; Zergoun and Vaid 1994; Lefebvre and Pfendler 1996; Boulanger et al 1998). The influence of loading rate is further illustrated in these results by noting that the ratio τ_{cyc}/s_u exceeds unity for failure in one loading cycle because the reference value of s_u is for conventional monotonic loading rates that are much slower. The results for these clays fall within a relatively narrow range, with a cyclic stress ratio of $\tau_{cyc}/s_u = 0.88$ to 1.01 (average 0.92 for DSS tests) required to trigger 3% strain in 15 uniform loading cycles at 1 Hz, as summarized in Table 2-1 along with results for additional soils that are discussed in subsequent sections. It is

also worth noting that Seed and Chan (1966) observed similar cyclic strength ratios for compacted sandy clay and compacted silty clay, suggesting that the cyclic strength ratios shown in these figures may also be applicable to compacted clays as well as natural sedimentary clays.

The roles of effective consolidation stress and stress history on the cyclic strength of clay are adequately represented by their effects on the clay's monotonic undrained shear strength. The practical consequence of this, in comparison to the behavior of clean sands, is that there is no need to introduce an overburden correction factor for clay (i.e., K_σ is not required).

2.4 Transitions between clay-like and sand-like behavior of fine-grained soils

Behavior of three blended silt mixtures in tests by Romero

The transition of a fine-grained soil from behaving like a sand-like soil to that of a clay-like soil is illustrated by the series of monotonic and cyclic undrained triaxial tests performed on three blended silt mixtures by Romero (1995). The three silts were bulk prepared by blending soils collected from different locations within an aggregate mine's tailings pond. All samples were prepared by a slurry sedimentation procedure, with the initial slurry water contents being 2.1 to 2.3 times the silt's liquid limit. Index characteristics for the three silts, all of which classified as ML, were as follows.

- Silt #1: PI=0, LL=26
  81% finer than 74 μm, 5% finer than 5μm, 3% finer than 2μm.
- Silt #2: PI=4, LL=30
  84% finer than 74 μm, 17% finer than 5μm, 11% finer than 2μm.
- Silt #3: PI=10.5, LL=36.5
  87% finer than 74 μm, 25% finer than 5μm, 19% finer than 2μm.

The monotonic undrained stress-strain and stress-path responses of the three silts, when normally consolidated, are illustrated by the triaxial compression test results shown in Fig. 2-13. Silt #3 showed a very plastic stress-strain response with deviator stress and excess pore pressure remaining relatively constant as axial strains increased from about 2 to 20%. This stress strain response and the corresponding q-p' path are very similar to what is observed for normally consolidated clays. In contrast, silt #1 exhibited strain hardening throughout the test, accompanied by excess pore pressures that increased during initial loading but subsequently progressively decreased (incrementally dilative behavior) as axial strains exceeded about 3%. This behavior is manifested in the q-p' plot as a path that initial moves left toward the failure envelope, followed by phase transformation and a dilative path at a relatively constant q/p' ratio. This behavior is very similar to that observed for loose sands at comparable initial consolidation stresses. Silt #2, with a PI of only 4, exhibited behavior that more closely resembles the clay-like soil behavior of silt #3, but with a very slight tendency toward some strain hardening and phase transformation behavior.

The critical state lines (CSL), quasi-steady state lines (QSSL; point of phase transformation), and isotropic consolidation lines (ICL) from isotropically-consolidated undrained (ICU) triaxial compression tests on the three silts are shown in Fig. 2-14. The ICL and CSL for silt #1 are not

parallel, as expected for a sand-like soil. In addition, the ICL for silt #1 was below the CSL over the range of confining stresses studied. Silt #3 had essentially parallel ICL and CSL lines and did not exhibit QSSL behavior, which is consistent with behaviors observed for mechanically consolidated clays. Lastly, silt #2 had approximately parallel ICL and CSL lines like silt #3, but with a QSSL that reflects the previously noted tendency toward very slight post-phase transformation strain hardening (i.e., the QSSL is offset slightly below the CSL).

The cyclic stress-strain responses of normally consolidated specimens of silts #1 and #3, as compared in Fig. 2-15, exhibit the characteristics expected from sand-like and clay-like soils, respectively. Silt #3, with its higher plasticity, had broader hysteresis loops and did not develop the nearly zero stiffness intervals that were exhibited by silt #1 after r_u=100% had been triggered. The effect of plasticity on the hysteresis loops is further illustrated in Fig. 2-16 comparing individual stress-strain loops for three silt specimens at similar strain levels. As expected, silt #2 exhibited hysteretic behavior that was intermediate to that of silts #1 and #3.

The cyclic strength parameters versus number of uniform loading cycles for normally consolidated specimens of the three silts are summarized in Fig. 2-17. In the upper plot, the cyclic stresses were normalized by the initial consolidation stress. These results show that the cyclic strength was lowest for the nonplastic silt #1, intermediate for silt #2, and greatest for silt #3. The cyclic strengths were further normalized by their values at 15 uniform stress cycles, as shown in the middle plot. This plot shows that the slope of the CRR-versus-N relation decreases with increasing plasticity, which is consistent with the established differences between clay-like and sand-like soils (discussed at greater length in section 3). Lastly, the cyclic strengths of silts #2 and #3 were normalized by their respective undrained shear strengths to produce the lower plot. The resulting τ_{cyc}/s_u ratios are smaller than observed for the natural clays summarized in Fig. 2-12. These slurry sedimented silts were tested shortly after reaching the end of primary consolidation, and thus can be expected to have substantially smaller cyclic resistances than natural silts that have aged in situ for hundreds or thousands of years. In addition, the differences in fabric between reconstituted specimens and relatively undisturbed field samples of natural silts appear to have strong effects on undrained shearing behavior, as Hoeg et al. (2000) illustrated through tests for both a natural silt and a silty sand tailings material. For these reasons, the test results by Romero (1995) cannot be viewed as representing the strengths (static or cyclic) expected for field deposits of similar materials, but rather as providing insight into how the soil mechanics behavior changed as the clay content was increased for these mixtures. The τ_{cyc}/s_u ratio for these mixtures may also be significantly different from that for natural deposits of similar soils, although perhaps less so than the differences in τ_{cyc} and s_u individually (since both would be affected in the same way). These issues are discussed further in Section 3.

Behavior of low plasticity tailing slimes

The monotonic and cyclic stress-strain responses of copper tailing slimes summarized by Moriwaki et al. (1982) also provide examples of behavior that help bound the transition between clay-like and sand-like soil behavior. These copper tailing slimes classified as CL and CL-ML, had Atterberg limits that plot just above and parallel to the A-line [Fig. 2-18(a)], had 75-90% fines (finer than 74 μm), and 15-23% clay-size (finer than 2 μm). These slimes exhibited clay-like soil behavior in triaxial and direct simple shear tests on normally consolidated samples with

effective consolidation stresses of about 144 and 478 kPa. The cyclic stress ratio (τ_{cyc}/s_u) to cause 5% peak-peak shear strain during uniform cyclic loading is plotted in Fig. 2-18(b), with the ratios being approximately 20% lower for the triaxial tests. The monotonic undrained strength ratios (s_u/σ_{vc}') were, however, about 68% greater for the triaxial tests (0.404 for triaxial versus 0.241 for direct simple shear), such that the stress-normalized cyclic strengths (τ_{cyc}/σ_{vc}') were about 35% greater for the triaxial than for the direct simple shear tests (Table 2-1). These results are within the range of cyclic strength ratios observed for natural clays with greater plasticity (i.e., PI's of 20-36 for the natural clays in Fig. 2-12 and Table 2-1, versus an average PI of 13 for these slimes).

The Atterberg Limits data for these copper tailing slimes, as shown in Fig. 2-18(a), also illustrate the practical difficulty in describing a soil deposit using single values of LL and PI. For example, the PI values for these slimes ranged from 5 to 19 with an average of 13 and the LL values ranged from 25-40 with an average of 35. In this regard, it is important to note that the four samples with PI values of 5 to 9 showed behaviors consistent with the remaining samples that were more plastic with PI values of 12 to 19.

Soil heterogeneity is an even greater complication when sand-like and clay-like soils are finely inter-layered, as is well illustrated by the results of laboratory tests by Tawil (1997) on tube samples of an iron ore tailing slime. This finely inter-layered slime had portions that were described as a sandy silt slime (PI=0) and portions described as a clayey silt slime (average PI=9.6). The results of monotonic undrained DSS tests shown in Fig. 2-19 include data for four test samples cut from the same sampling tube. These four samples, SS-38, CS-39, SS-40, and CS-41, were taken from sequential layers of sandy silt, clayey silt, sandy silt, and clayey silt, respectively. The observed stress-strain responses clearly demonstrate that the sandy silt exhibited sand-like behavior while the clayey silt exhibited clay-like behavior. Thus, these data illustrate how a deposit of fine-grained soils can contain finely inter-layered soils that exhibit clay-like and sand-like behaviors, and thus careful attention must be given to describing the index characteristics of the different soils comprising the inter-layers, especially when some of them are of very low plasticity (i.e., averaging the PI across the sandy silt and clayey silt portions of this tailing deposit would have obscured important information).

2.5 Index tests for distinguishing between clay-like and sand-like soil behavior

Choice of index tests and their purpose

Existing guidelines for identifying "potentially liquefiable fine-grained soils" have been developed around the Atterberg limits, grain size characteristics, and natural water content, in various combinations as reviewed in Section 1. Atterberg limits have long been used in useful correlations to important fine-grained soil characteristics, such as compressibility and shear strength. They are shown herein to also be a useful index for distinguishing between soils that exhibit clay-like versus sand-like behavior during undrained loading. The role of grain size characteristics in distinguishing between clay-like and sand-like soil behavior is more limited while the role of water content needs to be put in the context of consequences. These latter two

indices are discussed first, before proceeding with the development of guidelines based on Atterberg limits.

The percentage of clay-sized materials, whether using 5 μm or 2 μm, is not a reliable index test for distinguishing between clay-like and sand-like behavior in a fine-grained soil. Mineralogy, which is more important for distinguishing soil behavior, does not correlate reliably with the clay-size fraction. For example, to obtain a reasonable correlation to clay mineralogy, Skempton (1953) had to introduce the activity, A, where A is the ratio of the PI to the percent clay-size (2 μm). Subsequently, the Atterberg limits have proven sufficient on their own for correlating to the stress-strain characteristics of soils, while neither activity nor clay size have proven particularly useful in practice for this purpose.

Comparison of a soil's natural water content (w_n) to its Atterberg limits can provide useful information on the potential for strength loss, but the Chinese Criteria's use of the ratio w_n/LL to evaluate whether a soil is susceptible to liquefaction or not is misleading. The first question is whether the ratio w_n/LL can distinguish between sand-like and clay-like soil behavior, and the fact that it cannot is clear when one considers that either soil type can have high or low ratios depending on its depositional environment and stress history. The second question is whether the ratio w_n/LL can provide insight on the potential for strength loss, and the fact that it can has been well established in the literature, albeit in slightly different forms. The more common representation is in terms of the liquidity index (LI),

$$LI = \frac{w_n - PL}{LL - PL} \tag{2-3}$$

which compares the w_n relative to both the LL and plastic limit (PL). LI has been shown to provide reasonable correlations to a soil's sensitivity (S_t), which is the ratio of the soil's peak s_u to its fully remolded (residual) undrained shear strength (s_{ur}),

$$S_t = \frac{s_u}{s_{ur}} \tag{2-4}$$

For example, Fig. 2-20 shows a correlation between S_t, LI, and effective vertical consolidation stress, while Fig. 2-21 shows the corresponding correlation between LI and remolded undrained shear strength. The following terminology is commonly used for describing sensitive clays (Mitchell 1976):

Clay description	S_t
Insensitive	≈1
Slightly sensitive	1 to 2
Medium sensitive	2 to 4
Very sensitive	4 to 8
Slightly quick	8 to 16
Medium quick	16 to 32
Very quick	32 to 64
Extra quick	> 64

Source: Mitchell (1976)

Thus, high w_n/LL or high LI ratios generally correspond to high S_t values, such that these indices do provide some indication of a soil's susceptibility to strength loss following cyclic failure during earthquake shaking.

For low-plasticity fine-grained soils (e.g., PI in single digit range), the use of either LI or w_n/LL for evaluating the soil's S_t can be complicated by their sensitivity to the normal variances in each of the three measurements (w_n, LL, PL). In the case of nonplastic fine-grained soils, the LI cannot be computed and the usefulness of w_n/LL in practice is not clear, especially since the measurement errors in w_n and LL are potentially greater for nearly nonplastic soils. In summary, it is concluded that comparing a soil's w_n to its Atterberg Limits does not provide a means for distinguishing between sand-like and clay-like soil behavior, but may assist in evaluating the potential for strength loss if earthquake shaking is sufficiently strong to trigger a drop to remolded or residual shear strengths.

Atterberg Limits for distinguishing between clay-like and sand-like soil behavior

Atterberg Limits for fine-grained soils reported to exhibit clay-like behavior were compiled from the literature, as presented in Table 2-2. These data come from both laboratory and field studies on a broad range of fine-grained soils that exhibited clay-like soil behavior. While often not stated in the literature, it is believed that the reported Atterberg Limits for each of these soils are most likely average or representative values.

Atterberg Limits were similarly tabulated in Table 2-2 for sand-like and intermediate behaviors of fine-grained soils. These data include results from a more detailed examination of the behavior of individual samples for a number of studies where the heterogeneity of the source material resulted in test samples that spanned a range of Atterberg Limit values. For example, consider the results shown in Fig. 2-19 for undrained DSS tests on four samples cut from the same sampling tube obtained from an iron ore tailings pond. Two of the samples exhibited sand-like behavior (38 & 40) while two exhibited clay-like soil behavior (39 & 41). For cyclic tests, the distinction was based on comparisons of the stress-strain loops and the peak excess pore pressure ratios, with sand-like soils behaving similarly to that shown in Fig. 2-3 and clay-like soils behaving similarly to that shown in Fig. 2-11.

The values of Atterberg Limits listed in Table 2-2 for fine-grained soils exhibiting clay-like, intermediate, and sand-like behavior are plotted in parts (a), (b), and (c), respectively, of Fig. 2-22. The soils exhibiting clay-like behavior included some ML soils with PI values as low as 9 and some CL-ML soils with PI values as low as 4. Intermediate behavior was observed for samples classifying as CL-ML and ML with PI values of 4 to 5. Sand-like behavior was observed only for ML soils (below the A-line), and with one sample having an average PI of 8.5 (this sample was highly inter-layered with PI values of 6 and 11 obtained in two different portions of the sample).

The LL values in Table 2-2 likely include results from both Casagrande cup (most common in the US) and fall cone (most common in Europe) devices. The Casagrande cup device tends to give LL values that are a few percentage points lower than values obtained with a fall cone device (e.g., Koester 1992). If we adopt the Casagrande cup as our reference test, then many of

the LL values reported by European sources would have to be slightly reduced and the corresponding PI values would also be slightly reduced. Nonetheless, the results in Table 2-2 were left as reported values given the approximations involved in designating single representative values for most natural clay deposits and the general absence of explicit statements regarding the LL testing devices that were used.

The Atterberg Limits for all three groups of soils are plotted together in Fig. 2-23, with a focus on the low plasticity portion of the chart. In addition, detailed results from four individual testing programs are similarly plotted together in Fig. 2-24. Together, these data can be used to develop criteria for distinguishing between soils that exhibit sand-like versus clay-like behavior, as discussed below.

The transition between sand-like and clay-like behavior in fine-grained soils undoubtedly spans across a range of Atterberg Limits, both because the actual soil behavior would smoothly transition with increasing plasticity (or clay content) and because a simple index test like the Atterberg Limits cannot be expected to provide a perfect correlation to a soil's complex stress-strain characteristics. This transition is schematically illustrated in Fig. 2-25 showing how the cyclic strength of a soil may reasonably transition as the PI increases from about 3 to 8. In addition, the data in Figs. 2-23 and 2-24 would suggest that CL-ML soils would transition more toward the left side of the plotted transition zone while ML soils would transition more toward the right side of the plotted transition zone. Note that the LL by itself would not be able to distinguish between the observed behaviors.

For engineering practice, it is recommended that fine-grained soils be considered clay-like if they have PI $\geq$ 7 and sand-like if they have PI < 7. This criterion provides a slightly conservative interpretation of the likely transition interval (Fig. 2-25) which is considered appropriate in the absence of detailed in situ or laboratory testing that shows otherwise. If a soil plots as CL-ML, the PI criterion may be reduced by 1.5 points and still be consistent with the data in Figs. 2-23 and 2-24. The LL and PI values should be based on the Casagrande cup device. For soils whose Atterberg Limits plot significantly away from the data points in these figures (e.g., an unusual combination of high LL and low PI), it would be prudent to perform an appropriate program of in situ and laboratory testing to evaluate the soils' behavioral characteristics. In all cases, the practical application of these criteria will require careful attention to minimizing testing errors and judgment in dealing with the heterogeneity of soil deposits.

Fines content at which the fines fraction constitutes the soil matrix

The preceding discussions have focused on fine-grained soils (i.e., silts and clays) for which the fines content (percent passing the No. 200 sieve) is greater than 50% by definition, but the same findings may be extended to soils with slightly lower fines contents in certain cases. The key issue is whether or not the fines fraction constitutes the stress-carrying matrix or skeleton for the soil mass, with the larger sand-sized (or larger) particles essentially floating (isolated from each other) within the matrix. For many soils, it is likely that the fines fraction forms the load-carrying matrix when the fines fraction exceeds roughly 35%, but the transition may occur at higher or lower fines contents in any specific soil depending on factors such as the soil's full gradational characteristics, mineralogical composition, particle shapes, and depositional

environment or fabric (e.g., see Mitchell 1976). For projects where this transition point is of critical importance, it would be prudent to perform an appropriate program of in situ and laboratory testing to evaluate the soil' behavior characteristics prior to extending these criteria to fines contents less than 50%.

2.6 Effect of static shear stresses on cyclic strength

The cyclic resistance of saturated sand or clay is affected by the presence of an initial static shear stress, as has been shown through numerous laboratory and physical modeling studies. These effects have been presented differently for sands and clays due to their differences in engineering behaviors. For this study, it was advantageous to re-cast the experimental results for clay in the same framework as used for sands. Consequently, the framework for sands is described first, followed by a review of results for clays and the derivation of relations that are convenient for implementation in practice.

Sand-like soils

Seed (1983) developed the K_α correction factor to represent the effects of an initial static shear stress ratio (α) on the liquefaction resistance of sands, and used it to extend the semi-empirical SPT-based liquefaction correlations from level-ground conditions to sloping-ground conditions. K_α relations have been obtained from laboratory studies using:

$$K_\alpha = \frac{(CRR)_{\alpha=\alpha}}{(CRR)_{\alpha=0}} \tag{2-5}$$

which is simply the CRR for some value of α, divided by the CRR for α=0. The term α is the initial static shear stress divided by the effective normal consolidation stress on the plane of interest. For application to field conditions, reference is usually made to horizontal planes such that,

$$\alpha = \frac{\tau_s}{\sigma'_{vc}} \tag{2-6}$$

where τ_s is the horizontal shear stress. The resulting K_α relations are then applied in practice as:

$$(CRR_{M=7.5})_{\alpha=\alpha} = K_\alpha (CRR_{M=7.5})_{\alpha=0} \tag{2-7}$$

where the $(CRR_{M=7.5})_{\alpha=0}$ is obtained from a semi-empirical correlation that corresponds to level ground conditions (α=0) and an earthquake magnitude of 7.5, such as the those shown in Figs. 2-4 and 2-5.

The K_α factor depends on both D_R and σ_{vc}' because of the fact that the relative state of sand depends on both of these parameters. Boulanger (2003a) showed that K_α could be expressed as a function of the relative state of a sand (Fig. 2-6), from which Idriss and Boulanger (2003)

derived expressions relating K_α to SPT or CPT penetration resistances and σ_{vc}'. The resulting relations were used to generate the plots in Fig. 2-26 for a range of SPT penetration resistances and σ_{vc}' of 1 and 4 atm. For sands that are close to the critical state line or on the contractive side of the critical state line, the K_α factor becomes progressively smaller than unity with increasing α. For sands that are considerably dense of critical, the K_α factor becomes progressively greater than unity with increasing α. In this latter situation, the sand's tendency to be dilative in monotonic shearing and the reduction in shear stress reversals with increasing α both contribute to a slower generation of excess pore water pressures and shear strains during undrained cyclic loading.

Clay-like soils

The cyclic resistance of saturated clay is also affected by the presence of an initial static shear stress, as demonstrated in numerous laboratory studies. Figs. 2-27 to 2-29 show results of three such studies. Figure 2-27 shows data from a study by Seed and Chan (1966) involving triaxial testing on compacted silty clay, compacted sandy clay, and undisturbed silty clay. The two compacted soils were only partially saturated, with the degree of saturation being about 95%, while the natural soil was saturated. Samples were subjected to a static sustained stress (without allowing drainage) and then subjected to a cyclic axial stress. The static sustained stress and the cyclic stress were both normalized by the soil's monotonic undrained shear strength, and the combination of stresses producing failure (defined as the stresses at which strains rapidly exceeded the limits of the test device) in 1 or 30 cycles is shown Fig. 2-27. The cyclic strength decreases with increasing static sustained stress, with the resulting relation between τ_{cyc}/s_u versus τ_s/s_u being very similar for all three soils.

Similar results were observed for Drammen clay in direct simple shear tests by Goulois et al. (1985) and Andersen et al. (1988), as summarized in Figs. 2-28 and 2-29, respectively. In the tests by Goulois et al. (1985), all the samples were normally consolidated and were allowed to consolidate (drain) under the sustained static shear stress prior to undrained cyclic loading. In the tests by Andersen et al. (1988), samples were tested at OCR of 1, 4, and 40 (only OCR of 1 and 4 are presented herein) and the samples were not allowed to consolidate under the sustained static shear stress. In these figures, the terms γ_a and γ_{ave} refer to the average shear strain in any one cycle of loading, while γ_{cy} refers to the amplitude of the cyclic component of shear strain in any one cycle. The average shear strain includes the strain induced by the applied static shear stress.

A K_α factor for clay-like soils can now be developed following the same approach used for sand-like soils, but plotting K_α versus τ_s/s_u instead of K_α versus α. Results are shown in Fig. 2-30 for the tests on Drammen clay (OCR of 1 and 4) plus tests on St. Alban clay by Lefebvre and Pfendler (1996). This figure was generated for 10 loading cycles to cause failure. Failure was defined as about 3% peak shear strain (not including strains induced by the static shear stresses), which required interpolation of the published data in some cases. The results are, however, relatively unaffected by the choice of number of loading cycles or failure strain. The resulting K_α curves for Drammen clay are lower for those tests that did not allow consolidation under the sustained static shear stress compared to those tests that did allow consolidation under the static shear stress. This difference in behavior simply reflects the fact that the undrained shear strength of a clay-like soil increases when it is consolidated under a sustained static shear stress (e.g.,

Ladd 1991). The tests on St. Alban clay (at an OCR of 2.2) also did not allow consolidation under the sustained static shear stress, but the resulting K_α values are actually slightly higher than those for the Drammen clay with consolidation under the static shear stress. Nonetheless, the combined set of data in this figure all fall within a relatively narrow band, particularly for $\tau_s/(s_u)_{\alpha=0}$ less than about 0.5.

The K_α results for the Drammen clay with consolidation under the static shear stress was adopted as reasonably representative of the overall results and being more applicable to most situations of interest in seismic design. In particular, most designs for seismic loading would assume that the clay-like soils would have sufficient time to consolidate under the sustained loading of some structure or embankment prior to the occurrence of the seismic design event. Subsequently, the following expression,

$$K_\alpha = 1.344 - \frac{0.344}{\left(1 - \frac{\tau_s}{s_u}\right)^{0.638}} \tag{2-8}$$

was derived to approximate the Drammen clay results, as shown by the comparison in Fig. 2-31. While the data in Fig. 2-31 are for normally consolidated clay, the test results by Andersen et al. (1988) showed very similar relationships for OCR of 1, 4, and 40 when the specimens were not consolidated under the static shear stress. Consequently, it appears reasonable to tentatively assume that the relation shown in Fig. 2-31 is reasonably applicable over a wide range of OCR.

The above expression for K_α can also be recast as a function of the initial static shear stress ratio (α) as used for sand-like soils. This is accomplished by dividing both the numerator and denominator of the τ_s/s_u term by σ_{vc}', and then replacing the resulting s_u/σ_{vc}' term with an appropriate empirical relation as follows:

$$\frac{\tau_s}{s_u} = \frac{\tau_s}{s_u} \cdot \frac{1/\sigma_{vc}'}{1/\sigma_{vc}'} = \frac{\alpha}{s_u/\sigma_{vc}'} = \frac{\alpha}{0.22 \cdot OCR^{0.8}} \tag{2-9}$$

which then produces the expression,

$$K_\alpha = 1.344 - \frac{0.344}{\left(1 - \frac{\alpha}{0.22 \cdot OCR^{0.8}}\right)^{0.638}} \tag{2-10}$$

This expression may be used where an estimate of α is more readily made and it enables a direct comparison of K_α relations for clay-like and sand-like soils.

The K_α versus α relation for clay-like soils, as computed using the above expression, is plotted in Fig. 2-32 for OCR of 1, 2, 4, and 8. The K_α values are lowest for normally consolidated soils and increase with increasing OCR at a given value of α. These curves show

how the cyclic strength of normally consolidated clay-like soils may be negligible if they are already sustaining a static shear stress that is close to their undrained shear strength. Conversely, the cyclic strength of an OCR=8 clay-like soil is only reduced slightly by an α as high as 0.30. This pattern is consistent with that observed for sand-like soils (Figs. 2-26) in that an increasing OCR reduces the contractive tendencies of a clay-like soil in shear. Thus, the results for both clay-like and sand-like soils show that for a given static shear stress ratio, the effect of the static shear stress on cyclic strength is most detrimental for contractive soils.

Table 2-1: Fitting parameters for τ_{cyc}/s_u causing cyclic failure (3% shear strain) versus number of uniform undrained loading cycles

Soil name (Reference source)	**PI**	**Test type**	**OCR**	**Parameter a**	**Parameter b**	**$(\tau_{cyc}/s_u)_{N=15}$**	**(s_u/σ_{vc}') for OCR=1**	**$(\tau_{cyc}/\sigma_{vc}')_{N=15}$ for OCR=1**
Drammen clay (Andersen et al. 1988)	27	DSS	1 & 4	1.289	0.116	0.94	0.214	0.201
Boston Blue clay (Azzouz et al. 1989)	21	DSS	1, 1.38, & 2	1.382	0.149	0.92	0.205	0.189
Cloverdale clay (Zergoun & Vaid 1994)	36	TX	1	1.242	0.129	0.88	0.280	0.246
St. Alban clay (Lefebvre & Pfendler 1996)	20	DSS	2.2	1.426	0.129	1.01	0.248	0.250
Itsukaichi clay (Hyodo et al. 1994)	73	TX	1	1.190	0.095	0.92	0.390	0.359
Copper tailings slime (Moriwaki et al. 1982)	13	TX	1	0.931	0.137	0.64	0.404	0.260
		DSS	1	1.20	0.149	0.80	0.241	0.193
Aggregate tailings slime (Romero 1995)	10½	TX	1	0.830	0.073	0.68	0.340	0.231
				Average for DSS = 1.32	Average for DSS = 0.135	Average for DSS = 0.92	Average for DSS = 0.227	Average for DSS = 0.208

Notes:

[a] Fitting parameters are for $(\tau_{cyc}/s_u) = aN^{-b}$, with N = number of loading cycles. All test data adjusted to equivalent 1 Hz loading prior to fitting.

[b] DSS is direct simple shear, TX is triaxial.

[c] For TX tests, $s_u = q_{peak}/2$ and $\tau_{cyc} = q_{cyc}/2$.

Table 2-2: Atterberg Limits for fine-grained soils that have exhibited clay-like, intermediate, and sand-like soil behavior.

	Soil name	USCS	LL	PI	Reference
(a) Cohesive soil behavior					
	Connecticut valley varved clay - silt varves	CL	39	15	Ladd (1991)
	B2 marine clay - James Bay	CL	24	8	Ladd (1991), Ladd & DeGroot (personal files)
	B6 marine clay - James Bay	CL	37	13	Ladd (1991), Ladd & DeGroot (personal files)
	resedimented BBC	CL	44	21	Ladd (1991), Azzouz et al. (1989)
	AGS marine clay	CH	73	43	Ladd (1991), Ladd & DeGroot (personal files)
	Omaha Nebr. Clay	CH	92	60	Ladd (1991), Ladd & DeGroot (personal files)
	Arctic silt A	ML	50	15	Ladd (1991), Ladd & DeGroot (personal files)
	Arctic silt B	MH	68	30	Ladd (1991), Ladd & DeGroot (personal files)
	EABPL clay	CH	95	75	Ladd (1991), Ladd & DeGroot (personal files)
	Tailings slime (copper ore)	CL	32	10	Ladd (1991)
	Cloverdale clay	CL/CH	50	24	Zergoun and Vaid (1994)
	Drammen clay	CH	55	27	Andersen et al. (1988), Goulois et al. (1985)
	Itsukaichi clay	MH	124	73	Hyodo et al. (1994)
	Kaolinite clay	CH	65	40	Ansal and Erken(1989)
	San Francisco Bay Mud	MH	88	43	Seed and Chan (1966), Thiers and Seed (1968)
	Compacted silty clay	CL	37	14	Seed and Chan (1966)
	Compacted sandy clay	CL	35	16	Seed and Chan (1966)
	Newfield glacial lake clay	CL	28	10	Sangrey et al. (1969)
	Studenterlunden	CL	37	20	Berre and Bjerrum (1973), from Larson (1980)
	Ellingsrud (lab & embankment failure)	ML	24.5	4.5	Aas 1976a,b (from Larson 1980)
	Drammen lean clay	CL	33	10	Berre and Bjerrum (1973), from Larson (1980)
	Manglerud	CL	28	9	Berre (1972), from Larson (1980)
	Mastemyr	CL	29	7	Berre (1972), from Larson (1980)
	Olav Kyrres Plass	CL-ML	25	4.5	Karlsrud and Myrvoll (1976)
	Bekkelaget (quick clay slide)	CL	27	7.5	Eide (1955), from Larson (1980)
	Portsmouth NH (embankment failure)	CL	35	15	Ladd (1972), from Larson (1980)
	Trogstad (long slope failure)	CL	25	7	Gregersen (1976), from Larson (1980)
	Furre (quick clay slide)	CL	32	10	Gjerrum et al. (1960), from Larson (1980)
	Mastenyr (embankment failure)	CL	30	10	Clausen (1970), from Larson (1980)
	Rupert 7 (embankment failure)	CL	33	13	Dascal and Tournier (1975), from Larson (1980)
	Tailings slime (copper ore)	CL	35.2	12.6	Moriwaki et al. (1982)
	Bootlegger cove clay (4th Avenue slide)	CL	39	14	Idriss (1985), Stark & Contreras (1998)
	CWOC silt -- higher plasticity samples	ML	41	10	Woodward Clyde Consultants (1992a)
	Iron ore tailings - clayey silt slime	ML	35.3	9.6	Tawil (1997)
	Silty clay at MLML -- average ML	ML	35.5	9	Boulanger et al. (1995)
	Silty clay at MLML -- average CL	CL	37.5	16.3	Boulanger et al. (1995)
	Aggregate mine tailings - mixture #3	ML	36.5	10.5	Romero (1995)
	St. Alban clay	CL	41	20	Lefebvre & Pfendler (1996)
(b) Intermediate soil behavior					
	Piedmont reservoir	CL-ML	23	5	Boulanger and Dismuke (personal files 2003)
	CWOC silt -- lower plasticity samples	ML	35	5	Woodward Clyde Consultants (1992a)
	Aggregate mine tailings - mixture #2	ML	30	4	Romero (1995)
(c) Cohesionless soil behavior					
	Silica flour	ML	20	0	Shen et al. (1989)
	Silt at Moss Landing (MLR3)	ML	33.5	6-11	Boulanger et al. (1998)
	Chino tailings slime (typical properties)	ML	24.5	3.5	Woodward Clyde Consultants (1992b)
	Iron ore tailings - sandy silt slime	ML	24	0	Tawil (1997)
	Aggregate mine tailings - mixture #1	ML	26	0	Romero (1995)
	Borlange silt	ML	n.a.	5[c]	Hoeg et al. (2000)

[a] USCS, Unified Soil Classification System.

[b] Representative values for liquid limit (LL) and plasticity index (PI).

[c] LL likely by fall cone method. PI likely smaller for a LL by the Casagrande cup method (Dyvik, personal communication)

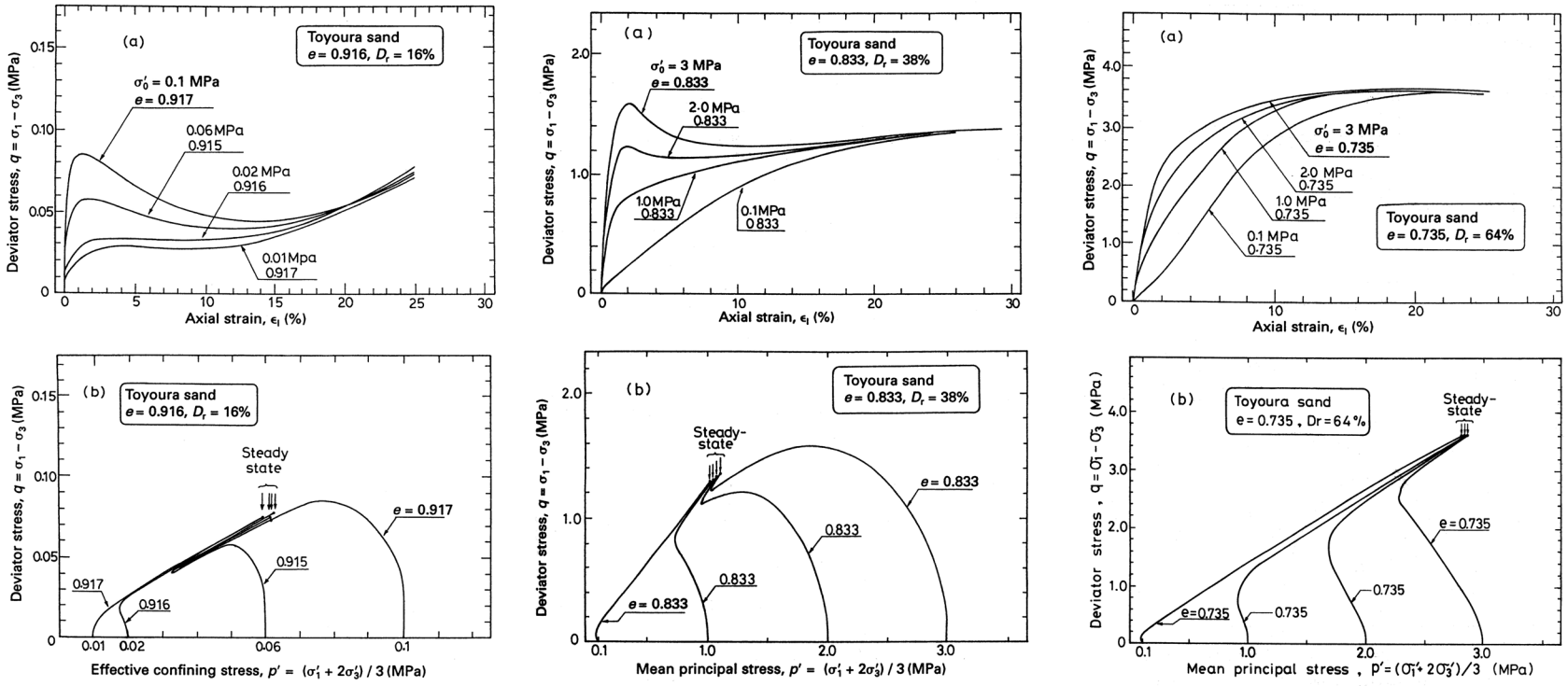

FIG. 2-1: Monotonic loading response of saturated Toyoura sand in isotropically-consolidated undrained triaxial compression tests: (a) D_R =16%, (b) D_R =38%, (c) D_R =64% (Ishihara 1993).

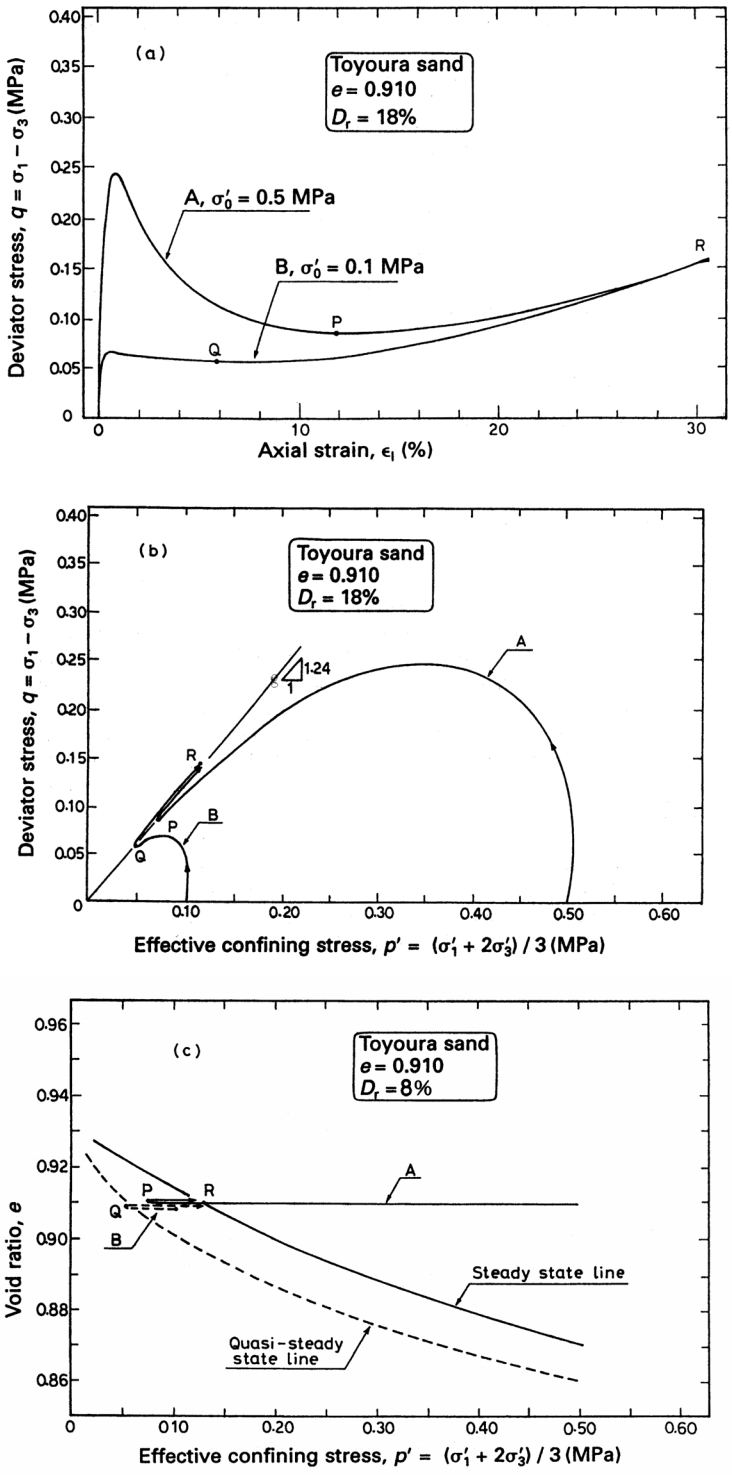

FIG. 2-2: Quasi-steady state (QSS) and steady state behavior of very loose Toyoura sand in ICU triaxial compression tests (Ishihara 1996).

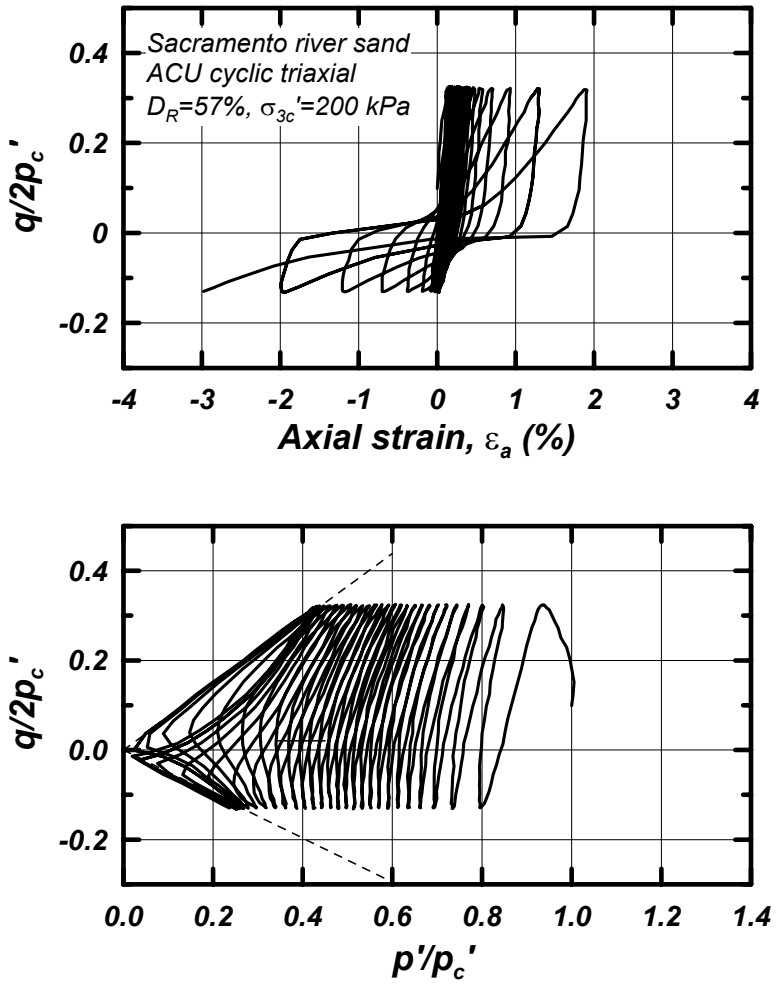

FIG. 2-3: Stress-strain response and effective stress path for Sacramento River sand during undrained cyclic triaxial loading (from Boulanger and Truman 1996).

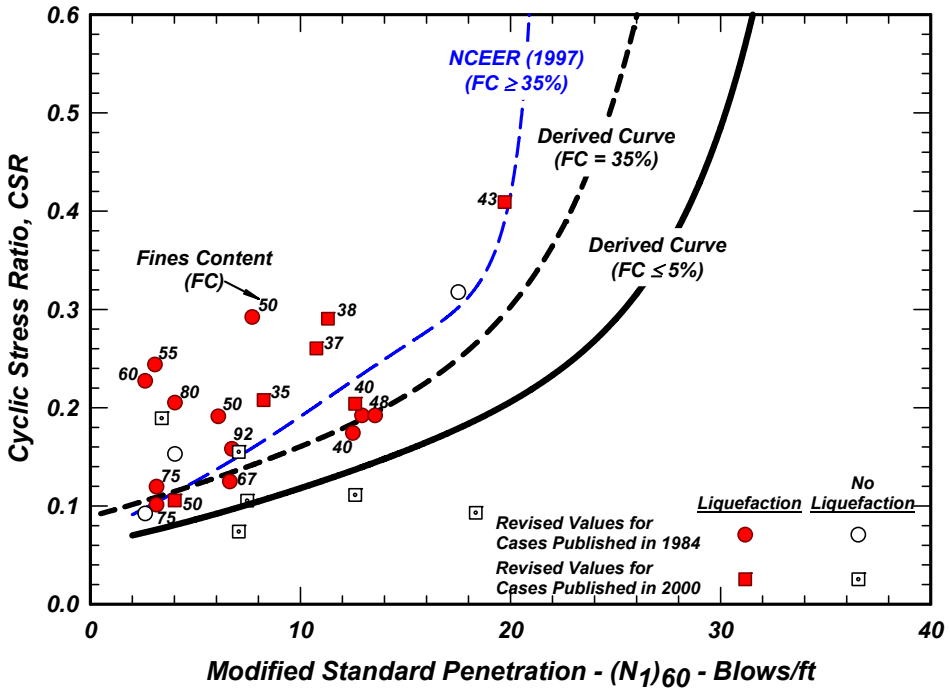

FIG. 2-4: SPT case histories of silty sands, sandy silts, and silts with $FC \geq 35\%$, the NCEER Workshop (1997) curve for $FC = 35\%$, and the Idriss and Boulanger (2004) curves for both clean sand and for $FC = 35\%$ for $M = 7½$ and $\sigma'_{vo} = 1$ atm (≈ 1 tsf). [Idriss and Boulanger 2004].

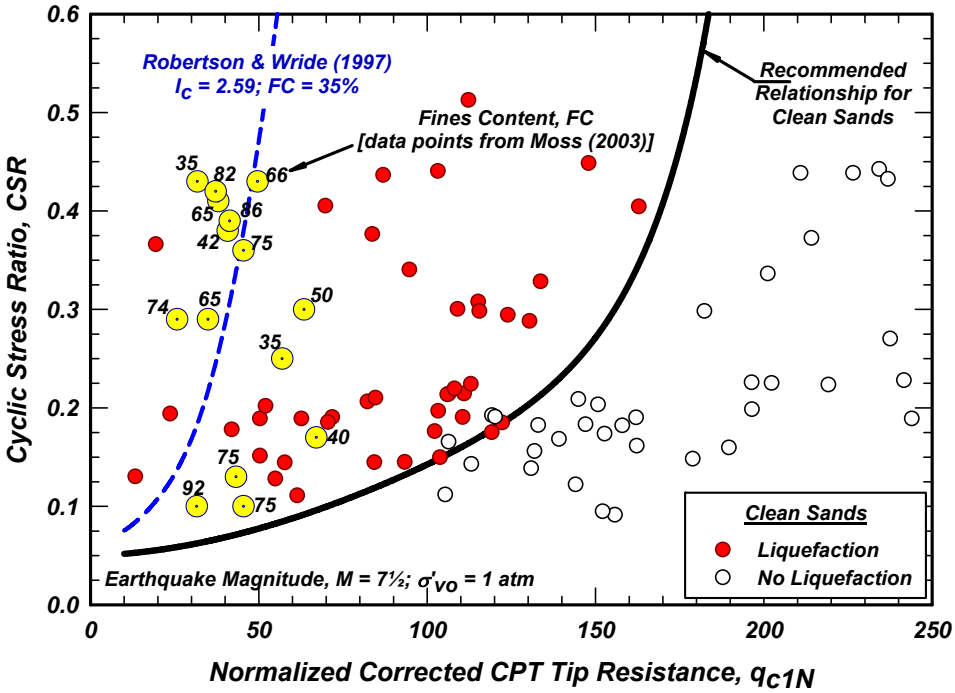

FIG. 2-5: Comparison of field case histories for silty sands, sandy silts, and silts and the curve proposed by Robertson & Wride (1997) for soils with $I_c = 2.59$ (apparent $FC = 35\%$) [Idriss and Boulanger 2004].

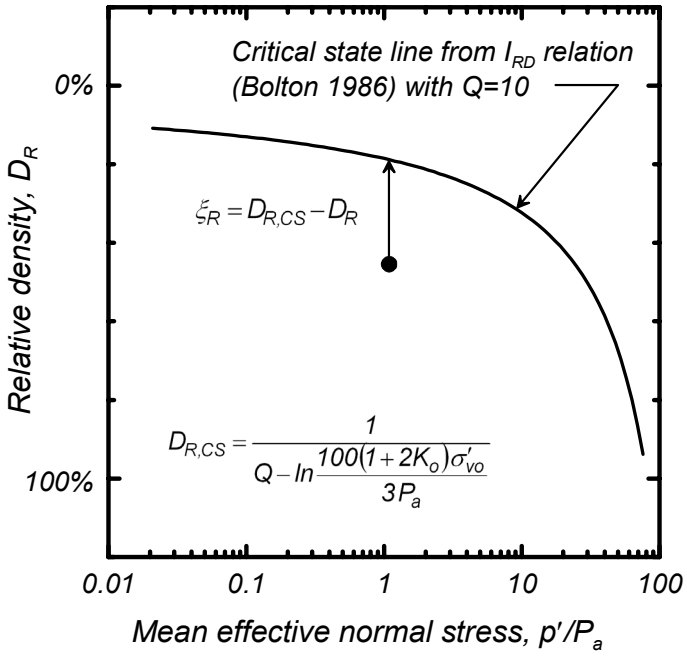

FIG. 2-6: Definition of the relative state parameter index (after Boulanger 2003a).

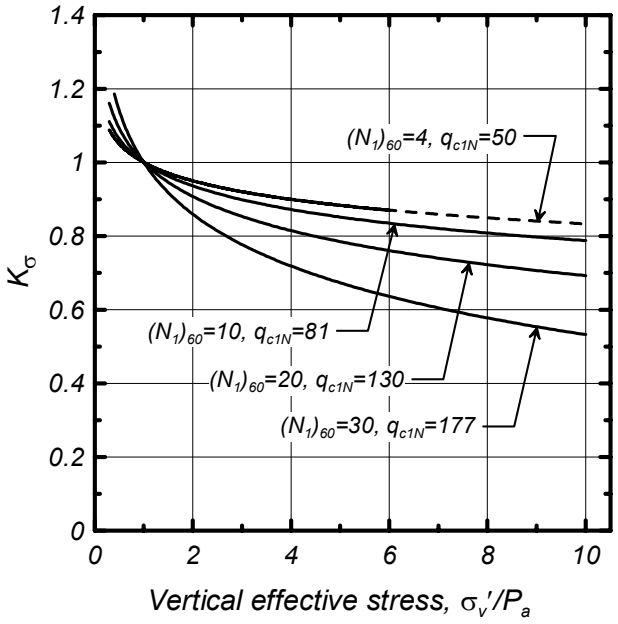

FIG. 2-7: κ_σ relations derived from ξ_R relations (Boulanger and Idriss 2004).

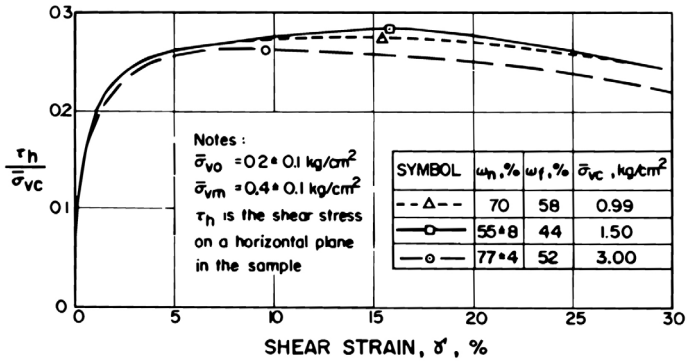

FIG. 2-8: Normalized shear stress versus shear strain response of normally consolidated Maine Organic clay in undrained direct simple shear tests (Ladd and Foott 1974).

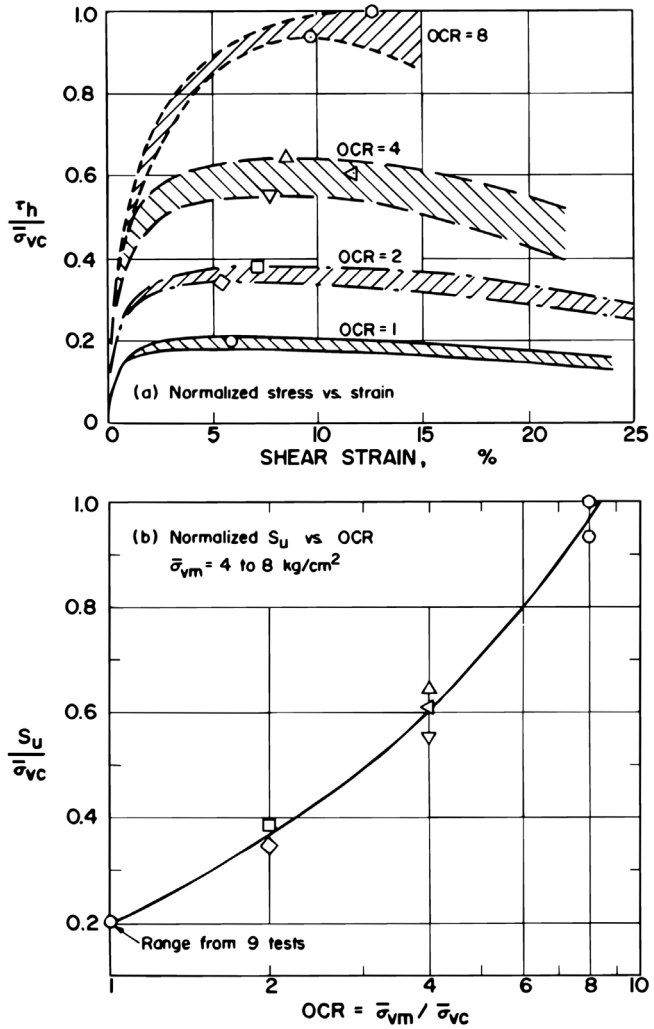

FIG. 2-9: Normalized shear stress versus shear strain response of Boston Blue clay in undrained direct simple shear tests on samples with preconsolidation stresses of 400 to 800 kPa and OCR of 1, 2, 4 and 8, and the variation of normalized shear strength versus OCR (Ladd and Foot 1974).

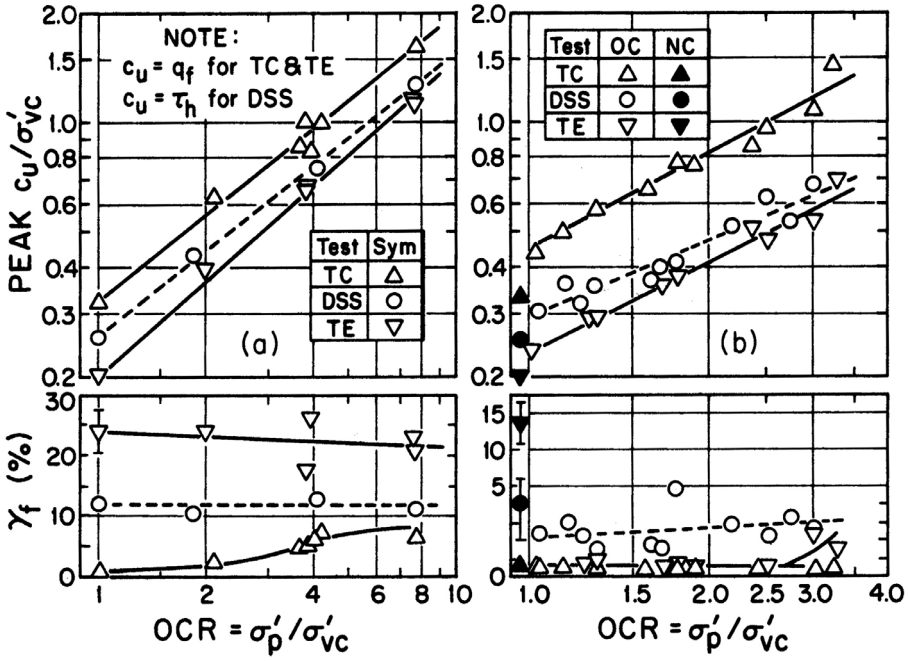

FIG. 2-10: Undrained shear strength ratios versus OCR and shear strain at failure versus OCR for CK_oU tests on (a) AGS plastic marine clay via SHANSEP and (b) James Bay sensitive marine clay via recompression. [from Ladd 1991]

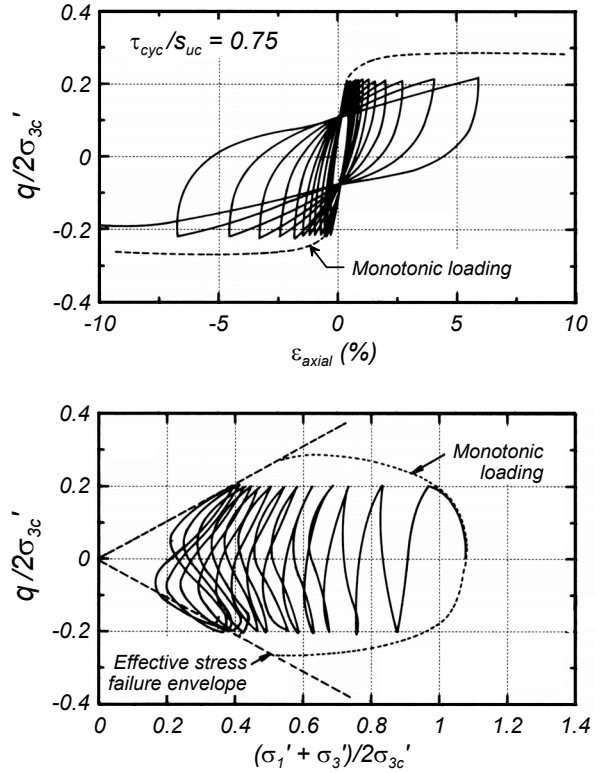

FIG. 2-11: Stress-strain response and effective stress paths for Cloverdale clay during undrained slow cyclic loading (Zergoun and Vaid 1994).

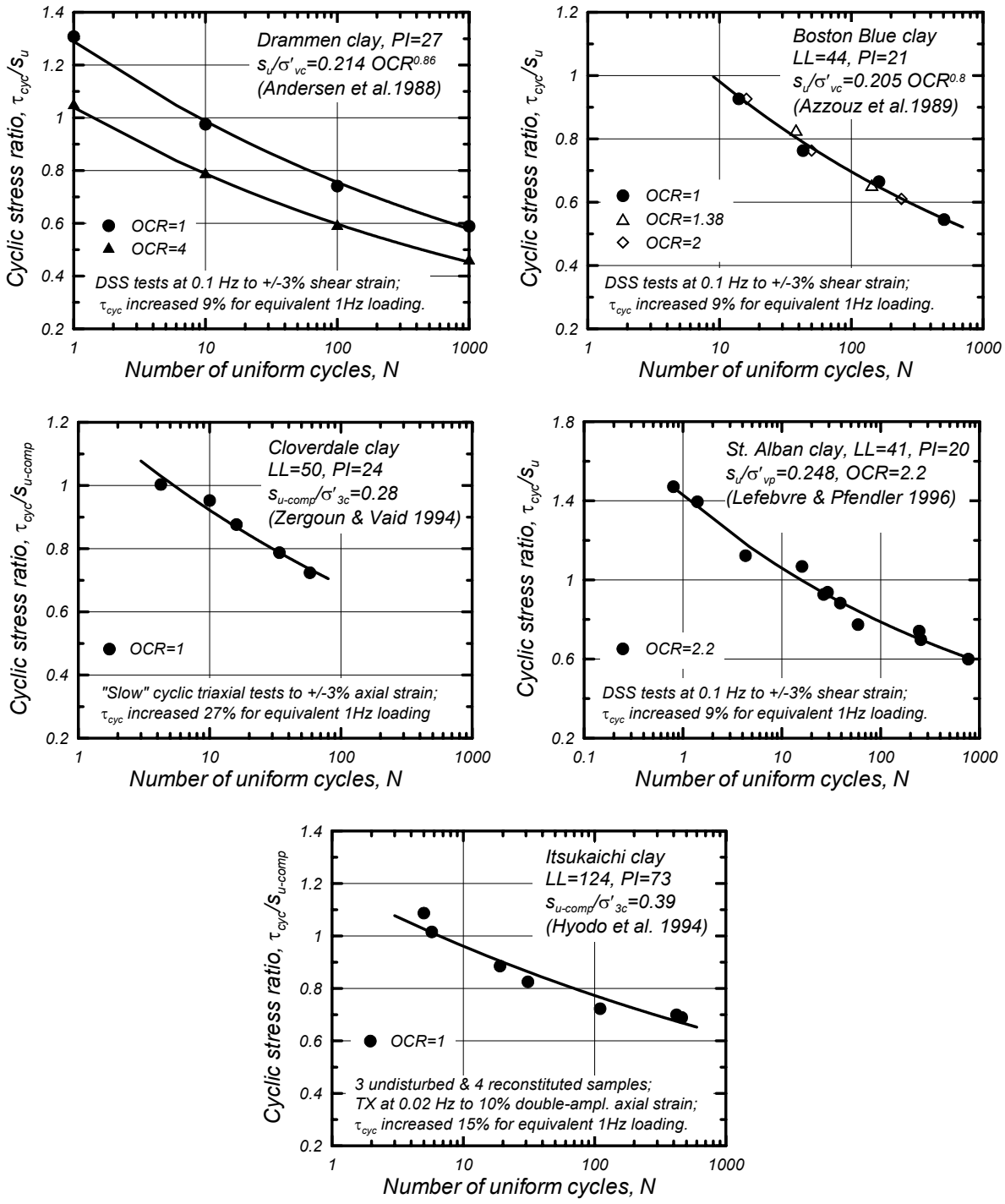

FIG. 2-12: Cyclic strength ratios for uniform cyclic loading of five saturated clays: (a) Drammen clay with OCR of 1 and 4, (b) Boston Blue clay with OCR of 1, 1.38, and 2, (c) Cloverdale clay with OCR of 1, (d) St. Alban clay with OCR of 2.2, and (e) Itsukaichi clay with OCR of 1.

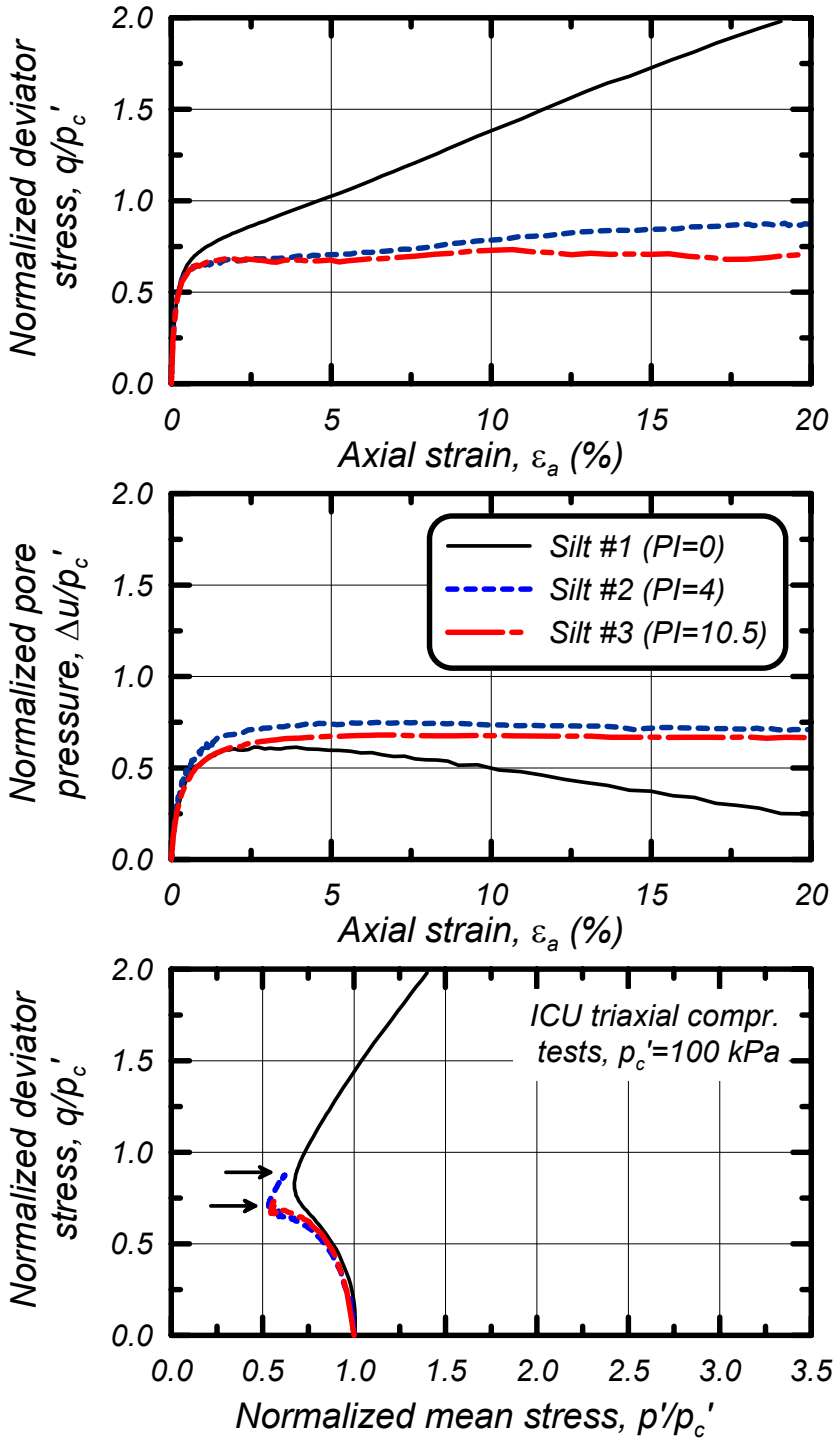

FIG. 2-13: Results of ICU triaxial compression tests on normally consolidated specimens of three blended silt mixtures (after Romero 1995)

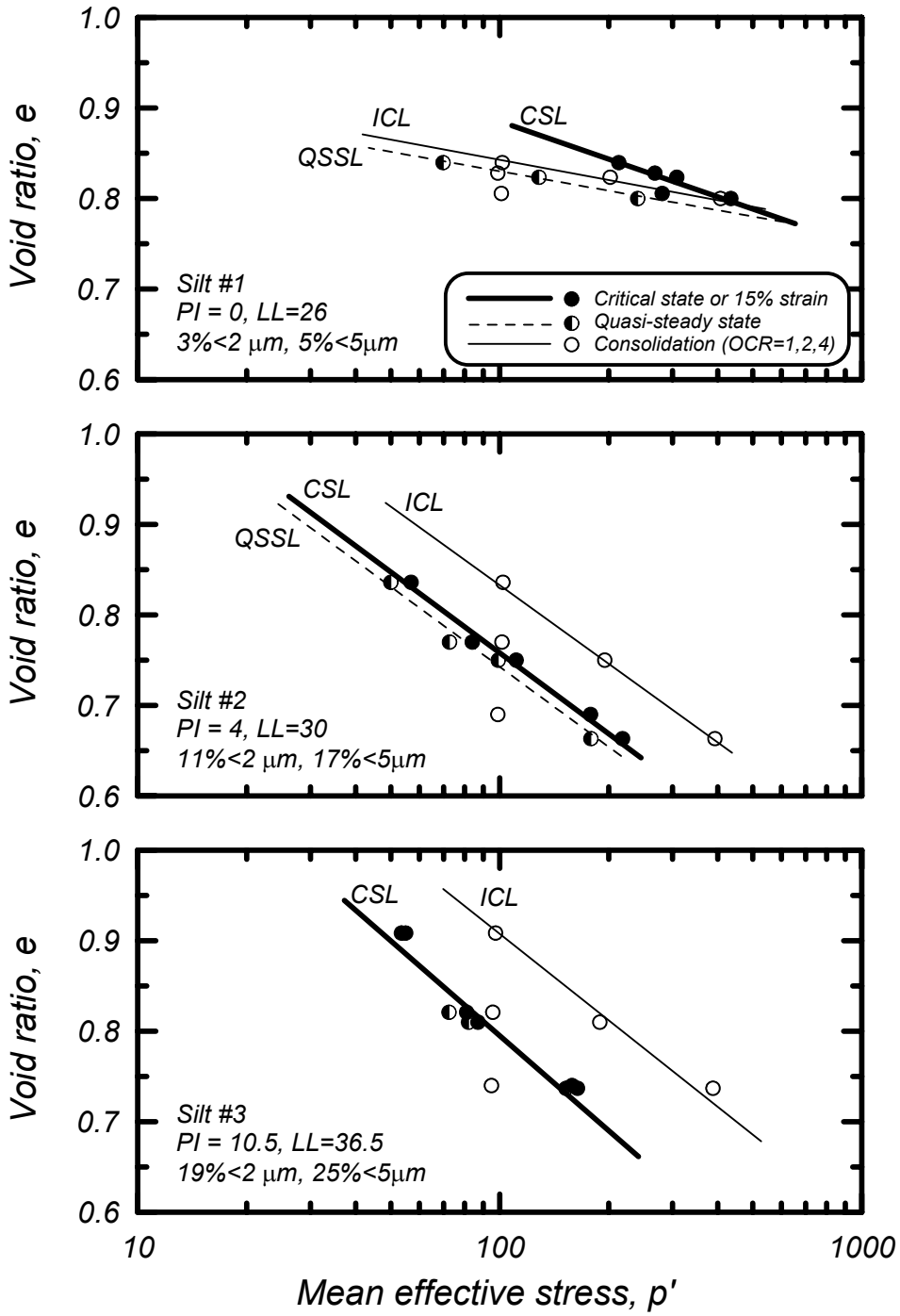

FIG. 2-14: Critical state lines (CSL), quasi-steady state lines (QSSL), and isotropic consolidation lines (ICL) from ICU triaxial compression tests on three blended silt mixtures (after Romero 1995)

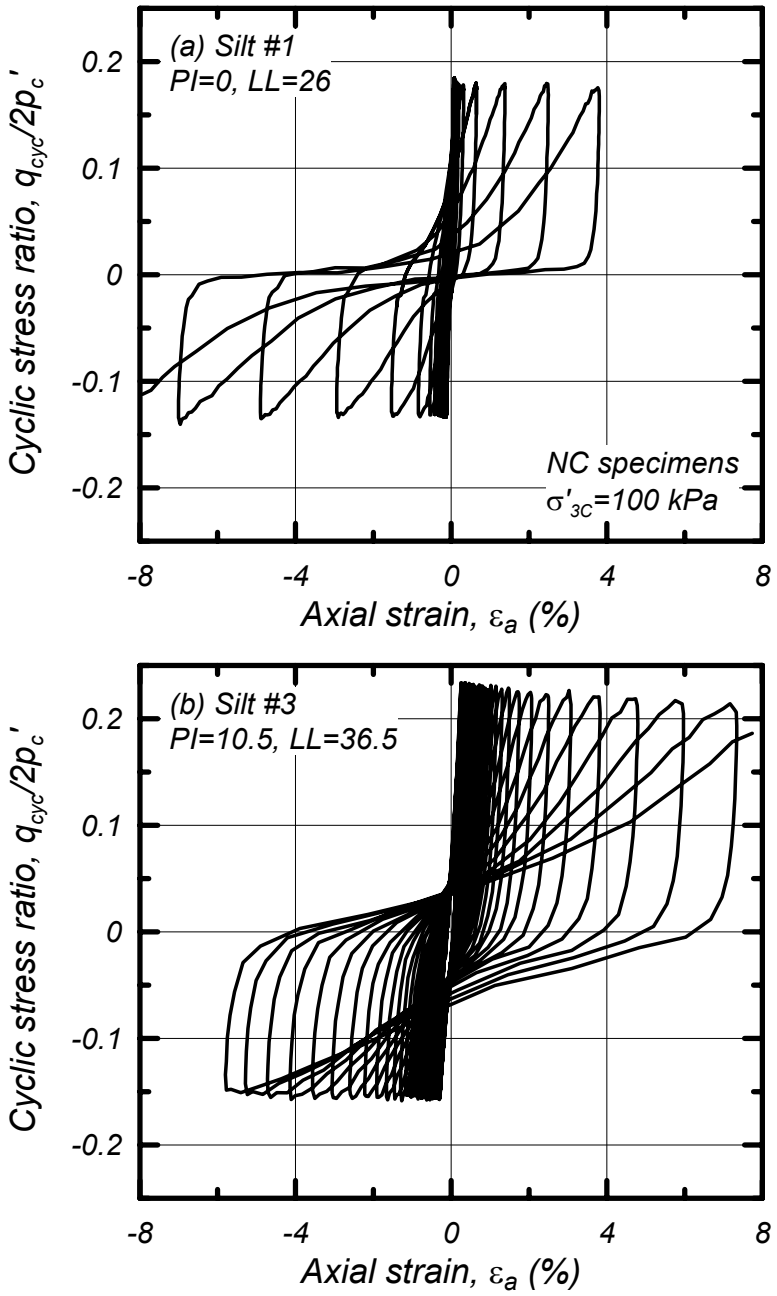

FIG. 2-15: Stress-strain response for normally consolidated specimens of two silt mixtures during undrained cyclic triaxial loading (after Romero 1995)

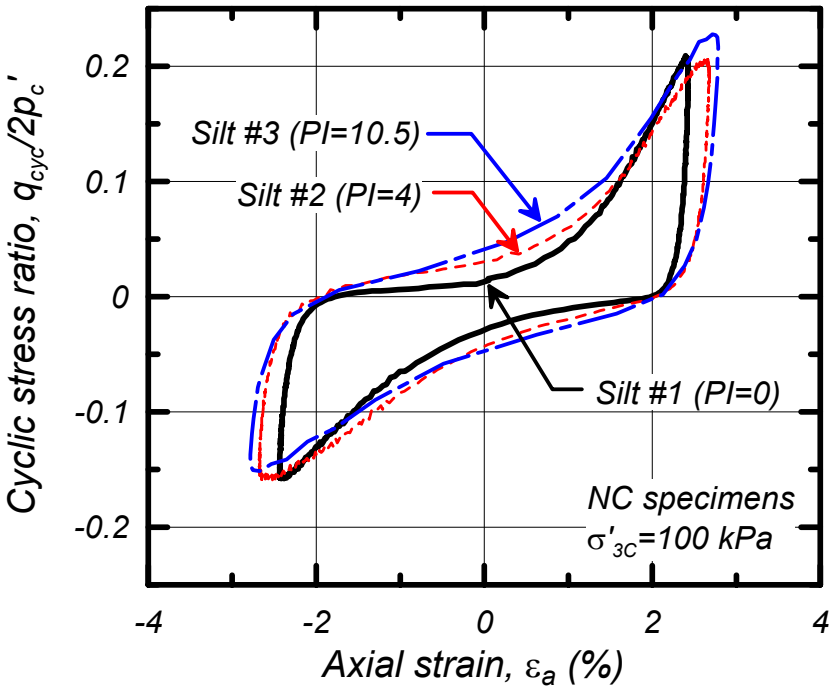

FIG. 2-16: Stress-strain loops for normally consolidated specimens of three blended silt mixtures at similar strain levels during undrained cyclic triaxial loading (after Romero 1995)

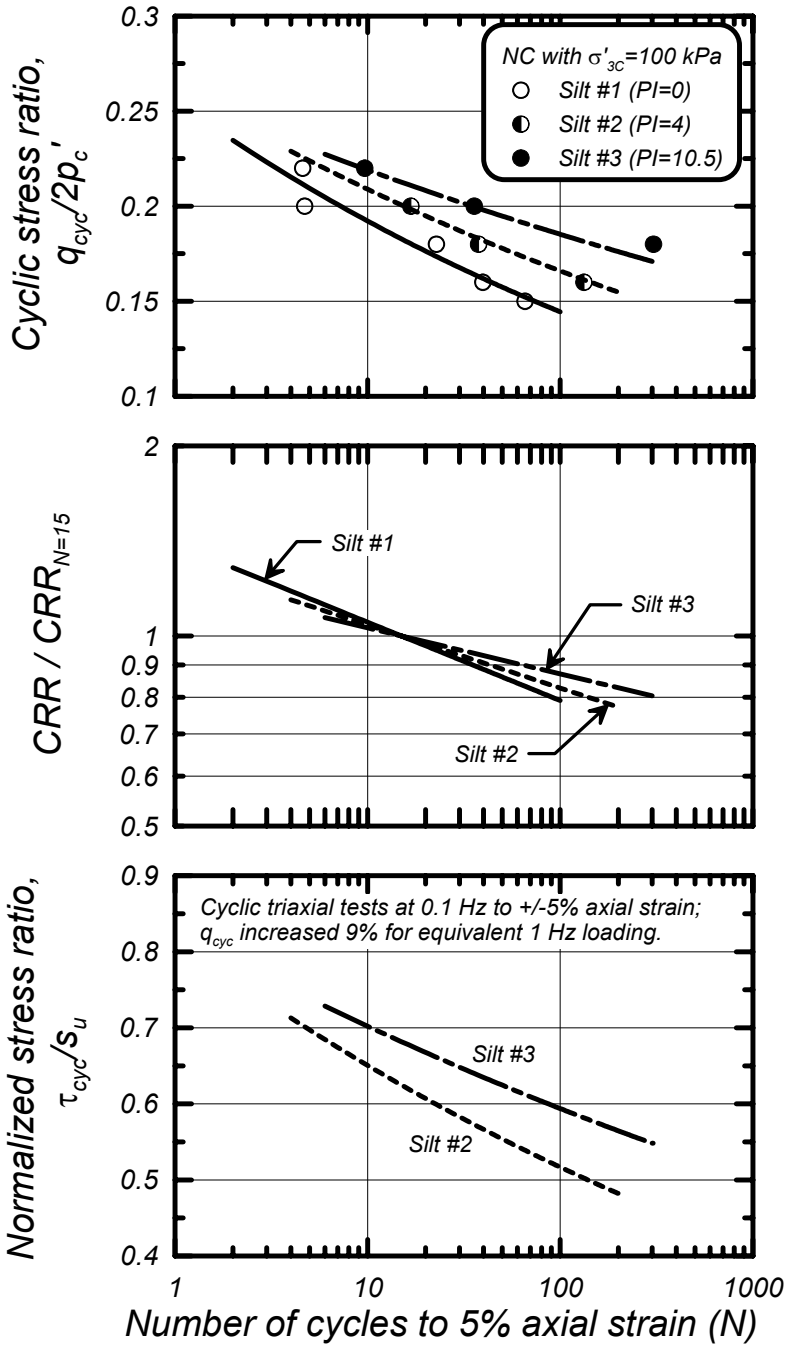

FIG. 2-17: Normalized cyclic stress ratios to cause 5% peak axial strain on normally consolidated specimens of three blended silt mixtures (data from Romero 1995)

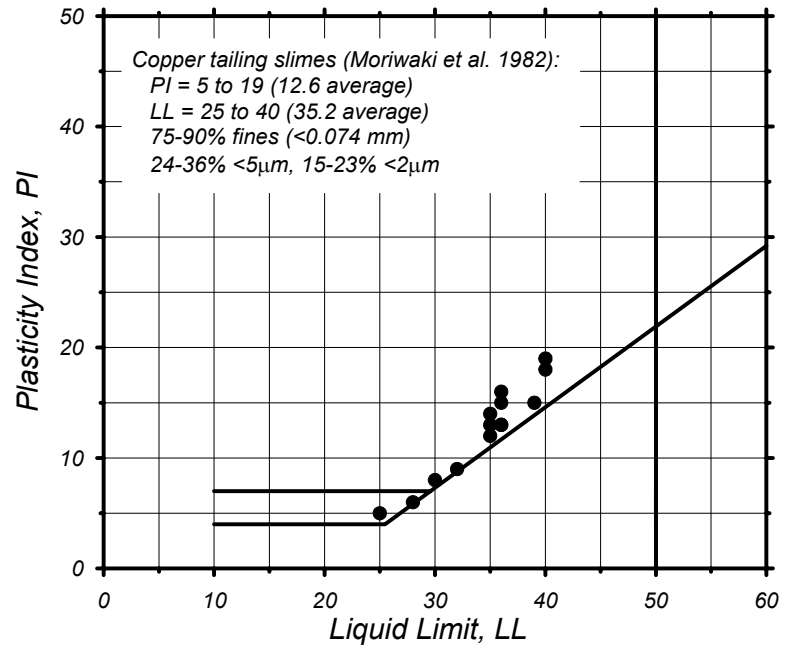

(a)

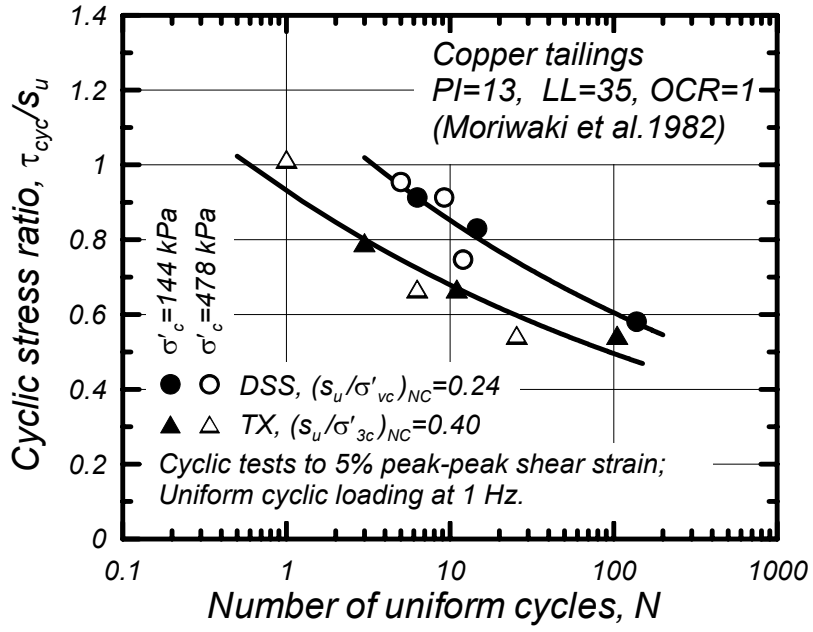

(b)

FIG. 2-18: Cyclic testing results for copper tailing slimes (data from Moriwaki et al. 1982):
(a) Atterberg limits for test specimens, and
(b) Cyclic strength ratio versus number of uniform loading cycles.

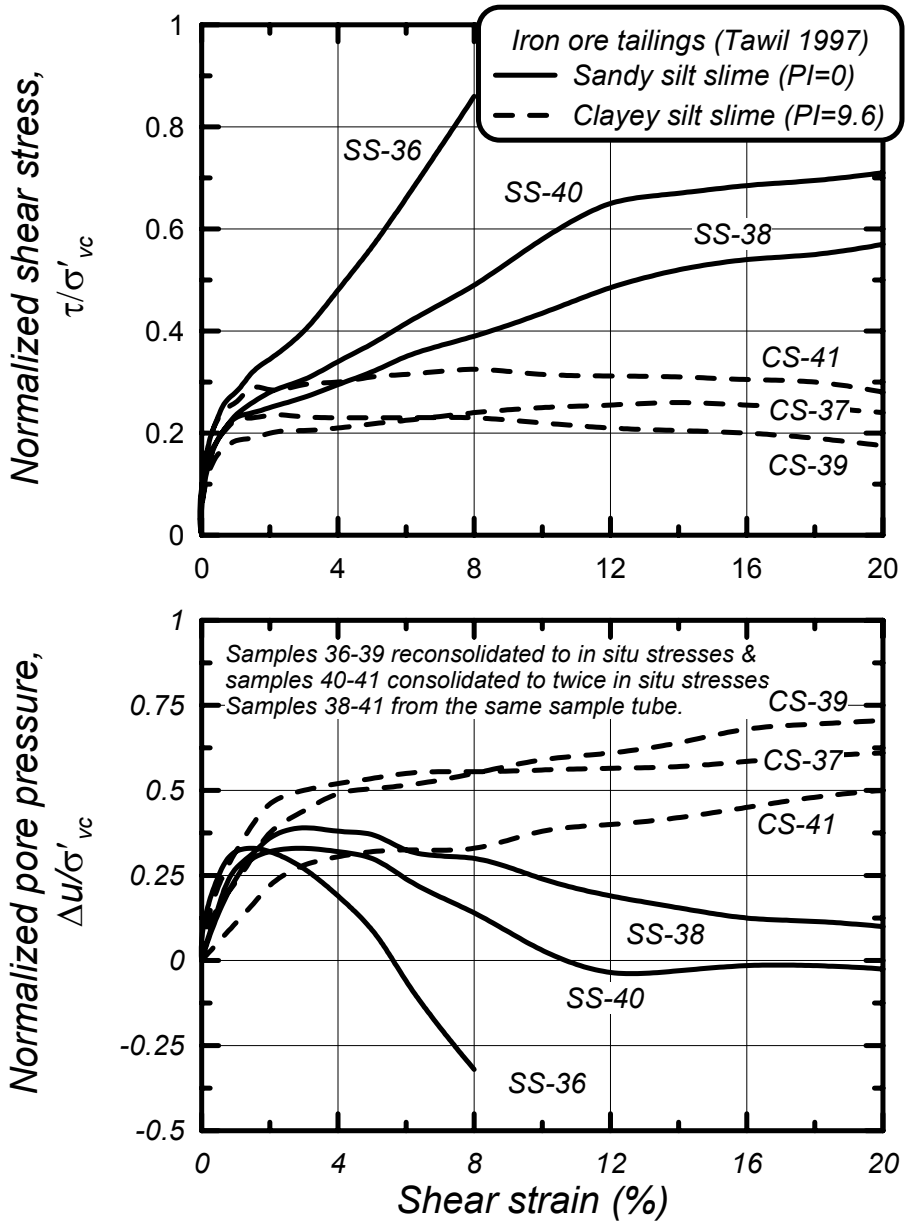

FIG. 2-19: Undrained DSS test results for tube specimens of iron ore tailings that included sandy silt slimes (SS) and clayey silt slimes (CS); Note that samples 36 & 37 had in situ vertical stresses of about 270 kPa while samples 38-41, which were all from the same tube, had in situ vertical stresses of about 360 kPa (after Tawil 1997)

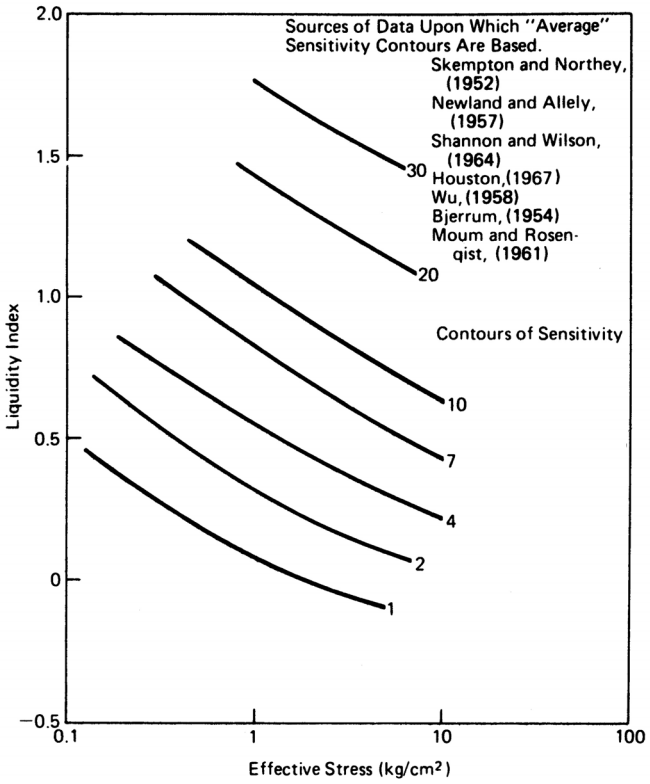

FIG. 2-20: Relationship between sensitivity, liquidity index, and effective consolidation stress (Mitchell 1993)

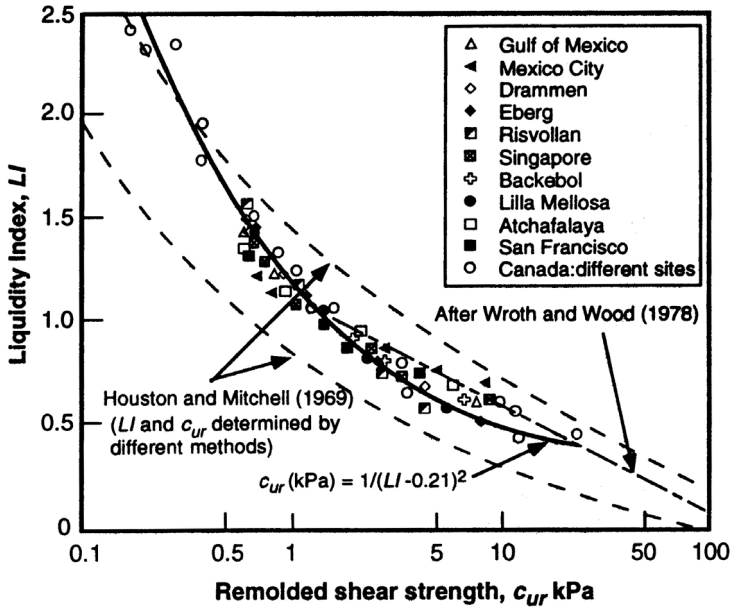

FIG. 2-21: Relationship between liquidity index and remolded undrained shear strength (Mitchell 1993)

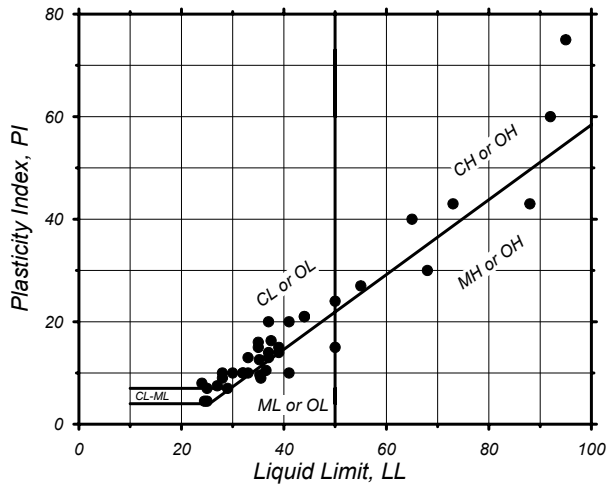

(a)

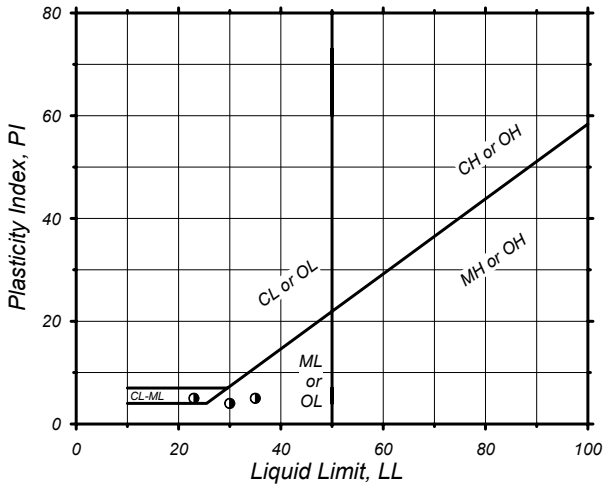

(b)

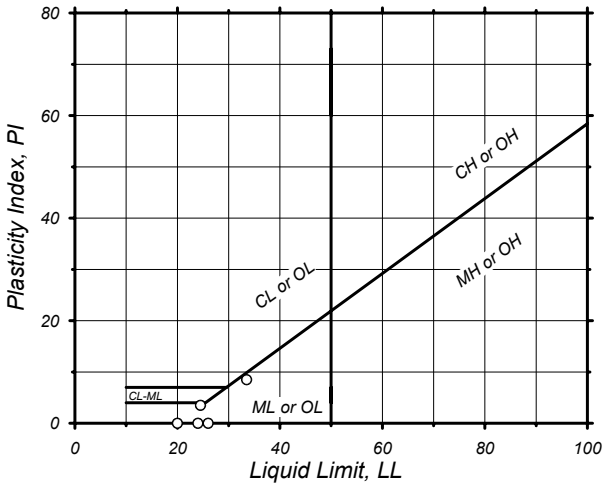

(c)

FIG. 2-22: Atterberg limits chart showing fine-grained soils that exhibit (a) clay-like behavior, (b) intermediate behavior, and (c) sand-like behavior.

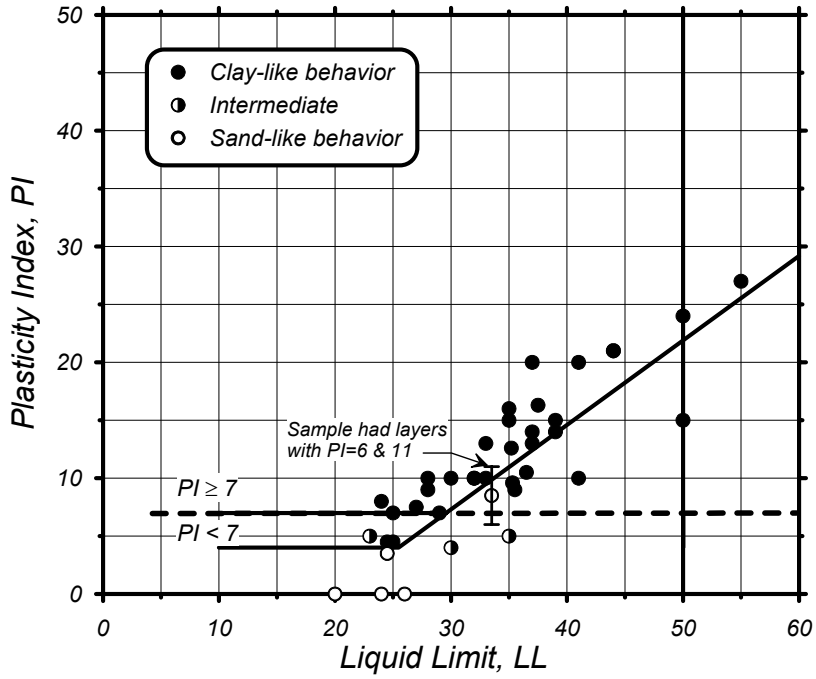

FIG. 2-23: Atterberg limits chart showing representative values for each soil that exhibited clay-like, sand-like, or intermediate behavior.

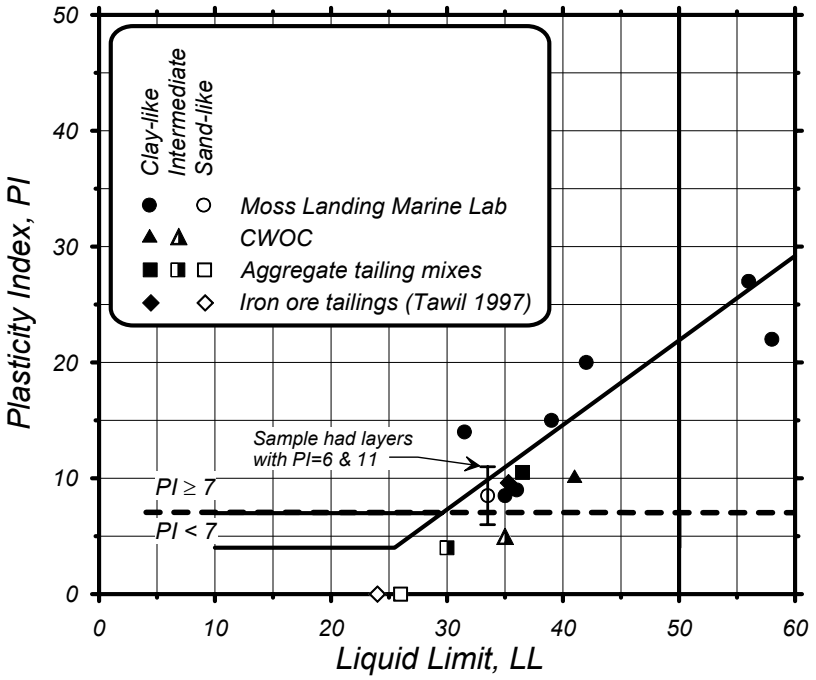

FIG. 2-24: Atterberg limits for four sites where samples taken in close proximity and tested in undrained cyclic loading showed behaviors ranging from clay-like to sand-like.

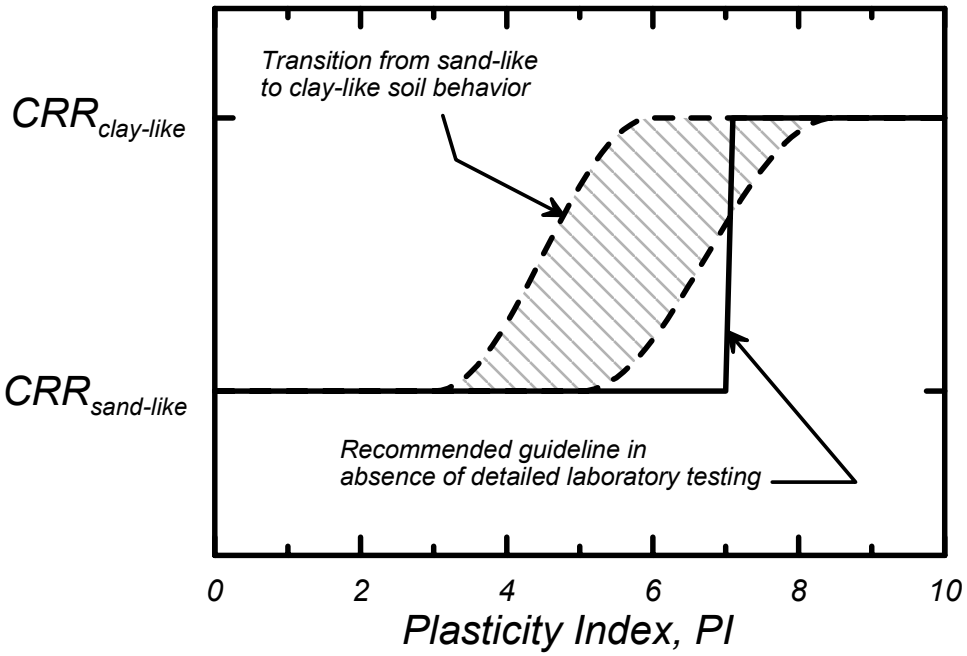

FIG.2-25: Schematic illustration of the transition from sand-like to clay-like behavior for fine-grained soils with increasing PI, and the recommended guideline for practice.

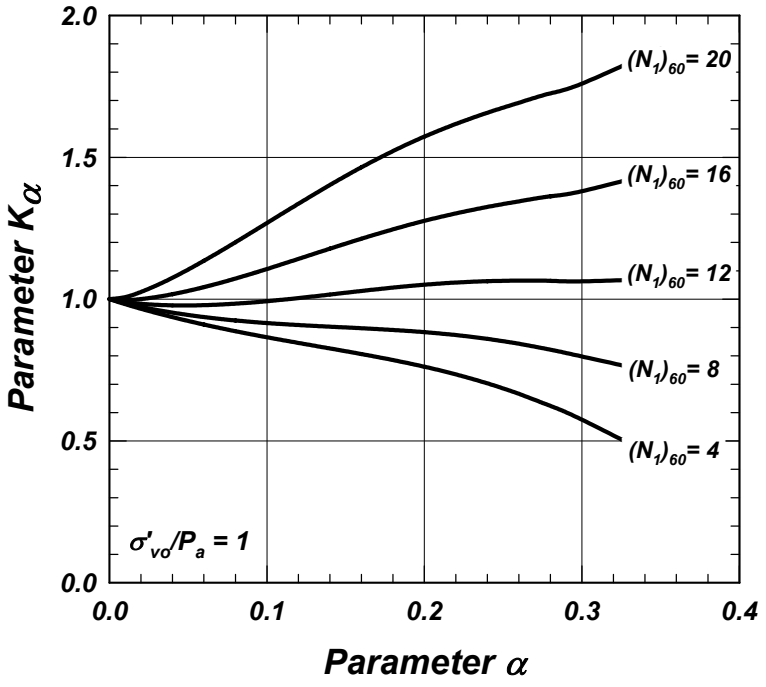

(a)

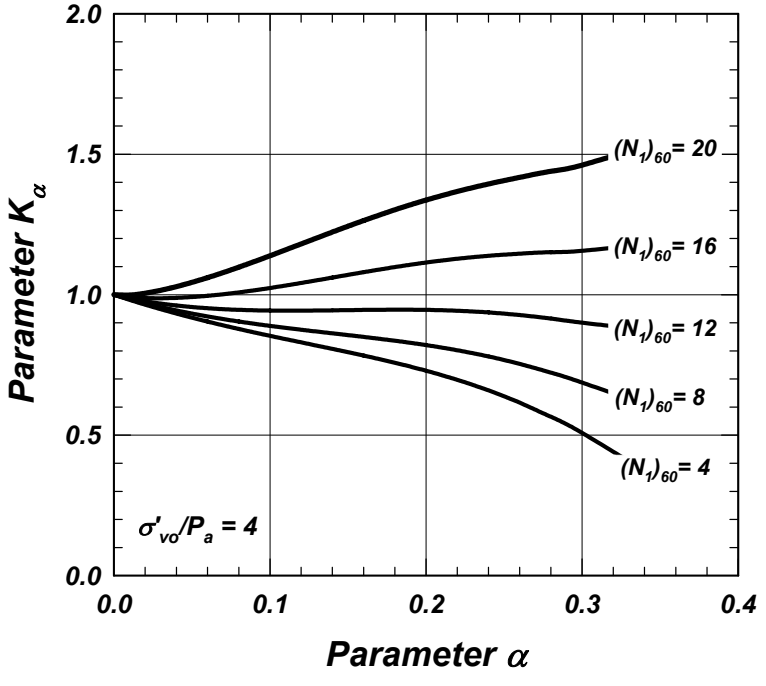

(b)

FIG. 2-26: Variation of the static shear stress correction factor (K_α) for sands at: (a) an effective overburden stress of 1 atm, and (b) an effective overburden stress of 4 atm. (Idriss and Boulanger 2003)

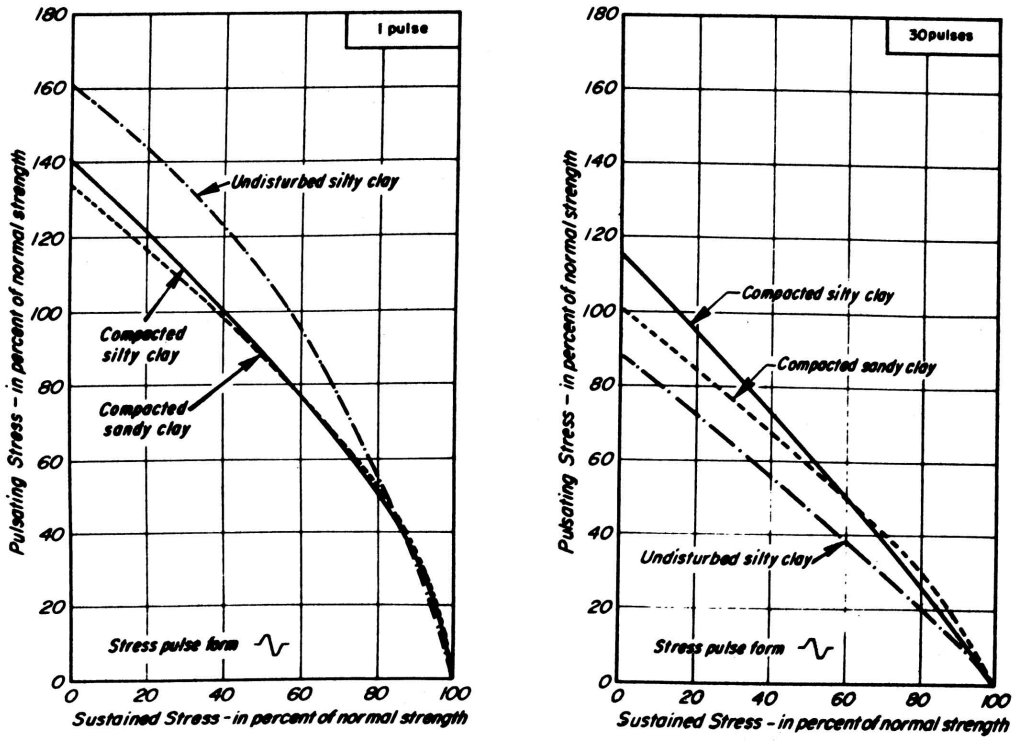

FIG. 2-27: Normalized stress ratios (τ_{cyc}/s_u) causing failure in 1 and 30 cycles of loading on a undisturbed soft sensitive silty clay, a compacted silty clay (LL=37, PI=14), and a compacted sandy clay (LL=35, PI=16) (Seed and Chan 1966).

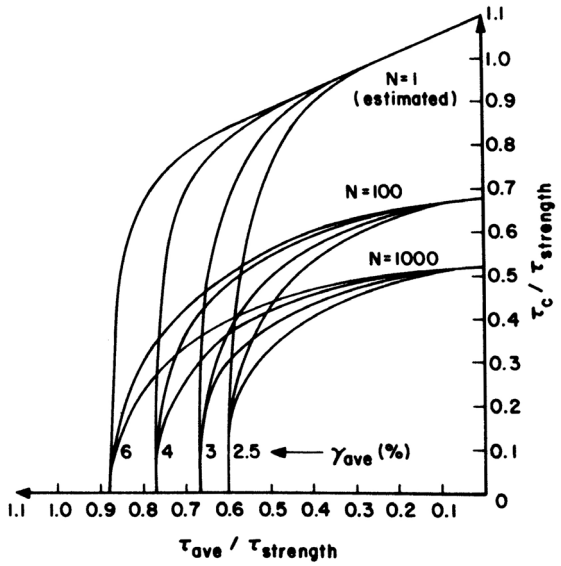

FIG. 2-28: Influence of static consolidation shear stress (τ_{ave}) on cyclic shear strength (τ_c) of normally consolidated Drammen Clay in DSS tests, normalized by the static undrained shear strength ($\tau_{strength}$) [Goulois et al. 1985].

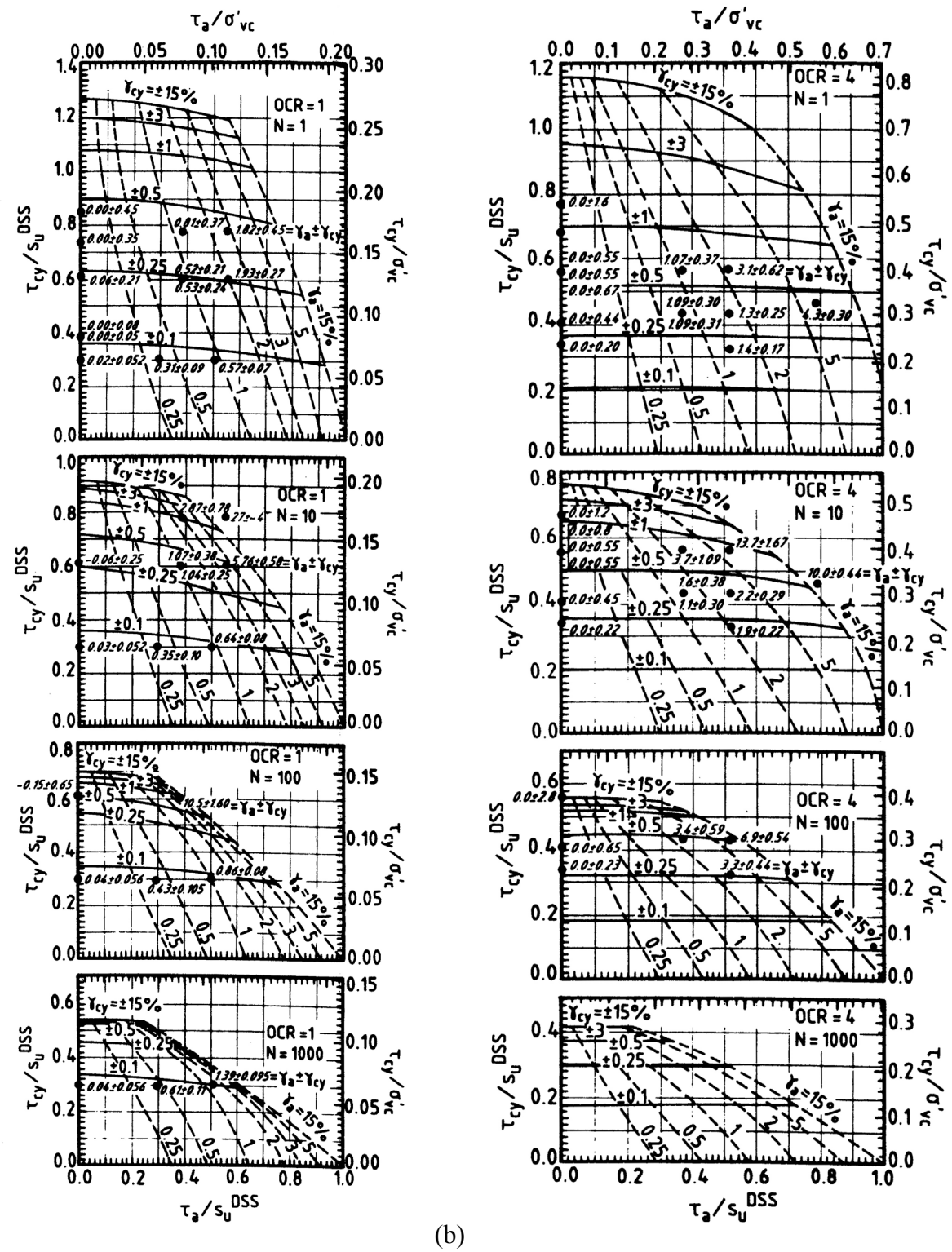

FIG. 2-29: Influence of undrained static shear stress (τ_a) on cyclic shear strength (τ_{cy}) of Drammen Clay in DSS tests: (a) OCR=1, (b) OCR=4 [Andersen et al. 1988]

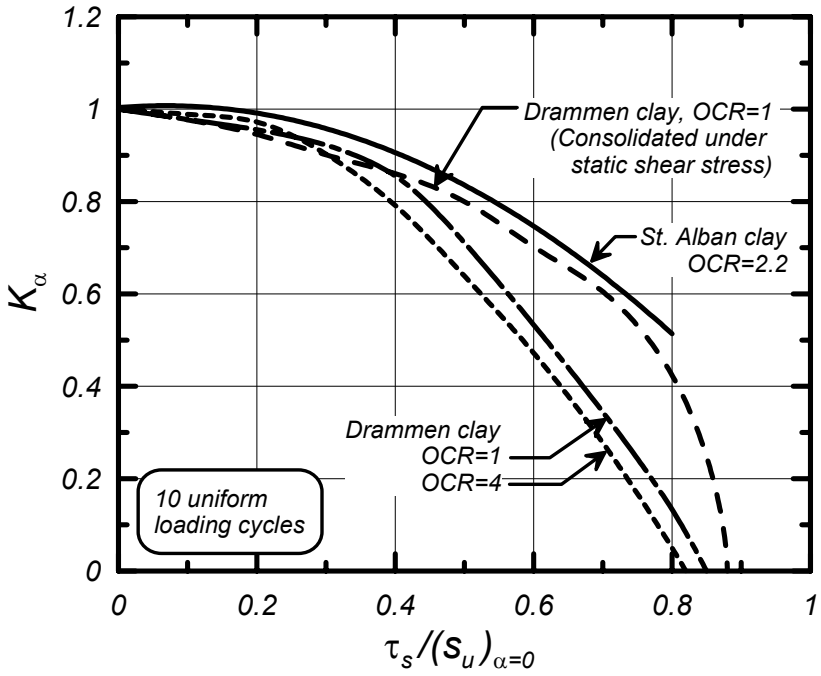

FIG. 2-30: K_α versus $(\tau_s/s_u)_{\alpha=0}$ relations for clays based on published data by Goulois et al. (1985), Andersen et al. (1988), and Lefebvre and Pfendler (1996). Note that specimens were not consolidated under the applied static shear stresses, except as otherwise labeled.

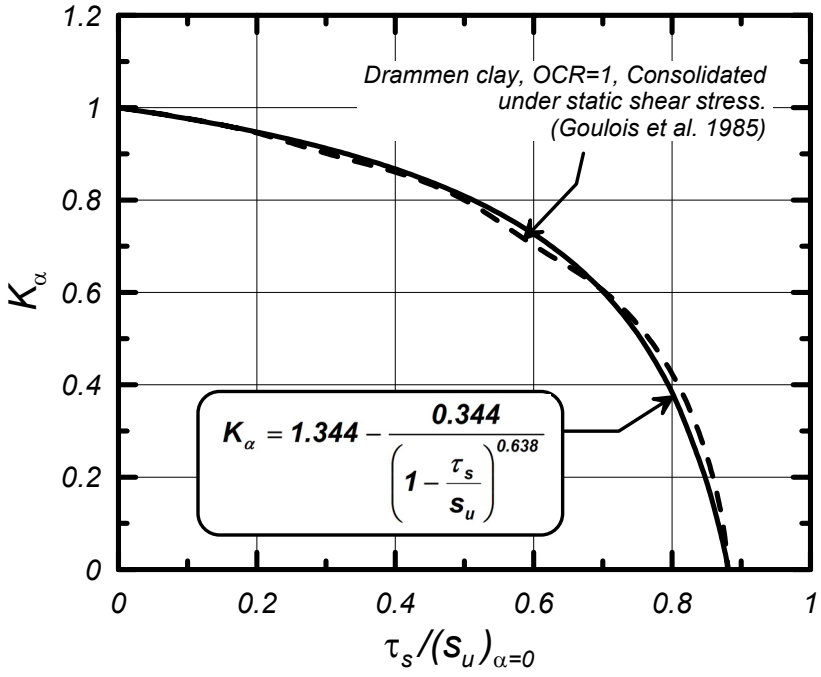

FIG. 2-31: Derived K_α versus $(\tau_s/s_u)_{\alpha=0}$ relation for clay-like soil consolidated under the static shear stress and the results for NC Drammen clay by Goulois et al. (1985).

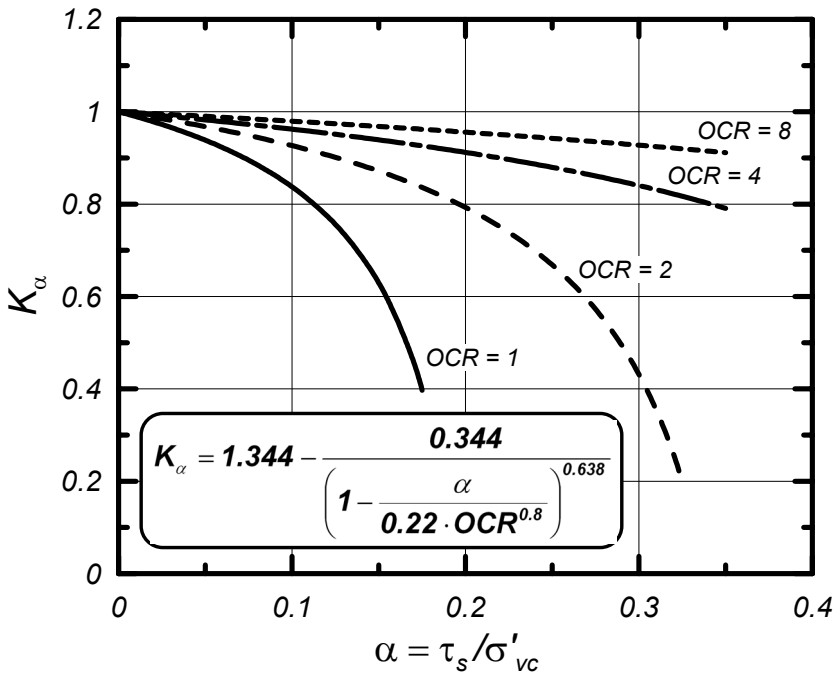

FIG. 2-32: K_α versus α relation for clay-like soil at various OCR and consolidated under the imposed static shear stress.

3. PROCEDURES FOR EVALUATING THE CYCLIC FAILURE POTENTIAL OF CLAY-LIKE FINE-GRAINED SOILS

Semi-empirical procedures for predicting liquefaction of sand-like soil have utilized the Seed-Idriss (1971) simplified procedure for estimating cyclic shear stresses during earthquakes, but similar analysis procedures have not been developed for predicting the cyclic failure of clay-like soil. This section presents the development of analysis procedures for evaluating cyclic failure of clay-like soils as follows.

- Section 3.1 presents a brief review of the Seed-Idriss simplified procedure for estimating cyclic stresses induced by earthquakes.
- Section 3.2 reviews the relations between magnitude scaling factors (MSF) and equivalent uniform cyclic loading, and subsequently presents the derivation of MSF relations for clay-like soil.
- Section 3.3 presents the development of relations for the CRR of clay-like soils, taking into consideration the different approaches that are used to characterize such soils.
- Section 3.4 discusses the consequences of triggering cyclic failure in clay-like soils.

The procedures developed in this section will later be illustrated through their application to case histories in Section 4.

3.1 Seed-Idriss simplified procedure for estimating cyclic stresses

The Seed-Idriss (1971) simplified procedure provides a means for estimating the in situ cyclic stresses that are induced by the vertical propagation of shear waves through level sites during earthquake shaking. The peak cyclic stress ratio (CSR_{peak}) is computed as:

$$CSR_{peak} = \frac{\tau_{peak}}{\sigma'_{vc}} = a_{max} \frac{\sigma_{vc}}{\sigma'_{vc}} r_d \tag{3-1}$$

where a_{max} is the peak ground surface acceleration (in g's), σ_{vc} is the total vertical stress, σ_{vc}' is the effective vertical consolidation stress, and r_d is a stress reduction coefficient that accounts for the flexibility of the soil column (i.e., r_d=1 corresponds to rigid body behavior). The CSR_{peak} is then scaled by a factor of 0.65 to produce a CSR that is considered representative of the most significant cycles over the full duration of loading, resulting in the following expression:

$$CSR = 0.65 \cdot a_{max} \frac{\sigma_{vc}}{\sigma'_{vc}} r_d \tag{3-2}$$

The stress reduction coefficient can be estimated using the following expressions (Idriss 1999, Idriss and Boulanger 2004):

$$r_d = exp(\alpha(z) + \beta(z)M) \tag{3-3a}$$

$$\alpha(z) = -1.012 - 1.126 \sin\left(\frac{z}{11.73} + 5.133\right) \tag{3-3b}$$

$$\beta(z) = 0.106 + 0.118 \sin\left(\frac{z}{11.28} + 5.142\right) \tag{3-3c}$$

where M is the moment magnitude of the earthquake and z is the depth in meters. Plots of r_d calculated using the above expressions for M of 5½, 6½, 7½ and 8 are presented in Fig. 3-1. The uncertainty in these relations for r_d increases with depth such that they should only be applied for depths less than about 20± m. For greater depths, the CSR should be estimated using site response studies, provided that a high quality response calculation can be completed for the site.

3.2 Equivalent uniform cyclic loading and magnitude scaling factors

A magnitude scaling factor (MSF) is used to adjust the CSR and/or CRR to a common value of M (conventionally taken as M=7.5) because the CRR depends on the number of loading cycles which correlates to M (Seed et al. 1975b). The basic definition of the MSF is:

$$MSF = \frac{CRR_M}{CRR_{M=7.5}} \tag{3-4}$$

Idriss and Boulanger (2004) reviewed various MSF relations that have been proposed for liquefaction analyses of sand-like soils, and subsequently adopted the relation by Idriss (1999):

$$MSF = 6.9 \cdot \exp\left(\frac{-M}{4}\right) - 0.058 \le 1.8 \tag{3-5}$$

The resulting MSF values for sand-like soils range from MSF=1.8 at M ≤ 5.25 to MSF=0.77 at M=8.5, as shown in plots later in this section. MSF relations have not been derived for clay-like soils, and thus their development is described herein.

MSF relations can be derived by combining: (1) correlations of the number of equivalent uniform cycles versus earthquake magnitude, and (2) laboratory-based relations between CRR and number of uniform stress cycles. These two relations are inter-dependent, as described below, and thus must be developed in parallel to maintain compatibility.

Converting irregular stress time series to equivalent uniform time series

Methods for converting an irregular time series to equivalent uniform cycles involve concepts similar to those used in fatigue studies. First, the relation between the CRR (liquefaction for sand-like soils, cyclic failure for clay-like soils) and the number of uniform stress cycles (N) is developed, such as shown in Fig. 3-2. This figure shows results for both sand-like and clay-like soils with the cyclic strengths normalized by their respective cyclic strengths at 15 uniform stress cycles. The data for either soil type is closely approximated using the form:

$$CRR = a \cdot N^{-b} \tag{3-6}$$

which produces a straight line with a slope of –b on a log(CRR) versus log (N) plot. The value of b = 0.337 for clean sand was used by Idriss (1999) to derive an MSF relation for sand-like soils. The value of b = 0.135 for clay is based on the average of the direct simple shear test results for clays (i.e., average of 0.116, 0.129, 0.149, and 0.149) as were summarized in Table 2-1 and presented in Figs. 2-12 and 2-18. Now consider two individual stress cycles having magnitudes CSR_A and CSR_B, respectively. The relative number of cycles to cause failure at these two stress ratios would be obtained using the above equation relating CRR to N; hence:

$$\frac{N_A}{N_B} = \left(\frac{CSR_B}{CSR_A}\right)^{1/b} \tag{3-7}$$

The damage from one cycle of stress at CSR_B is then assumed to be equivalent to the damage from X_A cycles at CSR_A if their numbers of cycles are an equal fraction of the number of cycles to failure at their respective CSR. This means that X_A can be computed as:

$$\frac{X_A \ cycles}{N_A} = \frac{1 \ cycle}{N_B} \tag{3-8}$$

which leads to the expression,

$$X_A = \left(\frac{CSR_B}{CSR_A}\right)^{1/b} (1 \ cycle) \tag{3-9}$$

This expression is used to convert individual stress cycles to an equivalent number of cycles at some reference stress level. Note that the above form of the CRR-N relation is necessary for the conversion to produce a unique result, and that the number of equivalent uniform cycles is controlled by the choice of the reference stress level.

The conversion of an irregular stress time series into an equivalent number of uniform stress cycles for sand-like and clay-like soils is illustrated using the simple example summarized in Table 3-1. In this example, the time series consists of five individual cycles at shear stress ratios of 1.0, 0.8, 0.65, 0.5 and 0.35, respectively. Consider first the conversion of this time series into an equivalent number of loading cycles at a uniform stress ratio equal to 65% of the peak stress ratio (i.e., 65% of 1.0 equals 0.65 in this example) for a sand-like soil (b=0.337). Cycle #5 is at the lowest stress ratio of 0.35, for which it would take $(0.65/0.35)^{1/0.337} = 6.27$ times as many cycles to be as damaging as a stress ratio of 0.65. Consequently, cycle #5 is equivalent to 1/6.27 = 0.16 cycles at a stress ratio of 0.65. Cycle #1 is at the strongest stress ratio of 1.0, which is equivalent to 3.55 cycles at a stress ratio of 0.65. Completing the process for all five cycles and summing the results converts this irregular stress time series to an equivalent 7.02 uniform cycles at a stress ratio of 0.65 for a sand-like soil.

Suppose that the reference stress ratio was instead taken as 100% of the peak stress ratio. In this case, Table 3-1 shows that the same process converts the same irregular stress time series to an equivalent 1.98 uniform cycles at a stress ratio of 1.0 for a sand-like soil.

The above two cases are then repeated for clay-like soil (b=0.135), with the same irregular stress time series converting to 33.6 and 1.22 uniform cycles at reference stress ratios of 0.65 and 1.0, respectively (Table 3-1). Thus, the number of equivalent uniform cycles is greater for clay-like soil than for sand-like soil when the reference stress is 0.65, but smaller when the reference stress is 1.0. These differences reflect the fact that the b value is smaller for clay-like soil (i.e., flatter slope in Fig. 3-2) and thus the cyclic behavior is more strongly dominated by the larger stress cycles in the time series.

Relating MSF, number of equivalent uniform stress cycles, and earthquake magnitude

Deriving an expression relating the number of equivalent uniform stress cycles (N) and earthquake magnitude (M) first requires specifying the reference stress level and the exponent "b" for the CRR versus N relation. For this study, the ratio of the reference stress to the peak stress is defined as r_e, such that the Seed-Idriss simplified procedure would be modified as follows:

$$CSR = r_e a_{max} \frac{\sigma_{vc}}{\sigma'_{vc}} r_d \tag{3-10}$$

Past studies have traditionally used r_e=0.65 per the original Seed-Idriss simplified procedure and have focused on sand-like soils. For example, Seed and Idriss (1982) and Idriss (1999) derived the relations between N and M shown in Fig. 3-3 for sand-like soil and r_e = 0.65. These relations and others (e.g., Liu et al. 2001) are based on applying the previously described procedure to bins of recorded ground motion time series and assuming that acceleration time series can directly represent stress time series.

The inter-relationships between MSF, N, and M are useful to review, as they can help guide the limits on the resulting relations for practice. The MSF is directly related to the N versus M relation through the equation:

$$MSF = \frac{CRR_M}{CRR_{M=7.5}} = \left(\frac{N_{M=7.5}}{N_M} \right)^b \tag{3-11}$$

where $N_{M=7.5}$ is number of uniform cycles for M=7.5 (e.g., $N_{M=7.5}$ = 15 cycles for sand with r_e = 0.65, as shown in Fig. 3-3). Limiting values for MSF can be derived for very small magnitude earthquakes where a single peak stress dominates the entire time series. Consider a time series dominated by single pulse of stress (i.e., ½ to 1 full cycle depending on its symmetry) with all other stress cycles being sufficiently small to neglect. Considering that this limiting case to consist of ¾ of a cycle at the peak stress, the equivalent number of uniform cycles corresponding to r_e = 0.65 for sand-like soils would be:

$$N_{min} = \left(\frac{1.0}{0.65}\right)^{1/0.337}\left(\frac{3}{4}\,cycle\right) = 2.69 \tag{3-12}$$

The maximum value for MSF would then be computed for sand-like soils as:

$$(MSF)_{max,cohesionless} = \left(\frac{15}{2.69}\right)^{0.337} = 1.78 \tag{3-13}$$

The above limit was incorporated into the MSF relation by Idriss (1999), which is compared to those by other investigators in Fig. 3-4.

The relations for clay-like soil are derived herein by repeating the above process for a set of 124 time histories recorded at deep soil sites (Geomatrix site category D) in 13 different earthquakes with M_w between 7 and 8 (Table 3-2). These earthquakes, in order of decreasing M_w, were the 2002 Denali, 1999 Chi-Chi, 1979 St. Elias, 1999 Kocaeli, 1990 Manjil, 1952 Kern County, 1978 Tabas, 1986 SMART1 (45), 1992 Landers, 1976 Calidran, 1999 Duzce, 1999 Hector Mine, and 1992 Cape Mendocino earthquakes. For each time series, the equivalent number of uniform loading cycles was determined for both sand (b=0.337) and clay (b=0.135) at a reference stress ratio of r_e = 0.65 as illustrated by the example in Fig. 3-5. For this example time series, N_{clay} = 43.2 and N_{sand} = 18.4, giving a ratio of N_{clay}/N_{sand} = 2.35.

The variation of N_{sand} and N_{clay} with M_w for all the records is shown in Fig. 3-6. As expected, the data show substantial variability with a general trend of increasing number of cycles with increasing M_w. At M_w = 7.5, the median relations give N_{sand} = 16.9 and N_{clay} = 32.1, from which the N_{clay}/N_{sand} ratio would be 1.90. The median value for N_{sand} at M_w=7.5 is only slightly larger than the value of 15 adopted by Seed and Idriss (1982) and Idriss (1999) and slightly lower than the values obtained by Liu et al. (2001). A second set of estimates for N_{sand} and N_{clay} at M_w = 7.5 was obtained from these data by tabulating the median values for each earthquake in this magnitude bin and then taking the median of those values. The resulting estimates were N_{sand} = 16.2 and N_{clay} = 30.8, which are both only slightly smaller than the values obtained from the regression lines in Fig. 3-6. The fact that the set of time series used herein produced N_{sand} values consistent with prior studies suggests that the estimated N_{clay} value would be unlikely to change significantly with further expansion of the time series data set or with a more detailed statistical analysis.

The ratio of N_{clay}/N_{sand} obtained for individual records is plotted versus the value of N_{sand} in Fig. 3-7. The ratio N_{clay}/N_{sand} decreases with increasing N_{sand}, which is expected because the single strongest peak has a smaller overall influence as the total number of cycles in the record increases. The residuals in the N_{clay}/N_{sand} versus N_{sand} relation showed only a very slight dependence on distance or magnitude, which can be neglected for practical purposes. The variance in the ratio N_{clay}/N_{sand} is smaller than the variance in the N_{clay} or N_{sand} versus M_w relations shown in Fig. 3-6, which simply reflects the fact that N_{clay} and N_{sand} are correlated through the duration of any given record. The median value for the ratio N_{clay}/N_{sand} is 1.93 at N_{sand} = 15. If N_{sand} = 15 for M_w = 7.5, then this ratio produces a corresponding N_{clay} value of 29, which is only slightly smaller than the N_{clay} values of 31-32 derived from Fig. 3-6.

Taking the above estimates into consideration [i.e., $(N_{clay}/N_{sand}) \times 15 = 29$, versus $N_{clay} = 31$ to 32 from Fig. 3-6], a value of $N_{clay} = 30$ was adopted as being representative for M_w=7.5 earthquakes when using $r_e = 0.65$. Note that this estimate pertains to the number of loading cycles in one direction only, while the additional effects of shaking in the orthogonal direction will need to be considered separately.

The role of r_e is illustrated in Fig. 3-8 showing how N varies with r_e for both sand-like and clay-like soils at a single earthquake magnitude (M = 7.5 for this figure). This figure illustrates that when the reference stress is defined by r_e values less than about 0.8, then the smaller b value for clay-like soil results in having a larger number of equivalent uniform loading cycles than for sand-like soils. In contrast, if the reference stress was instead defined by r_e values greater than about 0.8, then clay-like soil would have a fewer number of equivalent uniform loading cycles.

An MSF relation for clay-like fine-grained soil was subsequently developed following the same logic previously described for sands. First, the limiting value of MSF was computed for ½ cycle at the peak stress (the flatter b value suggests that ½ cycle is a better limit than the ¾ cycle used for sand-like soil). This gives a minimum N for $r_e = 0.65$ of:

$$N_{min} = \left(\frac{1.0}{0.65}\right)^{1/0.135}\left(\frac{1}{2}\,cycle\right) = 12.2 \tag{3-14}$$

This minimum N value was used to compute the maximum (limiting) MSF value as:

$$(MSF)_{max,cohesive} = \left(\frac{30}{12.2}\right)^{0.135} = 1.13 \tag{3-15}$$

which is assumed to be applicable for M less then about 5¼. The resulting MSF relation for clay-like soil, following the same form as used for sand, is:

$$MSF = 1.12 \cdot exp\left(\frac{-M}{4}\right) + 0.828$$
$$MSF \le 1.13 \tag{3-16}$$

This MSF relation is plotted in Fig. 3-9, along with the relation developed by Idriss (1999) for sands. The smaller b value for clay-like soils produces a much flatter MSF relation because the response is more strongly controlled by the few strongest cycles in a time series. In addition, the MSF relation for clay-like soils is relatively insensitive to variations in the selected parameters (e.g., b value, $N_{M=7.5}$ value). For example, if the equivalent number of loading cycles for a M=7.5 earthquake was instead taken as 35 cycles, the limiting MSF value from Equation 3-15 would only increase by about 2% to 1.15. Or if the value of b was taken as 0.149 (the largest value from Table 2-2) while keeping $N_{M=7.5} = 30$ (the higher b value would, in fact, cause this value to decrease), then Equations 3-14 and 3-15 would produce a limiting MSF value of 1.20 (a 6% increase). Thus, the derived MSF relation provides a reasonable means for incorporating the effects of shaking duration on the cyclic strength of clay-like fine-grained soils, and is unlikely to be significantly affected by a more extensive analysis of other recorded earthquake time series.

Implementation of the magnitude scaling factor

MSF factors may be implemented in either of two ways. For liquefaction triggering analyses of sands, the common SPT or CPT correlations provide an estimate of CRR that corresponds to M = 7.5 [i.e., $(CRR)_{M=7.5}$]. It has become common to adjust the CSR computed for a site subjected to earthquake ground motions caused by an earthquake with magnitude M [i.e., $(CSR)_M$] to the equivalent CSR for a M = 7.5 earthquake [i.e., $(CSR)_{M=7.5}$] and then compare these values in computing the factor of safety (F):

$$(CSR)_{M=7.5} = \frac{(CSR)_M}{MSF} \tag{3-17}$$

$$F = \frac{(CRR)_{M=7.5}}{(CSR)_{M=7.5}} \tag{3-18}$$

Alternatively, the CSR and CRR may be compared at the design earthquake magnitude, in which case the CRR is adjusted while the CSR is not:

$$(CRR)_M = (CRR)_{M=7.5} MSF \tag{3-19}$$

$$F = \frac{(CRR)_M}{(CSR)_M} \tag{3-20}$$

The above two approaches are equivalent, but the latter approach has a strong advantage when analyzing a soil profile containing both clay-like and sand-like soils. The advantage stems from the fact that the MSF is different for sand-like and clay-like soils, and it is therefore convenient to use the MSF to adjust CRR rather than have the computed CSR varying with soil type.

3.3 Cyclic resistance ratios for clay-like fine-grained soil

The cyclic strength of clay-like fine-grained soils (identified as PI ≥ 7 in Section 2) can be evaluated through cyclic laboratory testing or estimated as a ratio of the soil's monotonic undrained shear strength (s_u). In turn, s_u may be measured using in situ or laboratory testing, or estimated using empirical correlations. Consequently, the $CRR_{M=7.5}$ of clay-like soils may be evaluated using the following three approaches:

- Approach A: Measure CRR by cyclic laboratory testing.
- Approach B: Measure s_u by in situ or laboratory testing, and then multiply it by an empirical factor to obtain the CRR.
- Approach C: Empirically estimate CRR based on the stress history profile.

The latter approach C requires knowledge of the consolidation stress history for the clay-like soil, after which empirical relations can be used to estimate s_u and/or CRR. The direct measurement of s_u in approach B provides increased confidence in the estimated CRR, while the

direct measurement of CRR in approach A provides the highest level of insight and confidence. These different approachs provide the opportunity to evaluate a site with progressively increasing levels of confidence, while considering the potential benefits that additional information may provide given the uncertainties in the current level of analysis.

Approach A is the most direct approach and does not require further discussion, other than to note that careful attention to the laboratory testing protocols is essential and that the results can be interpreted using the framework presented earlier in this report.

The various approaches for measuring s_u by in situ and laboratory testing are discussed first, followed by the development of the procedures for approaches B and C.

Comments on estimating s_u profiles based on in situ and laboratory tests

Profiles of s_u for a clay-like fine-grained soil deposit are often evaluated using in situ tests like the vane shear test (VST) or cone penetration test (CPT). The SPT N value has also been correlated to s_u, but the scatter in such correlations is large enough that any resulting estimate is highly uncertain. VST tests provide perhaps the most direct measurement of the soil's peak s_u which can then be empirically adjusted to a field value that is more appropriate for analyzing the stability of an embankment on soft clay (i.e., for the effects of a different loading paths and rates) (Bjerrum 1972). This empirical adjustment is computed as:

$$(s_u)_{field} = \mu \cdot (s_u)_{VST} \tag{3-21}$$

where the vane shear correction factor (μ) varies with PI as shown in Fig. 3-10 (from Ladd and DeGroot 2003). The VST also normally provides a measurement of the soil's fully remolded (residual) strength, s_{ur}, from which the sensitivity S_t can be obtained.

The CPT provides a less direct measurement of s_u in that the cone tip resistance is related to s_u through the relation:

$$s_u = \frac{q_{cT} - \sigma_v}{N_k} \tag{3-22}$$

The cone factor N_k depends on the soil's reference shear strength (e.g., VST, ACU triaxial compression test, DSS), the shear modulus (G or G/s_u ratio), the coefficient of lateral earth pressure at rest (K_o), and other factors such as inherent anisotropy, fissuring, and cone surface roughness (e.g., Yu et al. 2000). Empirical relations for N_k (e.g., Kulhawy and Mayne 1990) show values ranging mainly between about 10 and 30, which leaves considerable uncertainty in an estimate of s_u based solely on CPT data. In addition, the cone tip resistance in soft clays must be corrected for pore water pressure effects (i.e., the corrected value is referred to as q_{cT} in the above relation) and can be affected by other factors such as calibration errors or electronic drift For these and other reasons, N_k factors are best confirmed by site specific correlations using independent measurements of s_u.

Ladd (1991) and Ladd and DeGroot (2003) provide a detailed discussion of various techniques and issues involved in obtained s_u profiles from laboratory testing programs, and the reader should refer to these or other references for a thorough treatment of the subject. Consolidated undrained (CU) tests provide better information than unconsolidated undrained (UU) tests. The preferred procedures for consolidation of samples in the laboratory depends on the nature of the soils, with the SHANSEP approach (Ladd and Foot 1974) being advantageous for mechanically consolidated "ordinary" clays while the NGI Recompression technique (e.g., Bjerrum 1973) is advantageous for highly structured or cemented clay-like soils. CU tests enable the interpretation of strength data in terms of stress normalized parameters, which is particularly advantageous for the analysis of staged construction projects that progressively alter the consolidation stress history of the foundation soils.

Unconsolidated-undrained (UU) or unconfined compression tests provide estimates of a soil's s_u for the current in situ consolidation state. Estimates of s_u from UU or unconfined compression tests have more uncertainty compared to estimates from CU tests because of the greater effects of sample disturbance.

Undrained strengths vary substantially with the loading path, as was illustrated in Fig. 2-10; triaxial compression (TC) giving the highest strength, direct simple shear (DSS) being intermediate, and triaxial extension (TE) giving the lowest strength. The average strength for a failure surface that includes portions that mimic TC, DSS, and TE conditions is generally close to (or slightly greater than) the strength obtained from direct simple shear tests. For this reason, direct simple shear tests would be the preferred choice when only one type of test device is being used to evaluate the seismic response/stability of many structures. In cases where equipment availability has led to the use of triaxial compression tests, the resulting s_u values should be reduced by approximately 20% to 35% based on empirical correlations (e.g., Kulhawy and Mayne 1990) to represent a strength appropriate for average or direct shear loading conditions (like horizontal shaking).

Approach B: Estimating CRR from the measured s_u profile

Values of cyclic strength, $\tau_{cyc,}$ may be empirically estimated based on the measured s_u profile for a clay-like fine-grained soil deposit. When the reference stress level is taken as 65% of the peak seismic stress (i.e., $r_e = 0.65$), the resulting relation for the CRR of clay-like soils in M=7½ earthquakes can be computed as,

$$CRR_{M=7.5} = C_{2D} \cdot \left(\frac{\tau_{cyc}}{s_u} \right)_{N=30} \cdot \frac{s_u}{\sigma'_{vc}} \cdot K_\alpha \qquad (3\text{-}23)$$

where C_{2D} is a correction factor for the effects of two-dimensional shaking in the field (discussed later in this section) and K_α is the static shear stress correction factor described in Section 2.5.

Normalized cyclic strength ratios are summarized in Table 3-3 for several soils, including those previously listed in Table 2-1, the two compacted clays from Fig. 2-27, and the natural silt that is described in Fig. 3-11. The data in Table 3-3 include representative Atterberg Limits, the type of cyclic tests performed (DSS versus TX), the as-tested overconsolidation ratio (OCR), the

undrained shear strength ratio (s_u/σ_{vc}') when normally consolidated (OCR=1), the τ_{cyc}/s_u ratios required to trigger peak shear strains of 3% in 15 and 30 uniform cycles of undrained loading, and the τ_{cyc}/σ_{vc}' ratios required to trigger peak shear strains of 3% in 15 and 30 uniform cycles of undrained loading when normally consolidated (OCR=1). The triaxial test data for the compacted clays by Seed and Chan (1966) and the direct simple shear test data for the thin-walled tube samples of the natural "CWOC" silt by Woodward-Clyde (1992) do not include data for normally consolidated conditions.

The τ_{cyc}/s_u ratio for N=30 cycles is plotted against PI in Fig. 3-12(a) for the soils summarized in Table 3-3. The different types of soils and test conditions are highlighted in this figure, from which the following observations can be made:

- The tailing slimes gave the lowest ratios of τ_{cyc}/s_u, perhaps being about 20% lower than the natural silts and clays. The tailing slimes data cover a lower range of PI's (10.5 to 13) than the natural silts and clays (10 to 73) and are much younger (hours in the case of the tests by Romero) than the natural silts and clays. Consequently, it is not clear how much of this difference in τ_{cyc}/s_u ratios is due to differences in PI or age.
- The compacted silty clay and compacted sandy clay by Seed and Chan (1966) gave the highest ratios of τ_{cyc}/s_u. These specimens were partially saturated and tested in unconsolidated-undrained conditions, such that their state of effective stress was not known.
- The triaxial and DSS tests gave comparable τ_{cyc}/s_u ratios for the natural silts and clays, while the triaxial tests on tailings slimes appeared to give τ_{cyc}/s_u ratios that were about 15 to 20% lower than obtained in DSS tests on tailings slimes.

It is clear that the data summarized in Fig. 3-12(a) are insufficient to clearly define the various factors that may affect the τ_{cyc}/s_u ratio, such as age, PI, soil type, OCR, and test type. Despite these uncertainties, the data for natural soils do tend to fall within relatively narrow ranges. It is subsequently suggested that the $(\tau_{cyc}/s_u)_{N=30}$ ratio be taken as 0.83 (±15%) for natural clay-like soils subjected to direct simple shear loading conditions, with due recognition that the continued compilation of laboratory test data can lead to future refinements in this estimate and its uncertainty.

The $(\tau_{cyc}/s_u)_{N=30}$ ratios in Fig. 3-12(a) are based on s_u values determined at standard loading rates for monotonic CU (consolidated undrained) laboratory tests. Conceptually, these ratios may be adjusted whenever the s_u value pertains to a significantly different loading rate. For example, corrected vane shear strengths correspond to the long-term strain rate in the field (through the empirical VST correction factor) which is considerably slower than the standard strain rate in CU laboratory tests. Conversely, unconsolidated undrained triaxial tests use a much higher loading rate than is used for CU tests, but then their strengths are affected considerably more by sample disturbance. In most situations, an additional correction for different s_u loading rates will be small relative to the uncertainties that arise from the natural soil heterogeneity, limitations in laboratory and in situ test results, and limitations in the various empirical relations that may be used (e.g., the vane shear correction factor; the $(\tau_{cyc}/s_u)_{N=30}$ ratio from Fig. 3-12). While future studies may provide improved guidance on this issue, such a refinement does not seem warranted at this time.

The effects of two-directional shaking would be expected to slightly reduce the available CRR for clay-like soils, as it does for sands. Seed (1979) reviewed experimental data on the effects of two-directional cyclic loading on the CRR of saturated sands, and recommended that the CRR for two-dimensional shaking could be estimated as 0.9 times the CRR for one-dimensional cyclic loading. Similar experimental data are not available for clays, but there are good reasons to expect that the effect of two-directional cyclic loading is smaller for clays than for sands. For example, suppose that the correction factor for two-dimensional cyclic loading (C_{2D}) was primarily due to the effects of additional loading cycles. In this case, C_{2D} could be expressed as:

$$C_{2D} = \left(\frac{N_{1D}}{N_{2D}}\right)^{b} \tag{3-24}$$

where N_{1D} and N_{2D} are the equivalent numbers of uniform loading cycles imposed by one-dimensional and two-dimensional shaking, respectively. If C_{2D} is taken as 0.9 for sands, then the ratio of N_{2D}/N_{1D} would be computed as 1.37 based on b = 0.337; i.e., the effect of two-directional shaking would be equivalent to increasing the number of one-dimensional loading cycles by 37%. The above equation can then be rearranged to estimate a C_{2D} for clays that is consistent with the value of 0.9 for sands:

$$(C_{2D})_{clay} = [(C_{2D})_{sand}]^{\frac{(b)_{clay}}{(b)_{sand}}} \tag{3-25}$$

$$(C_{2D})_{clay} = 0.9^{\frac{0.135}{0.337}} = 0.96 \tag{3-26}$$

Thus, the expected effect of two-dimensional shaking on clays may be estimated as about a 4% reduction in CRR, versus the 10% reduction expected for sands. This estimate of C_{2D} for clays is adopted herein pending the availability of direct experimental data regarding this effect.

The $CRR_{M=7.5}$ for natural deposits of clay-like fine-grained soils can then be estimated as:

$$CRR_{M=7.5} = C_{2D} \cdot \left(\frac{\tau_{cyc}}{s_u}\right)_{N=30} \cdot \frac{s_u}{\sigma'_{vc}} \cdot K_{\alpha} \tag{3-27}$$

$$CRR_{M=7.5} = 0.96 \cdot 0.83 \cdot \frac{s_u}{\sigma'_{vc}} \cdot K_{\alpha} \tag{3-28}$$

$$CRR_{M=7.5} = 0.8 \cdot \frac{s_u}{\sigma'_{vc}} \cdot K_{\alpha} \tag{3-29}$$

For tailing slimes, the above estimate of CRR should tentatively be reduced by about 20% as suggested by the data in Fig. 3-12. In many situations, the uncertainty in the s_u profiles will be greater than the uncertainty in the $(\tau_{cyc}/s_u)_{N=30}$ ratio, but for those cases where the uncertainty in the $(\tau_{cyc}/s_u)_{N=30}$ ratio is important, a detailed cyclic laboratory testing program would be warranted.

Approach C: Empirically estimating CRR based on the consolidation stress history profile

Cyclic strengths may be similarly computed from empirical s_u relations in conjunction with an established consolidation stress history profile. As noted in Section 2.0 of this report, the undrained shear strength, s_u, can be related to σ'_{vc} and OCR as follows:

$$\frac{s_u}{\sigma'_{vc}} = S \cdot OCR^m \tag{3-30}$$

An accurate assessment of the stress history (i.e., OCR) is generally more important than refined estimates of the parameters m and S for defining s_u for clay-like soils. For this reason, the parameters m and S are sometimes estimated empirically while engineering efforts focus on the stress history of a site. The $CRR_{M=7.5}$ can then be estimated by combining this expression with the relations presented in approach B to arrive at:

$$CRR_{M=7.5} = 0.8 \cdot S \cdot OCR^m \cdot K_\alpha \tag{3-31}$$

For homogenous, low- and high-plasticity, sedimentary clays (CL and CH), the simplest representation may be to use S = 0.22 and m = 0.8 (Ladd 1991), such that the CRR is estimated as:

$$CRR_{M=7.5} = 0.8 \cdot 0.22 \cdot OCR^{0.8} \cdot K_\alpha = 0.18 \cdot OCR^{0.8} \cdot K_\alpha \tag{3-32}$$

Measured values of $(\tau_{cyc}/\sigma_{vc}')_{N=30}$ for the several normally consolidated soils in Table 3-3 are plotted versus PI in Fig. 3-12(b). The following observations can be made from this figure:

- The tailings slimes had similar $(\tau_{cyc}/\sigma_{vc}')_{N=30}$ values to those for the natural clays, despite their differences in PI and age.
- The cyclic DSS tests appear to give $(\tau_{cyc}/\sigma_{vc}')_{N=30}$ values that are about 20% smaller than those obtained in cyclic triaxial tests. As noted in Table 3-3, the monotonic and cyclic shear stresses in TX tests were computed as $\tau = q/2$. If the shear stresses were instead computed for the eventual shear plane as $\tau = (q/2)\cdot\cos(\phi')$, then the $(\tau_{cyc}/\sigma_{vc}')_{N=30}$ values for TX tests would have been about 15% smaller (i.e, $\phi' \approx 32°$) and the difference between DSS and TX test results in Fig. 3-12(b) would have been very small. [Note that the ratio τ_{cyc}/s_u for TX tests is the same for either interpretation of shear stresses.]
- The one natural silt (MH) had the highest $(\tau_{cyc}/\sigma_{vc}')_{N=30}$ value, which may be attributable to its very high PI. However, the other data show no apparent trend with PI.

It is suggested that the $(\tau_{cyc}/\sigma_{vc}')_{N=30}$ ratio might reasonably be estimated as 0.183, independent of PI, for normally consolidated clay-like fine-grained soils subjected to one-dimensional direct simple shear loading (as shown on Fig. 3-12(b)). The corresponding $CRR_{M=7.5}$ value for two-dimensional shaking would then be approximately 0.18, independent of PI. This value is consistent with the above derivation based on S = 0.22, $(\tau_{cyc}/s_u)_{N=30}$ = 0.83, and C_{2D} = 0.96, reflecting the fact that the adopted relations in Figs. 3-11(a) and (b) were partly chosen for their consistency.

For sedimentary deposits of silts and organic soils plotting below the A-line on the Atterberg Limits chart, Ladd (1991) suggested that the simplest representation may be to use S = 0.25 and m = 0.8 in Eq. (3-31). This S value is about 14% greater than the typical S = 0.22 value for homogenous sedimentary clays, which would imply that such silts and organics soils would have a 14% higher CRR if the $(\tau_{cyc}/s_u)_{N=30}$ ratio was the same for both soil types. The data in Figs. 3-11(a) and 3-11(b) are not, however, complete enough to clearly define the dependence of CRR values on the various factors of concern, including any potential differences between silts, organic soils, and clays. It is therefore suggested that the CRR of silt or organic soil plotting below the A-line but still having PI ≥7, may be estimated using the same expression given above for CL and CH soils; i.e.,

$$CRR_{M=7.5} = 0.18 \cdot OCR^{0.8} \cdot K_{\alpha} \tag{3-33}$$

Continued compilation of cyclic laboratory test data on clay-like fine-grained soils is needed to refine the relation between cyclic strength and consolidation stress history. Such compilations can be expected to result in more well-defined estimates of cyclic strength and the uncertainties in such relations.

Comparing CRR values estimated using clay-like versus sand-like relations

The significance of the procedures proposed herein are illustrated by a couple of very simple examples. First, consider a fine-grained clay-like soil with PI = 8 and LL = 31 at a depth of 5 m in a soil deposit with the water table at a depth of 1 m. The soil has an OCR of 1.2, such that the undrained shear strength is about 15 kPa [$=0.22\sigma_{vc}'(OCR)^{0.8}$] and the measured CPT and SPT penetration resistances would be about $q_{cN} = 3.2$ [$=15s_u + \sigma_{vo}$] and $N_{60} = 3$ [Kulhawy and Mayne 1990]. Such a soft soil would have a high water content and very reasonably could be classified as "liquefiable" by some of the existing criteria. In that case, it would be common practice to enter a CPT- or SPT-based liquefaction correlation and estimate this soil's $CRR_{M=7.5}$ to be about 0.11. In contrast, a value of $CRR_{M=7.5}$ of about 0.21 is obtained using the procedures proposed herein. This difference of about 90% can obviously be very important in many applications.

Now reconsider the same problem but suppose this soil has a LL of 36 with 15% finer than 2 μm and 25% finer than 5 μm. In this case, the soil may be classified as "nonliquefiable" by some existing criteria and many engineers would then incorrectly conclude that this soil did not represent a potential problem. However, the soil would have the same undrained shear strength and $CRR_{7.5}$ as in the previous example, in which case it very well could be the source of large ground deformations in certain situations (sloping ground, overlying building foundation, strong shaking).

3.4 Consequences of cyclic failure in clay-like fine-grained soil

The consequences of cyclic failure in clay-like fine-grained soils, in terms of potential deformations or instability, depend on the soil's sensitivity (i.e., S_t = ratio of peak to remolded undrained shear strength). Sensitivity of natural clay-like soil can be related to the soil's liquidity index (LI) and effective consolidation stress, as illustrated previously in Fig. 2-20 (Mitchell

1993). Soft normally-consolidated or lightly-overconsolidated clays will generally have higher natural water contents, higher LI values, and higher sensitivities, and will therefore be most prone to strength loss during earthquakes. Well compacted and heavily overconsolidated clays will have lower natural water contents, lower LI values, and be generally far less sensitive to remolding. Consequently, with all else equal, potential ground deformations that arise from cyclic failure may range from relatively severe in natural quick clays (i.e., $S_t > 8$) to relatively minor in well-compacted or heavily overconsolidated clays.

This aspect of behavior is analogous to the fact that the consequences of liquefaction in sands are much more severe for loose sands than for medium-dense sands, as reflected in the correlations that show residual shear strengths increasing, and potential shear strains decreasing, as the SPT $(N_1)_{60}$ value increases (e.g., Seed 1987, Ishihara 1996). Similarly, for clay-like fine-grained soils, their residual strength will increase and potential strains will decrease with decreasing LI (or w_n) or increasing OCR. Thus, cyclic failure of clay-like soils should not necessarily be assumed to imply that a major problem exists, but rather that it is necessary to next evaluate the potential deformations.

Potential deformations in clay-like fine-grained soils may be estimated by either a Newmark Sliding Block type of procedure or by integrating estimated strains (shear or volumetric) over the thickness of the deforming strata. The choice of method depends on the specific problem and the expected mode of deformations. In some cases the parallel application of both methods may provide valuable insights. In this regard, the future development of relationships between the factor of safety against cyclic failure and expected shear strains or volumetric (reconsolidation) strains would be beneficial.

Newmark-type procedures evaluate the accrual of displacements along a defined slip surface as inertial forces from shaking cause the shear strength of the soils to be exceeded. Newmark-type procedures are widely used in practice, with early examples of their application to slopes in clayey soils including the work by Makdisi and Seed (1978), Seed (1979), and Idriss (1985). These types of analyses can also be easily modified to account for loss of shear strength with increasing displacement, such as done by Idriss (1985) in analyzing the Fourth Avenue slide in Anchorage during the 1964 Alaskan earthquake. In that case, the soils had a sensitivity of about 3, and so the loss of soil strength due to remolding was very significant. Alternatively, the Newmark-type analyses may use a constant undrained shear strength that represents the degree of strength loss that is expected for that soil under the design earthquake loading.

The undrained shear strength of clay after cyclic loading will generally be less than the original static undrained shear strength, with the magnitude of the reduction depending on the clay's characteristics, the strains imposed by the cyclic loads, and the number of loading cycles (e.g., Thiers and Seed 1969, Andersen 1976). For example, Thiers and Seed (1969) summarized results for San Francisco Bay Mud and Anchorage silty clays that showed post-cyclic undrained shear strengths to be at least 90% of the static undrained shear strength when the peak cyclic strains were less than ½ the corresponding failure strain in a static undrained loading test. The same data show the post-cyclic undrained shear strengths dropping to less than 40% of the static undrained shear strength when the peak cyclic strains exceeded the corresponding failure strain in a static undrained loading test. Using the cyclic failure analysis procedures presented in this

report, a factor of safety of 1.0 against cyclic failure corresponds to about 3% shear strain, after which continued cyclic loading causes shears strains to rapidly increase. Thus, the onset of cyclic failure (i.e., a factor of safety of 1.0) corresponds to the point where the post-cyclic undrained shear strength of the clay will be transitioning from values near its original static strength to values nearer its residual or fully remolded strength.

The magnitude of strain or ground displacement that will reduce a clay's undrained shear strength to its fully remolded value is currently difficult to assess. It is generally recognized that it would take less ground displacement to fully remold a very brittle soil (e.g., quick clay) than it would take to remold a more ductile soil (i.e., relatively insensitive clay), but defining the transition from peak to remolded shear strengths is complicated by limitations in our experimental methods and our ability to predict shear localizations in the field. Experiences from case histories provide only limited guidance on this issue, and thus additional research is necessary before reliable methods for defining this aspect of behavior can be developed.

Determining the stress history and sensitivity of clay-like fine-grained soils are therefore two key tasks for evaluating both the potential for cyclic failure and the potential consequences of cyclic failure. The effect of increasing OCR on cyclic behavior of natural clay-like soils is very strong because it impacts both the resistance to cyclic failure (i.e., CRR) and the potential consequences of cyclic failure. For example, clay with an OCR of 8.0 versus 1.0 would have more than five times the cyclic strength, be far less affected by the presence of static shear stresses such as in slopes (Fig. 2-32), and generally be much less sensitive to remolding.

Table 3-1: Simple example illustrating conversion of an irregular stress time series to equivalent uniform cycles at different reference stresses for sand-like and clay-like soil.

	Shear stress ratio	Equivalent number of uniform loading cycles for sand-like soil with b=0.337		Equivalent number of uniform loading cycles for clay-like soil with b=0.135	
		@ 65% of the peak stress	@ 100% of the peak stress	@ 65% of the peak stress	@ 100% of the peak stress
cycle 1	1.00	3.55	1.00	27.49	1.00
cycle 2	0.80	1.84	0.52	4.94	0.18
cycle 3	0.65	1.00	0.28	1.00	0.04
cycle 4	0.50	0.46	0.13	0.13	0.00
cycle 5	0.35	0.16	0.05	0.01	0.00
Total number of uniform cycles =		7.02	1.98	33.57	1.22

[a] Based on CRR = $a(N)^{-b}$

Table 3-2: Stations at D sites during M_w =7 to 8 earthquakes whose records were used to compute equivalent numbers of uniform cycles.

Earthquake	M_w	Station	Closest Dist. (km)	PGA (g)
Denali, AK (2002)	7.9	Eagle River - AK	249	0.01
	7.9	NOAA Weather	278	0.02
	7.9	Anchorage NewFS1	269	0.02
	7.9	Anchorage Police Headquarters	272	0.01
	7.9	R109(temp)	49	0.08
	7.9	Fairbanks Ester FS	140	0.04
	7.9	K203	266	0.01
	7.9	K204	277	0.01
	7.9	K205	272	0.01
	7.9	K206	271	0.01
	7.9	Taps pump station 09	56	0.06
	7.9	Taps pump station 11	126	0.08
Chi-Chi, Taiwan (1999)	7.62	CHY002	25	0.13
	7.62	CHY008	40	0.12
	7.62	CHY025	19	0.16
	7.62	CHY039	32	0.11
	7.62	CHY092	23	0.10
	7.62	CHY104	18	0.17
	7.62	CHY107	51	0.10
	7.62	HWA012	57	0.07
	7.62	TAP010	102	0.10
	7.62	TCU056	11	0.13
	7.62	TCU111	22	0.12
	7.62	TCU116	12	0.17
St. Elias, Alaska (1979)	7.54	Icy Bay	5	0.13
	7.54	Yakutat	72	0.07
Kocaeli, Turkey (1999)	7.51	Attakoy	71	0.13
	7.51	Bornova	322	0.01
	7.51	Botas	140	0.10
	7.51	Bursa	67	0.11
	7.51	Canakkale	278	0.03
	7.51	Duzce	15	0.33
	7.51	Kuthaya	145	0.05
	7.51	Usak	227	0.01
	7.51	Yarimca Petkim	4.7	0.31
	7.51	Zeytinburnu	66	0.11
Manjil, Iran (1990)	7.37	Abbar	19	0.51
	7.37	Abhar	68	0.17
	7.37	Tehran - Sarif University	157	0.01
	7.37	Tonekabun	81	0.11
	7.37	Qazvin	40	0.16
	7.37	Rudsar	61	0.09
	7.37	Tehran - Building & Housing	159	0.03
Kern County, CA (1952)	7.36	LA - Hollywood Stor FF	113	0.05
Tabas, Iran (1978)	7.35	Ferdows	93	0.10
	7.35	Kashmar	201	0.04
SMART1(45) (1986)	7.3	C00	39	0.14
	7.3	O08	39	0.15
Landers, CA (1992)	7.28	5070 N. Palm Springs	27	0.14
	7.28	Barstow	37	0.13
	7.28	Boron Fire Station	91	0.10
	7.28	Yermo fire station	25	0.19
	7.28	San Bernadino - E&Hospit	80	0.08
	7.28	Palm Springs airport	36	0.08
	7.28	Indio	54	0.11
	7.28	Fort Irwin	64	0.12
	7.28	Hemet fire station	69	0.09
Calidran, Turkey (1976)	7.21	Maku	51	0.08
Duzce, Turkey (1999)	7.14	Aslan R.	131	0.03
	7.14	Yarimca Petkim	98	0.02
	7.14	Bolu	12	0.77
	7.14	Bursa Tofas factory	166	0.02
	7.14	Duzce	7	0.43
	7.14	Kutahya	168	0.02
Hector Mine, CA (1999)	7.13	Desert Hot Springs - fire station	56	0.07
	7.13	Fort Irwin	66	0.12
Cape Mendocino, CA (1992)	7.1	Eureka - Myrtle & West	33	0.17
	7.1	Fortuna Blvd	14	0.12

Table 3-3: Normalized cyclic strength ratios for various clay-like soils

Soil name (Reference source)	PI	LL	USCS[a]	Test type[b]	OCR	(s_u/σ_{vc}') for OCR=1	For 15 uniform cycles		For 30 uniform cycles	
							$(\tau_{cyc}/s_u)_{N=15}$	$(\tau_{cyc}/\sigma_{vc}')_{N=15}$ for OCR=1	$(\tau_{cyc}/s_u)_{N=30}$	$(\tau_{cyc}/\sigma_{vc}')_{N=30}$ for OCR=1
Drammen clay (Andersen et al. 1988)	27	55	CH	DSS	1 & 4	0.214	0.94	0.201	0.87	0.186
Boston Blue clay (Azzouz et al. 1989)	21	44	CL	DSS	1, 1.38, & 2	0.205	0.92	0.189	0.83	0.170
Cloverdale clay (Zergoun & Vaid 1994)	24	50	CL-CH	TX	1	0.280	0.88	0.246	0.80	0.224
St. Alban clay (Lefebvre & Pfendler 1996)	20	41	CL	DSS	2.2	0.248[c]	1.01	0.250	0.92	0.228
Itsukaichi clay (Hyodo et al. 1994)	73	124	MH	TX	1	0.390	0.92	0.359	0.87	0.339
Copper tailings slime (Moriwaki et al. 1982)	13	35	CL	TX	1	0.404	0.64	0.260	0.58	0.234
				DSS	1	0.241	0.80	0.193	0.72	0.174
Aggregate tailings slime (Romero 1995)	10 ½	36.5	ML	TX	1	0.340	0.68	0.231	0.648	0.220
Compacted silty clay (Seed & Chan 1966)	14	37	CL	TX	n.a.	n.a.	n.a	n.a.	1.15	n.a.
Compacted sandy clay (Seed & Chan 1966)	16	35	CL	TX	n.a.	n.a.	n.a	n.a.	1.00	n.a.
CWOC silt (Woodward-Clyde 1992)	10	42	ML	DSS	≈2	n.a.[d]	0.77	n.a.	0.71	n.a.

Notes:

[a] Unified Soil Classification System.

[b] DSS is direct simple shear, TX is triaxial. For TX tests, $s_u = q_{peak}/2$ and $\tau_{cyc} = q_{cyc}/2$.

[c] For St. Alban clay, the reported s_u/σ_{vp}' ratio is used for the value of s_u/σ_{vc}' at OCR=1.

[d] For CWOC silt, samples were reconsolidated to their in situ overburden stresses.

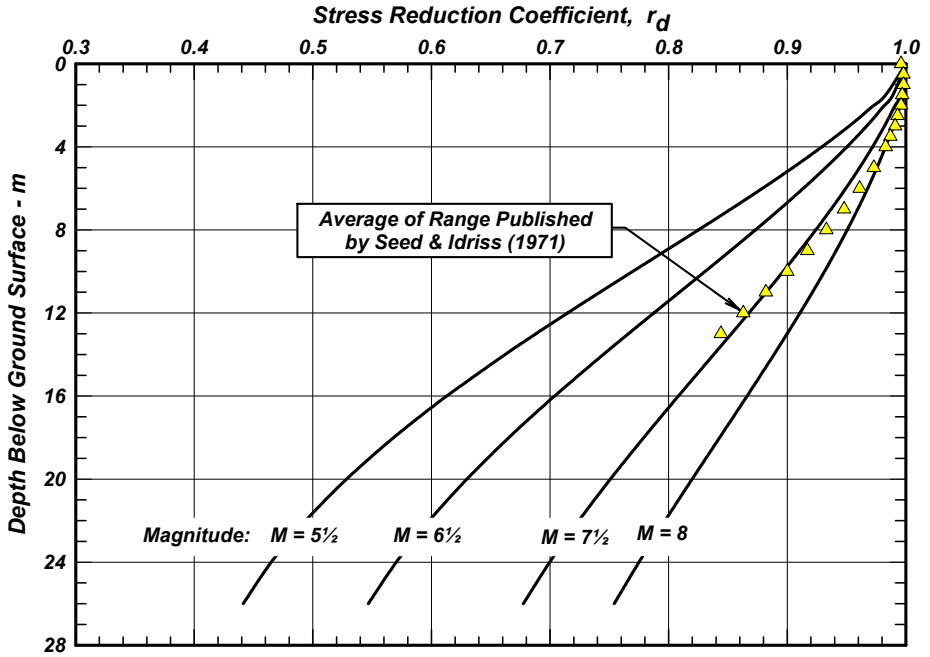

FIG. 3-1: Variation of stress reduction coefficient with depth and earthquake magnitude (from Idriss 1999).

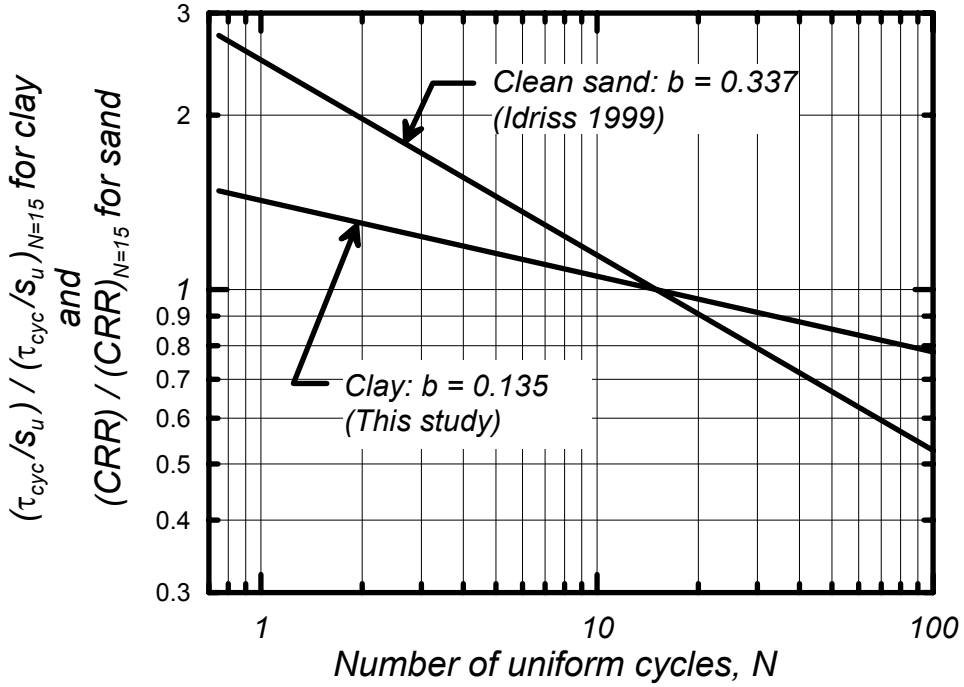

FIG. 3-2: Variation in cyclic strengths for clay (τ_{cyc}/s_u) and sand (CRR), normalized by the cyclic strength at 15 uniform loading cycles, versus number of uniform loading cycles

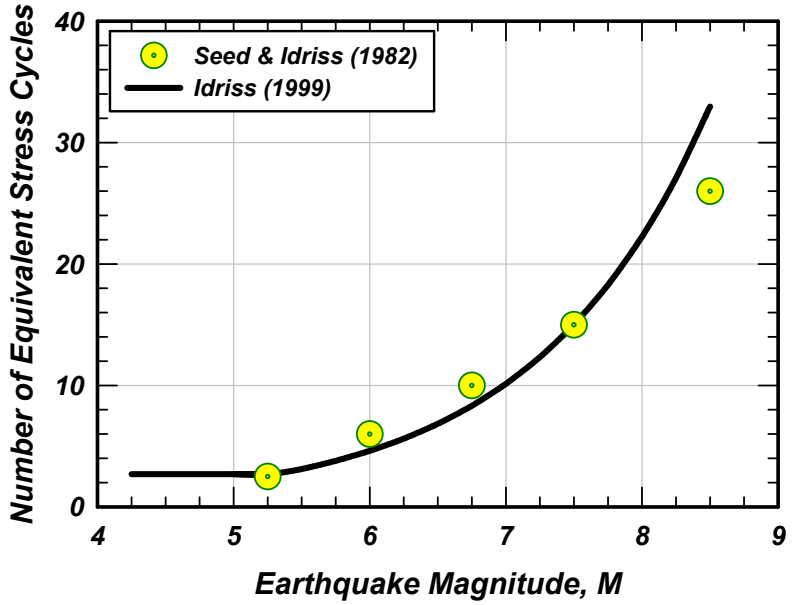

FIG. 3-3: Number of equivalent uniform cycles versus earthquake magnitude (M_w) for sand with r_e=0.65.

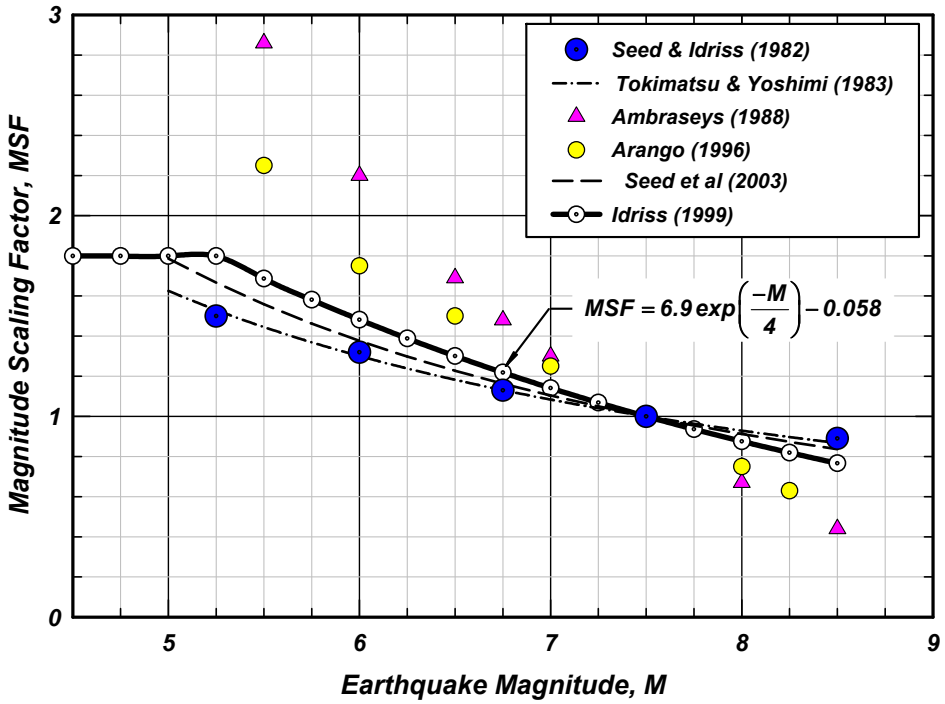

FIG. 3-4: Comparison of the recommended MSF relation (Idriss 1999) for sands to the MSF relations by other investigators.

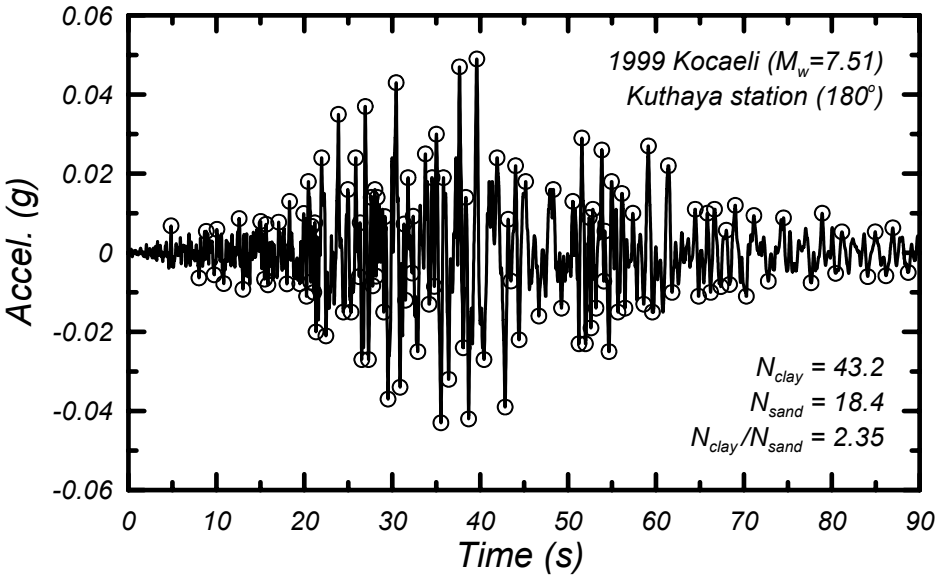

FIG. 3-5: Example time history showing the individual cycles that exceeded 10% of the record's peak acceleration and showing the equivalent number of uniform loading cycles for sand and clay with the reference stress based on r_e=0.65.

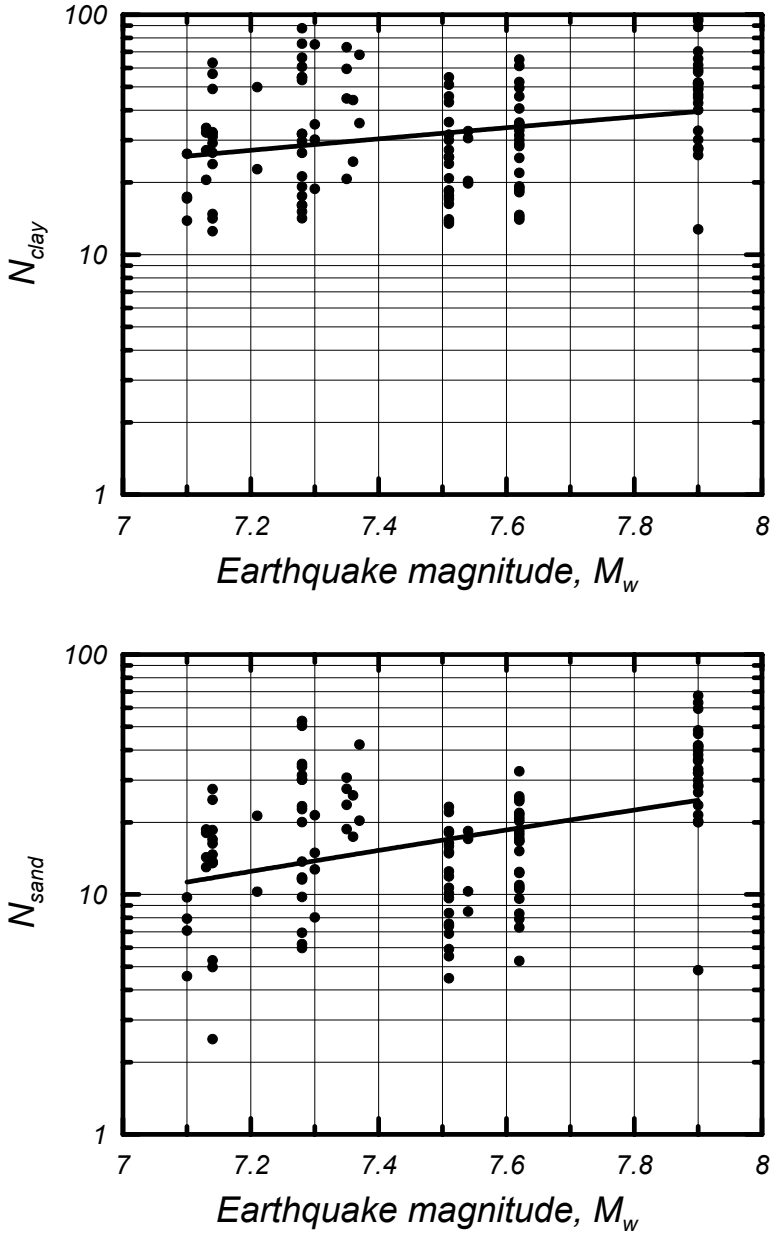

FIG. 3-6: Number of equivalent loading cycles for clay (b=0.135) and sand (b=0.337) from strong ground motion records at D sites during M_w = 7 to 8 earthquakes and based on a reference stress defined by r_e=0.65.

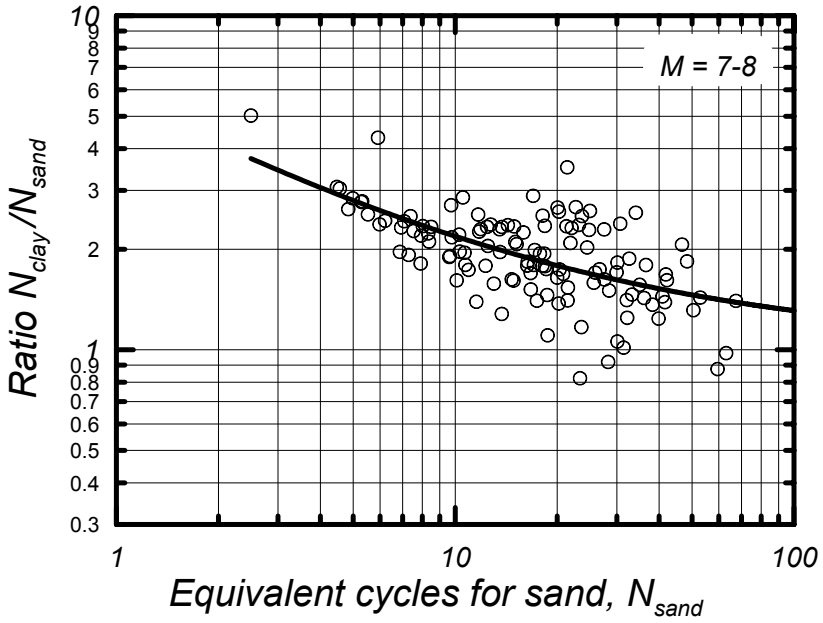

FIG. 3-7: Ratio of N_{clay} to N_{sand} for D sites with M_w of 7 to 8.

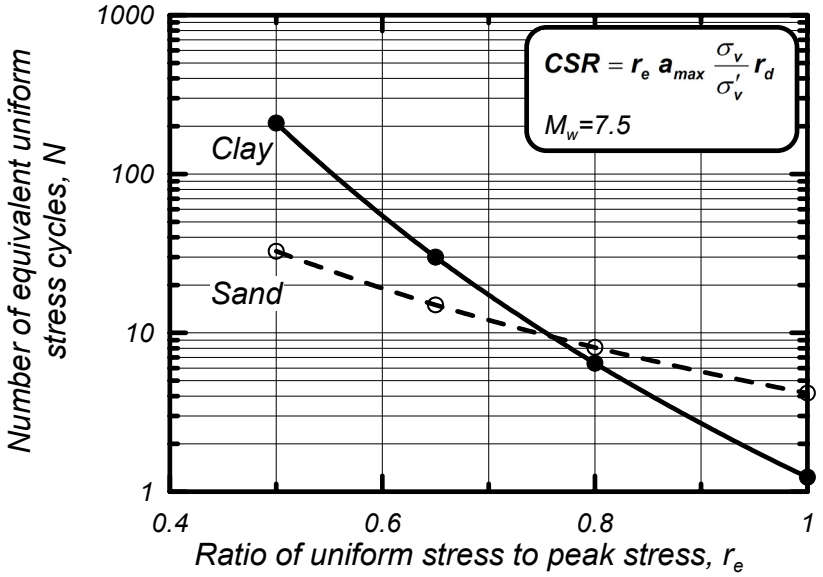

FIG. 3-8: Number of equivalent uniform stress cycles (N) versus the ratio of uniform stress to peak stress (r_e) for M_w=7.5 earthquakes for sand and clay.

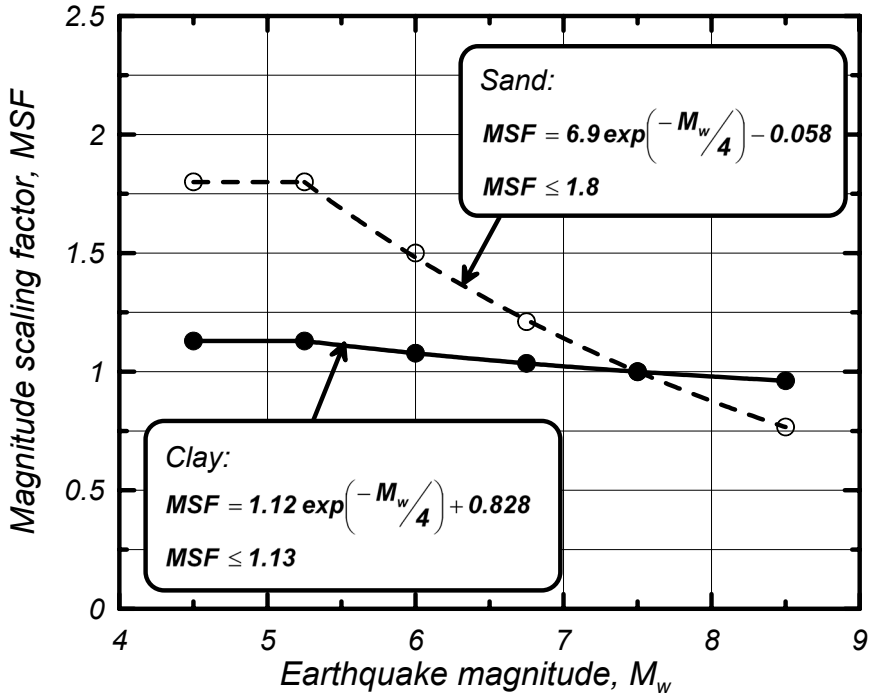

FIG. 3-9: Magnitude scaling factor (MSF) for converting a cyclic stress ratio to the equivalent cyclic stress ratio for an M_w=7.5 earthquake.

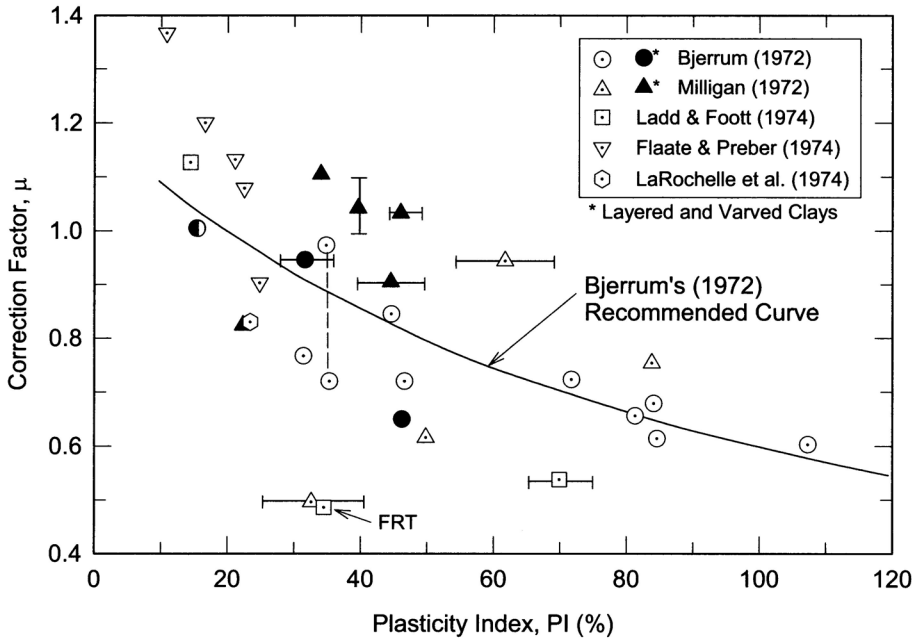

FIG. 3-10: Correction factor for VST measurements of undrained shear strength (Ladd and DeGroot 2003, after Ladd et al. 1977)

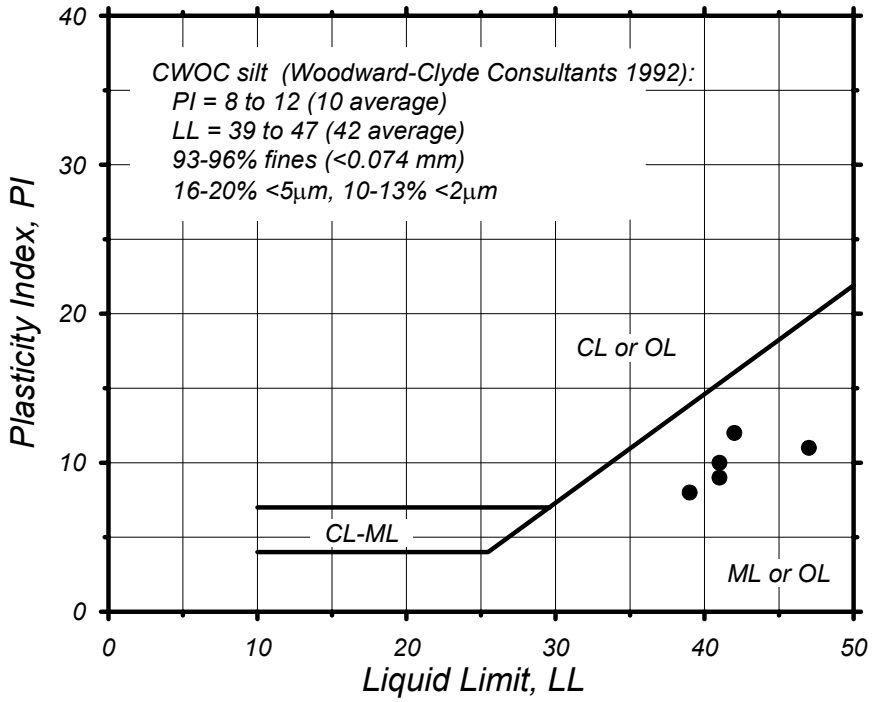

(a)

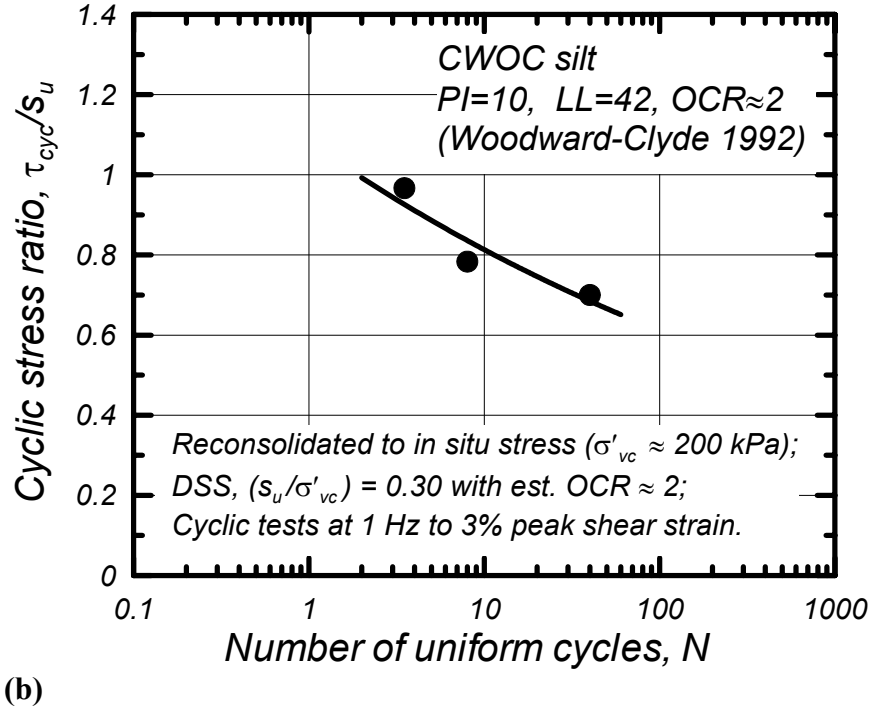

(b)

FIG. 3-11: Results of DSS tests on a natural silt from the CWOC site in Sacramento (Woodward-Clyde Consultants 1992): (a) Atterberg limits, and (b) Cyclic strength ratio versus number of uniform loading cycles.

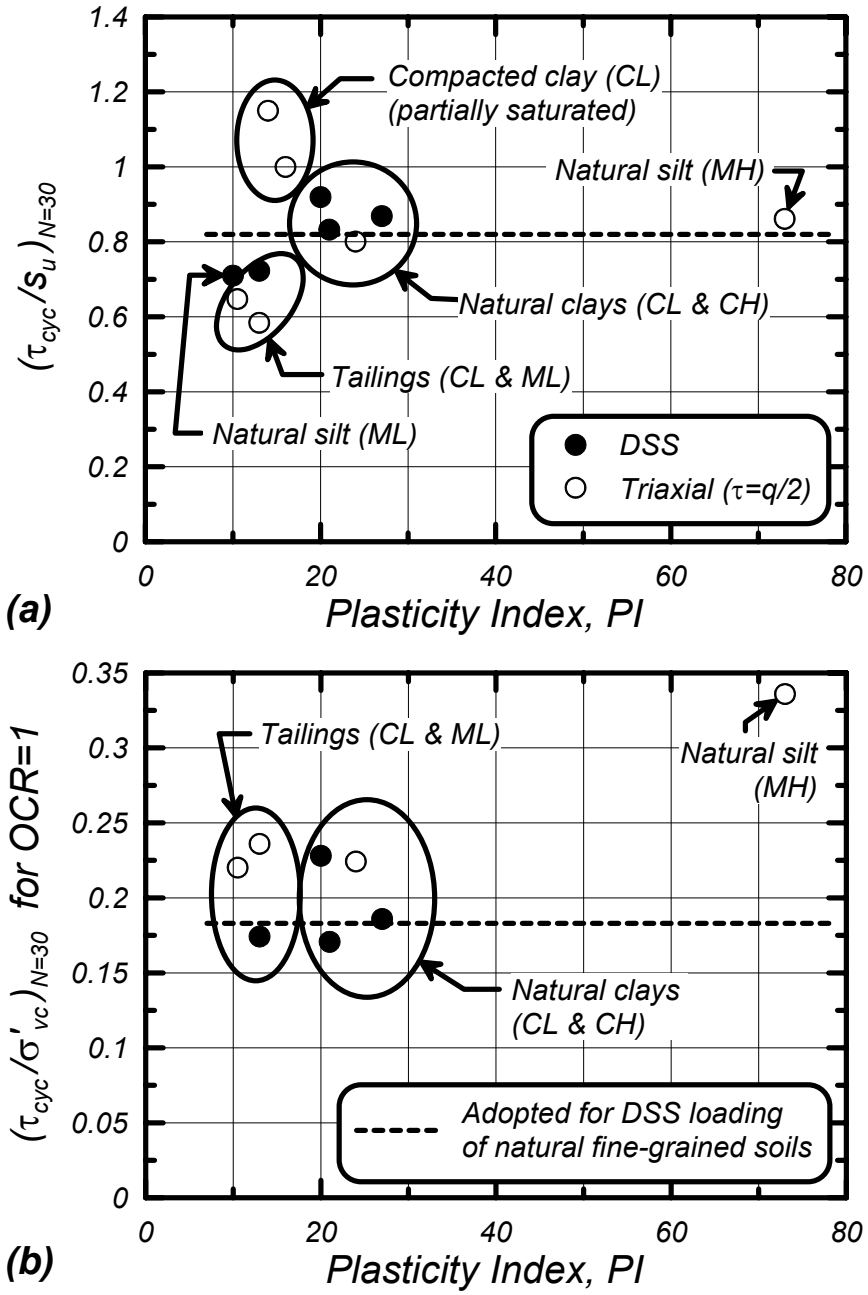

FIG. 3-12: Variations in cyclic strength ratios with plasticity index for clay-like fine-grained soils and proposed relations for design.

4. CASE HISTORY APPLICATIONS

4.1 Fourth Avenue slide in Anchorage during the 1964 Alaskan earthquake

The Fourth Avenue slide in Anchorage during the 1964 Alaskan Earthquake provides an opportunity to evaluate the proposed procedure's abilities to distinguish between the areas that experienced large ground displacements and the areas where movements were relatively small. A brief overview of background information from Idriss (1985) is provided before presenting the analysis results.

The Fourth Avenue slide damaged an area about 1,600 feet long and 900 feet wide between Fourth and First Avenues and between E Street and slightly east of A Street in Anchorage. The photograph in Fig. 4-1 shows the nature of the dramatic ground deformations along Fourth Avenue at the head of the landslide. Three cross-sections across the landslide are shown in Fig. 4-2, illustrating how the sliding was primarily translational toward the bluff along the adjacent channel (Ship Creek). The lateral sliding created grabens, within which vertical movements of up to 10 feet were measured. The lateral movements were up to 19 feet between the bluff and the first graben, up to 11 feet between the first and second grabens, and less than a few inches behind the second graben.

The 1964 Alaskan Earthquake (M_w=9.2) was estimated to have produced a peak ground surface acceleration of about 0.15g to 0.20g in Anchorage based on observed patterns of damage to structures and their contents. No strong ground motion recordings were obtained. Eyewitness reports indicated that the sliding initiated about 1.5 to 2 minutes after the start of shaking and that sliding ceased when shaking stopped (duration of strong shaking was about 2 to 3 minutes in other areas while felt motions in Anchorage were reported to range from 4 to 7 minutes).

The soil profile along D Street is illustrated by the cross-section in Fig. 4-3 and the boring/CPT sounding results in Fig. 4-4. These and other exploration results indicate that the upper 35 to 40 feet consists of very dense gravels and sands (Naptowne Outwash), which is underlain by 30 to 35 feet of interbedded layers of clays (Bootlegger Cove clay), silty sands and sandy silts. The clays in this interbedded zone are stiff to very stiff and have OCR of 3 to 4. The silty sands and sandy silts are dense to very dense, as illustrated by the high SPT N values and high CPT tip resistances in Fig. 4-4. The interbedded zone is underlain by a uniform layer of Bootlegger Cove clay to depths greater than 150 feet (limit of exploration). This clay classifies as CL based on typical LL and PI values of 39 and 14, respectively, and was lightly overconsolidated with OCR of about 1.2 to 1.5, as illustrated by the consolidation test data plotted in Fig. 4-5.

The base of the slide was determined to have formed within the Bootlegger Cove clay just beneath the interbedded zone. It is highly unlikely that liquefaction occurred in the dense silty sands and sandy silts in the interbedded zone given their very high penetration resistances, and as indicated by liquefaction analyses that result in very high factors of safety against liquefaction. Failure of the clays in the interbedded zone is also highly unlikely, given that they were more overconsolidated and stiffer than the underlying Bootlegger Cove clay.

The undrained shear strength of the uniform Bootlegger Cove clay layer was assessed using SHANSEP testing of high quality tube samples. The normalized strength results are summarized in Fig. 4-6. In addition, the clay exhibited medium sensitivity with laboratory measurements giving sensitivities (S_t) of about 3 or less (Idriss 1985). The fully remolded shear strength of the clay at large displacements would therefore be expected to be about 1/3 of the peak undrained shear strength.

The potential for cyclic failure of the Bootlegger Cove clay during the 1964 earthquake can now be evaluated using the procedures recommended in this report. The analysis steps are summarized in Table 4-1, showing results for conditions: (a) within the slide mass between the bluff and the first graben, and (b) outside the slide mass. In addition, the calculations are repeated for various values of OCR to illustrate the importance of stress history on the cyclic strength of clay-like soil. The induced CSR was computed for a peak ground surface acceleration of 0.20 g and using the r_d relation by Idriss (1999). Other parts of the analyses are described below.

The static shear stress ratio (α) along the horizontal portions of the slide failure plane was approximated using static equilibrium of three representative soil blocks along B Street. The first soil block extended 180 feet back from the bluff edge and encompassed the zone of greatest ground displacement (i.e., from the bluff to the first graben). The second block was also 180 feet long, extending from 180 to 360 feet back from the bluff and encompassing the remaining zones where ground displacements were several feet (i.e., between the first and second grabens). The third block was again 180 feet long and extended back into the region where ground displacements were less than ½ foot (i.e., behind the second graben). Ground surface and water table elevations are listed in Table 4-1. The upslope side of each block was bounded by a vertical face carrying a horizontal pressure distribution that corresponds to a coefficient of earth pressure K, and the base of each block was assumed to have a constant value of α.

The values of α were then determined for a range of possible assumptions to evaluate likely magnitudes. For example, suppose that K is 0.55 for all three blocks. This value of K is likely smaller than the coefficient of lateral earth pressure at rest (K_o) for the soils above the eventual slide plane because these soils are known to be significantly over-consolidated. Nonetheless, this value of K might be reasonable given that some amount of lateral straining toward the channel might reduce K below the ideal level-ground K_o value. Analyzing the blocks in succession, with K = 0.55 for all three blocks, produces calculated α values of 0.103, 0.055, and 0.0 for blocks 1, 2, and 3, respectively. Alternatively, suppose that K was 0.55, 0.6, and 0.65 for blocks 1, 2, and 3, respectively, as a consequence of being different distances from the channel. In this case, the successive analysis of each block produces calculated α values of 0.095, 0.061, and 0.01 for blocks 1, 2, and 3, respectively. These and other analysis scenarios suggest that α might reasonably be estimated as being about 0.10 near the bluff and 0.01 outside the slide mass for the purpose of illustrating the potential effect that static shear stresses can have on computed CRR values.

K_α values can then be estimated for the critical surface both near the bluff (inside the slide mass) and outside the slide mass (where movements were less than ½ foot). The K_α values estimated using the previously derived relation (Fig. 2-32) for clay-like soils are about 0.87 near

the bluff and 0.99 outside the slide mass, which is a difference of about 12%. This difference in K_α contributes to the reason why the potential for ground displacements decreases with distance from the bluff. In fact, they are consistent with retrogressive sliding wherein failure would initiate very close to the bluff where α is greatest (likely much larger than the average of 0.10 assumed over the nearest 180 feet of slide mass). As the soil strength drops to its residual value along the base of the initiating slide mass, there would be an increase of shear stresses on the soils behind it (i.e., a transfer of shear stress to the still stable regions). The mass of soil immediately behind the initiating slide mass would then have the greatest static shear stress ratio and thus be most likely to fail next. In this manner, the slide would progress retrogressively in-land over the duration of shaking.

The computed CRR for both locations are plotted versus assumed OCR in Fig. 4-7, and the corresponding factors of safety against cyclic failure are plotted in Fig. 4-8. The CSR were approximately equal at the two locations, despite the differences in soil and water table depths to the bases of these blocks. The values of $CRR_{7.5}$ were computed as 0.8 times the undrained shear strength ratio, as recommended in Section 3.3. The CRR in the stable zone outside the slide mass was greater than the CRR within the slide mass for two reasons. First, the OCR outside the slide mass was closer to 1.3 compared to the OCR within the slide mass of about 1.2, which produces a difference in CRR of about 7%. Second, the difference in static shear stress ratio at these locations, as discussed above, results in K_α values that are about 12% smaller for the area in the slide mass versus the area outside the slide mass. Together, these differences result in computed factors of safety of about 0.94 for the slide mass and about 1.13 for the zone outside the slide mass. These results are in good agreement with the observed behavior given the uncertainty in the estimated ground motions. Particularly noteworthy is the fact that the analysis results can differentiate between the zones of large versus small deformations.

The consequences of cyclic failure near the bluff, in terms of potential displacements, could now be estimated using Newmark-type sliding block analysis procedures, as was done by Idriss (1985) for this case history. In those analyses, Idriss (1985) showed that the ground deformations were reasonably estimated using a Newmark sliding block approach coupled with the relation shown in Fig. 4-9 that describes how the clay's undrained strength was assumed to vary with ground surface displacement. This transition in clay strength from it peak value to its fully remolded (residual) strength as strains or displacement increase is, however, an issue that continues to be poorly understood, as previously discussed in Section 3.4.

4.2 Carrefour Shopping Center in Turkey during the 1999 Kocaeli earthquake

The Carrefour Shopping Center case history (Martin et al. 2004) provided a unique set of in situ ground deformation measurements from settlement extensometers during the 1999 Kocaeli earthquake, in addition to observations on the performance of jet grouted areas. These in situ measurements showed significant vertical strains in CL and CH strata, from which Martin et al. concluded that the CL layer had exhibited "liquefaction-type behavior" while "a definitive explanation for significant earthquake-induced settlements in a high-plasticity clay stratum (CH) in Lot C has not yet been found." This case history provides an excellent example of how fine-grained soils can develop significant strains and an opportunity to evaluate the procedures

developed herein. A brief overview of background information from Martin et al. (2004) is provided before presenting the analysis results.

Site conditions and Settlement Extensometer Records

The settlement extensometer (SE) measurements were obtained from Lot C in the Carrefour Shopping Center, as located in Fig. 4-10. The shopping center is located along Izmit Bay in relatively flat area that had been reclaimed by placing sandy fills over the soft alluvial sediments. A typical soil profile at the shopping center, prior to any ground improvements, is shown in Fig. 4-11. A surcharge of 3.3 m of additional fill was placed, along with wick drains to a depth of 20 m, across Lot C to preload the soft sediments. Settlement extensometer SE-2 was located about 10 to 15 m from the edge of the preload as shown in Fig. 4-10, and its rings were located at the depths shown in Fig. 4-12. The SE-2 measurements in Fig. 4-13 indicate that approximately 70-90% of the ultimate consolidation settlements had already occurred prior to the earthquake.

The soil profile and SE-2 measurement intervals at Lot C are shown in Fig. 4-12, with the soil conditions being similar to the profile shown in Fig. 4-11. The surface layer consisted of approximately 2 m of medium dense fill (GC), which likely was unsaturated since the water table was at a depth of about 2 m. The next 5 m of soil consists of saturated, soft to firm, low-plasticity fine-grained soil (ML/CL) having average PI and LL values of 10 and 33, respectively. The average natural water content was 32%, which implies an average liquidity index of LI=0.9. This layer is underlain by about 1.2 m of loose-to-medium, silty sand and sand (SP/SM) having an average of 30% fines and a typical equivalent clean sand SPT corrected blow count [$(N_1)_{60\text{-}cs}$] value of about 12. The sand layer is underlain by about 0.9 m of ML/CL soils, followed by medium to stiff, high plasticity clay (CH) that extends to depths greater than 35 m, and has average PI and LL values of 37 and 66, respectively. Its average natural water content was 55%, which implies an average LI of 0.7. This lower CH layer becomes much stiffer below depths of about 25 m.

The Kocaeli earthquake (M_w=7.4) was estimated to have produced a peak ground acceleration of about 0.24 g at the Carrefour Shopping Center, based on the strong ground motion recordings in the area and the results of one-dimensional site response analyses (Martin et al. 2004). SE measurements before and after the earthquake showed that the earthquake had caused significant vertical strains within the upper 20 m of the soil profile, as illustrated in Fig. 4-13 and corresponding to the intervals A-D in Fig. 4-12. The total earthquake-induced settlement was almost 12 cm.

The sources of the relative settlements caused by the earthquake over each of the five SE-2 measurement intervals (A-E) can be examined using the information in Figs. 4-12 and 4-13. The 2.5 cm of compression over interval A was attributed to the soft ML/CL soils because the unsaturated medium dense GC fill was unlikely to have strained significantly. The 4.6 cm of compression over interval B may have come from both the ML/CL and SP/SM layers, while the 3.6 cm and 1.1 cm of compression over intervals C and D, respectively, could only be associated with straining in the CH layer.

The vertical strains induced in the fine-grained soil layers by the earthquake are largely attributed to undrained shear deformations beneath the surcharge, as illustrated by the schematic cross-section in Fig. 4-14, with some possible contribution from the dissipation of excess pore water pressures prior to the first post-earthquake reading of the slope extensometer. The settlement records in Fig. 4-13 do not show any significant change in the rate of settlement from just before the earthquake to just after the earthquake (i.e., excluding the jumps that occurred between the last pre-earthquake and first post-earthquake readings). This suggests that the excess pore water pressures shortly after the earthquake are not significantly higher than they were before the earthquake. In that case, it is unlikely that the dissipation of excess pore pressures contributed significantly to the observed jumps in settlement on the day of the earthquake. Thus, it is reasoned that the earthquake likely induced only moderate excess pore pressures and that the jump in settlements on August 17th were largely due to undrained shear deformations (e.g., as illustrated in Fig. 4-14).

An estimate of the earthquake-induced shear strains in the clays can be obtained by considering the mechanism for undrained shear deformation beneath the surcharge as illustrated by the schematic cross-section in Fig. 4-14. The vertical strains in the fine-grained soils within intervals A, B, C, and D due to the earthquake, are approximately 0.8%, 1.0%, 1.0%, and 0.2%, respectively. Shearing at SE-2 was likely close to plane strain conditions because SE-2 appears to have been located about 10 to 15 m inward from the middle of one edge of the surcharge (which was roughly 100 m in length; Fig. 4-10). For undrained plane-strain conditions, the vertical compression strains must have been accompanied by equal horizontal extension strains. If the vertical and horizontal strains are principal strains (which assumes that γ_{xy} is zero), then the maximum shear strains in these soils would have been twice the vertical strains, or about 2% as shown by the inner Mohr diagram for strains in Fig. 4-15. If there was additional horizontal shear strain ($\gamma_{xy} > 0$), then the maximum shear strains in these soils would have been greater than 2% (e.g., suppose $\gamma_{xy} = 2\%$ with $\varepsilon_x = -\varepsilon_y = 1\%$, then $\gamma_{max} = 2.8\%$ as shown in Fig. 4-15). Overall, the SE measurements indicate that intervals A to C experienced shear strains that are consistent with the soils being close to cyclic failure.

Preconsolidation stress profile at time of shaking

The estimation of cyclic strength for the clay requires knowledge of the preconsolidation stress profile, which can be obtained by inverse analyses of the consolidation settlement records. For example, the relative vertical compressions over intervals A, B, and C, neglecting the increment associated with the earthquake, correspond to vertical strains of approximately 7.8%, 4.2%, and 1.9%, respectively. For a reasonable range of estimated virgin compression index (C_c) and recompression index (C_r) values, the above strains can only be explained by the soil having eventually become normally consolidated (NC) under the imposed surcharge. The relative compressions over intervals D and E, however, correspond to vertical strains of only 0.6% and 0.4%, respectively, which can only be explained by the soils having been initially overconsolidated and either having just become NC under the imposed surcharge or even staying OC under the imposed surcharge. For example, the observed consolidation settlements over intervals D and E can be reasonably approximated by assuming C_c=PI/74 and C_r=PI/370 (Kulhawy and Mayne 1990) and using an initial OCR of 1.3 at all depths in the interval. These calculations, as presented in Table 4-2, suggest that final OCR, after the clay was fully

consolidated under the surcharge, would range from 1.0 at the top of interval D to 1.1 at the bottom of interval E. Different C_c and C_r estimates along with different assumptions regarding the initial preconsolidation stress profile can produce the same predicted settlements, but all reasonable parameter selections lead to the conclusion that the soils are NC at the shallower depths and are either nearly NC or lightly OC at the larger depths at the time of the earthquake. Consequently, the interpretation of the site's preconsolidation stress history that was used in Table 4-2 was adopted for the purpose of estimating cyclic resistances for the clay-like soils.

Analysis of liquefaction and cyclic failure potential

The potential for liquefaction or cyclic failure during the Kocaeli earthquake can be evaluated using the procedures recommended in this report. The analysis steps and results are summarized in Table 4-3. The sand layers are treated as sand-like while the ML/CL and CH layers are treated as clay-like since the PI values in these layers exceed 7. The vertical effective stress and OCR values in the clay-like soils at the time of the earthquake were computed based on an estimated average degree of consolidation of 80% using the settlement measurements in Fig. 4-13. The induced CSR is computed using the r_d relation by Idriss (1999).

For the clay-like soils, the OCR and CRR values at the time of the earthquake were estimated using the normalized cyclic strength relations derived in Section 3.3 and presented in Fig. 3-11. The presence of the surcharge imposes static shear stresses on the underlying soils, and these static shear stresses must be estimated to determine the value of K_α. The average static shear stress at various depths was estimated as a fraction of the soil's undrained shear strength, with this ratio being directly related to the factor of safety (F) obtained from a limit equilibrium analysis as:

$$\frac{\tau_s}{s_u} = \frac{1}{F} \tag{4-1}$$

Since the soil profile is dominated by clay-like soils, the factor of safety against a bearing failure to any given depth was estimated using a limit-equilibrium-based chart solution (Taylor 1948) as:

$$F = \frac{5.5 \cdot (s_u)_{average}}{H_{fill}\gamma_{fill}} \tag{4-2}$$

where $(s_u)_{average}$ is the average s_u between the ground surface and the depth of interest, with $(s_u)_{average}$ being no less than the average strength to a depth of 10 m. This latter limit on $(s_u)_{average}$ was imposed because SE-2 was located 10 to 15 m from the edge of the surcharge, and thus the smallest potential failure circle that could influence SE-2 was estimated as having to extend to a depth of at least 10 m. The value of F is therefore constant in the upper 10 m, and then increases at larger depths because the $(s_u)_{average}$ increases with depth. The value of τ_s/s_u at each depth was estimated as the inverse of F for that depth, and the K_α value was then determined using the expression derived in Section 2. The K_α values range from 0.86 at the top of the ML/CL layer, to 0.91 at a depth of 25 m. The presence of static shear stresses is also important as they drive the accumulation of shear strain in a biased direction during earthquake shaking, which is the

mechanism by which vertical settlements could develop during undrained loading of these clays (Fig. 4-14). The MSF is near unity because the magnitude is close to 7.5. The calculated factors of safety against cyclic failure in the upper ML/CL layer and the lower CH layer are less than 1.0, indicating that significant strains would be expected to occur, as were in fact observed.

For the sands (SP/SM), the potential for liquefaction was calculated using the procedures and relations recommended in Idriss and Boulanger (2004). These soils would be expected to liquefy during the earthquake, which is consistent with the various observations that were made across the entire Carrefour Shopping Center site (Martin et al. 2004).

Discussion of analysis results

The computed CSR and CRR values are plotted versus depth in Fig. 4-16, illustrating that both the clay-like soils and the sands had factors of safety less than unity against significant straining during this earthquake. Since the proposed CRR relations for clay-like soils used to analyze this case history are based on a failure criterion of about 3% shear strain, the computed factors of safety (FS = 0.74 to 0.90) would suggest that shear strains somewhat greater than 3% might have been expected. The shear strains inferred from the SE measurements are on the order of 2 to 3%, which suggests that the actual factors of safety were not quite as small as shown in Fig. 4-16. Thus, the computed factors of safety appear to be slightly conservative, which is quite reasonable given the various uncertainties in some of the analysis parameters.

The analysis results might be improved, for example, by using a detailed site response analysis to calculate the earthquake-induced CSR or using advanced laboratory testing to obtain site-specific CRR values. The potential effects of the latter point are illustrated by considering the range of the $CRR_{M=7.5}$ values in the data set that was used to derive the empirical CRR relation. Referring to Fig. 3-12(b), the $(\tau_{cyc}/\sigma_{vc}')_{N=30}$ values for one-directional DSS loading of normally-consolidated clay-like soils range from 0.171 to 0.228, from which a reasonably conservative $CRR_{M=7.5}$ value of 0.18 was adopted for the empirical relation in Section 3. If the actual $CRR_{M=7.5}$ value for normally consolidated conditions was 0.22 (i.e., the highest of the three DSS values in Table 3-3 for natural soils multiplied by the correction factor for two-dimensional shaking), then the computed factors of safety would instead range from 0.90 to 1.10, as plotted in Fig. 4-17. Thus, as illustrated by this simple example, the factors of safety computed using the proposed empirical relation for CRR are in quite reasonable agreement with the shear strains inferred from the SE measurements at this site given the various uncertainties in the analysis parameters.

An additional point worth noting is that the observed strains in the fine-grained soils were not large enough to cause their strengths to drop to fully remolded values, otherwise there could have been much larger deformations. The estimated LI values of 0.9 and 0.7 for the ML/CL and CH soils, respectively, along with the correlation to sensitivity in Fig. 2-20, suggest that these soils may classify as very sensitive (S_t of 4 to 8), but not as quick. Future compilations of this type of information are considered necessary for establishing guidelines on how clay-like soil strengths drop toward remolded values with increasing strain or displacement.

The observed behaviors of the ML/CL and CH soil layers can also be qualitatively evaluated relative to the liquefaction susceptibility criteria by Seed et al. (2003) in Fig. 1-4 or Bray et al. (2004a). According to either of these criteria, the ML/CL layer would be categorized as "liquefiable" because its PI (about 10) is less than 12 and its w/LL ratio is greater than 0.85, while the underlying CH layer would be categorized as not susceptible to liquefaction because its PI (about 37) is greater than 20. However, both the ML/CL and CH soil layers developed similar strains despite having very different categorizations by these criteria. In contrast, the results presented herein show that analyzing both soil layers as clay-like produces similar calculated factors of safety, and hence similar expectations for strains, in both soil layers.

The SE measurements at Lot C proved invaluable in understanding the source of the surface deformations in this case history, and provided a useful check on the proposed analysis procedures. A more detailed investigation of this site, including tasks such as in situ vane shear testing and cyclic laboratory testing of high-quality tube samples, would be highly desirable.

4.3 Site A at Wufeng in Taiwan during the 1999 Chi-Chi earthquake

The area referred to as Site A in Wufeng, Taiwan (Chu et al. 2003, Stewart et al. 2004, Chu et al. 2004) provides an excellent opportunity to evaluate the proposed procedure's abilities to differentiate between observations of ground failure and no ground failure around buildings founded over a deposit containing thick layers of fine-grained soils. A brief overview of background observations is provided, before presenting the analysis results, based on information from Chu et al. (2003, 2004), Stewart et al. (2004), and Chu and Stewart (personal communications, 2004).

Site A in Wufeng included areas where ground failure and building settlements were observed and areas where no distress was observed, as shown in Fig. 4-18. An expanded map of Site A with the locations of explorations is shown in Fig. 4-19. The photographs in Fig. 4-20 pertain to four specific locations within site A (as marked in Fig. 4-19) where site explorations included a boring and an adjacent CPT sounding were performed.

- Boring WAS-3 and CPT sounding WAC-8 were at the location of a 6-story building that experienced foundation failure and significant settlement, along with structural damage, as shown in photos (a), (b) & (c). Note that the ground surface away from the buildings showed relatively little evidence of ground failure.
- Boring WAS-4 and CPT sounding WAC-9 were at the location of a 5-story building that experienced foundation failure and significant settlements, along with structural damage, as also shown in photos (a), (b) & (c). Again, the ground surface away from the buildings in this area showed relatively little evidence of ground failure.
- Boring WAS-2 and CPT sounding WAC-6 were located near 3-story buildings, with the buildings to the south of WAS-2 having to be demolished while the building to the north of WAS-2 still exists. Field observations included some ground failure (cracking, differential settlements) in the area around the standing building [photos (d) and (e)], while settlement of the building itself was not particularly notable.

- Boring WAS-1 and CPT sounding WAC-2 were in an area of 1-story buildings that showed no evidence of building settlements or ground failure away from the buildings, as illustrated by photo (f).

The overall pattern of observations, as illustrated by these four specific building locations, was that the taller buildings (5- and 6-story) tended to experience significant settlements or foundation failures, while there tended to be little or no ground failure in the free field or beneath 1-story buildings.

A strong ground motion instrument (TCU065) was located about 1 km north of Site A, as shown in Fig. 4-18, during the 1999 Chi-Chi earthquake. The two horizontal accelerograms recorded at this station are shown in Fig. 4-21. The peak ground surface acceleration of the E-W component was 0.814g and that of the N-S component was 0.603g. The geometric mean for these two components is 0.70g, which is the value used in the subsequent analyses of potential ground failure at Site A. No ground failure was observed near the accelerometer location.

Site explorations included CPT soundings, borings with SPT tests, vane shear tests, and shear wave velocity measurements; the results are available at the website for Stewart et al. (2004). The soil profiles at site A generally consisted of 1 to 2 m of fill overlying 4 to 7 m of firm to stiff, fine-grained CL, ML, and CL-ML soils. The fine-grained soils are underlain by primarily medium-dense and dense silty sands with inter-layers of stiff to very stiff silts and clays, extending to depths of 15 m or more (approximate limit of exploration at most locations). The water table depth ranged from 0.5 to 1.1 m. Soil profiles for the four building locations are presented in Figs. 4-22 to 4-25.

The firm to stiff silt and clay stratum

The characteristics of the 4- to 7-m thick layer of firm to stiff clay-like soils (CL, ML, and CL-ML) that is present at the four exploration locations are of primary importance to the analyses of these sites. In evaluating these characteristics, the information from the four exploration locations can be considered together because it is a common geologic stratum that does not appear to vary substantially across these locations based on comparisons of the CPT and borehole data. The PI values obtained from 20 samples in this stratum are plotted in Fig. 4-26; three samples (15%) had PI ≤ 3, six samples (30%) had PI = 5 or 6, and eleven samples (55%) had PI ≥ 7. These values would suggest that slightly less than half of the samples would classify as sand-like (PI < 7) according to the criteria recommended in Section 2.5, while slightly greater than half would classify as clay-like. However, 5 of the 6 samples that had PI values of 5 or 6 classified as CL-ML soils (Fig. 4-26), for which a slightly lower criterion was acknowledged in Section 2.5 as being equally consistent with the empirical data. If these 5 samples that classified as CL-ML are considered as clay-like, then only 20% of the 20 samples would classify as sand-like while 80% would classify as clay-like. In addition, occasional thin lenses of sands appear to be present within this stratum based on the CPT soundings.

The s_u values measured by vane shear tests in the firm to stiff clay-like soil stratum ranged from 35 to 64 kPa (average of 48 kPa), and had a general trend of increasing with depth. Sensitivities obtained from the vane shear tests ranged from 1.2 to 3.1, with an average of about 2, making this a slightly sensitive to medium sensitivity soil. As discussed in the following

section, the CPT tip resistances provided comparable estimates of s_u values throughout the majority of the stratum (excluding what appear to be sand lenses).

The sand-like portions of this stratum would be expected to liquefy based on established liquefaction analyses because these soils have low penetration resistances and the levels of shaking are very high. The consequences of these sand-like portions having liquefied depend on their relative extent and spatial distribution within the stratum. Consider the following two possibilities.

- If almost half of the stratum is considered sand-like (based on the PI < 7 criterion), then liquefaction of the sand-like soils would be expected to result in ground failure throughout the area. In this situation, the challenge would be explaining the general trend of greater damage beneath buildings while the free-field areas showed no or relatively little ground failure.
- If only 20% of the stratum is considered sand-like (i.e., assuming the CL-ML soils with PI values of 5 or 6 behave as clay-like), then liquefaction of these portions may have contributed to the observed ground failure patterns and to any observed soil boils, but it is most likely that the overall pattern of damage was controlled by the clay-like sediments within this strata.

A detailed laboratory testing program would be very useful for evaluating the stress-strain behavior of these low-plasticity fine-grained soils and thereby potentially justifying the classification of the CL-ML soils at this site as clay-like in behavior (an important option discussed in Sections 2 and 3). Furthermore, the criterion of PI < 7 was adopted as a reasonably conservative indicator of the range of PI values over which fine-grained soil transitions from sand-like to clay-like behavior, whereas it may be more appropriate to use a best-estimate criterion in the analysis of a case history. In any event, it appears necessary to at least consider the potential that either of the above two possibilities is more appropriate. The outcome of the first possibility (i.e., half the stratum is sand-like) is easily foreseen to be the prediction of widespread liquefaction, which is not supported by the observations and hence is not pursued herein. The second possibility (i.e., 80% of the stratum is clay-like) provides an opportunity to evaluate the analysis procedures recommended herein. Consequently, the following analyses will focus on the potential for cyclic failure of the clay-like soil portions of the stratum and on whether the computed factors of safety are consistent with the observed damage patterns throughout site A.

The photographs in Fig. 4-27 show the surface fill and the top of the underlying clay-like stratum, as exposed by the test pits that were excavated for performing additional VST tests near borings WAS-4.

Estimating undrained shear strength profiles for the clay-like soil layer

Undrained shear strength (s_u) profiles were developed using the VST and CPT results, as summarized in Figs. 4-22 to 4-25 for each of the four building locations. The s_u profiles at the locations of borings WAS-3 and WAS-4 were determined first because that is where the vane shear tests were performed. The vane shear strengths were multiplied by a vane shear correction factor of 1.1 based on the typical PI values of 5 to 10 and the correction factor relation shown in Fig. 3-10. The choice of cone bearing factor (N_k) for computing s_u from CPT data was then

chosen to provide a reasonable fit with the vane shear test results. As shown in Figs. 4-22 and 4-23, an N_k value of 15 provides reasonably good agreement between the VST and CPT estimates of s_u. The dashed lines in this figure represent the s_u values chosen for subsequent analyses of cyclic failure potential. In choosing representative s_u values, it should be recognized that the individual spikes in q_{cN} (=q_c/P_a, with P_a = atmospheric pressure) within this clay-like soil layer are likely due to thin lenses of sandy silt or silty sand, and thus may not represent locally larger s_u values.

The s_u profiles at the other two building locations (Figs. 4-24 and 4-25) were subsequently developed based on the nearby CPT soundings using the N_k=15 value that had been calibrated by VST results in the same geologic strata. Again, dashed lines identify the representative s_u values chosen for subsequent analyses of cyclic failure potential.

The VST data were measured at locations where the buildings had been demolished, which means that the effective overburden stress at the time of VST testing was smaller than existed beneath the buildings at the time of the earthquake. This is unlikely to have significantly affected the measured undrained shear strengths because they are most strongly dependent on the soil's preconsolidation stress and would only be slightly affected by changes in the current overburden stress because these soils are overconsolidated. Given the uncertainties associated with spatial variability and other factors, the measured VST strengths were assumed to be representative of the undrained strengths both beneath the buildings and in the surrounding free field at the time of the earthquake.

Foundation types and loads

The foundation types and loads for the buildings at each location were estimated based on information provided by Chu (personal communication, 2004), which was based on visual inspections and discussions with some local structural engineers and contractors. The estimated loads and dimensions are somewhat uncertain given that they are not based on actual building plans, but reasonable variations in the estimated values do not change the major conclusions drawn from subsequent analyses.

The 5- and 6-story buildings by WAS-4 and WAS-3, respectively, had shallow mat foundations over the rear 2/3 of the building footprint and spread footings (assumed square) beneath the columns at the front of the building; photo 4-20(c) shows the individual columns at the front of a building. It is reportedly common to have an underground water storage tank built into the mat foundation for these types of buildings, but this aspect was not included in the analyses given the lack of specific information for these buildings. The average net building loads were estimated at 10 kPa per floor over the entire building footprint, which corresponds to net contact pressures of 50 kPa and 60 kPa on the mat portions of the 5- and 6-story buildings, respectively. The front columns were assumed to be supported on 2-m-square footings with net contact pressures of 150 kPa for both buildings.

The 3-story building by WAS-2 was assumed to be supported on shallow strip footings with widths of 1.5 m and net contact pressures of 120 kPa. When averaged over the entire building footprint, this was assumed to correspond to an average net contact pressure of 30 kPa.

The 1-story building by WAS-1 was assumed to be supported on shallow strip footings with widths of 0.6 m and net contact pressures of 60 kPa. When averaged over the entire building footprint, this was assumed to correspond to an average net contact pressure of 6 kPa.

The embedment depth for the shallow foundations (both mats and spread footings) beneath all four buildings was taken as 1.0 m for simplicity. A backhoe pit adjacent to the building by WAS-3 showed the mat foundation to be embedded 1.2 m, while embedment depths for other buildings might have varied depending on the depth of the water table (which ranged from depths of 0.5 to 1.1 m). The key observation is that the foundations appear to have been founded near the bottom of the surface fill or directly on the underlying clay-like soils.

Estimating the effects of foundation loads on the seismic shear stresses

The horizontal cyclic shear stresses induced on the soil by the earthquake will be affected by the presence of the overlying buildings. One approach to incorporate this effect would be to compute the vertical stresses beneath the building and then use those values in computing the induced CSR by the Seed-Idriss simplified procedure. Such an approach, however, would likely over-estimate the building's contribution to the horizontal cyclic stresses because it implicitly assumes that the building's peak inertial load would occur at the same time as the peak ground surface acceleration. Some level of yielding in the building would reduce its contribution to cyclic stresses in the soil, and thus the following simplified approximation was adopted for the analyses presented herein,

$$\left(\frac{\tau_{cyc}}{\sigma'_{vc}}\right) = \left(\frac{0.65 \cdot a_{max} r_d \cdot (\sigma_v)_{soil} + k \cdot \Delta\sigma_{v,building}}{\sigma'_{vc}}\right) \quad (4\text{-}3)$$

where $(\sigma_v)_{soil}$ is the total vertical stress without the influence of the building, $\Delta\sigma_v$ is the increase in total vertical stress due to the building, σ'_{vc} is the vertical effective consolidation stress which includes the influence of the building, and k is a coefficient that depends on the building's lateral strength and dynamic response relative to the soil column.

The estimation of k for the buildings at Site A is subjective given the limited information available, and the desire to maintain simplicity in the analysis procedures. A value of k = 0.2 was adopted based on consideration of reasonable lateral strengths and the fact that a yielding building would produce several cycles of stress at that yield value (i.e., the ratio of representative cyclic stress to peak cyclic stress would be closer to 1.0 for the building than to the 0.65 used for cyclic stresses from soil inertia). Comparing k = 0.2 to the value of $0.65a_{max} = 0.455$ shows that this approach reduces the cyclic stresses from the building to less than ½ the value that would have been computed if the building had just been treated as increasing σ_v in the Seed-Idriss simplified procedure.

The $\Delta\sigma_v$ imposed on the soil by the buildings was estimated using 2:1 load spreading. For rectangular areas of width B and length L carrying a net contact pressure q_{net}, the $\Delta\sigma_v$ at a depth z below the footing is estimated as,

$$(\Delta\sigma_v) = q_{net}\frac{(B \cdot L)}{(B+z)(L+z)} \tag{4-4}$$

For strip footings with L/B being large, this reduces to,

$$(\Delta\sigma_v) = q_{net}\frac{(B)}{(B+z)} \tag{4-5}$$

For spread footings, the $\Delta\sigma_v$ will be dominated by the footing contact stress near the ground surface, and then later at depth will begin to include overlapping stresses from adjacent footings. The effect of overlapping stresses at larger depths can be approximated by treating the building as a uniformly loaded area over its full footprint (with the corresponding average net contact pressure). The $\Delta\sigma_v$ at any given depth beneath a building on spread footings would then be estimated as the larger of the above two cases.

Estimating the static shear stresses beneath building foundations for computing K_α

The value of K_α was computed using the expression between K_α and τ/s_u that was presented in section 2.5. The ratio τ/s_u can be estimated based on the factor of safety ($F=s_u/\tau$) against bearing failure to a given depth. The static factor of safety against bearing failure for shallow foundations can be estimated using the general bearing capacity equation as,

$$F_{static} = \frac{q_{ult,net}}{q_{net}} = \frac{N_c s_u F_{cs} + (N_q - 1)\gamma D_f F_{qs} + \frac{1}{2}\gamma N_\gamma B F_{\gamma s}}{q_{net}} \tag{4-6}$$

Since the foundations are embedded into (or very close to) the underlying clay-like stratum, the static bearing capacity is governed by the undrained strength of the clay-like soils. For this condition ($\phi_u=0$), the factor of safety reduces to,

$$F_{static} = \frac{5.1 s_u F_{cs}}{q_{net}} \tag{4-7}$$

where the shape factor F_{cs} is 1.0 for strip footings and 1.2 for square footings, and s_u is the average undrained shear strength along the potential bearing failure surface. If the footing width is B, then the bearing failure surface would be expected to extend to a depth of slightly less than B below the footing base. Therefore, the value of F computed using the above expression was taken as applicable for all depths less than or equal to B below the footing base. The footings will still exert significant shear stresses on soils at greater depths, but the factor of safety against such deeper-seated failure surfaces is greater and thus do not govern footing design. For potential failure surfaces that extend to a depth z (below the footing base) that is greater than the footing width B, the factor of safety computed by the above expressions was multiplied by the ratio z/B. This correction approximates the fact that the average shear stresses induced by a footing will decrease with increasing depth.

The seismic response of the building will impose cyclic vertical loads, horizontal loads, and overturning moments on the building foundations. These loads can only be crudely estimated without a detailed analysis of the building which would also require more information about the building configuration. Despite this uncertainty, it is necessary to include at least a rough estimate or allowance for the effects of these cyclic loads. This was subsequently accomplished by reducing the static factor of safety against bearing failure, F_{static}, by a factor of 1.3.

$$F_{seismic} = \frac{F_{static}}{1.3} \tag{4-8}$$

The value of F for seismic loading was then used in the computation of K_α, which assumes that the additional shear stresses from the cyclic vertical, horizontal, and overturning loads on footings can be reasonably accounted for through the K_α factor. This approximation is considered a reasonable approach because it maintains simplicity in the analysis approach while providing a first-order estimate of the expected effects of cyclic footing loads.

Analyses of the potential for cyclic failure in the clay-like soils at the four building locations

The analysis results for the cyclic failure potential of the clay-like soils at each of the four building locations during the 1999 earthquake are presented in Fig. 4-28 and tabulated in Table 4-4. The calculations are only presented for the clay-like soils because the underlying dense silty sands are not expected to have been the primary cause of the observed patterns of ground failure, even if they developed high excess pore pressures, because they are dense enough to develop only limited strains. The induced CSR was computed for a peak ground surface acceleration of 0.70 g and using the r_d relation by Idriss (1999). The $CRR_{7.5}$ was estimated as $0.8s_u/\sigma_{vc}'$, as recommended in Section 3.3. The CRR and factor of safety against cyclic failure are computed for both the free-field conditions and beneath the building. For the 5-story and 6-story buildings, this includes analyses for the spread footings under the front columns and for the mat foundations over the rear portions of the buildings. The tabulated results are presented mainly at depth increments of 1 m.

For the 6-story building near boring WAS-3, the analysis results in Fig. 4-28(a) show that the factor of safety against cyclic failure beneath the column spread footings was less than 1.0 throughout most of the clay-like stratum (from depths of 1.0 to 8.2 m), which is consistent with the observed bearing failures [e.g., photo in Fig. 4-20(c)]. The factors of safety beneath the mat portion were slightly greater but still predict cyclic failure throughout much of the clay-like stratum, which is again consistent with the observed foundation settlements. For the free-field, the factors of safety are substantially larger and cyclic failure is only predicted within thin intervals at depths of 3.5, 6, and 8 m. Cyclic failure in thin zones in the free field would not be expected to result in significant ground distress because the site is relatively flat and the soils are only slightly sensitive. Thus, the free-field analysis results are consistent with the field observations of relatively little ground distress away from the influence of the building.

For the 5-story building near boring WAS-4, the analysis results in Fig. 4-28(b) show similarly good agreement with the field observations. Cyclic failure is predicted beneath the spread footings, with the lowest factors of safety occurring directly beneath the footings in the

depth range of 1.0 to 3.0 m. For the free-field, the factors of safety against cyclic failure are well above 1.0 except for a thin interval at a depth of 5.5 m. Intermediate factors of safety are computed beneath the mat foundation portion of the building, with cyclic failure predicted in sufficiently thick intervals to explain the observed foundation settlements. Thus, the analysis results are again consistent with the field observations of significant foundation settlements and relatively minor ground distress away from the influence of the building.

For the 3-story building near boring WAS-2, the analysis results in Fig. 4-28(c) show factors of safety that are close to unity at almost all depths in the clay-like stratum beneath the spread footings, and factors of safety that are generally greater than unity at all depths in the free-field (except for thin zones at 5.5 and 8 m depths). The field observations for this building were more ambiguous, with minor ground distress having been reported in the free-field but no significant foundation settlements were reported.

For the 1-story buildings near boring WAS-1, the analysis results in Fig. 4-28(d) show that cyclic failure would not be expected at any depth in either the free-field or beneath the buildings. These results are in good agreement with the observed absence of ground distress or building settlements in this area [e.g., photo in Fig. 4-20(f)].

Spatial heterogeneity in the undrained shear strengths of the clay-like soil layer in the depth range of about 1 to 8 m, are an important consideration when evaluating the results of the above analyses. For example, the undrained shear strengths between depths of 2 and 3 m (an important depth interval for support of the shallow foundations) were about 40, 60, 32, and 38 kPa near borings WAS-1, 2, 3, and 4, respectively, which represents a factor of about 2 between the strongest and weakest values. The undrained shear strengths at other depths within this clay-like soil layer varied, from strongest to weakest, by factors of about 1.3 to 1.9. In this regard, it is important to recognize that the soil explorations (borings, CPT soundings, and vane shear tests) were not necessarily fully representative of the conditions across the footprint of the buildings being analyzed. Thus, the actual undrained shear strengths at each of the four building locations could reasonably vary from the values estimated herein, with only small variations being necessary to increase or decrease computed factors of safety above or below unity. Recognizing this inherent limitation, it is concluded that the computed potential for cyclic failure of the clay-like soils at these four buildings are entirely consistent with the general pattern of field observations showing significant settlements for the tallest buildings and the absence of deformations in the free-field or beneath 1-story buildings.

The role of the buildings on the computed potential for cyclic failure in the clay-like soil layer has several important components that are illustrated by the tabulated calculation steps in Table 4-4.

- The static load from a building produces static shear stresses that reduce the underlying clay-like soil's CRR, as represented through the K_α value.
- The horizontal inertia of a building increases the cyclic horizontal shear stresses (or CSR) in the underlying soil.
- The horizontal inertia of a building also produces cyclic loads on its foundation elements (vertical, horizontal, and overturning loads) that further increase the potential for cyclic

failure in the underlying soils. This effect was approximated by computing K_α using a factor of safety against bearing failure that was reduced for seismic loading conditions.

- Each of these effects decreases with depth below the building because the stresses from the building become smaller (relative to those from the soil alone) with increasing depth.

Another important factor that is not explicitly represented in Table 4-4 is the fact that cyclic failure of soils beneath a building will be accompanied by the accumulation of biased strains and deformations under the building's static weight. Without a building or with a very light building, cyclic failure of clay-like soils over limited depths in a level-ground area may not necessarily be accompanied by the accumulation of permanent displacements and therefore the ground surface may not exhibit any signs of deformation or damage.

The observed consequences of cyclic failure in the clay-like soils also appear to be consistent with the available data on their sensitivity. The VST measurements produced S_t values of 1.2 to 3, which suggest that their fully remolded strengths would still be on the order of ½ their pre-earthquake values. This range of values would appear consistent with the observations of buildings in this level-ground area having settled various amounts, but not having developed dramatic bearing failures (such as might be expected if the soils had been highly sensitive or quick).

The analysis results for Site A show that the recommended procedures are able to distinguish between conditions leading to ground failure or building settlements and conditions where ground failure did not occur. The analyses could be better refined with more information about the building loads and configurations, and the development of improved methods for representing the effects of buildings on the cyclic failure potential of underlying soils. While such improvements are needed, the main conclusions presented herein are unlikely to be affected. In contrast, if the clay-like soils between depths of 1 and 8 m had been classified as "liquefiable" based on their index test characteristics [e.g., 64% of the samples classify as liquefiable (Zone A) by Seed et al.'s (2003) criteria in Fig. 1-4], then a liquefaction analysis based on SPT or CPT penetration resistances would have predicted widespread ground failure beneath the buildings and in the free-field, and thus could not have distinguished between the areas of good and poor performance.

Table 4-1: Results from the analyses of the potential for cyclic failure in the Bootlegger Cove clay at Fourth Avenue in Anchorage during the 1964 Alaskan earthquake.

Ground surface elevation (ft)	Depth to failure surface (ft)	Depth to water table (ft)	σ_v (ksf)	σ_{vc}' (ksf)	a_{max} (g)	r_d	MSF	$CSR_{7.5}$	OCR	s_u/σ_{vc}'	Static shear stress ratio, α	K_α	$CRR_{7.5}$	FS
(a) Slide mass within 180 feet of bluff														
90	50	35	6.25	5.31	0.20	1.00	0.94	0.163	1	0.190	0.10	0.838	0.127	0.78
									1.1	0.205	0.10	0.856	0.140	0.86
									1.2	0.219	0.10	0.871	0.153	0.94
									1.3	0.233	0.10	0.883	0.165	1.01
									1.4	0.247	0.10	0.892	0.176	1.08
									1.6	0.274	0.10	0.907	0.199	1.22
									1.8	0.301	0.10	0.918	0.221	1.36
(b) Outside slide mass (from 360 to 540 feet away from bluff)														
105	65	45	8.125	6.88	0.20	1.00	0.94	0.163	1	0.190	0.01	0.990	0.150	0.92
									1.1	0.205	0.01	0.990	0.162	0.99
									1.2	0.219	0.01	0.991	0.174	1.06
									1.3	0.233	0.01	0.992	0.185	1.13
									1.4	0.247	0.01	0.992	0.196	1.20
									1.6	0.274	0.01	0.993	0.218	1.33
									1.8	0.301	0.01	0.994	0.239	1.46

Notes:

[a] Earthquake parameters: M=9.2, a_{max}=0.20g

[b] Total unit weight of 125 pcf for all soils above slide plane.

[c] For clays, used $CRR_{7.5} = 0.8\ s_u/\sigma_{vc}'$.

Table 4-2: Results of one-dimensional consolidation settlement calculations for Lot C in the Carrefour Shopping Center.

Soil layer	Depth to top of layer (m)	Depth to bottom of layer (m)	Layer thickness (m)	Unit weight (kN/m^3)	Void ratio	σ_{vo} at mid layer (kPa)	σ_{vo}' at mid layer (kPa)	$\Delta\sigma_v$ (kPa)	After surcharge σ_{vf}' (kPa)	Initial OCR	σ_{vp}' (kPa)	Final OCR	PI	C_c	C_r	Vertical strain (%)	ΔH for sublayer (m)	Calculated ΔH_{ult} over interval (m)	Observed ΔH_{ult} over interval (m)
Existing fill (GC)	0	2	2	20	0.64	20	20	65	85	--	--	--	--	--	--	--	--	*Interval A (0.0 - 5.0 m)*	
ML/CL	2	3	1	18.6	0.85	49	44	63	107	1	44	1.00	10	0.135	0.027	2.79	0.028		
" "	3	4	1	18.6	0.85	68	53	62	115	1	53	1.00	10	0.135	0.027	2.43	0.024		
" "	4	5	1	18.6	0.85	87	62	60	122	1	62	1.00	10	0.135	0.027	2.15	0.022	0.074	0.235
" "	5	6	1	18.6	0.85	105	71	59	130	1	71	1.00	10	0.135	0.027	1.93	0.019	*Interval B (5.0 - 9.5 m)*	
" "	6	7.2	1.2	18.6	0.85	126	80	58	139	1	80	1.00	10	0.135	0.027	1.72	0.021		
SM with SP/SC	7.2	8.4	1.2	20	--	149	92	57	149	--	--	--	--	--	--	--	--		
ML/CL	8.4	9.5	1.1	18.6	0.85	171	103	56	158	1.3	134	1.00	10	0.135	0.027	0.70	0.008	0.048	0.187
CH	9.5	10	0.5	16.4	0.85	185	109	55	164	1.3	142	1.00	37	0.500	0.100	2.30	0.012	*Interval C (9.5 - 13.2 m)*	
"	10	11	1	16.4	1.47	198	114	54	168	1.3	148	1.00	37	0.500	0.100	1.56	0.016		
"	11	12	1	16.4	1.47	214	121	53	174	1.3	157	1.00	37	0.500	0.100	1.36	0.014		
"	12	13.2	1.2	16.4	1.47	232	128	52	180	1.3	166	1.00	37	0.500	0.100	1.15	0.014	0.055	0.069
"	13.2	14	0.8	16.4	1.47	248	135	51	186	1.3	175	1.00	37	0.500	0.100	0.99	0.008	*Interval D (13.2 - 20.5 m)*	
"	14	15	1	16.4	1.47	263	141	50	191	1.3	183	1.00	37	0.500	0.100	0.85	0.008		
"	15	16	1	16.4	1.47	280	147	49	197	1.3	191	1.00	37	0.500	0.100	0.70	0.007		
"	16	17	1	16.4	1.47	296	154	49	202	1.3	200	1.00	37	0.500	0.100	0.57	0.006		
"	17	18	1	16.4	1.47	312	160	48	208	1.3	208	1.00	37	0.500	0.100	0.46	0.005		
"	18	19	1	16.4	1.47	329	167	47	214	1.3	217	1.01	37	0.500	0.100	0.44	0.004		
"	19	20.5	1.5	16.4	1.47	349	175	46	221	1.3	228	1.03	37	0.500	0.100	0.41	0.006	0.044	0.041
"	20.5	22	1.5	16.4	1.47	374	185	45	230	1.3	241	1.05	37	0.500	0.100	0.38	0.006	*Interval E (20.5 - 25.0 m)*	
"	22	23	1	16.4	1.47	394	193	44	237	1.3	251	1.06	37	0.500	0.100	0.36	0.004		
"	23	24	1	16.4	1.47	411	200	43	243	1.3	260	1.07	37	0.500	0.100	0.34	0.003		
"	24	25	1	16.4	1.47	427	206	43	249	1.3	268	1.08	37	0.500	0.100	0.33	0.003	0.016	0.015

[a] Water table at a depth of 2 m.

[b] Consolidation settlements calculated for one-dimensional (vertical) strains. Shear distortion under the fill would increase the vertical strains.

[c] Compression index and recompression index estimated using C_c = PI/74 and C_r = PI/370.

[d] The sand layer and gravelly clay fill layer are assumed to have developed negligible vertical strain under static loading.

Table 4-3: Results from the analyses of the potential for liquefaction of the sand-like soils or cyclic failure of the clay-like soils at Lot C in the Carrefour Shopping Center during the 1999 Kocaeli earthquake.

									Clay-like soils								Sand-like soils					
Soil layer	Depth below original surface (m)	Initial σ_{vo} (kPa)	Initial σ_{vo}' (kPa)	Surcharge $\Delta\sigma_v$ (kPa)	Final σ_{vf} (kPa)	σ_{vc}' at earthquake (kPa)	r_d	CSR	OCR at earthquake	s_u/σ_{vc}'	Estimated s_u at earthquake (kPa)	FS against bearing failure to this depth	K_α	MSF	CRR	FS	$(N_1)_{60,cs}$	$CRR_{M=7.5}$ for α=0	K_α	MSF	CRR	FS
Existing fill (GC)	0	0	0	66	66	53																
	2	40	40	63	103	91																
ML/CL	2	40	40	63	103	91	0.95	0.17	1.00	0.220	20	2.3	0.85	1.00	0.15	0.90						
	3	59	49	62	121	99	0.94	0.18	1.00	0.220	22	2.3	0.85	1.00	0.15	0.85						
	4	77	58	61	138	106	0.93	0.19	1.00	0.220	23	2.3	0.85	1.00	0.15	0.81						
	5	96	66	60	156	114	0.91	0.19	1.00	0.220	25	2.3	0.85	1.00	0.15	0.79						
	6	114	75	59	173	122	0.90	0.20	1.00	0.220	27	2.3	0.85	1.00	0.15	0.77						
	7.2	137	86	57	194	132	0.88	0.20	1.00	0.220	29	2.3	0.85	1.00	0.15	0.75						
SM with SP, SC lenses	7.2	137	86	57	194	143	0.88	0.19				2.3					12	0.13	0.99	1.03	0.14	0.72
	8.4	161	98	56	217	154	0.86	0.19				2.3					12	0.13	0.99	1.03	0.14	0.71
CH (with ML/CL at top)	8.4	161	98	56	217	143	0.86	0.20	1.00	0.220	31	2.3	0.85	1.00	0.15	0.75						
	10	187	108	55	242	152	0.84	0.21	1.00	0.220	33	2.3	0.85	1.00	0.15	0.74						
	11	203	115	54	257	158	0.82	0.21	1.00	0.220	35	2.4	0.86	1.00	0.15	0.74						
	12	220	122	53	272	164	0.81	0.21	1.00	0.220	36	2.4	0.86	1.00	0.15	0.74						
	13	236	128	52	288	170	0.79	0.21	1.00	0.220	37	2.5	0.87	1.00	0.16	0.74						
	14	253	135	51	303	175	0.78	0.21	1.00	0.220	39	2.5	0.87	1.00	0.16	0.74						
	15	269	141	50	319	181	0.76	0.21	1.01	0.222	40	2.6	0.87	1.00	0.16	0.76						
	16	285	148	49	334	187	0.75	0.21	1.03	0.225	42	2.6	0.88	1.00	0.16	0.77						
	17	302	155	48	350	193	0.73	0.21	1.04	0.227	44	2.7	0.88	1.00	0.16	0.79						
	18	318	161	47	366	199	0.72	0.21	1.05	0.229	46	2.7	0.88	1.00	0.17	0.80						
	19	335	168	47	381	205	0.71	0.20	1.06	0.231	47	2.8	0.89	1.00	0.17	0.82						
	20	351	174	46	397	211	0.69	0.20	1.07	0.233	49	2.9	0.89	1.00	0.17	0.83						
	21	367	181	45	412	217	0.68	0.20	1.08	0.235	51	2.9	0.89	1.00	0.17	0.85						
	22	384	188	44	428	223	0.67	0.20	1.09	0.236	53	3.0	0.90	1.00	0.17	0.86						
	23	400	194	44	444	229	0.66	0.20	1.10	0.238	54	3.0	0.90	1.00	0.17	0.87						
	24	417	201	43	459	235	0.65	0.20	1.11	0.239	56	3.1	0.90	1.00	0.18	0.89						
	25	433	207	42	475	241	0.64	0.20	1.12	0.241	58	3.2	0.91	1.00	0.18	0.90						

Notes:

[a] Earthquake parameters: M_o=7.4, a_{max}=0.24g

[b] Water table at 2 m depth. Total unit weights: 20 kN/m^3 for the surcharge, GC and SM layers, 18.6 kN/m^3 for ML/CL layers, and 16.4 kN/m^3 for CH layer.

[c] Surcharge of 3.3. m was assumed to act over a 100 m by 100 m area, and the vertical stress increase at depth was estimated using the simplified 2:1 load spreading method.

[d] The average degree of consolidation in the fine-grained soils was taken as 80% at the time of the earthquake.

[e] For cohesive soils, used $s_u = 0.22\ OCR^{0.8}$ and $CRR_{M=7.5} = 0.18\ OCR^{0.8}$.

[f] Estimated representative SPT value for Lot C based on data in Martin et al. (2004).

[g] CH layer assigned an OCR of 1.3 prior to surcharging.

[h] Factor of safety against bearing failure to a given depth estimated as $F = 5.5\ (s_u)_{average}/(q_{surcharge})$, with $(s_u)_{average}$ being no less than the average strength to a depth of 10 m.

Table 4-4: Results from the analyses of the potential for cyclic failure in the clay-like soil layer at Site A in Wufeng, Taiwan, during the 1999 Chi-Chi earthquake.

			Free field					Beneath spread footings								Beneath mat portion of foundation							
Site	Depth below surface (m)	Estimated s_u for analysis (kPa)	Free field σ_{vo}' (kPa)	r_d	CSR	CRR	FS	$\Delta\sigma_v$ beneath footings (kPa)	σ_{vo}' beneath footings (kPa)	CSR	Static FS for bearing failure to this depth	τ/s_u	K_α	CRR	FS	$\Delta\sigma_v$ beneath footings (kPa)	σ_{vo}' beneath footings (kPa)	CSR	Static FS for bearing failure to this depth	τ/s_u	K_α	CRR	FS
(a) 6-story building near boring WAS-3, CPT sounding WAC-8, and VST-1 & 2									Square footings beneath columns at front of building									Mat foundation over rear 2/3 of buiding					
	1	60	16	1.00	0.54	2.97	5.52	150	166	0.23	1.8	0.73	0.55	0.16	0.68	60	76	0.27	5.64	0.23	0.94	0.59	2.17
	1.5	60	21	1.00	0.63	2.31	3.70	96	117	0.28	1.8	0.73	0.55	0.23	0.82	56	77	0.31	5.64	0.23	0.94	0.58	1.85
	2	32	25	0.99	0.68	1.01	1.48	67	92	0.33	1.8	0.73	0.55	0.15	0.46	53	78	0.36	5.64	0.23	0.94	0.31	0.86
	2.5	32	30	0.99	0.71	0.85	1.19	49	79	0.40	1.8	0.73	0.55	0.18	0.45	50	79	0.39	5.64	0.23	0.94	0.30	0.76
	3	32	34	0.98	0.74	0.74	1.00	38	72	0.46	1.7	0.74	0.52	0.18	0.40	47	81	0.43	5.64	0.23	0.94	0.29	0.68
	4	65	44	0.97	0.77	1.18	1.54	24	68	0.57	2.7	0.48	0.82	0.63	1.11	42	85	0.49	5.64	0.23	0.94	0.57	1.15
	5	55	53	0.96	0.79	0.83	1.05	17	70	0.65	3.9	0.33	0.90	0.57	0.88	37	90	0.54	5.64	0.23	0.94	0.45	0.83
	6	55	62	0.95	0.80	0.71	0.89	12	74	0.70	5.0	0.26	0.93	0.55	0.78	34	96	0.59	5.64	0.23	0.94	0.43	0.73
	7	75	71	0.94	0.80	0.84	1.05	9	81	0.73	6.6	0.20	0.95	0.70	0.96	31	102	0.62	5.64	0.23	0.94	0.55	0.89
	8	60	80	0.93	0.80	0.59	0.74	7	88	0.75	7.8	0.17	0.96	0.52	0.70	28	108	0.64	5.64	0.23	0.94	0.41	0.64
(b) 5-story building near boring WAS-4, CPT sounding WAC-9, and VST-3 & 4									Square footings beneath columns at front of building									Mat foundation over rear 2/3 of buiding					
	1	38	14	1.00	0.61	2.13	3.48	150	164	0.24	1.7	0.75	0.51	0.09	0.40	50	64	0.29	7.98	0.16	0.96	0.45	1.55
	1.5	38	19	1.00	0.69	1.61	2.33	96	115	0.28	1.7	0.75	0.51	0.13	0.48	47	66	0.34	7.98	0.16	0.96	0.44	1.30
	2	38	23	0.99	0.74	1.29	1.75	67	90	0.34	1.7	0.75	0.51	0.17	0.51	44	67	0.39	7.98	0.16	0.96	0.43	1.11
	2.5	38	28	0.99	0.77	1.08	1.41	49	77	0.41	1.7	0.75	0.51	0.20	0.49	41	69	0.43	7.98	0.16	0.96	0.42	0.97
	3	65	33	0.98	0.78	1.58	2.02	38	70	0.47	1.7	0.75	0.51	0.38	0.80	39	71	0.47	7.98	0.16	0.96	0.69	1.48
	4	65	42	0.97	0.81	1.23	1.53	24	66	0.59	3.0	0.43	0.85	0.67	1.14	35	76	0.53	7.98	0.16	0.96	0.65	1.21
	5	52	51	0.96	0.82	0.81	0.99	17	68	0.67	4.1	0.32	0.91	0.55	0.83	31	82	0.58	7.98	0.16	0.96	0.48	0.82
	6	68	60	0.95	0.82	0.90	1.09	12	72	0.72	5.4	0.24	0.93	0.70	0.97	28	88	0.62	7.98	0.16	0.96	0.59	0.94
	7	100	69	0.94	0.82	1.14	1.39	9	79	0.75	7.2	0.18	0.95	0.96	1.28	26	95	0.65	7.98	0.16	0.96	0.80	1.22
	8	100	79	0.93	0.82	1.01	1.23	7	86	0.77	9.2	0.14	0.96	0.89	1.16	23	102	0.68	7.98	0.16	0.96	0.75	1.10
(c) 3-story building near boring WAS-2 and CPT sounding WAC-6									Strip footings														
	1	60	20	1.00	0.43	2.38	5.50	120	140	0.23	2.6	0.51	0.80	0.27	1.17								
	1.5	60	25	1.00	0.53	1.93	3.68	90	115	0.27	2.6	0.51	0.80	0.33	1.23								
	2	60	29	0.99	0.59	1.63	2.77	72	101	0.31	2.6	0.51	0.80	0.38	1.21								
	2.5	60	34	0.99	0.63	1.41	2.23	60	94	0.36	2.6	0.51	0.80	0.41	1.14								
	3	60	38	0.98	0.66	1.24	1.86	51	90	0.40	3.4	0.38	0.88	0.46	1.16								
	4	50	48	0.97	0.71	0.83	1.18	40	88	0.48	5.0	0.26	0.93	0.42	0.88								
	5	50	57	0.96	0.73	0.70	0.95	33	90	0.54	6.4	0.20	0.95	0.42	0.78								
	6	77	66	0.95	0.75	0.92	1.23	28	94	0.59	8.4	0.15	0.96	0.63	1.07								
	7	77	75	0.94	0.76	0.81	1.07	24	99	0.62	10.5	0.12	0.97	0.60	0.96								
	8	77	84	0.93	0.76	0.72	0.95	21	106	0.65	12.7	0.10	0.98	0.56	0.87								
(d) 1-story home near boring WAS-1 and CPT sounding WAC-2									Strip footings														
	1	60	20	1.00	0.43	2.38	5.50	60	80	0.26	5.5	0.23	0.94	0.56	2.15								
	1.5	60	25	1.00	0.53	1.93	3.68	18	42	0.39	5.5	0.23	0.94	1.05	2.70								
	2	40	29	0.99	0.59	1.09	1.85	8	38	0.50	9.2	0.14	0.97	0.81	1.62								
	2.5	40	34	0.99	0.63	0.94	1.48	5	39	0.58	12.8	0.10	0.98	0.80	1.38								
	3	40	38	0.98	0.66	0.83	1.24	3	42	0.63	16.4	0.08	0.98	0.75	1.19								
	4	50	48	0.97	0.71	0.83	1.18	2	49	0.69	23.9	0.05	0.99	0.79	1.15								
	5	65	57	0.96	0.73	0.91	1.24	1	58	0.72	34.4	0.04	0.99	0.88	1.22								

Notes:

[a] Earthquake parameters: M=7.6, a_{max}=0.70g, and MSF=0.99.

[b] Total unit weight of 19 kN/m^3 for all soils. Water table at depths of 0.7, 0.5, 1.1, and 1.1 m for a-d, respectively.

[c] For clay-like soils, used $CRR_{M=7.5} = 0.8(s_u/\sigma_{vc}')K_\alpha MSF$.

[d] Vertical stresses beneath footings is the larger of (a) 2:1 spreading beneath individual square footings, and (b) 2:1 spreading of the average building stress over its full footprint.

[e] α/s_u estimated as $1/FS_{seismic}$, with $FS_{seismic}$ estimated as $FS_{static}/1.3$.

FIG. 4-1: Photograph at the head of the 4th Avenue slide in Anchorage, Alaska, 1964 (Hansen 1971).

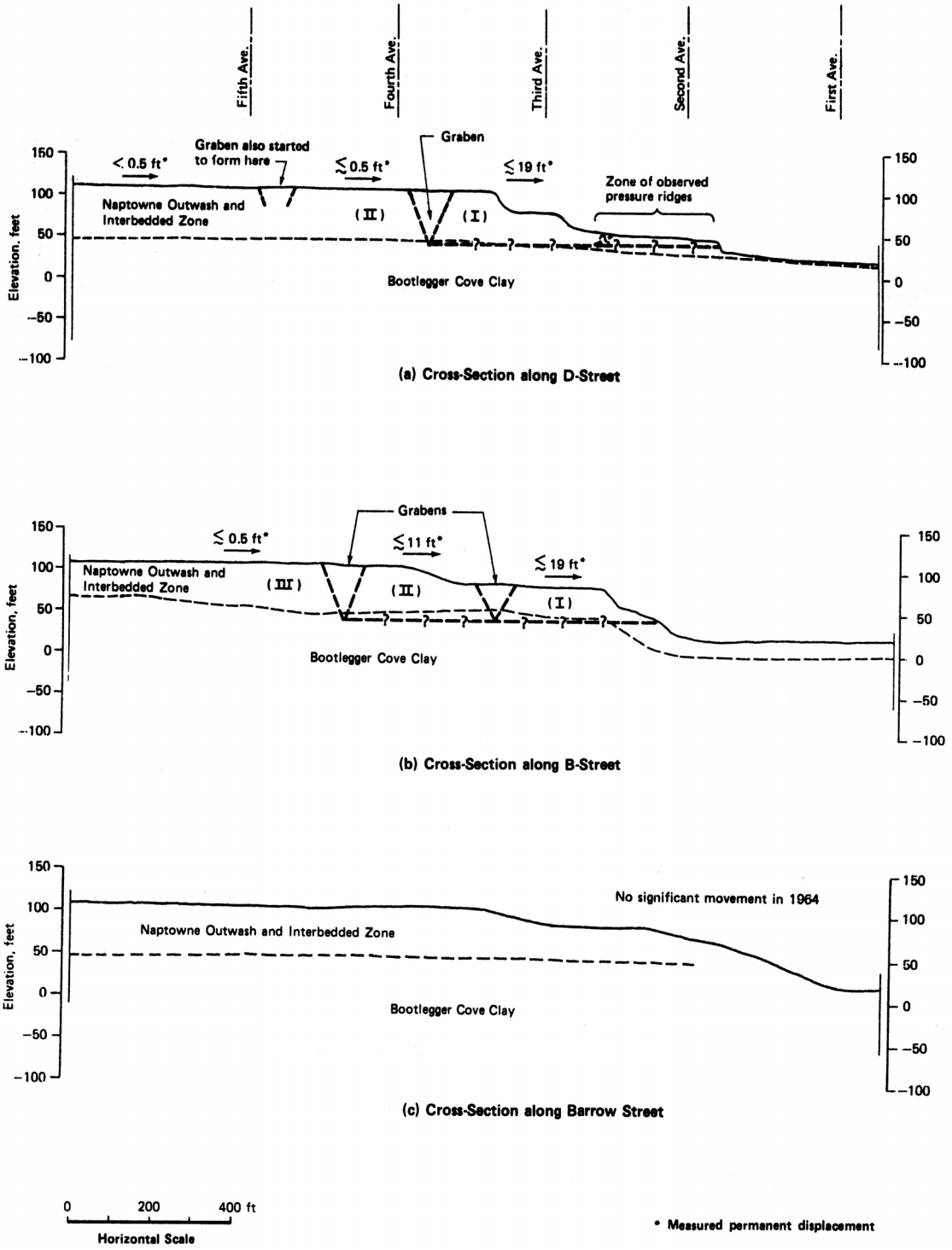

FIG. 4-2: Cross-sections across Fourth Avenue Slide (from Idriss 1985)

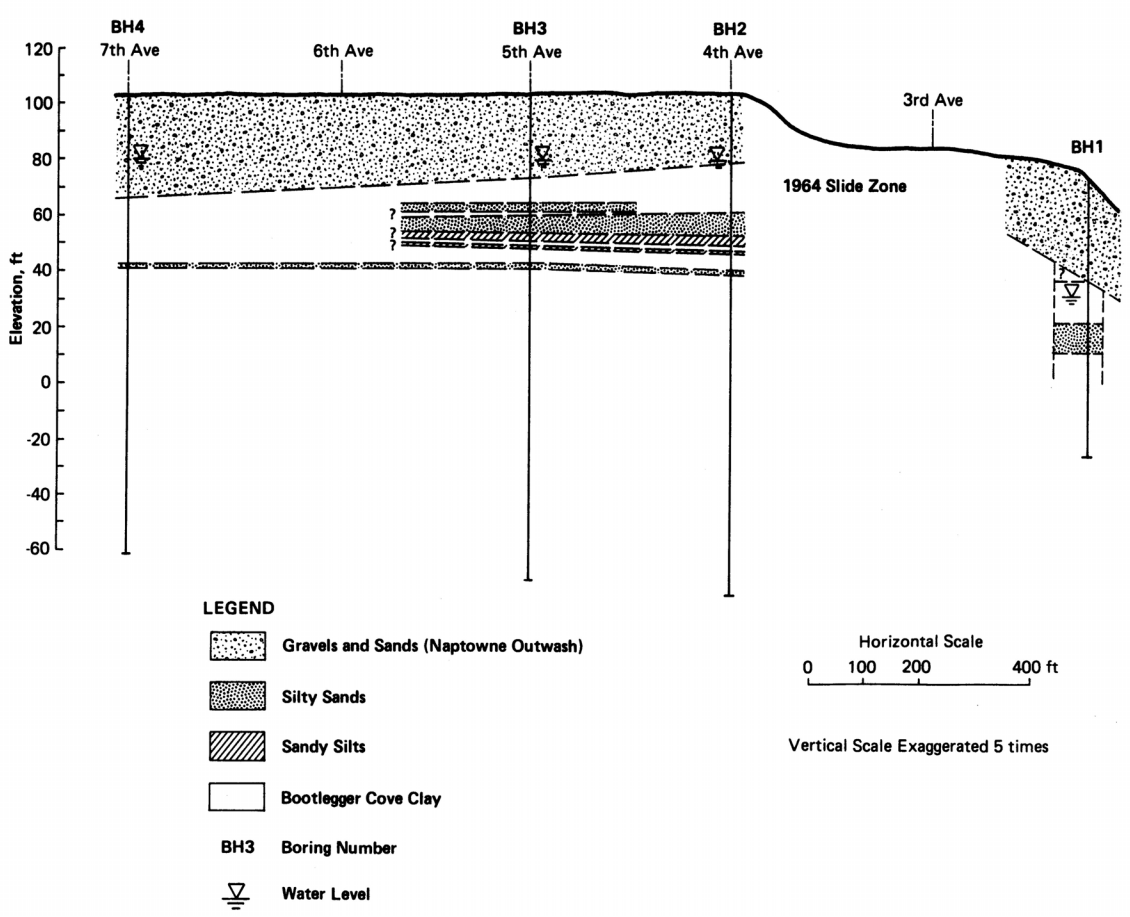

FIG. 4-3: Subsurface conditions along D Street (from Idriss 1985)

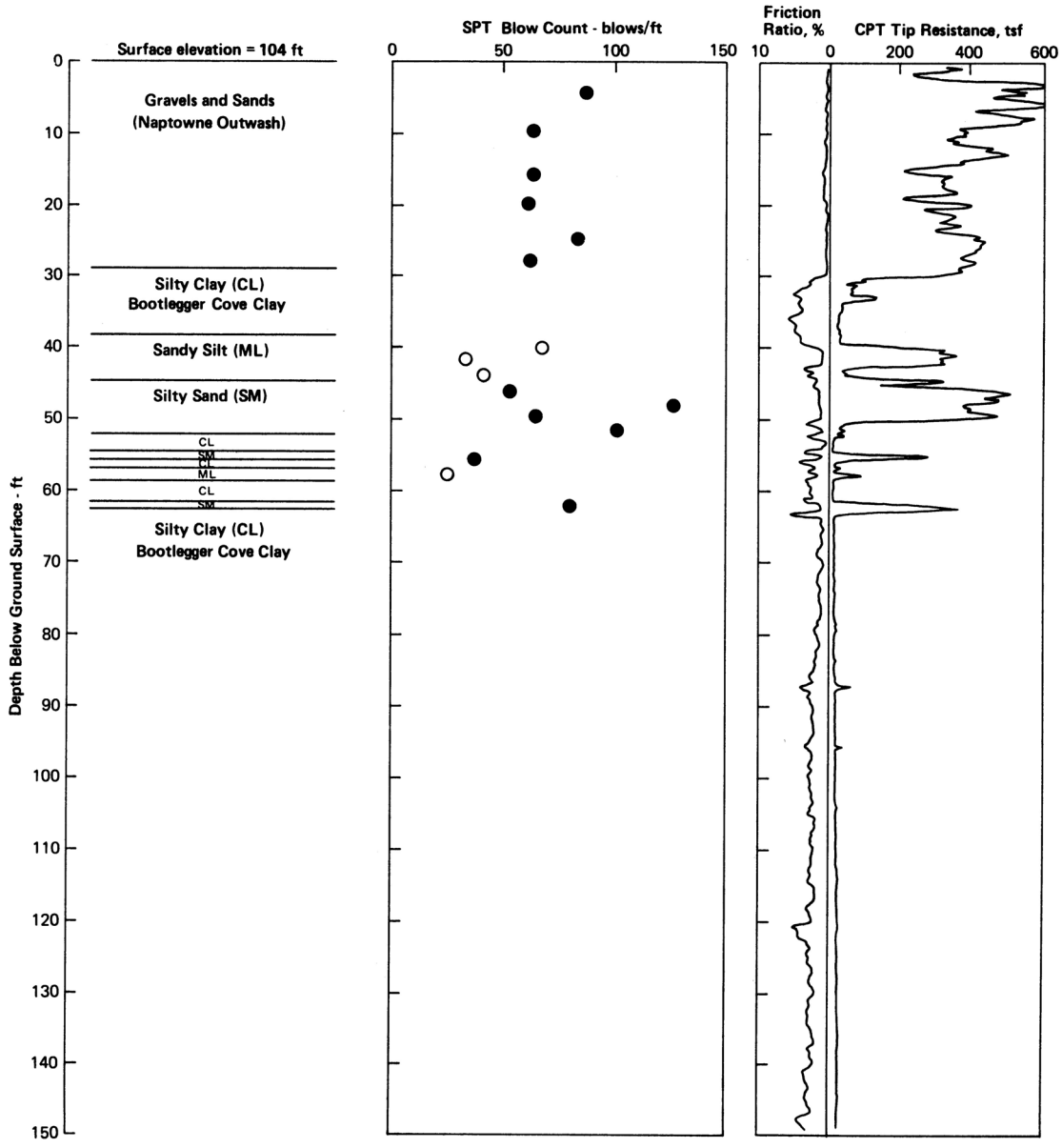

FIG. 4-4: Log of boring BH3 and CPT record [open circles are for SPT N values in sand silt (ML) soils and filled circles are for N values in Naptowne Outwash and silty sand (SM) soils] (from Idriss 1985)

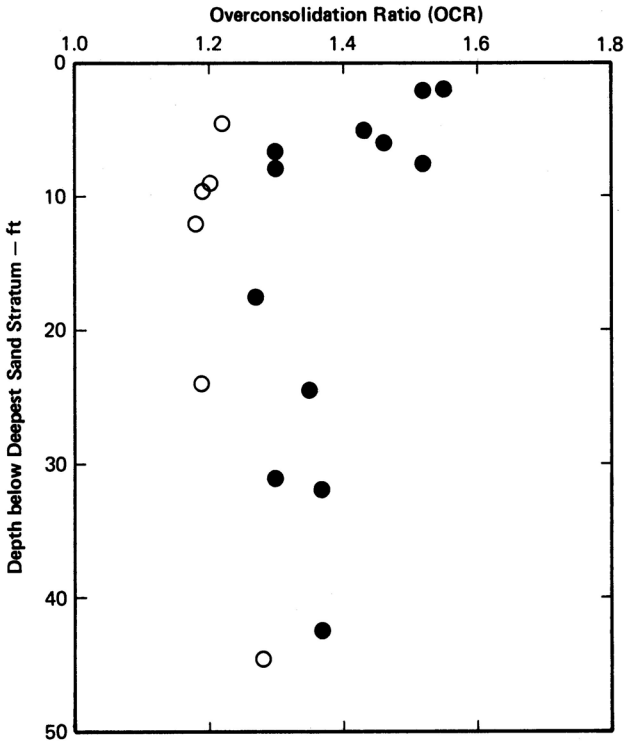

FIG. 4-5: Overconsolidation ratios in Bootlegger Cove clay below the interbedded zone (open circles are for samples from borings near the bluff, and filled circles are for borings away from the bluff) (from Idriss 1985)

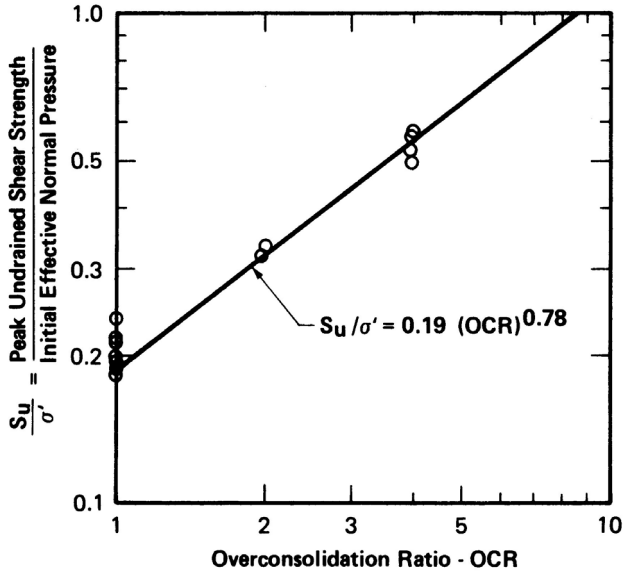

FIG. 4-6: Normalized undrained shear strength of Bootlegger Cove clay based on DSS tests (from Idriss 1985)

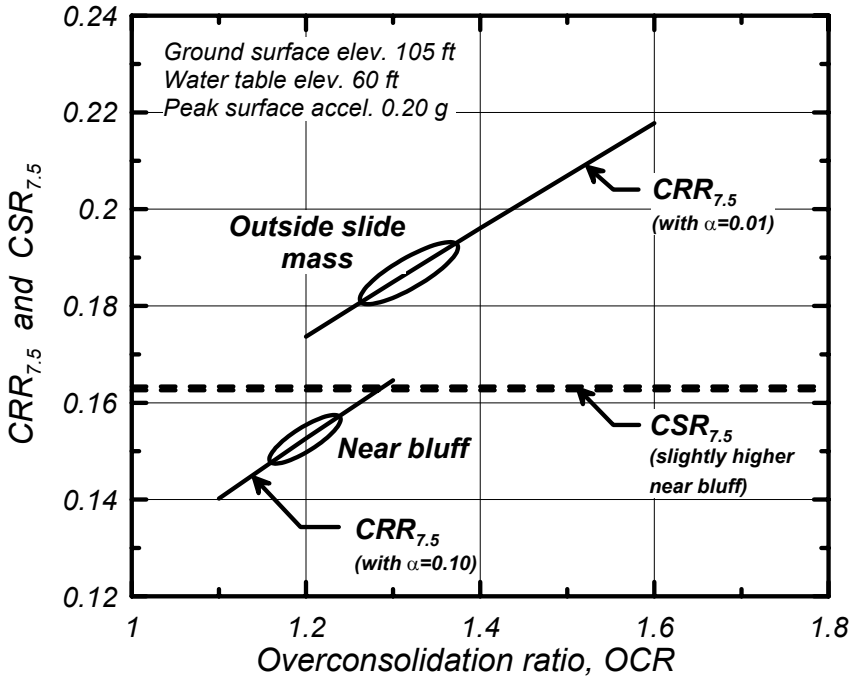

FIG. 4-7: Cyclic resistance ratio and induced cyclic stress ratio versus overconsolidation ratio for the Bootlegger Cove clay at Fourth Street.

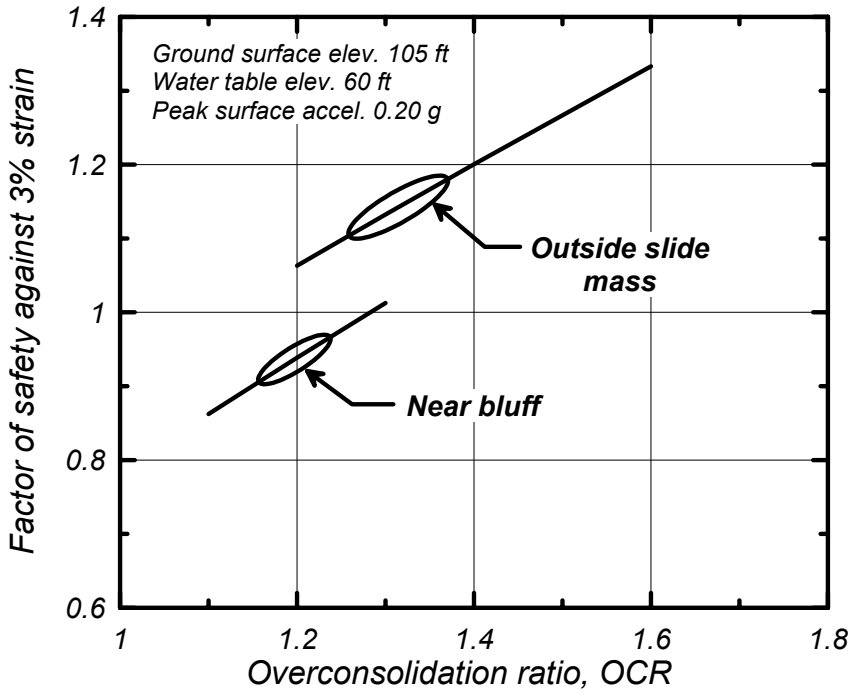

FIG. 4-8: Factor of safety against onset of 3% shear strain versus overconsolidation ratio for the Bootlegger Cove clay at Fourth Street.

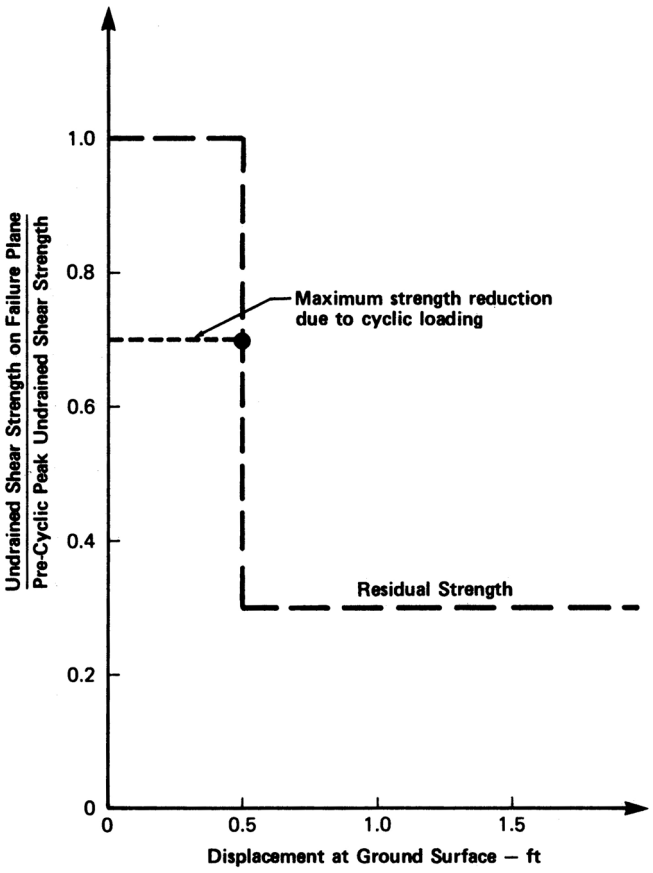

FIG. 4-9: Variation of undrained shear strength in the Bootlegger Cove clay versus ground surface displacement at Fourth Street, Anchorage (Idriss 1985).

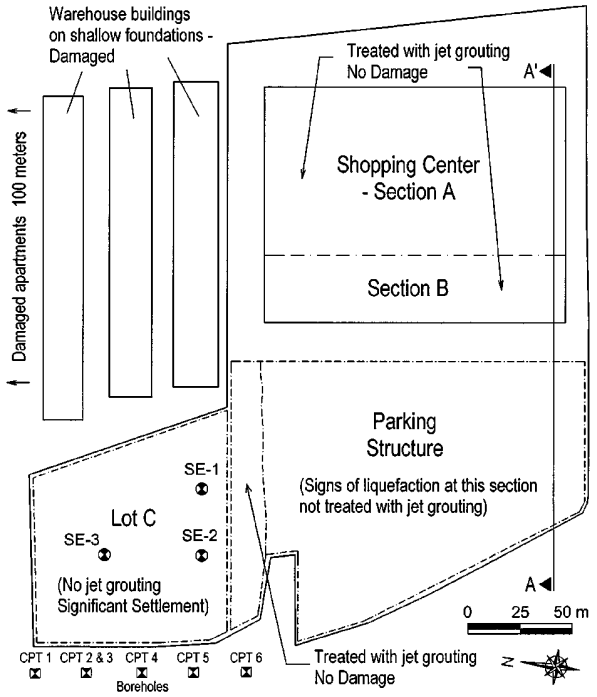

FIG. 4-10: Site plan of Carrefour Shopping Center showing Lot C with settlement extensometers (SE) (Martin et al. 2004).

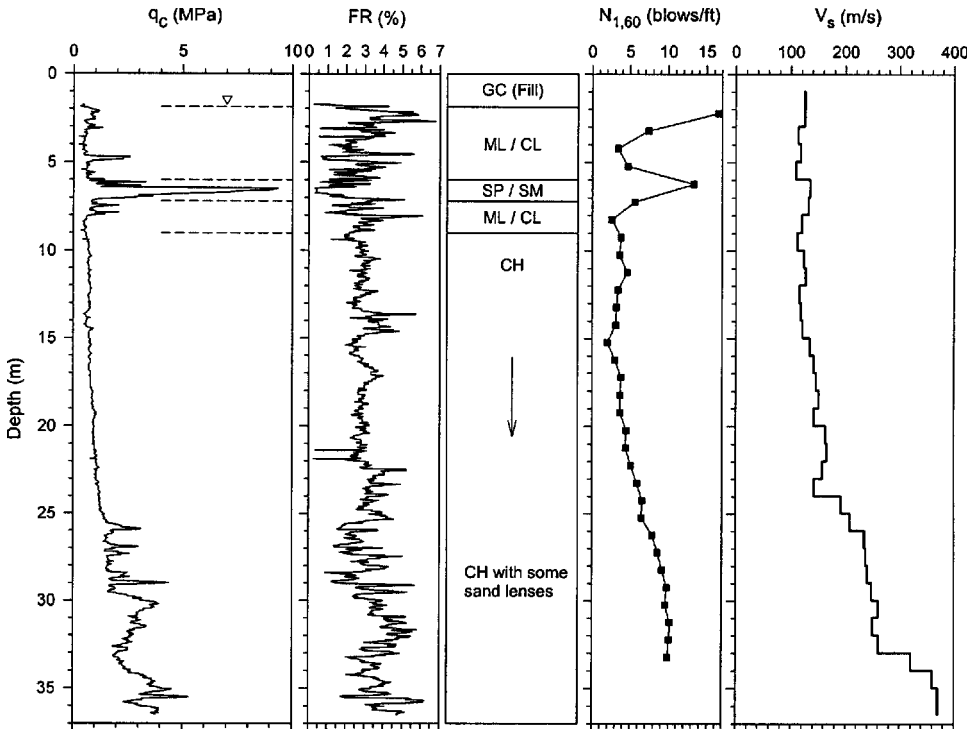

FIG. 4-11: Typical pre-improvement profile at the Carrefour site (Martin et al. 2004)

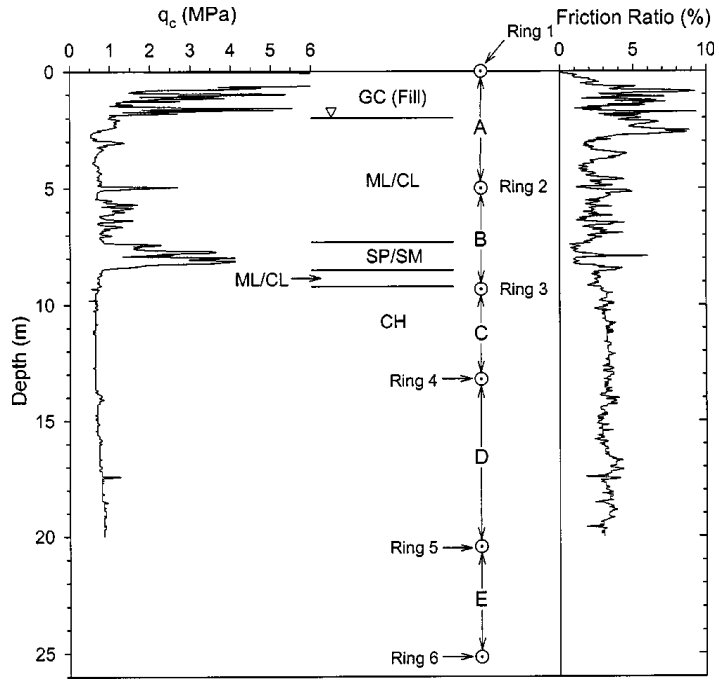

FIG. 4-12: CPT sounding and details for settlement extensometer SE2 in Lot C (Martin et al. 2004).

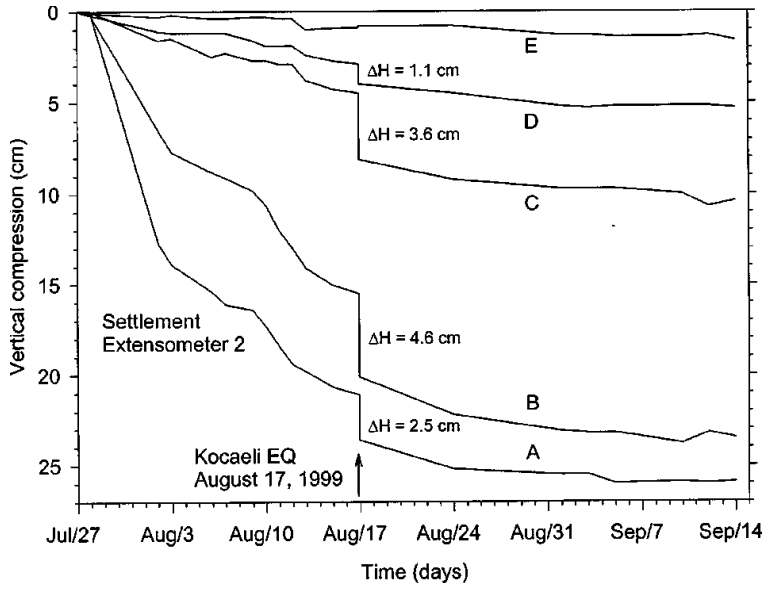

FIG. 4-13: Relative settlements between extensometer rings (see next Figure for layer intervals) versus time under the surcharge fill in Lot C (Martin et al. 2004).

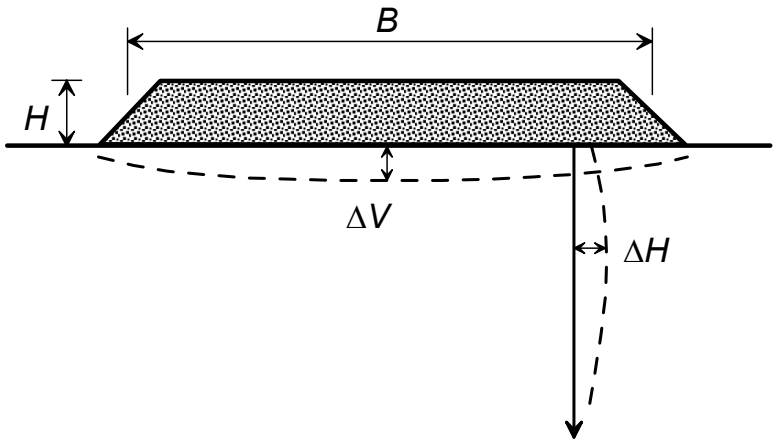

FIG. 4-14: Schematic illustration of the expected pattern of vertical and lateral strains beneath the surcharge fill at Lot C of the Carrefour Shopping Center.

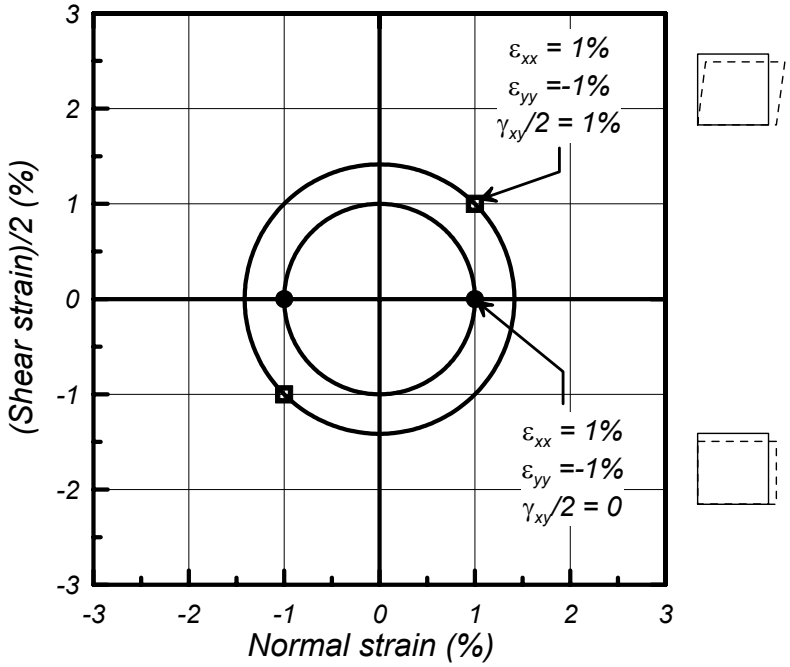

FIG. 4-15: Mohr diagram illustrating examples of how vertical strains beneath the surcharge fill may be related to shear strains in the clay-like soils.

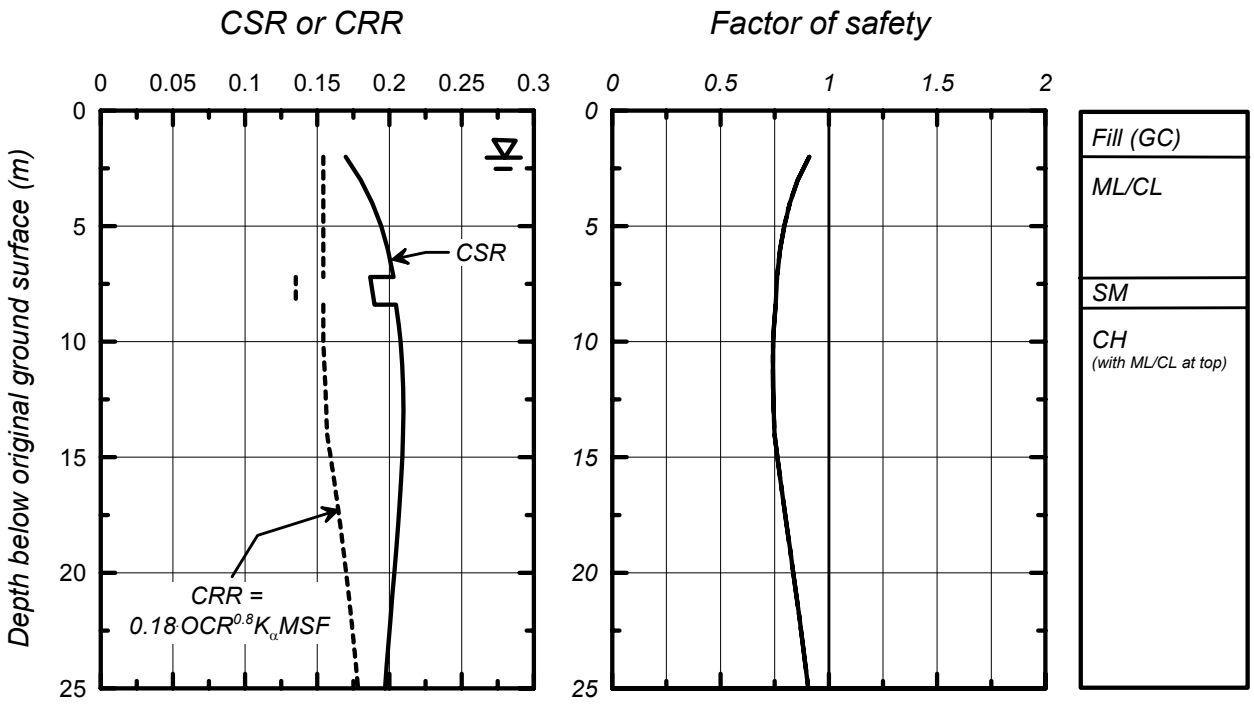

FIG. 4-16: Comparison of induced CSR to the CRR of both the clay-like and sand-like soils at the location of SE2 in Lot C.

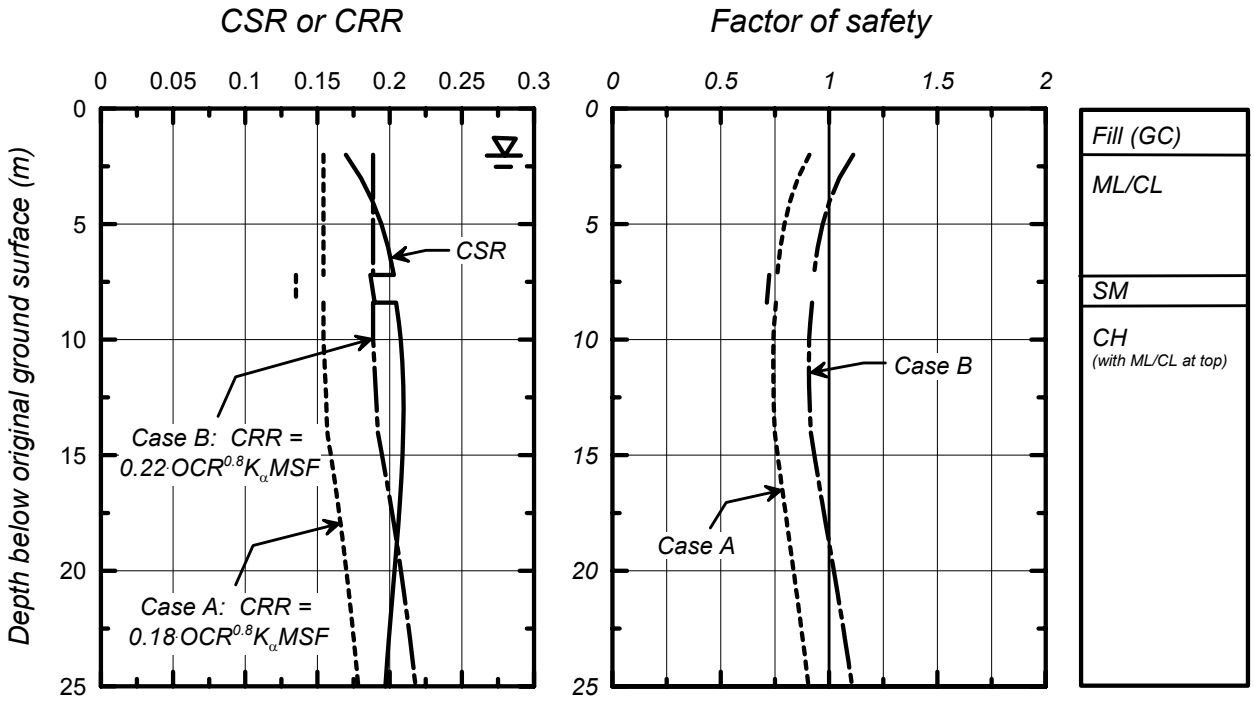

FIG. 4-17: Effect of uncertainty in the empirical CRR relation for clay-like soil on the computed factors of safety versus depth at the location of SE2 in Lot C.

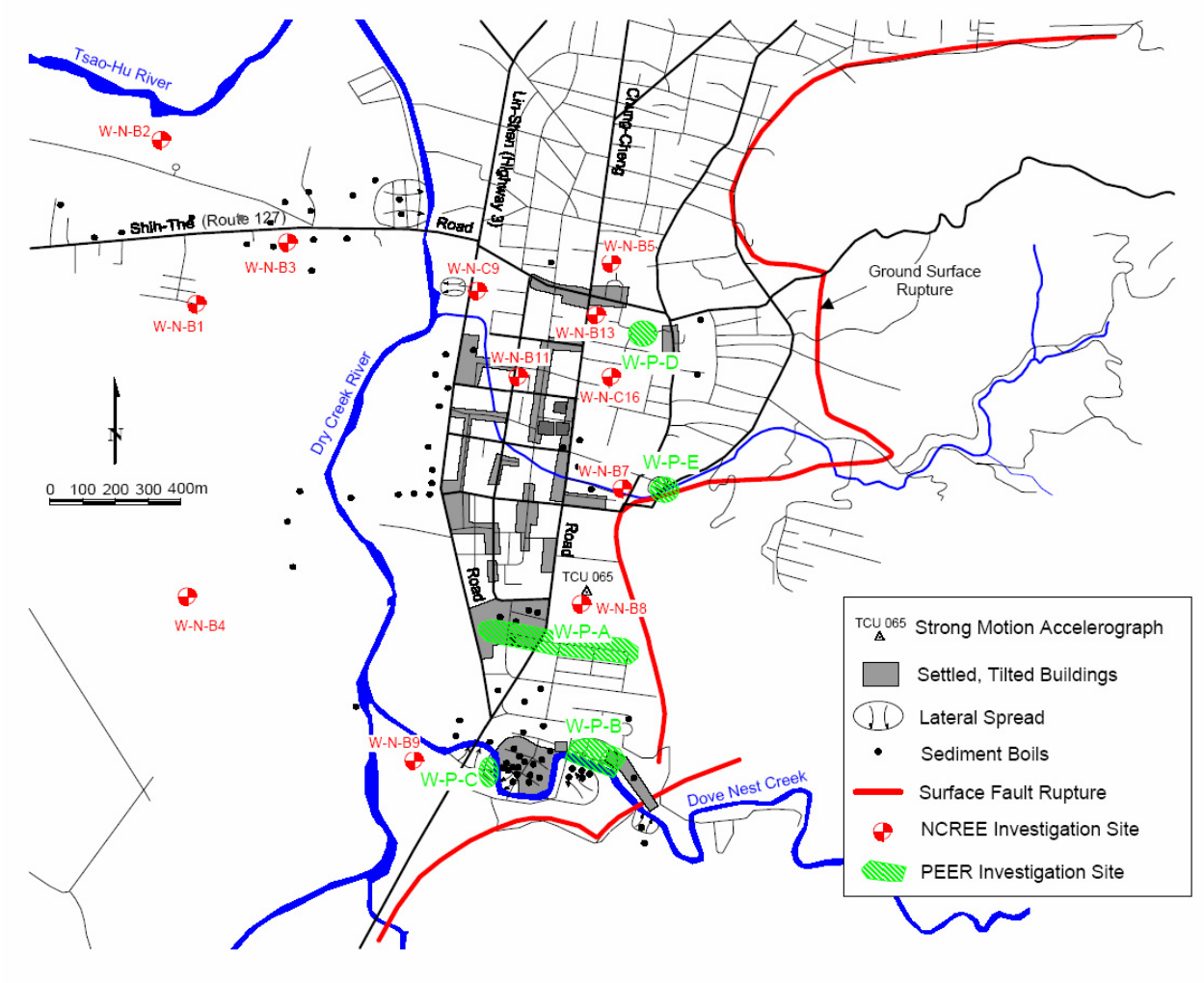

FIG. 4-18: Map of Wufeng showing areas of ground failure and investigations (Chu et al. 2003)

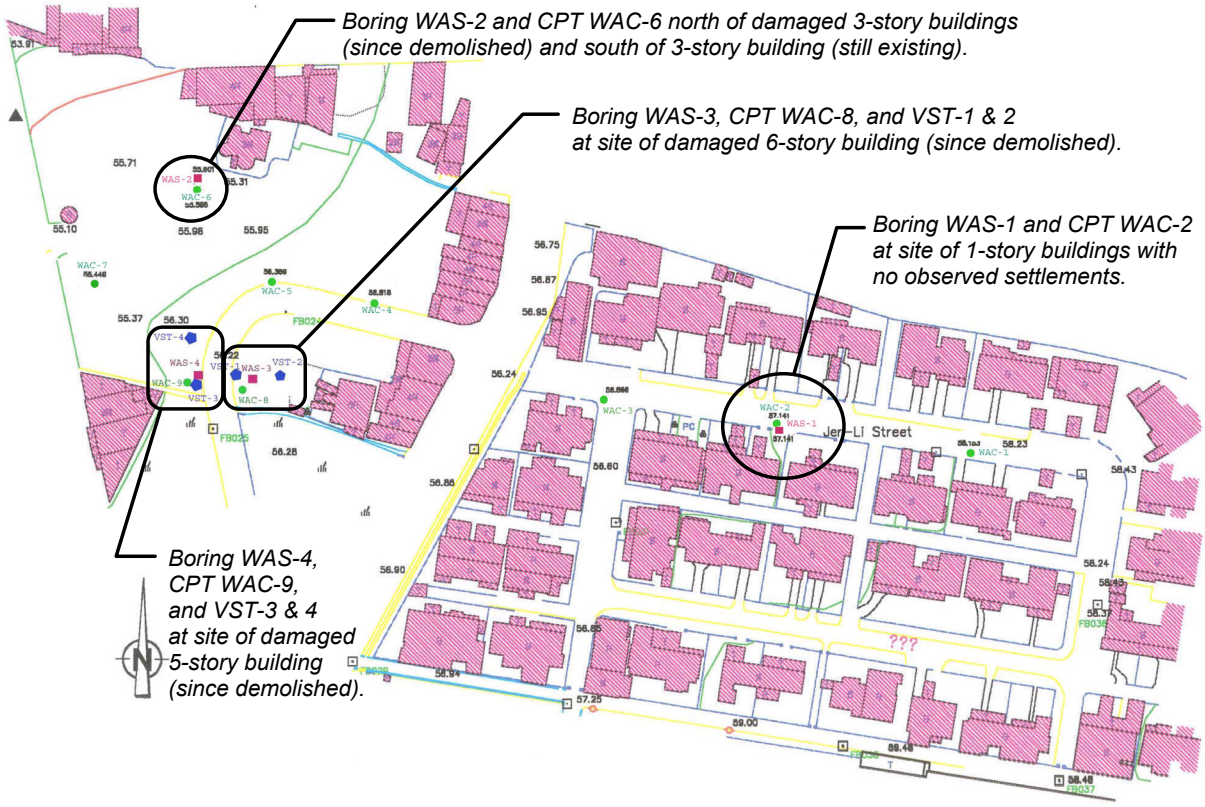

FIG. 4-19: Map of site A in Wufeng showing location of borings and soundings relative to buildings that were not demolished after the earthquake.
(Stewart et al. 2004)

(a) 5- and 6-story buildings with foundation failures near the locations of borings WAS-3 and WAS-4 (photo by R. B. Seed)

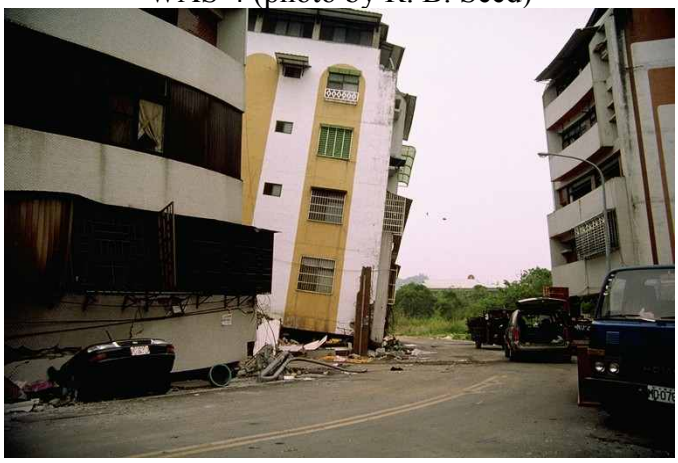

(b) 5- and 6-story buildings with foundation failures near the locations of borings WAS-3 and WAS-4 (photo by R. B. Seed)

(c) Close-up view of foundation failures beneath a building [seen on left side of photo (a)] near the locations of borings WAS-3 and WAS-4 (photo by R. B. Seed)

(d) 3-story building near the location of boring WAS-2 (photo by R. B. Seed)

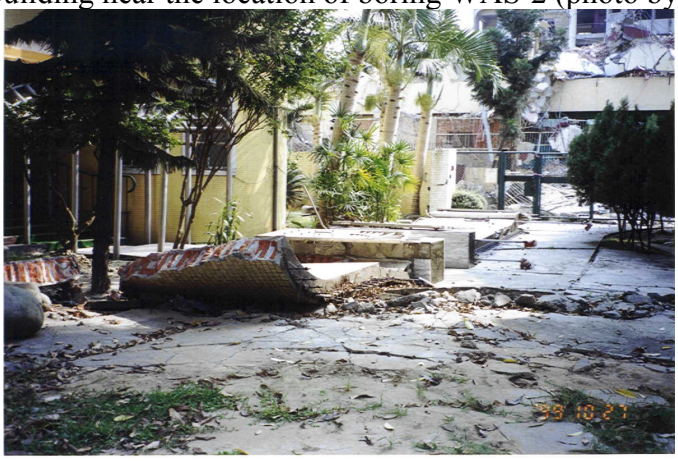

(e) 3-story building near the location of boring WAS-2 (photo by R. B. Seed)

(f) 1-story buildings without evident ground failure or building settlement near the location of boring WAS-1

FIG. 4-20: Photographs of buildings at locations within Site A at Wufeng (http://peer.berkeley.edu/lifelines/research_projects/3A02/).

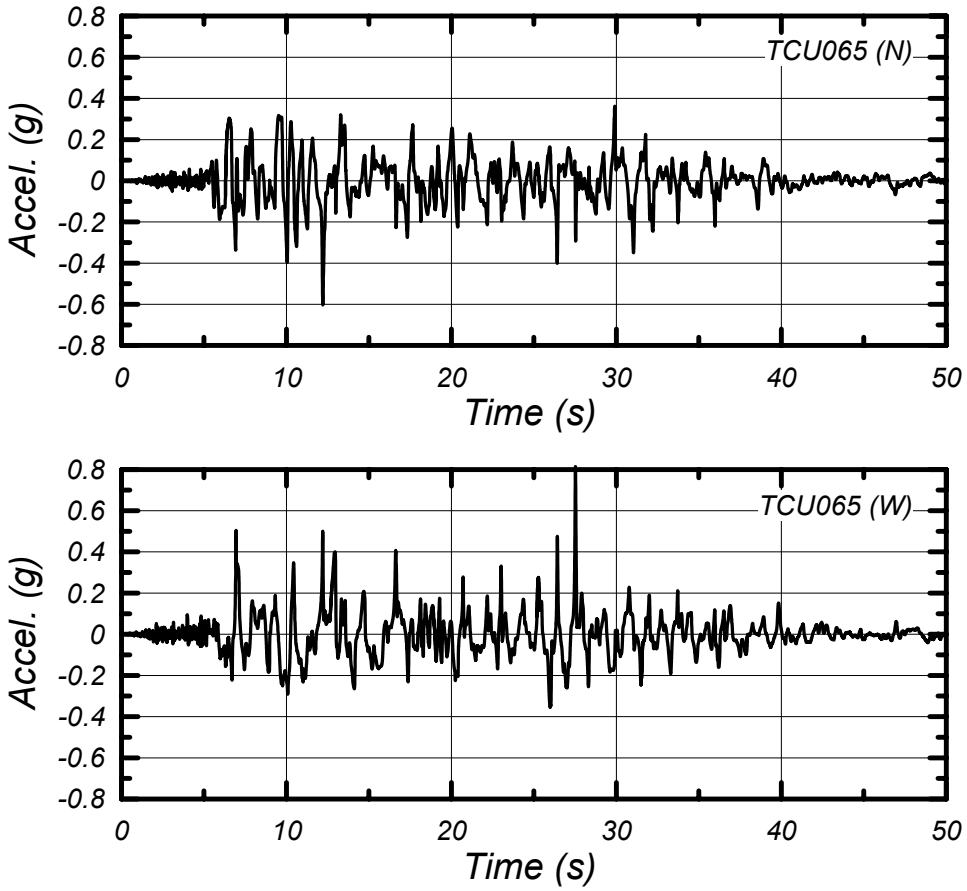

FIG. 4-21: Horizontal acceleration time histories recorded at TCU065 within 1 km of Site A, Wufeng, Taiwan, during the 1999 Chi-Chi earthquake.

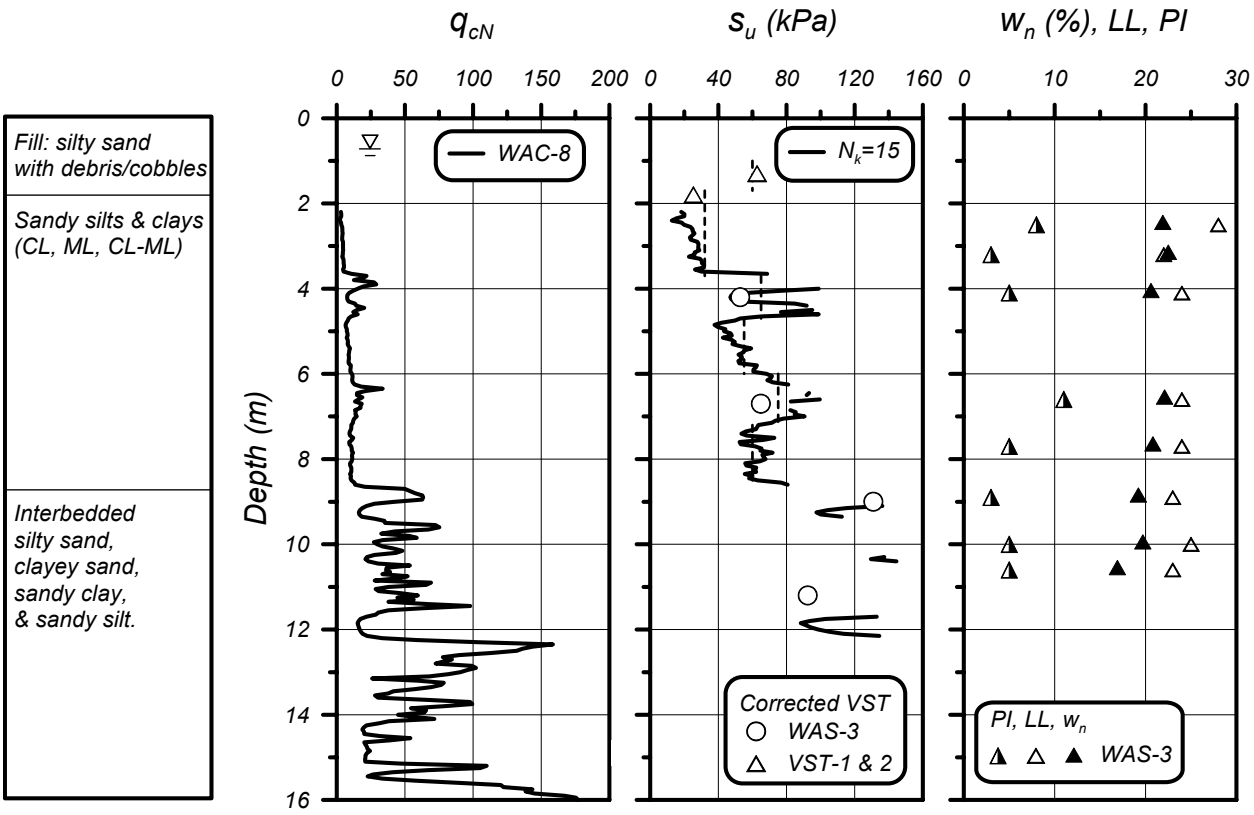

FIG. 4-22: Boring WAS-3, CPT WAC-8, and VST-1 and 2 data at the location of a 6-story building that experienced significant foundation settlements at Site A in Wufeng (source: http://peer.berkeley.edu/lifelines/research_projects/3A02/)

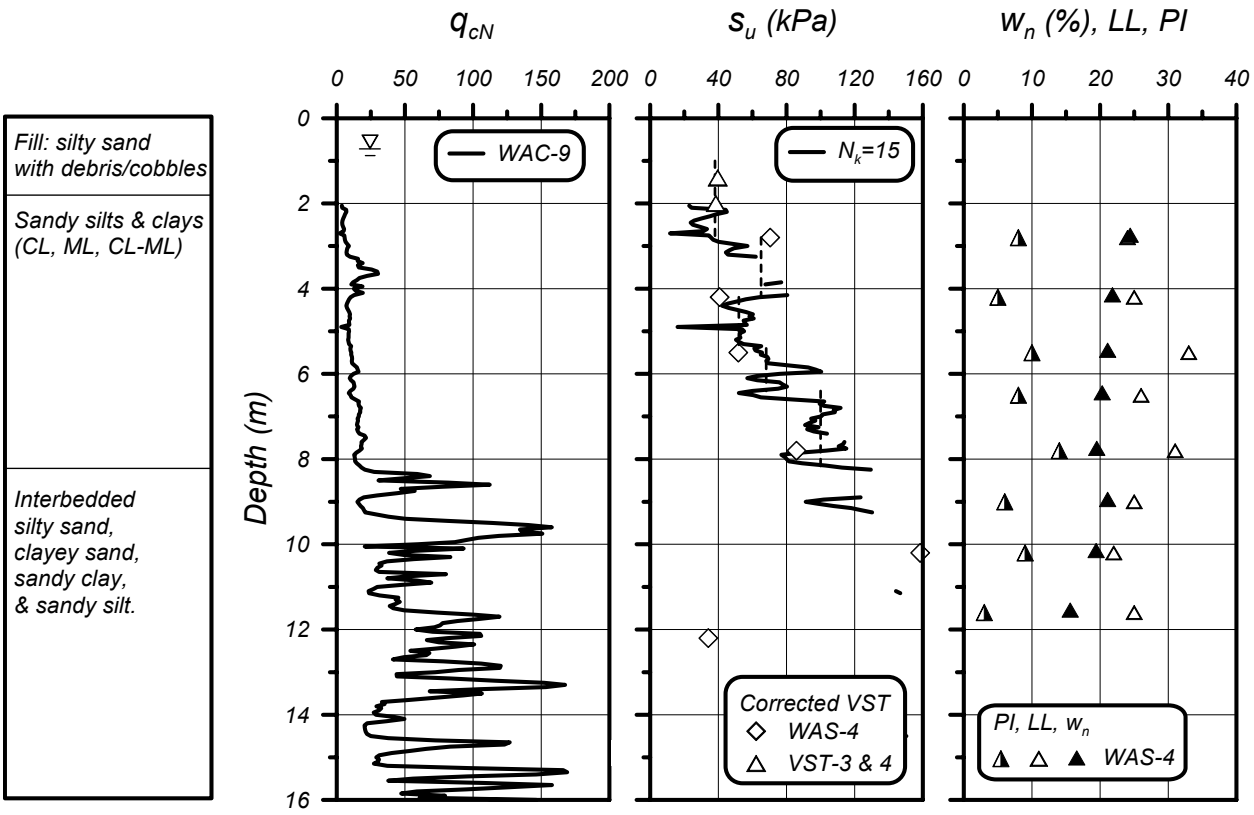

FIG. 4-23: Boring WAS-4, CPT WAC-9, and VST-3 and 4 data at the location of a 5-story building that experienced significant foundation settlements at Site A in Wufeng (source: http://peer.berkeley.edu/lifelines/research_projects/3A02/)

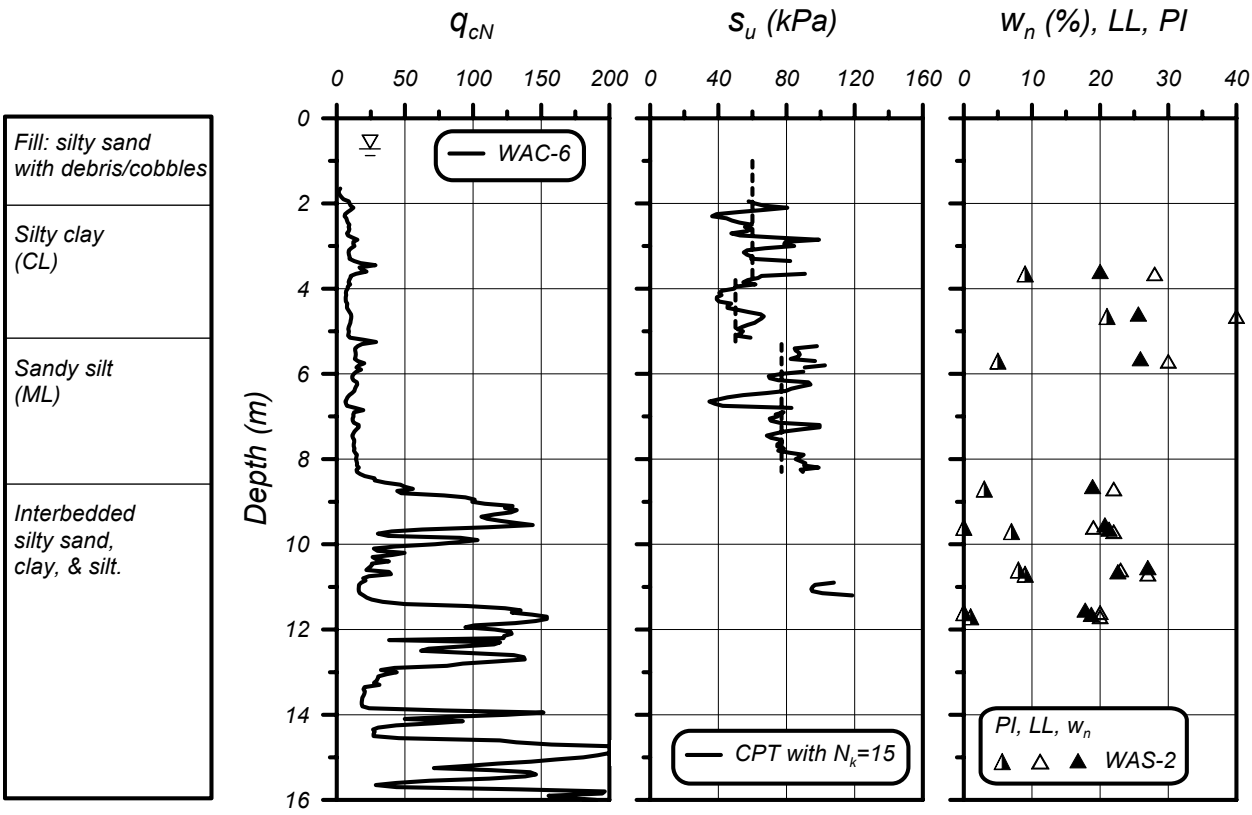

FIG. 4-24: Boring WAS-2 and CPT WAC-6 data at the location of 3-story buildings that showed some ground distress around its perimeter but no notable building settlements (source: http://peer.berkeley.edu/lifelines/research_projects/3A02/)

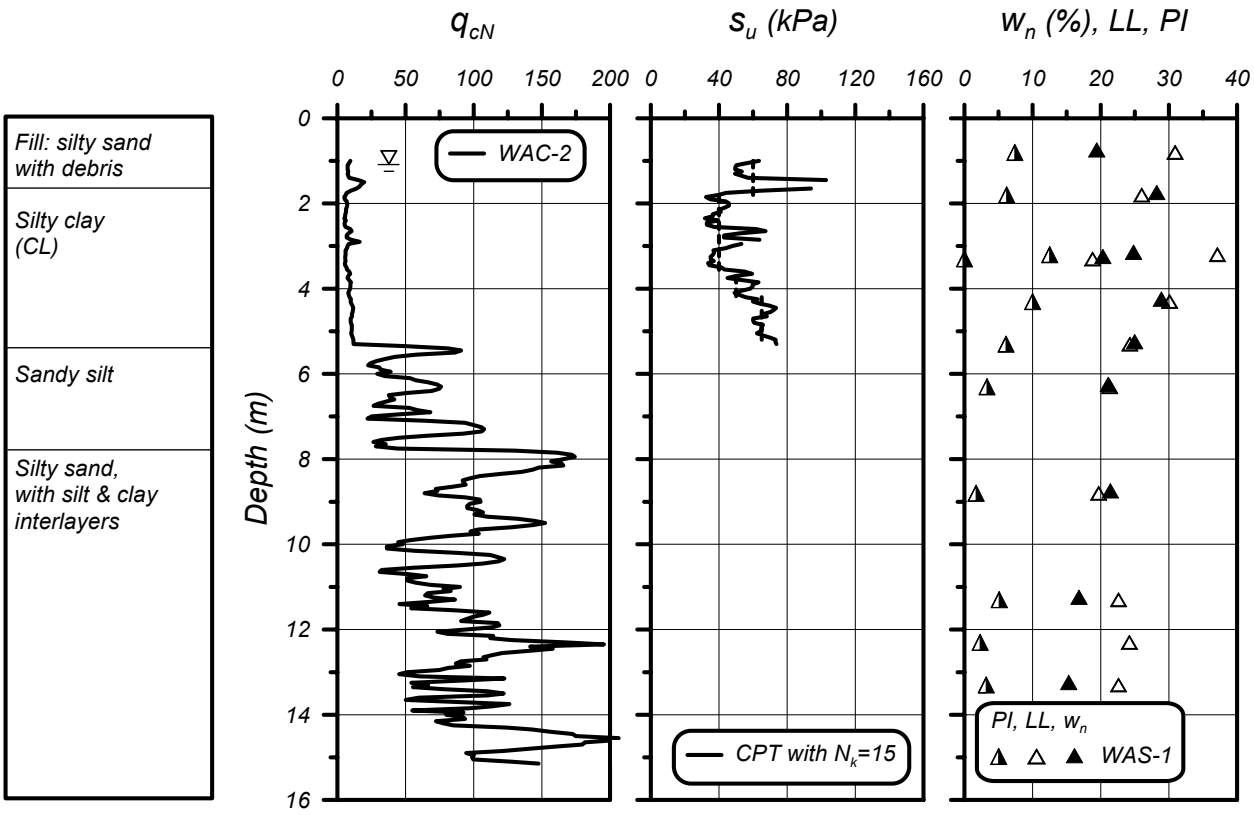

FIG. 4-25: Boring WAS-1 and CPT WAC-2 data at the location of 1-story buildings with no signs of settlement or ground failure at Site A in Wufeng
(source: http://peer.berkeley.edu/lifelines/research_projects/3A02/)

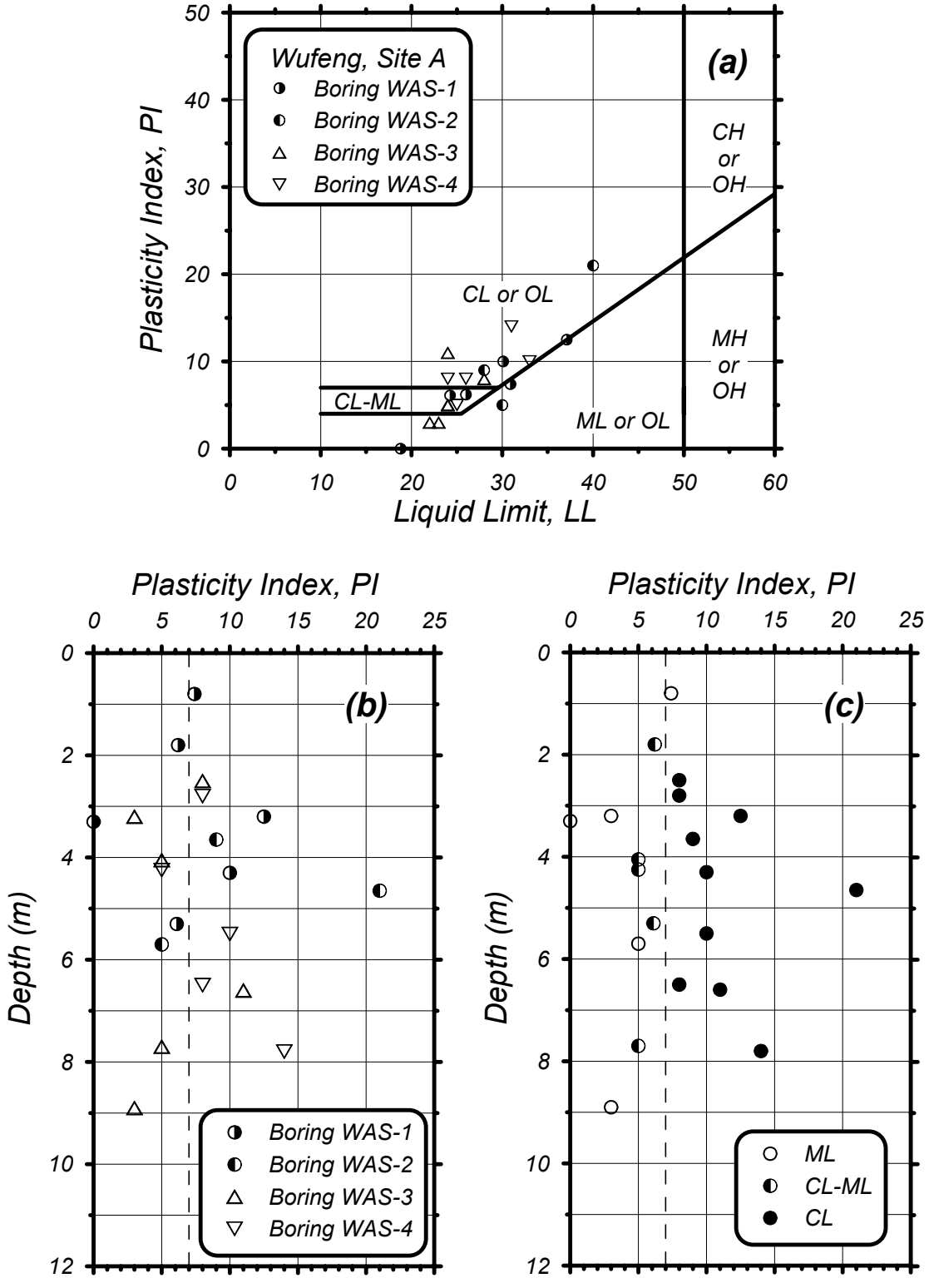

FIG. 4-26: Atterberg Limits for the clay-like stratum at Wufeng, Site A: (a) Atterberg limits from borings WAS 1 to 4, (b) PI versus depth for different borings, and (c) PI versus depth for different USCS classifications.

FIG. 4-27: Photographs of test pits for vane shear tests VST-3 and 4 that show the characteristics of the surface fill and underlying fine-grained soils.
(source: http://peer.berkeley.edu/lifelines/research_projects/3A02/)

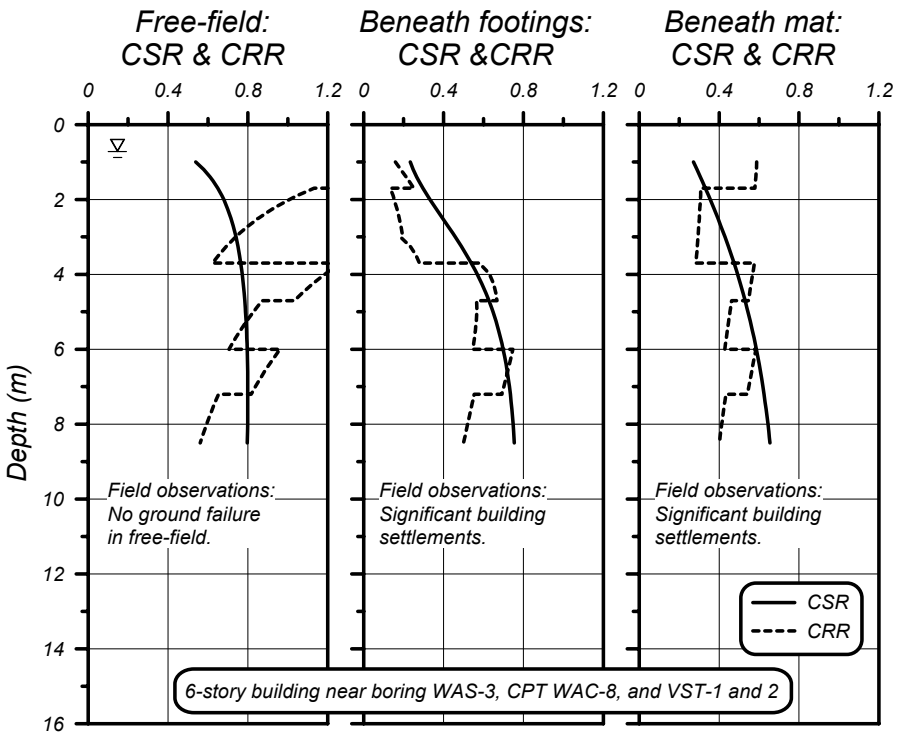
Free-field:
CSR & CRR
Beneath footings:
CSR &CRR
Beneath mat:
CSR & CRR
0
0.4
0.8
1.2
Depth (m)
0
2
4
6
8
10
12
14
16
Field observations:
No ground failure
in free-field.
Field observations:
Significant building
settlements.
Field observations:
Significant building
settlements.
CSR
CRR
6-story building near boring WAS-3, CPT WAC-8, and VST-1 and 2

(a)

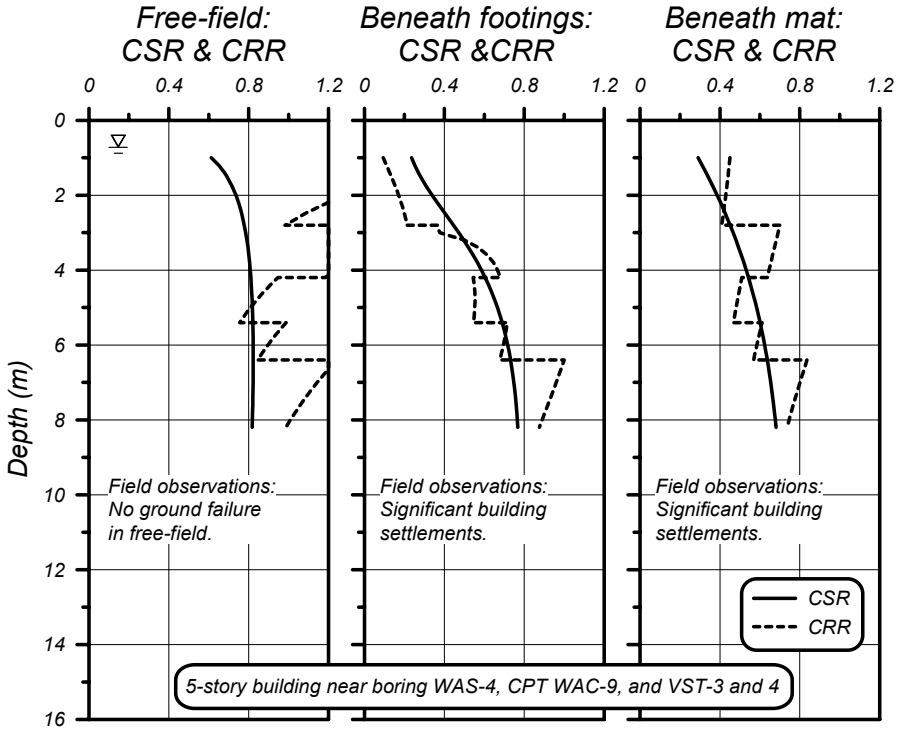
Free-field:
CSR & CRR
Beneath footings:
CSR &CRR
Beneath mat:
CSR & CRR
0
0.4
0.8
1.2
Depth (m)
0
2
4
6
8
10
12
14
16
Field observations:
No ground failure
in free-field.
Field observations:
Significant building
settlements.
Field observations:
Significant building
settlements.
CSR
CRR
5-story building near boring WAS-4, CPT WAC-9, and VST-3 and 4

(b)

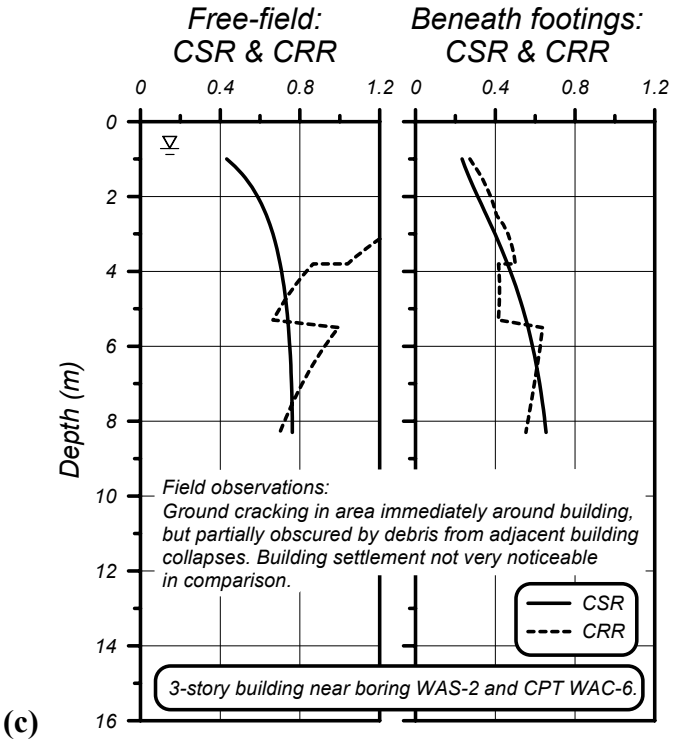

(c)

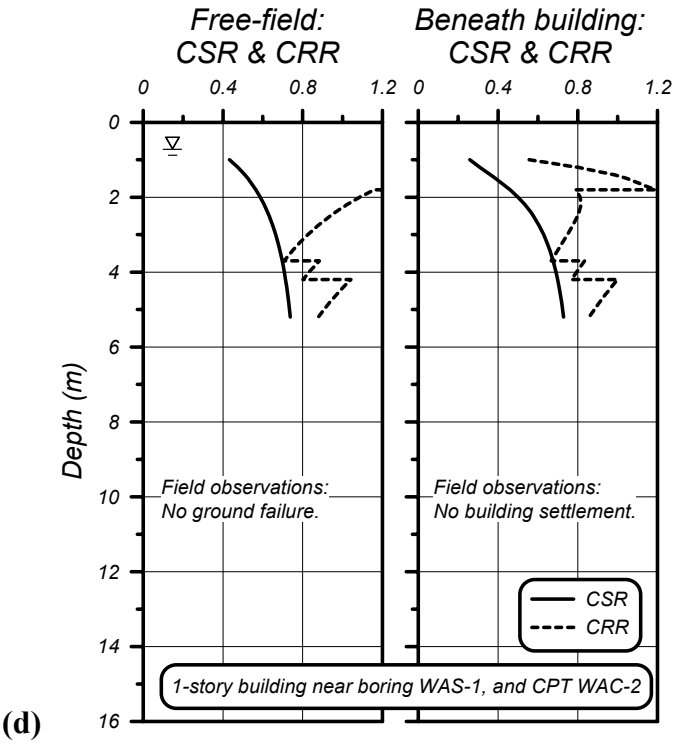

(d)

FIG. 4-28: Comparison of CSR and CRR for the clay-like soils in the free-field and beneath the buildings at Site A in Wufeng: (a) 6-story building near WAS-3, (b) 5-story building near WAS-4, (c) 3-story building near WAS-2, and (d) 1-story building near WAS-1.

5. SUMMARY AND RECOMMENDATIONS

Liquefaction susceptibility criteria for fine-grained soils

The first step in evaluating the potential for ground failure in silts and clays during earthquakes is to determine the appropriate framework and engineering procedures to be used in the evaluation. For practical purposes, it was shown that silts and clays could be separated into two categories. "Sand-like" fine-grained soils are those that exhibit monotonic and cyclic undrained shear loading behavior that is fundamentally most similar to that of sands, and are best evaluated using engineering procedures that adapted from those for sands. "Clay-like" fine-grained soils are those that exhibit monotonic and cyclic undrained shear loading behavior that is fundamentally most similar to that of clays, and are best evaluated using engineering procedures that are adapted from those used for clays. For clarity, it is recommended that the term "liquefaction" be reserved for sands and sand-like fine-grained soils, and the term "cyclic failure" be reserved for clays and clay-like fine-grained soils.

Fine-grained soils transition from sand-like to clay-like behavior at plasticity indices (PI) between about 3 and 8, with the transition point appearing to be slightly lower for ML-CL soils than for ML soils. For practical purposes, it is recommended that fine-grained soils be categorized as sand-like (i.e., susceptible to liquefaction) if they have a $PI < 7$ and clay-like (i.e., susceptible to cyclic failure, not liquefaction) if they have a $PI \geq 7$. This criterion may be adjusted on a site-specific basis if justified by the results of detailed in situ and laboratory testing.

The use of the Chinese Criteria should be discontinued. Similar empirical index-test-based criteria that do not adequately consider the differences between sand-like and clay-like behavior may envelope soil conditions where certain types of ground failure have been observed in past earthquakes, but generally do not provide adequate distinctions with regard to the engineering procedures that are appropriate for predicting potential ground failure in future earthquakes.

Analysis procedures for liquefaction and cyclic failure

For sand-like fine-grained soils, it is recommended that the potential for triggering of liquefaction be evaluated using CPT- and SPT-based liquefaction correlations. These correlations have been derived and applied in conjunction with the Seed-Idriss (1971) simplified procedure for estimating earthquake-induced stresses. Idriss and Boulanger (2004) provided a recent re-examination of these correlations along with updated relations for the simplified procedure.

For clay-like fine-grained soils, it is recommended that the potential for triggering of cyclic failure be evaluated using the procedures presented in this report. The proposed procedures have been cast for use in conjunction with the Seed-Idriss simplified procedure because it enables parallel analyses of clay-like and sand-like soils within the same soil profile. The cyclic strength of clay-like soil is related to its monotonic

undrained shear strength, which can be evaluated in several ways (in situ testing, laboratory testing of high quality tube samples, or empirical relations). Guidelines were provided for estimating cyclic resistance ratios for clay-like fine-grained soils when using these different approaches to characterize the soil's undrained shear strength profile.

The potential consequences of cyclic failure in clay-like fine-grained soils can range from relatively severe to inconsequential, depending on the soil's sensitivity, the specific site conditions (e.g., presence of a slope or building foundation), and the level and duration of earthquake motions. Thus, the triggering of cyclic failure in clay-like fine-grained soils should not be assumed to necessarily imply that a major problem exists, but rather that it is necessary to next evaluate the potential ground deformations.

Case history analyses

Three case histories involving ground failure in fine-grained soils during earthquakes were analyzed using the procedures proposed herein. The analyses showed that the observed ground deformations (and absence of deformations) could be predicted reasonably well using procedures applicable to clays. Ground failure in the clay-like soils at these sites had many of the same characteristics as ground failures in sands in other earthquakes, illustrating the fact that field observations are sometimes insufficient for distinguishing between sand-like and clay-like behavior of fine-grained soils or for identifying the appropriate means for predicting that behavior.

- Fourth Avenue in Anchorage during the 1964 Alaskan earthquake.
  The proposed procedures distinguished why ground failure (with movements up to 19 feet) occurred near the bluff, while the movements were small (less than 6 inches) at greater distances from the bluff. The key factors contributing to these different behaviors in the Bootlegger Cove clay were shown to be the slightly higher overconsolidation ratios and lower static shear stress ratios away from the bluff.

- Carrefour Shopping Center in Turkey during the 1999 Kocaeli earthquake.
  This unique case history reported by Martin et al. (2004) had in situ instrumentation that showed significant vertical strains in the CL and CH strata at the site, leading Martin et al to conclude that the CL layer had exhibited "liquefaction-type behavior" while "a definitive explanation for significant earthquake-induced settlements in a high-plasticity clay stratum (CH) in Lot C has not yet been found." The procedures proposed herein predicted that the seismic loading at this site would be expected to produce cyclic failure (significant permanent shear strains accompanied by vertical strains) in both the CL and CH strata, with both layers behaving as clay-like soils.

- Wufeng Site A in Taiwan during the 1999 Chi-Chi earthquake.
  Four locations were analyzed. At two locations, five- and six-story buildings experienced significant settlements while the surrounding free-field areas were relatively unaffected. At another location, one-story buildings and the surrounding free-field areas showed no signs of foundation settlement or ground failure. The remaining site was near 3-story buildings for which the observations were ambiguous,

but included minor distress in the free-field with no notice of building settlements. These sites were underlain by 1 to 2 m of fill overlying 4 to 7 m of soft to firm fine-grained CL, ML, and ML-CL soils. Analyses that focused on the potential for cyclic failure in these clay-like soil layers provided a reasonable means for explaining the occurrence of ground failure beneath the five- and six-story buildings and the general absence of ground failure in the free-field or beneath the one-story building.

Future research

There are several important research avenues that are needed to advance our abilities to predict ground failure in clay-like fine-grained soils during earthquakes. Further development and validation of the procedures proposed herein will require a systematic evaluation of the better-documented case histories involving ground failure in fine-grained soils and the collection of additional experimental data on fine-grained soils near the transition from sand-like to clay-like behavior. The consequences of cyclic failure in clay-like soils also need to be better defined with due consideration of how the strength of such soils may transition to fully remolded values with increasing levels of strain (or ground displacement). Questions also remain regarding the appropriate procedures for evaluating the behavior of clayey and silty sands with PI $\geq$ 7, and the procedures for predicting ground failure in strata comprised of highly inter-layered deposits of sand-like and clay-like soils. Some of these questions may benefit from centrifuge modeling studies that utilize the recent advances in in-flight characterization tools.

While a number of issues remain to be addressed, it is nonetheless hoped that the procedures recommended in this report will prove useful in engineering practice for assessing potential ground failure hazards in silts and clays during earthquakes. It is also hoped that the material included in this report will provide a framework and a springboard for future developments and refinements in this area.

ACKNOWLEDGMENTS

The experimental work on blended silt mixtures performed by Steve Romero was supported by the National Science Foundation under award CMS-95-9502530. Professor Jonathan P. Stewart and Dr. Daniel Chu provided the data on Wufeng Site A. Dr. Yoshi Moriwaki provided additional data on the slides in Anchorage and the testing of tailing slimes from his personal files. Dr. Lelio Mejia provided cyclic laboratory test data on the CWOC and Chino sites, as well as other testing data from his personal files. Professors C. C. Ladd and Don J. DeGroot provided insights and data on silts and clays from their personal records. The authors are also grateful for the many discussions and valuable review comments provided by Dr. Mejia, Dr. Moriwaki, Professor Stewart, Professor James K. Mitchell, Professor DeGroot, and Dr. Faiz Makdisi.

REFERENCES

Andersen, K, Kleven, A., and Heien, D. (1988). "Cyclic soil data for design of gravity structures," *Journal of the Geotechnical Engineering Div.*, ASCE, 114(5): 517-539.

Andersen, K. H. (1976). "Behavior of clay subjected to undrained cyclic loading." Proceedings, Conference on Behavior of Off-Shore Structures, Trondheim, Norway, Vol. 1, 392-403.

Andrews, D. C. A., and Martin, G. R. (2000). "Criteria for liquefaction of silty soils." *Proc. 12th World Conference on Earthquake Engineering*, Auckland, New Zealand.

Ansal, A, and Erken, A. (1989). "Undrained behavior of clay under cyclic shear stresses." Journal of Geotechnical Engineering, ASCE, 115(7), 968-983.

Azzouz, A. S., Malek, A. M., and Baligh, M. M. (1989). "Cyclic behavior of clays in undrained simple shear, *J.Geotechnical Engineering Div.*, ASCE, 115(5): 637-657.

Boulanger, R. W. (2003a). "Relating K_α to relative state parameter index." Journal of Geotechnical and Geoenvironmental Engineering, ASCE, 129(8), 770-773.

Boulanger, R. W. (2003b). "High overburden stress effects in liquefaction analyses." Journal of Geotechnical and Geoenvironmental Engineering, ASCE, 129(12), 1071-1082.

Boulanger, R. W. and Idriss, I. M. (2004). "State normalization of penetration resistances and the effect of overburden stress on liquefaction resistance." Proc., 11th Int. Conf. on Soil Dynamics and Earthquake Engineering, and 3rd Int. Conf. on Earthquake Geotechnical Engineering, D. Doolin et al., eds., Stallion Press, Vol. 2, 484-491.

Boulanger, R. W., Meyers, M. W., Mejia, L. H., and Idriss, I. M. (1998). "Behavior of a fine-grained soil during Loma Prieta earthquake." *Canadian Geotechnical J.*, 35: 146-158.

Boulanger, R. W., and Truman, S. P. (1996). "Void redistribution in sand under post-earthquake loading." Canadian Geotechnical Journal, 33, 829-834.

Bjerrum, L. (1973). "Problems of soil mechanics and construction on soft clays: SOA report." Proc., 8th Int. Conference on Soil Mechanics and Foundation Engineering, Moscow, USSR, 3, 111-159.

Bjerrum, L. (1972). "Embankments of soft ground." Proc., Specialty Conference on Performance of Earth and Earth-supported Structures, ASCE, Vol. 2, 1-54.

Bray, J. D., Sancio, R. B., Riemer, M. F., and Durgunoglu, T. (2004a). "Liquefaction susceptibility of fine-grained soils." 11th Int. Conf. on Soil Dynamics and Earthquake Engineering and 3rd Int. Conf. on Earthquake Geotechnical Engineering, D. Doolin et al., eds., Stallion Press, pp 655-662.

Bray, J. D., Sancio, R. B., Durgunoglu, T., Onalp, A., Youd, T. L., Stewart, J. P., Seed, R. B., Cetin, O. K., Bol, E., Baturay, M. B., Christensen, C., and Karadayilar, T. (2004b). "Subsurface characterization at ground failure sites in Adapazari, Turkey." J. Geotechnical and Geoenvironmental Engineering, ASCE, 130(7), 673-685.

Chu, D. B., Stewart, J. P., Lee, S., Tsai, J. S., Lin, P. S., Chu, B. L., Seed, R. B., Hsu, S. C., Yu, M. S., Wang, M. C. H. (2004). "Documentation of soil conditions at liquefaction and non-liquefaction sites from 1999 Chi-Chi (Taiwan) earthquake." Soil Dynamics and Earthquake Engineering, 24(9-10), 647-657.

Chu, D. B., Stewart, J. P., Lee, S., Tsai, J. S., Lin, P. S., Chu, B. L., Moss, R. E. S., Seed, R. B., Hsu, S. C., Yu, M. S., Wang, M. C. H. (2003). "Validation of liquefaction-related ground failure models using case histories from Chi-Chi, Taiwan earthquake." U.S.-Taiwan Workshop on Soil Liquefaction, Hsinchu, Taiwan, November 2-5, 2003.

Goulois, A. M., Whitman, R. V., and Hoeg, K. (1985). "Effects of sustained shear stresses on the cyclic degradation of clay," *Strength Testing of Marine Sediments: Laboratory and In-Situ Strength Measurements*, ASTM STP 883, R. C. Chaney and K. R. Demars, eds., ASTM, Philadelphia, pp. 336-351.

Hansen, W. R. (1971). Effects at Anchorage, The Great Alaska Earthquake of 1964, Geology, Part A, Naitonal Academy of Science, 5-43.

Hoeg, K., Dyvik, R., and Sandbaekken, G. (2000). "Strength of undisturbed versus reconstituted silt and silty sand specimens." Journal of Geotechnical and Geoenvironmental Engineering, ASCE, 126(7), 606-617.

Hyodo, M., Yamamoto, Y., and Sugiyama, M. (1994). "Undrained cyclic shear behavior of normally consolidated clay subjected to initial static shear stress," *Soils and Foundations*, JSSMFE, 34(4), 1-11.

Idriss, I. M. (1999). "An update to the Seed-Idriss simplified procedure for evaluating liquefaction potential." *Proc., TRB Workshop on New Approaches to Liquefaction*, January, Publication No. FHWA-RD-99-165, Federal Highway Administration.

Idriss, I. M. (1985). "Evaluating seismic risk in engineering practice," *Proc., 11th International Conference on Soil Mechanics and Foundation Engineering*, San Francisco, Balkema, Rotterdam, 265-320.

Idriss, I. M., and Boulanger, R. W. (2004). "Semi-empirical procedures for evaluating liquefaction potential during earthquakes." Proc., 11th Int. Conference on Soil Dynamics and Earthquake Engineering, and 3rd Int. Conference on Earthquake Geotechnical Engineering, D. Doolin et al., eds., Stallion Press, Vol. 1, 32-56.

Idriss, I. M., and Boulanger, R. W. (2003a). "Estimating K_α for use in evaluating cyclic resistance of sloping ground." *Proc. 8th US-Japan Workshop on Earthquake Resistant Design of Lifeline Facilities and Countermeasures against Liquefaction*, Hamada, O'Rourke, and Bardet, eds., Report MCEER-03-0003, MCEER, SUNY Buffalo, N.Y., 449-468.

Ishihara, K. (1996). *Soil Behavior in Earthquake Geotechnics*. The Oxford Engineering Science Series, No. 46.

Ishihara, K. (1993). "Liquefaction and flow failure during earthquakes." Geotechnique, 43(3), 351-415.

Ishihara, K, Tatsuoka, F., and Yasuda, S. (1975). "Undrained deformation and liquefaction of sand under cyclic stresses." Soils and Foundations, 15, 29-44.

Koester, J. P. (1992). "The influence of test procedure on correlation of Atterberg limits with liquefaction in fine-grained soils." Geotechnical Testing J., ASTM, 15(4): 352-360.

Koutsoftas, D. C., and Ladd, C. C. (1985). "Design strengths for an offshore clay." Journal of Geotechnical Engineering, ASCE, 111(3), 337-355.

Kulhawy, F. H., and Mayne, P. W. (1990). Manual on estimating soil properties for foundation design. Report EPRI EL-6800, Electric Power Research Institute, Palo Alto, California.

Ladd, C. C. (1991). "Stability evaluation during staged construction," *Journal of Geotechnical Engineering*, ASCE, 117(4), 540-615.

Ladd, C. C., and DeGroot, D. J. (2003). "Recommended practice for soft ground site characterization: Arthur Casagrande Lecture." Proc., Soil and Rock America, P.J. Culligan, H. H. Einstein, and A. J. Whittle, eds., Verlag Gluckauf GMBH, Essan, Germany, Vol. 1, 3-57.

Ladd, C. C., Foott, R., Ishihara, K., Schlosser, F., and Poulos, H. G. (1977). "Stress-deformation and strength characteristics: SOA report." Proc., 9th International Conference on Soil Mechanics and Foundation Engineering, 2, 421-494.

Ladd, C. C., and Foott, R. (1974). "New design procedure for stability of soft clays." *Journal of the Geotechnical Engineering Div.*, ASCE, 100(7), 763-786.

Larsson, R. (1980). "Undrained shear strength in stability calculation of embankments and foundations on soft clays." Canadian Geotechnical Journal, 17(4), 591-602).

Lefebvre, G., and Pfendler, P. (1996). "Strain rate and preshear effects in cyclic resistance of soft clay." J. Geotechnical and Geoenvironmental Engineering, ASCE, 122(1), 21-26.

Lefebvre, G., and LeBouef, D. (1987). "Rate effects and cyclic loading of sensitive clays," *Journal of Geotechnical Engineering*, ASCE, 113(5), 476-489.

Lefebvre, G., Ladd, C. C., Mesri, G., and Tavenas, F. (1983). "Report of the testing subcommittee." Committee of Specialists on Sensitive Clays on the NBR Complex, SEBJ, Montreal, Canada, Annexe I.

Liu, A. H., Stewart, J. P., Abrahamson, N. A., and Moriwaki, Y. (2001). "Equivalent Number of Uniform Stress Cycles for Soil Liquefaction Analysis," *J. Geotechnical & Geoenvironmental Engineering*, ASCE, 127(12), 1017-1026.

Makdisi, F. I., and Seed, H. B. (1978). "Simplified procedure for estimating dam and embankment earthquake-induced deformations." Journal of Geotechnical Engineering Division, ASCE, 104(GT7), 849-867.

Mitchell, J. K. (1993). *Fundamentals of Soil Behavior*, 2nd Edition, John Wiley and Sons, Inc.

Mitchell, J. K. (1976). *Fundamentals of Soil Behavior*, 1st Edition, John Wiley and Sons, Inc.

Martin, J. R., II, Olgun, C. G., Mitchell, J. K., Durgunoglu, H. T. (2004). "High modulus columns for liquefaction mitigation. Journal of Geotechnical and Geoenvironmental Engineering, ASCE, 130(6), 561-571.

Moriwaki, Y., Akky, M. R., Ebeling, R., Idriss, I. M., and Ladd, R. S. (1982). "Cyclic strength and properties of tailing slimes." Proc., Specialty Conference on Dynamic Stability of Tailings Dams, ASCE.

National Center for Earthquake Engineering Research (NCEER) (1997). *Proceedings of the NCEER Workshop on Evaluation of Liquefaction Resistance of Soils*, T. L. Youd and I. M. Idriss, Editors, Technical Report NCEER-97-022.

Perlea, V. G. (2000). "Liquefaction of cohesive soils." *Soil Dynamics and Liquefaction 2000*, Geotechnical Special Pub. 107, R. Y. S. Pak and J. Yamamuro, eds., ASCE, 58-76.

Polito, C. P. (1999). *The effects of non-plastic and plastic fines on the liquefaction resistance of sandy soils*. Ph.D. thesis, Virginia Polytechnic Institute and State University, Dec.

Robertson, P. K., and Wride, C. E. (1998). "Evaluating cyclic liquefaction potential using the cone penetration test." Canadian Geotechnical Journal, 35(3), 442-459.

Romero, S. (1995). *The behavior of silt as clay content is increased*. MS thesis, University of California, Davis, 108 pp.

Sangrey, D. A., Henkel, D. J., and Esrig, M. I. (1969). "The effective stress response of a saturated clay to repeated loading." Canadian Geotechnical Journal, 6(3), 241-252.

Seed, H. B. (1987). "Design problems in soil liquefaction." Journal of Geotechnical Engineering, ASCE, 113(8), 827-845.

Seed, H. B. (1983). "Earthquake resistant design of earth dams." *Proc., Symposium on Seismic Design of Embankments and Caverns*, Pennsylvania, ASCE, N.Y., 41-64.

Seed, H. B., and Idriss, I. M. (1982). *Ground motions and soil liquefaction during earthquakes*, Earthquake Engineering Research Institute, Berkeley, CA, 134 pp.

Seed, H. B. (1979). "Considerations in the earthquake-resistant design of earth and rockfill dams." Geotechnique, 29(3).

Seed, H. B., Idriss, I. M., Makdisi, F., and Banerjee, N. (1975b). "Representation of Irregular Stress Time Histories by Equivalent Uniform Stress Series in Liquefaction Analyses," Report No. EERC 75-29, Earthquake Engineering Research Center, University of California, Berkeley, October.

Seed, H. B., and Idriss, I. M. (1971). "Simplified procedure for evaluating soil liquefaction potential," *J. Soil Mechanics and Foundations Div.*, ASCE, 97:SM9, 1249-1273.

Seed, H. B., and Chan, C. K. (1966). "Clay strength under earthquake loading conditions." Journal of the Soil Mechanics and Foundations Division, ASCE, 92(SM2), 53-78.

Seed, R. B., Cetin, K. O., Moss, R. E. S., Kammerer, A., Wu, J., Pestana, J., Riemer, M., Sancio, R. B., Bray, J. D., Kayen, R. E., and Faris, A. (2003). "Recent advances in soil liquefaction engineering: A unified and consistent framework." Keynote presentation, 26th Annual ASCE Los Angeles Geotechnical Spring Seminar, Long Beach, CA.

Shen, C. K., Jeong, S., Wang, Z. L., and Dafalias, Y. (1989). "Behavior of silt under monotonic and cyclic loadings." Proc., 4th Soil Dynamics and Earthquake Engineering Conference, Mexico.

Skempton, A. W. (1953). "The colloidal activity of clay." Proc. Third International Conference on Soil Mechanics and Foundation Engineering, Vol. 1, 57-61.

Stark, T. D., and Contreras, I. A. (1998). "Fourth Avenue landslide during 1964 Alaskan earthquake." Journal of Geotechnical and Geoenvironmental Engineering, ASCE, 124(2), 99-109.

Stewart, J. P., Chu, D. B., Lee, S., Tsai, J. S., Lin, P. S., Chu, B. L., Moss, R. E. S., Seed, R. B., Hsu, S. C., Yu, M. S., and Wang, M. C. H. (2003). "Liquefaction and non-liquefaction from 1999 Chi-Chi, Taiwan, earthquake," *Advancing Mitigation Technologies and Disaster Response for Lifeline Systems*, Technical Council on Lifeline Earthquake Engineering, Monograph No. 25, J. E. Beavers ed., 1021-1030.

Stewart, J. P., Chu, D. B., Guglielmo, E., Chu, B. L, Hsu, S. C., Kayen, R., Lee, S., Lin, P. S., Seed, R. B., Tsai, J. S., Wang, M. C. H., and Yu, M. S. (2004). Documentation of soil conditions at liquefaction sites from 1999 Chi-Chi, Taiwan earthquake. PEER Lifelines website, http://peer.berkeley.edu/lifelines/research_projects/3A02/.

Tawil, M. R. (1997). Engineering properties of iron mine slimes for tailings dam stability. MS thesis, Massachusetts Institute of Technology, 280 pp.

Taylor, D. W. (1948). Fundamentals of Soil Mechanics, John Wiley and Sons.

Thiers, G. R., and Seed, H. B. (1969). "Strength and stress-strain characteristics of clays subjected to seismic loads." ASTM STP 450, Symposium on Vibration Effects of Earthquakes on Soils and Foundations, ASTM, 3-56.

Thiers, G. R., and Seed, H. B. (1968). "Cyclic stress-strain characteristics of clays," *J. Soil Mechanics and Foundations Div.*, ASCE, 94(2), 555-569.

Wang, W. S., "Some findings in soil liquefaction." Water Conservancy and Hydroelectric Power Scientific Research Institute, Beijing, China, 1979.

Woodward-Clyde Consultants (1992a). *California Water Operations Center – Site Evaluation and Remediation – Conceptual Design. Appendix E: CWOC Site Characterization Memo*. Oakland, California.

Woodward-Clyde Consultants (1992b). *Seismic Stability Evaluation and Piezometer Installation, Tailing Pond No. 7*. Denver, Colorado.

Yu, H. S., Herrmann, L. R., and Boulanger, R. W. (2000). "Analysis of steady cone penetration in clay." J. Geotechnical & Geoenvir. Engrg., ASCE, 126(7), 594-605.

Zergoun, M., and Vaid, Y. P. (1994). "Effective stress response of clay to undrained cyclic loading," *Canadian Geotechnical Journal*, 31: 714-727.